ISSN: 2408-2384 (Online)
ISSN: 1686-5456 (Print)

Environment and Natural Resources Journal

Volume 18, Number 4, October - December 2020

Environment and Natural Resources Journal (EnNRJ)

Volume 18, Number 4, October - December 2020 ISSN: 1686-5456 (Print)
ISSN: 2408-2384 (Online)

AIMS AND SCOPE

The Environment and Natural Resources Journal is a peer-reviewed journal, which provides insight scientific knowledge into the diverse dimensions of integrated environmental and natural resource management. The journal aims to provide a platform for exchange and distribution of the knowledge and cutting-edge research in the fields of environmental science and natural resource management to academicians, scientists and researchers. The journal accepts a varied array of manuscripts on all aspects of environmental science and natural resource management. The journal scope covers the integration of multidisciplinary sciences for prevention, control, treatment, environmental clean-up and restoration. The study of the existing or emerging problems of environment and natural resources in the region of Southeast Asia and the creation of novel knowledge and/or recommendations of mitigation measures for sustainable development policies are emphasized.

The subject areas are diverse, but specific topics of interest include:

- Biodiversity
- Climate change
- Detection and monitoring of polluted sources e.g., industry, mining
- Disaster e.g., forest fire, flooding, earthquake, tsunami, or tidal wave
- Ecological/Environmental modelling
- Emerging contaminants/hazardous wastes investigation and remediation
- Environmental dynamics e.g., coastal erosion, sea level rise
- Environmental assessment tools, policy and management e.g., GIS, remote sensing, Environmental Management System (EMS)
- Environmental pollution and other novel solutions to pollution
- Remediation technology of contaminated environments
- Transboundary pollution
- Waste and wastewater treatments and disposal technology

Schedule

Environment and Natural Resources Journal (EnNRJ) is a quarterly published journal in January-March, April-June, July-September and October-December.

Publication Fees

There is no cost of the article-processing and publication.

Ethics in publishing

EnNRJ follows closely a set of guidelines and recommendations published by Committee on Publication Ethics (COPE) (http://publicationethics.org/).

Environment and Natural Resources Journal (EnNRJ)

Volume 18, Number 4, October - December 2020 ISSN: 1686-5456 (Print)
ISSN: 2408-2384 (Online)

Editorial Office Address
Research and Academic Services Section,
Faculty of Environment and Resource Studies, Mahidol University
999, Phutthamonthon Sai 4 Road, Salaya, Phutthamonthon, Nakhon Pathom, Thailand, 73170
Phone +662 441 5000 ext. 2108 Fax. +662 441 9509-10
Website: https://ph02.tci-thaijo.org/index.php/ennrj/index
E-mail: ennrjournal@gmail.com

Environment and Natural Resources Journal (EnNRJ)

Volume 18, Number 4, October - December 2020 ISSN: 1686-5456 (Print)
ISSN: 2408-2384 (Online)

CONTENT

Impact of Odor from a Landfill Site on Surrounding Areas: A Case Study in Ho Chi Minh City, Vietnam

Linh Hoang Tran[1*], Takehiko Murayama[1], Chouzou Enomoto[2], and Shigeo Nishikizawa[1]

[1]*School of Environment and Society, Tokyo Institute of Technology, Japan*
[2]*Odor Analysis Laboratory, Technical Center, Environmental Control Center Co. Ltd., Japan*

ARTICLE INFO

Received: 15 Apr 2020
Received in revised: 30 Jun 2020
Accepted: 8 Jul 2020
Published online: 24 Jul 2020
DOI: 10.32526/ennrj.18.4.2020.31

Keywords:
Odor concentration/ Landfill/ Odor perception/ Health symptom/ Wind direction

*** Corresponding author:**
E-mail: thlinh171@gmail.com

ABSTRACT

Airborne and odor pollutions generated from landfill operations can adversely affect human health and social well-being. These pollutants should be thus controlled and regulated. Further, the dispersion of odors in the areas surrounding landfills can create public complaints regarding air quality and can increase social tension. Therefore, in this context, we investigated the odor emission from a landfill in surrounding areas using a combination of measuring odor concentrations and conducting a questionnaire survey. The odor measured in three areas, namely, 1, 2, and 3 were at a distance of 1.5 km, 8.2 km, and 10 km from the landfill site, respectively. Results show that the level of odor concentration in area 1 is much higher than the acceptance level of 10-15 ou/m^3 with a mean value of 109.75±39.46 ou/m^3. Odor concentration levels detected 8.2 km and 10 km from the landfill were 18.97±10.84 ou/m^3 and 10.97±10.50 ou/m^3, respectively. Additionally, odor concentration and people's perception of odor varied with geography. This study provides useful information for the management of odor from the Municipal Solid Waste (MSW) management facility in a developing country like Vietnam. Policymakers should consider public perception when framing regulations or making decisions about MSW facilities that also ensure environmental protection.

1. INTRODUCTION

Odor emissions can cause olfactory annoyance. Industries such as treatment plants for water and wastewater, food production facilities, waste disposal operations, and intensive farming activities generally emit odors that are also volatile organic compounds (VOCs). The majority of pollutants from these sources are VOCs, and they cause odor episodes at varying levels of annoyance (Gallego et al., 2008). Industries have an environmental and social obligation to ensure that their intended performance does not harm their surroundings (Parcsi et al., 2012), as detectable odors may influence daily moods and impact both psychology and physiology in individuals (Gallego et al., 2008; Ko et al., 2015). Odors are typically known as contaminants and are subject to specific environmental regulations (Nicell, 2009). Nuisances associated with odor pollution have been one of the most common public complaints to authorities regarding air quality (Hayes et al., 2014; Henshaw et al., 2006), and have become a larger social issue in developed countries (Blumberg and Sasson, 2001; Ranzato et al., 2012). Monitoring tools are necessary to prevent, manage, and mitigate odor impact in communities (Ranzato et al., 2012).

The influence of odors is a combination of interactive variables known as FIDOL: Odor frequency (F), perceived odor intensity (I), odor duration (D), offensive odors (O), and perceived odor location (L). The FIDOL factors encompass both odor patterns and the environment (Freeman and Cudmore, 2002; Nicell, 2009). An annoyance can be quantified, and there is a propensity of an odor to cause a disturbance within a population if it is exposed to an odor intermittently. The intensity of a perceived level of odor annoyance depends not only on odor quality but also on its perceived offensiveness (UK Environment Agency, 2002). Odor pollution is most disturbing when there is more industrial activity near residential areas (Capelli et al., 2011).

Citation: Tran LH, Murayama T, Enomoto C, Nishikizawa S. Impact of odor from a landfill site on surrounding areas: A case study in Ho Chi Minh City, Vietnam. Environ. Nat. Resour. J. 2020;18(4):322-332. (https://doi.org/10.32526/ennrj.18.4.2020.31)

A training process for evaluators (panelists), according to VDI (2006) (VDI- Association of German Engineers), may be used to perform odor assessment studies on a direct basis. In certain parts of Europe and the USA, this approach is now widespread. However, it is time-consuming, costly, and depends largely on local weather conditions (Naddeo et al., 2012; Zarra et al., 2011). An analysis of air quality related to odor perception can be conducted by using a questionnaire survey for the population affected by the odor source. Odor exposure is typically a human experience, so it can be beneficial to study a community for the purposes of odor evaluation (Capelli et al., 2013). A questionnaire assessment can be used to test community irritation levels from all odor sources. The findings of this assessment can be used to identify the origins of odor according to the accumulated stress in a community. This approach is limited to areas where there is an adequate population density to produce statistically significant results (New Zealand Ministry for the Environment, 2016).

The primary perception of public risks faced by residents living near a waste treatment facility is concerns about health issues, deterioration of environmental quality (pollution, dust, noise, odor), increased risk of technical incidents, damage from natural disasters, and devaluation of neighboring property. These concerns are heightened when residents are in close vicinity to the facility (Al-Khatib et al., 2014; Al-Yaqout et al., 2002; Giusti, 2009; Laner et al., 2009; Sankoh et al., 2013; Srangsriwong et al., 2019). The proximity of residents to a planned or current facility appears to be the most significant factors for influencing the residential perception. Many studies have shown that health problems are related to the proximity or exposure to sites (Sever, 1997; Vrijheid, 2000): the closer residents are to the sites, the more likely they are to worry about their adverse effects (De Feo et al., 2013; Furuseth and Johnson, 1988; Rahardyan et al., 2004). Among the anxiety, odor annoyance for those who live near the waste treatment center is considered to be the most directly perceived response. Thus, there is some correlation between proximity and odor annoyance (Aatamila et al., 2011).

In addition, previous studies only investigated the short distance of the odor effect. Particularly, a study in Canada investigated the perception of odor from an area that included a composting plant and a large landfill site. The study involved recruitment and training of 43 residents living adjacent to the site to make odor observations (Héroux et al., 2004). The observations of residents confirmed an impact radius of 1.5 km from the composting zone center. The area beyond 1.5 km was not covered in the study, and no maximum distance was identified. In a study in Germany, trained panelists have found that the relative frequency of odor annoyance ranged from less than 10 to 30% at a distance of 870 m from large composting plants (Albrecht et al., 2008; Fischer et al., 2008). In South Korea, a study investigated the concentration level and variation of odorous gases at the landfill site and in nearby areas within a radius of 5 km from the site. In most surrounding areas, offensive odor was not a significant pollution issue, with the exception of the high generation of the strong odour compounds such as acetaldehyde and propionaldehydes, within a 5 km radius of the site (Lim et al., 2018). In these studies, the levels of odor annoyance were not reported for longer distances. In Vietnam, however, a previous study indicated that areas surrounding Da Phuoc landfill in Ho Chi Minh City (HCMC) were under affected by odor levels, particularly in urban areas within 7 km from waste treatment facility (Tran et al., 2019). Therefore, the purpose of this research was to measure the odor concentration in affected areas in comparison with questionnaire survey results. The obtained results can help enhance environmental protection.

2. METHODOLOGY

2.1 Climate condition of survey area

The survey area is subject to tropical monsoons along with two traditional weather patterns that directly affect odor distribution. The first pattern is the high temperature in two separate seasons: the dry season between November and April, and the rainy season between May and October. The second pattern is the direction of the wind, which changes monthly: (i) from Jan to May in the South (S) or Southeast (SE) direction; (ii) from June to September in the West (W) or Southwest (SW) direction; (iii) from October to December in the Northeast (NE) direction (Tran et al., 2019). The windrose plot of the study area by each quarter for 2019 is shown in Figure 1. As seen in this figure, the wind direction of the survey location was SE from January to March, SW or SE from April to June, SW from July to September, and NE or Northwest (NW) or SE from October to December.

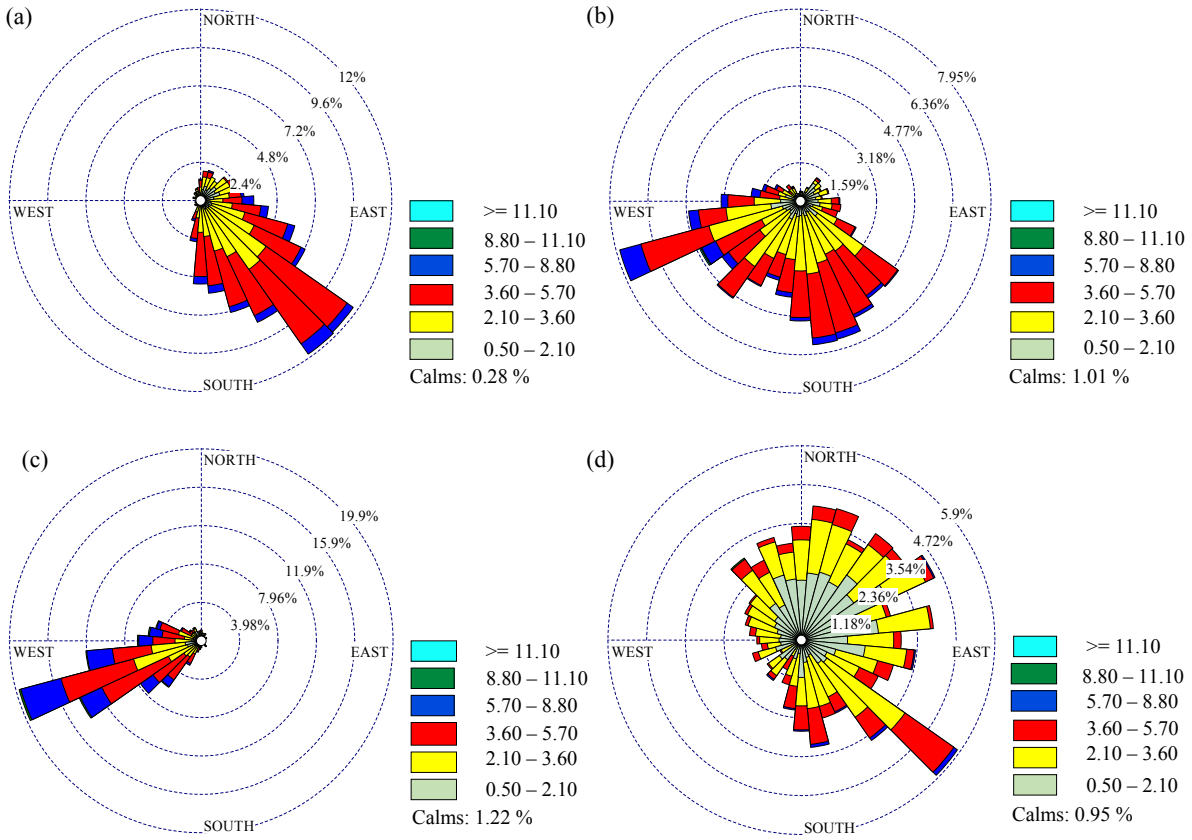

Figure 1. Windrose plot for study area in 2019: (a) From January to March; (b) From April to June; (c) From July to September; (d) From October to December. (Source: prepared from VVTS met data)

2.2 Survey location

2.2.1 Characteristics of MSW treatment facility

The Da Phuoc MSW management facility in HCMC was chosen as the target area for our study. This facility is the primary solid waste management facility in HCMC, and was established in 2007. It has the capacity to treat 5,200 tons of solid waste per day, and mostly relies on landfilling. Since the operation of this facility began, it has received around 22.8 Mt of solid waste. Even though this facility plays a vital role in reducing the substantial waste problem of this city, it causes pollution and odor that spreads to nearby residential areas and to its management areas. There have been more than 500 complaints received from residents living in urban areas approximately 7 km away from the landfill site. Surrounding residents have complained that they are unable to get fresh air inside their apartments. However, the response from authorities has not satisfied these residents.

2.2.2 Site description

Three areas were selected for our investigation zone, which was located in the center of the site with a radius of approximately 10 km (Figure 2). Table 1 show the characteristics of three sampling sites. Regions were classified as Areas 1, 2, and 3 based on odor reports provided by the environmental agency. The survey locations chosen were the same as a previous investigation (Tran et al., 2019) in order to provide consistent reporting and allow for comparative analysis. Area 1 is associated with a high exposure to odor, and it is located in a rural region. Areas 2 and 3 are associated with a high sensitivity to odor impact, and they are located in an urban area.

2.3 Structure of the questionnaire

The questionnaire survey consisted of face-to-face interviews with residents surrounding the MSW treatment facility. The questionnaire aimed to evaluate respondents' perception of odor and attitude toward the MSW treatment facility. It consisted of four components. The first component addressed demographics (gender, age, years of living in the current address). The second component investigated odor perception (frequency, intensity, duration, offensiveness of odors, and factors affecting odors) and included questions regarding the "time of day" and "time of year" that odors are perceived. The third component explored respondents' health issues related to odor impacts. It included the following aspects:

"concern about odors"; "respondent's odor-affected health"; "health symptoms" associated with odors (such as headache, cough, nausea, sleep problems, shortness breath, stuffy nose, anxiety, feeling unhappy and depressed and pain in the heart), and the final component was concerned with odor annoyance, odor issue management, and general attitude towards the MSW treatment facility.

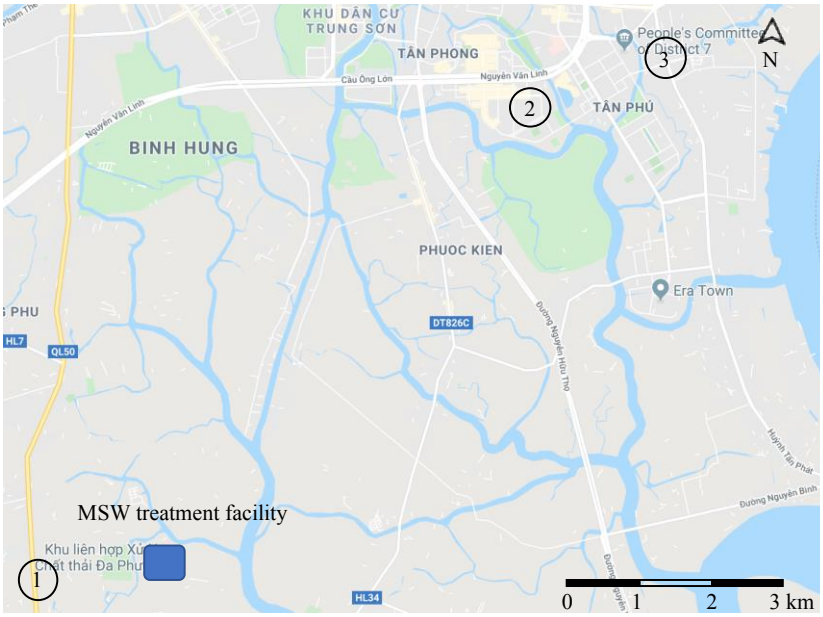

Figure 2. Survey location (Source: google map)

Table 1. Characteristics of sampling sites

	Area 1	Area 2	Area 3
Location	10°40'3.30"N 106°39'4.82"E	10°43'31.28"N 106°42'45.02"E	10°43'54.72"N 106°43'45.35"E
Altitude (above sea level)		Approximately a similar altitude	
Distance from the landfill	1.5 km	8.2 km	10.0 km
Type of land use	Suburban	Residential	Residential
Temperature (average annual)	26.6°C	27.0°C	27.0°c
Rainfall (annual)	1,400-1,700 mm	1,400-1,700 mm	1,400-1,700 mm
Humidity (average annual)	79.5%	80.0%	80.0%
Wind direction		S or SE (Jan-May) W or SW (Jun-Sep) NE (Oct-Dec)	

2.4 Data collection and processing

An odor level indicator XP-329III (New Cosmos Electric Co. Ltd.) was utilized to measure odor concentrations. The method for data collection entailed field sampling monitoring of sensitive receivers at each location within a radius of 10 km from the center of the landfill site. The readings were recorded for 10 min at each sampling area: 20 observations were recorded from area 1 on Sep 20th, 2019; 30 observations were recorded for area 2 on Sep 16th, 2019, and 41 observations were obtained from area 3 on Sep 17th, 2019. Meteorological data such as wind speed, wind direction, humidity, and temperature were collected during the odor concentration measurement. Data on wind speed and wind direction were collected from met station VVTS (Tan Son Nhat international airport) which is provided by BREEZE Software. The windrose map was prepared by using WRPLOT View software, which is freely available on the website of Lake Environment.

3. RESULTS AND DISCUSSION

3.1 Odor measurements

In area 1, the odor concentration ranged from 49 to 149 ou/m^3 with a mean value of 109.75±39.46 ou/m^3. This area is located 1.5 km from the landfill

site. The measured levels of odor concentration and the windrose plot for this area are shown in Figure 3. From this data, we can see that the odor concentration in area 1 was more than 7 times the acceptable level of 10-15 ou/m^3, which is the level specified by the Offensive Odor Control Law (Japan Ministry of the Environment, 2003). The rapid industrial expansion and urbanization of Japan during 1960s resulted in a mounting number of complaints related to air pollution, noise, and offensive odors. To tackle this chronic issue, the "Offensive Odor Control Law" was introduced in 1972. Since its inception, the regulation has helped reduce the number of offensive-odor related complaints dramatically. The odor levels in area 1 are consistent with the perception of the population that was surveyed, where the majority of the respondents (more than 55.0%) reported high odor nuisance levels. This is likely because the area is very close to the MSW treatment facility and is also located on the upwind side of the facility, as seen in Figure 2. However, the surrounding regions of the MSW treatment facility are profoundly affected by odor pollution regardless of the direction of the wind, a finding which is supported by previous studies (Badach et al., 2018; Che et al., 2013; Srangsriwong et al., 2019).

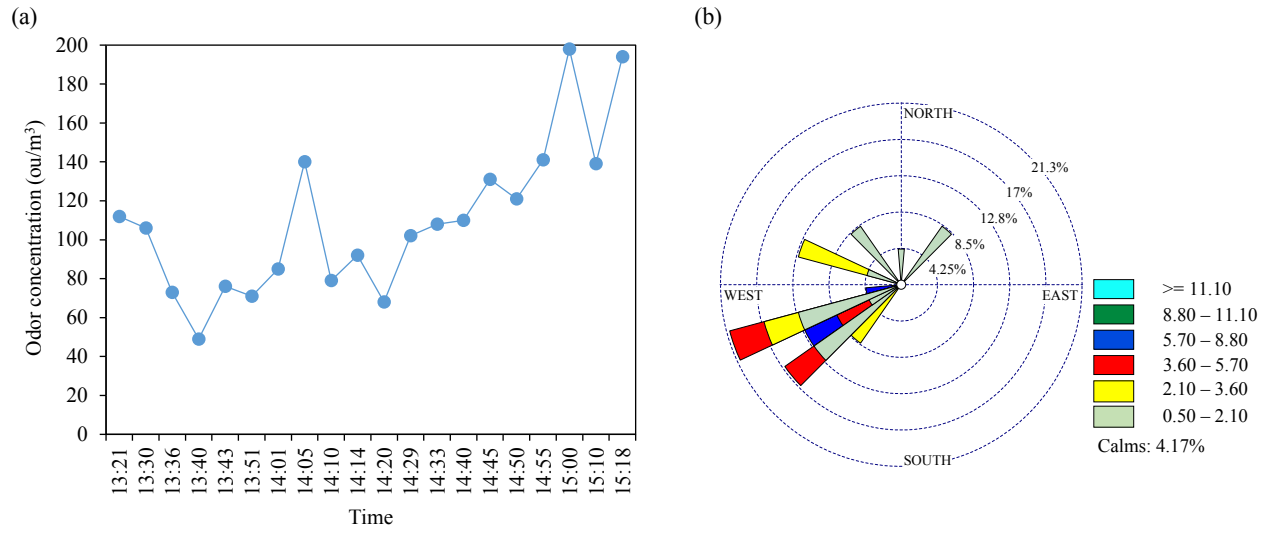

Figure 3. (a) Odor concentration; (b) Windrose plot for area 1 of Sep 20th, 2019 (Source: prepared from field survey 2019)

In area 2, which is located 8.2 km away from the facility, the odor concentration ranged between 2 and 44 ou/m^3 with a mean value of 18.97±10.84 ou/m^3. Figure 4 shows the results of odor concentration and the windrose plot for this area. In this area, the odor concentration is also above the acceptable limit for residential areas (Japan Ministry of the Environment, 2003). It is important to note that this area is a residential area, and is located in the southwest (SW) wind direction (Figure 2). This is a novel finding because this area is located more than 8 km from the MSW treatment plant, and people still reported odor nuisance here (almost 80.0% of respondents reported odor annoyance). However, this could be explained by the social demographics of respondents since odor perception is profoundly influenced by individual differences such as gender, age, and occupation (Bliss et al., 1996; Dalton, 1996).

In area 3, the odor concentration ranged from 1 to 40 ou m^{-3} with a mean value of 10.97±10.50 ou/m^3. The results of odor concentration and windrose plot for this area are shown in Figure 5. This area is located 10 km from the MSW plant, and includes approximately 86.0% of the respondents who reported odor nuisance in this survey. Area 3 is the sector with the highest perceived threat by odor emission from the MSW facility, and it exhibited the highest odor annoyance level in the survey. However, the average odor concentration in area 3 did not exceed the acceptable limit. When examining our monitoring data, we found that the maximum odor concentration here was 40 ou/m^3. From Figure 5, it is apparent that the odor concentration was highest during the period 18:00-19:00, i.e., 6 to 7 pm. This supports the results of the perception survey, where the majority of respondents claimed that odor nuisance was highest from 18:00-24:00, i.e., 6 pm to 12 am the next day (Figure 8). It should be noted that this is in good agreement with wind direction as seen in Figure 6 which shows the windrose plot for area 3 during the

evening time for September 2019. It is apparent that Southwest was the predominant wind direction during the evening time of September 2019, with a frequency of 57.0%. Moreover, in area 3, there are human activities such as development of infrastructure and high-rise buildings, which would affect the dispersion.

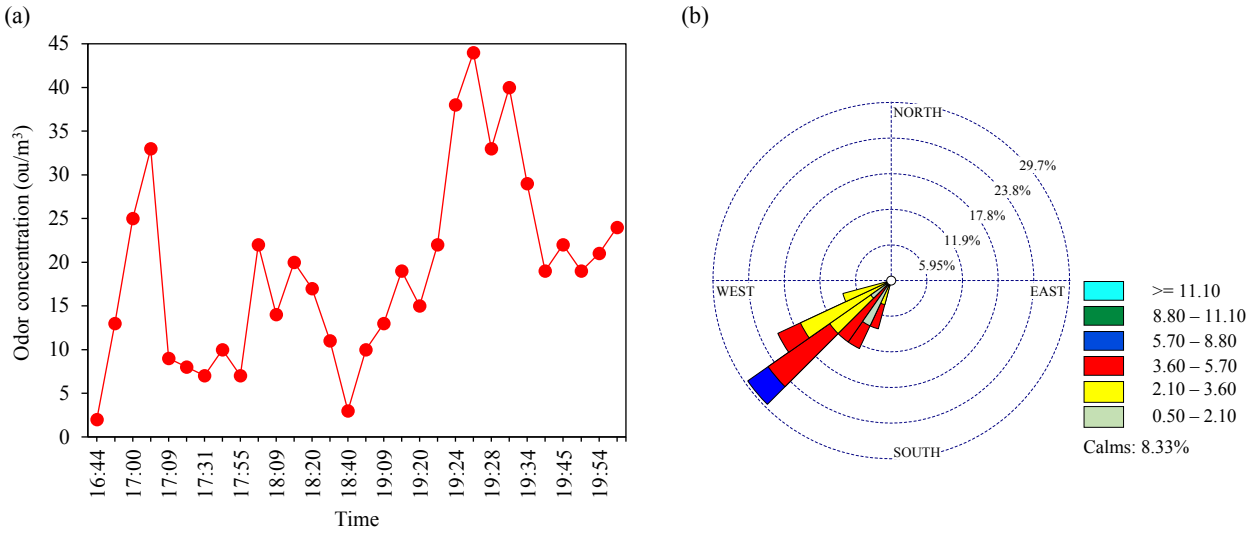

Figure 4. (a) Odor concentration; (b) Windrose plot for area 2 of Sep 16th, 2019 (Source: prepared from field survey 2019)

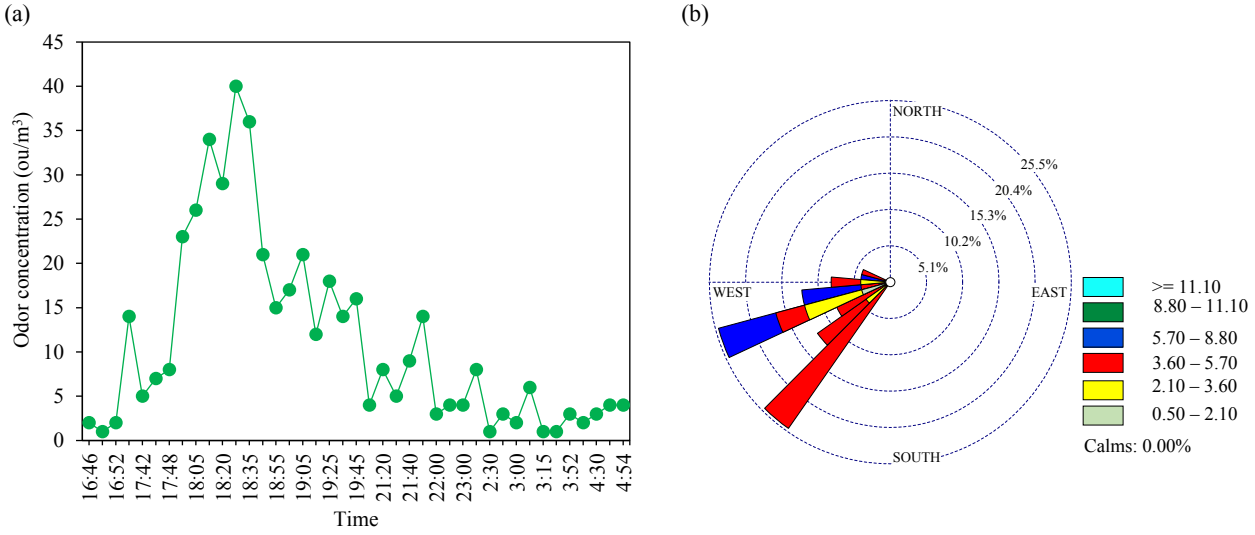

Figure 5. (a) Odor concentration; (b) Windrose plot for area 3 of Sep 17th, 2019 (Source: prepared from field survey 2019)

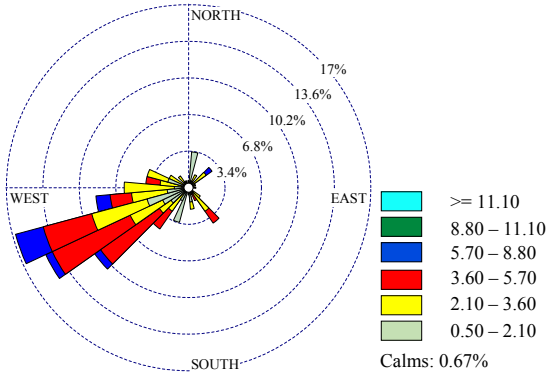

Figure 6. Windrose plot of area 3 in the evening time for Sep 2019 (Source: prepared from field survey 2019)

Figure 7 shows the difference in odor concentration in each area. It is clear that odor concentration decreases by distance. This finding is consistent with Gębicki et al. (2016), which determined that the odor concentration from the municipal landfill in Gda. sk, Poland ranged from 12.50 to 36.70 ou/m^3 along the north-east direction. Furthermore, other research has indicated that the spatial distribution of odor concentration from the municipal wastewater treatment plant in Poland was higher in the vicinity of the facility (Barczak and Kulig, 2016).

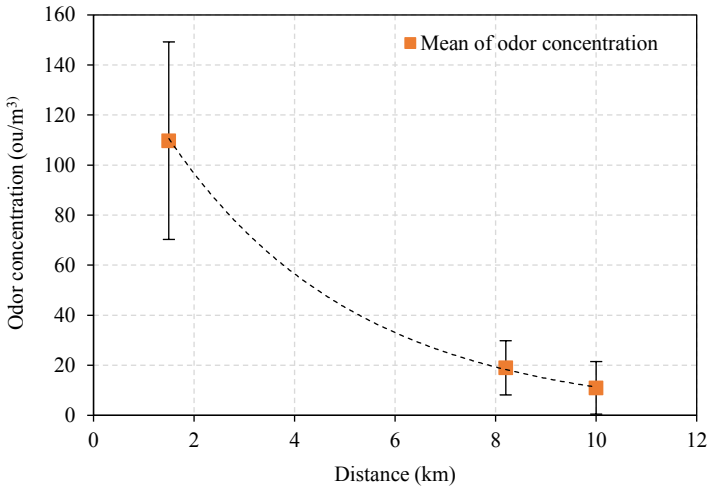

Figure 7. Odor concentration in each area (Source: field survey 2019)

3.2 Summary of community survey results

For a population of 76,602 inhabitants within the investigation area, a minimum number of 409 questionnaires were calculated and applied. Approximately 50.6% of the inhabitants studied were male and 49.4% were female. Further, 85.0% of the inhabitants were over the age of 30 years old. Questionnaire data, which dealt with the perception of odor (i.e., frequency, duration, level, and characteristic), is summarized in Table 2. The responses were classified according to a Likert scale; they were categorized as "not at all, a little bit, moderately, very, and extremely". In terms of response-related odor annoyance, if the response indicated that the person was "very annoyed" or "extremely annoyed," the answer was counted as "percent at-least annoyed" (Freeman and Cudmore, 2002).

Table 2. Results of odor perception by studied area (source: field survey 2018)

	Frequency	Duration	Level	Characteristic
<3 km	92.7% at least once a week	61.0% at least 1-4 h	64.6% at least annoyed	98.8% offensive
3-5 km	91.4% at least once a week	64.3% at least 1-4 h	45.7% at least annoyed	94.3% offensive
5-7 km	58.9% at least once a week	63.6% at least 1-4 h	77.7% at least annoyed	95.5% offensive
>7 km	76.6% at least once a week	54.5% at least 14 h	85.5% at least annoyed	93.8% offensive

The results of the community survey indicate that the odor impact was influenced by wind direction and seasonal change in the area investigated. The observed wind directions were 62.1%, 5.9%, and 1.2% corresponding to Southwest, West wind, and calm hour, respectively (Figure 1(c)). It is implied that the high concentration of odor dispersion probably occurred in the downwind side of the facility. As a result, nearly 46.2% of respondents perceived bad odors between June and August, followed by 33.0% of respondents from September to December. This finding is supported by previous works (Damuchali and Guo, 2020; Palmiotto et al., 2014), which have discovered the high concentrations of air pollutants downwind of the emission source. As seen in Table 2, the area of less than 3 km from the facility exhibited a high perception of odor frequency (i.e., 92.7% at least once a week). In other words, this area has high exposure to odor effects. It is also noteworthy that odors are continuously produced by the MSW facility, as odors in four areas were perceived for multiple hours daily. The majority of respondents reported that the odor from the MSW facility was offensive, and the area of less than 3 km from the facility again had the highest proportion with 98.8% of respondents reporting an offensive odor. Interestingly, the area of more than 7 km from the facility had the highest rate of odor level annoyance (85.5%). Nausea, shortness of breath, and feelings of unhappiness and depression were symptoms recorded in the population. Tran et al. (2019) indicated that residents who live more than 5 km away from the MSW facility had severe odor annoyance from June to October and the period of time during which respondents perceived the worst odor is

shown in Figure 8. As shown in Figure 8, the majority of respondents perceived odor pollution during a period between 18:00-24:00, i.e., 6 pm to 12 am in the next day. This is consistent with the community results.

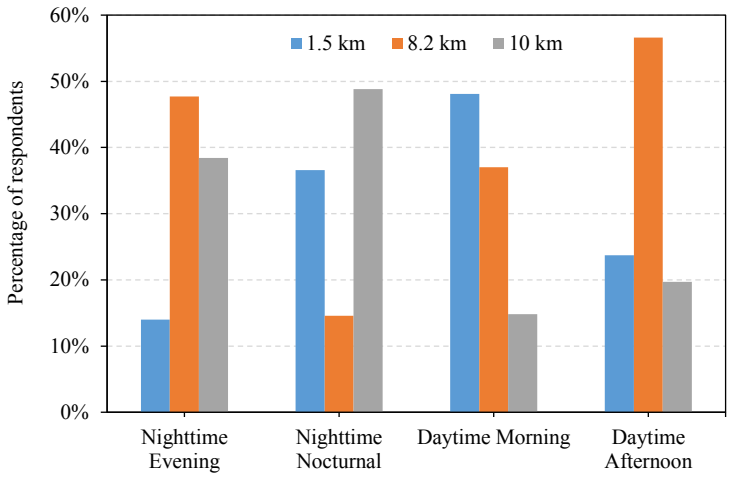

Figure 8. Period of perceived odor (Source: field survey 2018)

Table 3 summarizes the concern, annoyance, and reaction of an area's population that is dealing with odor pollution. The attitude of the populations toward the MSW facility operation is also summarized. The odor level has a strong effect on exposure and annoyance. Areas more than 7 km from the facility again had high proportions of respondents that were concerned and annoyed with odor effects (88.3% very/extremely worried and 85.5% very/extremely annoyed). From this data, it is apparent that most of the respondents in the four areas felt bad/very bad about MSW facility operation. To deal with odor issues, approximately 58.0% of people surveyed close their windows when they detect the odor, while 0.3% (2 out of 409) leave their homes. A proportion of respondents reported odor emissions in their living areas (i.e., informed authorities). From this, it can be inferred that all areas were affected when compared with an acceptable level of cumulative adverse odor effect. The criterion for this acceptable level is that ≤20% of the population are annoyed (Freeman and Cudmore, 2002).

Table 3. Results of community survey by studied area (source: field survey 2018)

	Concern	Annoyance	Reaction	Attitude
<3 km	75.6% very/extremely worried	59.8% very/extremely annoyed	62.2% informed authorities	76.8% bad/very bad
3-5 km	81.4% very/extremely worried	68.6% very/extremely annoyed	45.7% informed authorities	61.4% bad/very bad
5-7 km	75.9% very/extremely worried	71.4% very/extremely annoyed	69.6% informed authorities	88.4% bad/very bad
>7 km	88.3% very/extremely worried	85.5% very/extremely annoyed	60% informed authorities	87.6% bad/very bad

3.3 Comparison between physical condition of odor measurement and community survey results

The mean odor concentration of the three locations and the perceived odor intensity is plotted in Figure 9. As seen in this figure, there was a marked difference between mean odor concentration and intensity of odor perceived. All areas other than area 1 showed a remarkable difference in terms of mean odor concentration and perception of odor intensity. This is likely because odor perception relies on several parameters, such as climatic conditions, subjective consciousness, and the effect of different odors (Davoli et al., 2003; De Gisi et al., 2017; Gallego et al., 2008). Personal perception also is related to other environmental stressors, socioeconomic status, and disruptions in social activity (Nimmermark, 2004; Sucker et al., 2001). Cognitive differences when considering demographics such as age, gender, occupation, and lifestyle habits are regulated further by psychological variables in olfactory perception (Bowler et al., 1996; Davies and Davies, 1999; Doty, 1997; Hayes and Jinks, 2012). Thus, it is important to

note that residents with a higher level of education and a higher income level felt more annoyed from lower odor levels. These residents also exhibited greater concern about environmental issues in general.

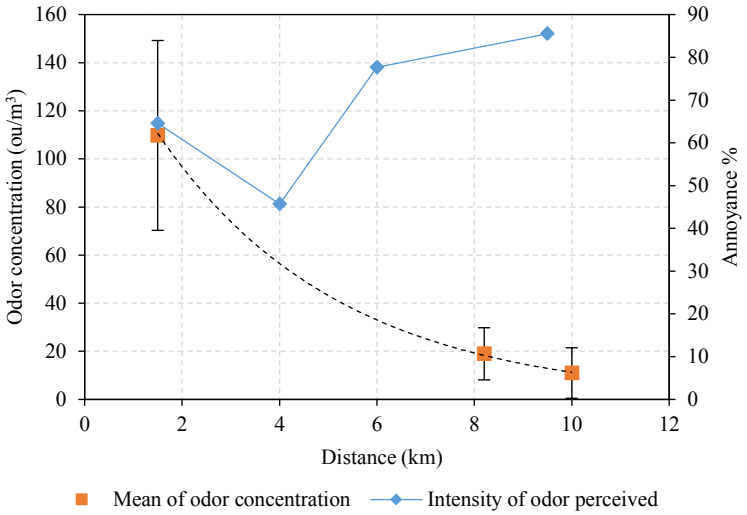

Figure 9. Comparison between odor concentration and odor annoyance (Source: field survey 2018 and 2019)

It is known that intermittent odor exposure may lead to adaptation or sensitivity of individuals, altering their capacity to perceive the odor through physiological changes (Dalton and Dilks, 1997; Press and Minta, 2000). However, because members of the community were exposed continuously to industrial smells, they were accustomed to odors at a peripheral level. When populations were less conscious of odors, their attitudes were more disagreeable and more negative (Dalton and Dilks, 1997). It is possible that people who had lived for less than five years at their current address were more sensitive to odor issues in comparison to those who had lived there for more than ten years.

4. CONCLUSION

In this study, we have investigated the level of odor concentration as well as the perception of odor impact in areas surrounding the MSW treatment plant in HCMC, Vietnam. Specifically, the odor level was measured in three areas, namely, area 1, 2, and 3. Area 1 is 1.5 km upwind, while areas 2 and 3 are downwind of the facility at distances of 8.2 and 10 km, respectively. From the investigation, it was observed that the odor concentration for area 1 was 109.75±39.46 ou/m^3. This is considerably higher than the acceptable level for an area within that radius, 10-15 ou/m^3. As a result, significant odor concentrations were detected in areas downwind of the facility with observed concentration levels in area 2 and 3 reading 18.97±10.84 ou/m^3 and 10.97±10.5 ou/m^3, respectively.

Additionally, odor concentration and respondents' perception of odor varied by geography. This study provides useful information for the management of odor from MSW management facilities in developing countries like Vietnam. Policymakers should consider public perception when developing regulation or making decisions about MSW facilities that also ensure environmental protection. Since there are no clear guidelines on odor management for landfill operations in Vietnam, this research suggests the Japanese Offensive Odor Control Law as a reference for Vietnamese authority. This piece of regulation is a good demonstration of how to deal with offensive odors from business activities for the protection of the living environment and human health. Public participation is a very important aspect of waste management facilities. We also recommend ensuring public consultation towards better landfill management. In addition, as touched upon in this study, socio-demographic parameters such as education level and income also significantly influence odor perception, and this can be explored in future research.

ACKNOWLEDGEMENTS

The authors would like to thank the respondents who provide all information during the field survey.

REFERENCES

Aatamila M, Verkasalo PK, Korhonen MJ, Suominen AL, Hirvonen MR, Viluksela MK, Nevalainen A. Odour annoyance and physical symptoms among residents living near waste treatment centres. Environmental Research 2011;111(1):164-70.

Albrecht A, Fischer G, Brunnemann-Stubbe G, Jäckel U, Kämpfer P. Recommendations for study design and sampling strategies for airborne microorganisms, MVOC and odours in the surrounding of composting facilities. International Journal of Hygiene and Environmental Health 2008;211(1-2):121-31.

Al-Khatib IA, Ajlouny H, Al-Sari' MI, Kontogianni S. Residents' concerns and attitudes toward solid waste management facilities in Palestine: A case study of Hebron district. Waste Management and Research 2014;32(3):228-36.

Al-Yaqout AF, Koushki PA, Hamoda MF. Public opinion and siting solid waste landfills in Kuwait. Resource, Conservation and Recycling 2002;35(4):215-27.

Badach J, Kolasi. ska P, Paciorek M, Wojnowski W, Dymerski T, Gębicki J, et al. A case study of odour nuisance evaluation in the context of integrated urban planning. Journal of Environmental Management 2018;213:417-24.

Barczak R, Kulig A. Odour monitoring of a municipal wastewater treatment plant in poland by field olfactometry. Chemical Engineering Transactions 2016;54:331-6.

Bliss PJ, Schulz TJ, Senger T, Kaye RB. Odor measurement-factors affecting olfactometry panel performance. Water Science and Technology 1996;34(3-4):549-56.

Blumberg DG, Sasson A. Municipal hotlines and automated weather stations as a tool for monitoring bad odour dispersion: The northern Negev case. Journal of Environmental Management 2001;63(1):103-11.

Bowler RM, Huel G, Mergler D, Cone J, Rauch S, Hartney C. Symptom base rates after chemical exposure for White, Hispanic and African Americans. Neurotoxicology 1996;17(3-4):793-802.

Capelli L, Sironi S, Del Rosso R, Céntola P, Rossi A, Austeri C. Olfactometric approach for the evaluation of citizens' exposure to industrial emissions in the city of Terni, Italy. Science of the Total Environment 2011;409(3):595-603.

Capelli L, Sironi S, Del Rosso R, Guillot JM. Measuring odours in the environment vs. dispersion modelling: A review. Atmospheric Environment 2013;79:731-43.

Che Y, Yang K, Jin Y, Zhang W, Shang Z, Tai J. Residents' concerns and attitudes toward a municipal solid waste landfill: Integrating a questionnaire survey and GIS techniques. Environmental Monitoring and Assessment 2013; 185(12):10001-13.

Dalton P. Odor perception and beliefs about risk. Chemical Senses 1996;21(4):447-58.

Dalton P, Dilks D. Odor, annoyance, and health symptoms in a residential community exposed to industrial odors. South Camden Citizens in Action; 1997. p. 1-21.

Damuchali AM, Guo H. Evaluation of odour properties, their relationships, and impact of an oil refinery plant on the surrounding environment using field measurements. Atmospheric Environment 2020;230:117480.

Davies CW, Davies S. Prediction of olfactory response based on age, gender and smoking habits. Journal of Medical Engineering and Technology 1999;23(2):73-6.

Davoli E, Gangai ML, Morselli L, Tonelli D. Characterisation of odorants emissions from landfills by SPME and GC/MS. Chemosphere 2003;51(5):357-68.

De Feo G, De Gisi S, Williams ID. Public perception of odour and environmental pollution attributed to MSW treatment and disposal facilities: A case study. Waste Management 2013;33(4):974-87.

De Gisi S, Casella P, Sabia G, Farina R, Landolfo P, Notarnicola M, et al. Assessing the public perception of islanders regarding the implementation of new technologies to optimize the municipal solid waste management system: A Mediterranean case study. Journal of Cleaner Production 2017;164:1586-601.

Doty RL. Studies of human olfaction from the university of Pennsylvania smell and taste center. Chemical Senses 1997;22:565-86.

Freeman T, Cudmore R. Review of odor management in New Zealand. Wellington: Ministry for the Environment [Internet]. 2002 [cited 2020 Jun 16]. 2002 Available from: https://www.mfe.govt.nz/sites/default/files/odour-tr-aug02.pdf.

Fischer G, Albrecht A, Jäckel U, Kämpfer P. Analysis of airborne microorganisms, MVOC and odour in the surrounding of composting facilities and implications for future investigations. International Journal of Hygiene and Environmental Health 2008;211(1-2):132-42.

Furuseth OJ, Johnson MS. Neighbourhood attitudes towards a sanitary landfill: A North Carolina study. Applied Geography 1988;8(2):135-45.

Gallego E, Soriano C, Roca FX, Perales JF, Alarcón M, Guardino X. Identification of the origin of odour episodes through social participation, chemical control and numerical modelling. Atmospheric Environment 2008;42(35):8150-60.

Gębicki J, Dymerski T, Namieśnik J. Evaluation of ambient air odour quality in vicinity of municipal landfill using electronic nose technique. Chemical Engineering Transactions 2016; 54:253-8.

Giusti L. A review of waste management practices and their impact on human health. Waste Management 2009;29:2227-39.

Hayes JE, Jinks AL. Evaluation of smoking on olfactory thresholds of phenyl ethyl alcohol and n-butanol. Physiology and Behavior 2012;107(2):177-80.

Hayes JE, Stevenson RJ, Stuetz RM. The impact of malodour on communities: A review of assessment techniques. Science of the Total Environment 2014;500:395-407.

Henshaw P, Nicell J, Sikdar A. Parameters for the assessment of odor impacts on communities. Atmospheric Environment 2006;40(6):1016-29.

Héroux M, Pagé T, Gélinas C, Guy C. Evaluating odour impacts from a landfilling and composting site: Involving citizens in the monitoring. Water Science and Technology 2004; 50(4):131-7.

Japan Ministry of the Environment. Odor Measurement Review (MOE) [Internet]. 2003 [cited 2020 Mar 9]. Available from: https://www.env.go.jp/en/air/odor/measure/index.html.

Ko JH, Xu Q, Jang YC. Emissions and control of hydrogen sulfide at landfills: A review. Critical Reviews in Environmental Science and Technology 2015;45(19):2043-83.

Laner D, Fellner J, Brunner PH. Flooding of municipal solid waste landfills-An environmental hazard? Science of the Total Environment 2009;407(12):3674-80.

Lim JH, Cha JS, Kong BJ, Baek SH. Characterization of odorous gases at landfill site and in surrounding areas. Journal of Environmental Management 2018;206:291-303.

Naddeo V, Zarra T, Giuliani S, Belgiorno V. Odour impact assessment in industrial areas. Chemical Engineering Transactions 2012;30:85-90.

New Zealand Ministry for the Environment. Good practice guide for assessing and managing odour [Internet]. 2016 [cited 2020 Apr 13]. Available from: https://www.mfe.govt.nz/sites/default/files/media/Air/good-practice-guide-odour.pdf.

Nicell JA. Assessment and regulation of odour impacts. Atmospheric Environment 2009;43(1):196-206.

Nimmermark S. Odour influence on well-being and health with specific focus on animal production emissions. Annals of Agricultural and Environmental Medicine 2004;11(2):163-73.

Palmiotto M, Fattore E, Paiano V, Celeste G, Colombo A, Davoli E. Influence of a municipal solid waste landfill in the surrounding environment: Toxicological risk and odor nuisance effects. Environment International 2014;68:16-24.

Parcsi G, Sivret EC, Wang X, Stuetz RM. Odor: Characterisation and transformation. Chemical Engineering Transactions 2012;30:193-8.

Press D, Minta SC. The smell of nature: olfaction, knowledge and the environment. Ethics, Place and Environment 2000;3(2):173-86.

Rahardyan B, Matsuto T, Kakuta Y, Tanaka N. Resident's concerns and attitudes towards Solid Waste Management facilities. Waste Management 2004;24(5):437-51.

Ranzato L, Barausse A, Mantovani A, Pittarello A, Benzo M, Palmeri L. A comparison of methods for the assessment of odor impacts on air quality: Field inspection (VDI 3940) and the air dispersion model CALPUFF. Atmospheric Environment 2012;61:570-9.

Sankoh FP, Yan X, Tran Q. Environmental and health impact of solid waste disposal in developing cities: A case study of Granville Brook dumpsite, Freetown, Sierra Leone. Journal of Environmental Protection 2013;04(07):665-70.

Sever LE. Environmental contamination and health effects: What is the evidence? Toxicology Industrial Health 1997;13(3):145-61.

Srangsriwong A, Olapiriyakul S, Yenradee P. Factors influencing public perception and impact distance of a municipal solid waste dumpsite in Thailand. Asia-Pacific Journal of Science and Technology 2019;24(1):APST-24-01-05.

Steinnes E, Hvatum OO, Bølviken B, Varskog P. Atmospheric pollutants and trace gases. Journal of Environmental Quality 2001;34(1):192-7.

Sucker K, Both R, Winneke G. Adverse effects of environmental odours: Reviewing studies on annoyance responses and symptom reporting. Water Science and Technology 2001;44(9):43-51.

Tran LH, Murayama T, Nishikizawa S. Social impact of odor induced by municipal solid waste treatment facilities in Ho Chi Minh city. Asian Journal of Environment and Ecology 2019;16:1-3.

UK Environment Agency. Assessment of community response to odorous emissions [Internet]. 2002 [cited 2020 Apr 13]. Available from: https://assets.publishing.service.gov.uk/government/uploads/system/uploads/attachment_data/file/290405/sp4-095-tr-e-e.pdf.

Verein Deutscher Ingenieure (VDI). Measurement of odor impact by field inspection-Measurement of the impact frequency of recognizable odors-Grid measurement, (VDI 3940). Verlag des Vereins Deutscher Ingenieure; 2006.

Vrijheid M. Health effects of residence near hazardous waste landfill sites: A review of epidemiologic literature. Environmental Health Perspectives 2000;108(Suppl 1):101-12.

Zarra T, Naddeo V, Giuliani S, Belgiorno V. Optimization of field inspection method for odor impact assessment. Chemical Engineering Transactions 2011;23:93-8.

Potential of Palm Kernel Alkanolamide Surfactant for Enhancing Oil Recovery from Sandstone Reservoir Rocks

Parichat Traiwiriyawong and Suratsawadee Kungsanant*

Department of Chemical Engineering, Faculty of Engineering, Prince of Songkla University, Hat-Yai, Songkhla 90110, Thailand

ARTICLE INFO

Received: 6 Mar 2020
Received in revised: 30 Jun 2020
Accepted: 10 Jul 2020
Published online: 29 Jul 2020
DOI: 10.32526/ennrj.18.4.2020.32

Keywords:
Alkanolamide surfactant/ Adsorption/ Crude oil solubilization/ Solubilization Equilibrium constant/ EOR

*** Corresponding author:**
E-mail: suratsawadee.k@psu.ac.th

ABSTRACT

The interest in using benign surfactants has been steadily increasing in the context of enhanced oil recovery (EOR). Palm kernel alkanolamide surfactant (PKA), a nonionic surfactant synthesized from palm kernel oil, was preliminarily assessed for EOR from sandstone reservoir rocks. The performance factors determined were surfactant loss due to adsorption on silica surface and crude oil solubilization for oil solubilizing efficiency. The performance of PKA was compared to two commercial ionic surfactants, SDS (anionic surfactant) and CTAB (cationic surfactant). The results show that PKA was less absorbed on silica than CTAB or SDS. The adsorption kinetics was well fit with a pseudo-second order model for all three surfactants. The adsorption equilibrium data for CTAB and PKA were fitted with a Langmuir isotherm, while a Freundlich isotherm fit well for SDS, indicating multilayer SDS adsorption on silica surfaces. The adsorption of PKA was not significantly affected by added NaCl or increased temperature. In addition, the solubilization equilibrium constant (K_s) had the rank order PKA>CTAB>SDS, and proportionally increased with added NaCl. PKA performance was also compared to two commercial nonionic surfactants, Tergitol 15-S-9 and Tergitol TMN-6, and the results indicate that PKA was the least adsorbed, and had the highest K_s among the tested nonionic surfactants.

1. INTRODUCTION

Nowadays, enhanced oil recovery (EOR) by surfactant flooding is continuously developed and widely used. The surfactant molecules used in EOR have amphipathic structures. The head part of the surfactant molecule is polar and hydrophilic, whereas its tail is non-polar and hydrophobic. When adding surfactants to the system, they tend to adsorb at crude/water or crude/rock interfaces, lowering interfacial tension, and this can release and mobilize crude oil from the pores of reservoir rocks. These phenomena can increase the amount of crude oil production significantly, by up to 60% (Belhaj et al., 2019; Emadi et al., 2017). In addition, surfactants can form micelles by pointing hydrophobic tails inwards and hydrophilic heads outwards. This phenomenon creates a hydrophobic region for crude oil partitioning and can make crude oil appear water soluble (Rosen, 1989).

However, there are some limitations to surfactant flooding techniques, such as the high cost of surfactants, surfactant loss during operation due to adsorption by reservoir rocks, and their toxicity to the environment, leading to high production costs and toxicity, especially in a sea environment (Bera et al., 2017). Thus, many studies have suggested that surfactants synthesized from natural resources could avoid the negative environmental impacts from surfactant loss during surfactant flooding, and still provide high recovery rate (Arabloo et al., 2015; Barati-Harooni et al., 2016; Iglauer et al., 2010).

Natural surfactants are typically synthesized from plants, seeds, or vegetable oil, depending on availability by locality. This facilitates agricultural waste minimization and can effectively generate value-added products. For example, Arabloo et al. (2015) studied adsorption of a saponin surfactant synthesized from *Glycyrrhiza Glabra* onto sandstone.

Citation: Traiwiriyawong P, Kungsanant S. Potential of palm kernel alkanolamide surfactant for enhancing oil recovery from sandstone reservoir rocks. Environ. Nat. Resour. J. 2020;18(4):333-344. (https://doi.org/10.32526/ennrj.18.4.2020.32)

The results show that *Glycyrrhiza Glabra* saponin decreased interfacial tension between oil and water from 31.6 mN/m to 6.5 mN/m and could be utilized in EOR. Barati-Harooni et al. (2016) studied adsorption of a nonionic surfactant synthesized from seeds of *Trigoonella foenum-graceum* (TFG) on sandstone minerals in EOR. The adsorption of TFG was lower than of other natural nonionic surfactants in controlled conditions. In addition, the price of TFG is lower than those of surfactants commonly used in the crude oil industry. Furthermore, TFG is available in the country of that study and is not harmful to the environment. Iglauer et al. (2010) studied new surfactant classes for their tertiary oil recovery potential. This study examined the adsorption of di-tridecyl sulfosuccinic acid ester, coconut diethanolamide, alkyl polyglycoside, and alkylpropoxy sulfate sodium salts on kaolin clay, with a view to surfactant loss. The results show that coconut diethanolamide was the least absorbed and increased tertiary oil recovery by up to 75%. The study suggested coconut diethanolamide as a new alternative surfactant with high tertiary oil recovery potential.

Therefore, this current work studied the potential of alkanolamide nonionic surfactant (palm kernel alkanolamide, PKA) synthesized from palm kernel oil for EOR. PKA is a natural nonionic surfactant with structure similar to coconut diethanolamide, which has been proven an effective surfactant for EOR (Iglauer et al., 2010). Typically, the alkanolamine synthesized from palm kernel oil is used as an additive in personal care products and has no significant effects on the environment (Wetchakul, 2013). Besides, the study of alkanolamine as EOR surfactant could support palm oil industry, especially in the Southeast Asian countries that are the main palm oil producers (Mukherjee and Sovacool, 2014).

Thus, the performance of PKA in EOR was studied and compared with four commercial surfactants. The selected surfactants are of anionic type, namely sodium dodecyl sulfate (SDS), of cationic type namely cetyltrimethylammonium bromide (CTAB), and of nonionic type, namely secondary alcohol ethoxylate (Tergitol 15-S-9) and a branched secondary alcohol ethoxylate (Tergitol TMN 6). All these surfactants are widely applied as good candidate surfactants in EOR studies. The experiment was divided into two parts, which are surfactant loss due to adsorption on reservoir rock surfaces, and crude oil solubilization ability of the surfactants. For surfactant adsorption, silica was applied as the model adsorbent representing reservoir rock. The studied factors interacting with surfactant adsorption were salinity and temperature. The surfactant adsorption behaviors were fit by models for both kinetics of adsorption and for equilibrium adsorption isotherm. In the crude oil solubilization study, all the surfactants were tested for crude oil solubilization performance in controlled conditions and compared. The influence of salinity on crude oil solubilization is discussed.

2. METHODOLOGY

2.1 Materials

The anionic surfactant, sodium dodecyl sulfate (SDS, 98% purity) was purchased from Sigma-Aldrich. The cationic surfactant cetyltrimethy-lammonium bromide (CTAB, 98% purity) was purchased from Ajax Finechem. Regarding the three nonionic surfactants, PKA (80% content) was supplied by Thai Flavour and Fragrance Co., Ltd.; and Tergitol 15-S-9 (90% content), and Tergitol TMN-6 (90% content) were both purchased from Sigma-Aldrich. The properties of the surfactants are summarized in Table 1. Additionally, silica (98% purity, particle size 18 μm) was purchased from Ajax Finechem. Crude oil was supplied by the Petroleum Authority of Thailand. Sodium chloride (NaCl) purchased from Ajax Finechem was used for brine solution preparation.

2.2 The study of surfactant adsorption on silica surface

2.2.1 Adsorption kinetics

The experiment was conducted by adding a 4-g quantity of silica in 50-mL of distilled water. These samples were combined individually with CTAB, PKA, and SDS. The initial surfactant concentrations were controlled above the CMC values of all surfactants to 15.6 mmol/L, in order to ensure full coverage of surfactant on silica surfaces. The sample bottles were shaken in an incubator with a shaking rate of 170 rpm at 30°C. The liquid samples of surfactant solution were collected for free surfactant concentration measurement using UV-vis spectro-photometry for CTAB (λ=195 nm) (Atia and Radwan, 1997; Park et al., 2015) or chemical oxygen demand (COD) (Bera et al., 2013) measurement method for PKA and SDS. The blank solution was prepared using 4-g of silica in 50-mL of distilled water to avoid interference of silica on surfactant concentration measurement. The equilibrium times were recorded from observing constant surfactant concentrations in

the supernatant liquid. The experimental results were used to fit models for adsorption kinetics.

The effects of NaCl and temperature on the adsorption of surfactants on silica were tested in 0.1 mol/L NaCl solution and 50°C. The bank solution was prepared without adding a surfactant. The experiment was similar as in prior literature (Bera et al., 2013).

Table 1. Properties of the selected surfactants

Surfactant (Trade name)	Chemical formula	MW (g/mol)	CMC (mmol/L)
Anionic surfactant			
SDS[a]	$C_{12}H_{25}NaO_4S$	288	8.2
Cationic surfactant			
CTAB[b]	$C_{19}H_{42}BrN$	364	0.82
Nonionic surfactants			
PKA[c]	$C_{13}H_{27}ON(CH_2CH_2OH)_2$	309	0.23
Tergitol 15-S-9[d]	$C_{12\text{-}14}H_{25\text{-}29}O(CH_2CH_2O)_9H$	596	0.09
Tergitol TMN-6[d]	$C_{12}H_{26}O(C_2H_4O)_6$	540	1.48

Remark: Letters a, b, c, and d indicate literature data from NCBI (2005), NCBI (2004), Wetchakul (2013), and Parnthong et al. (2018), respectively.

2.2.2 Adsorption isotherm

A 4-g silica sample was added in 50-mL of surfactant solution. The initial concentration of CTAB was controlled in the range of 0.274-15.6 mmol/L. The sample bottles were shaken with a shaking rate of 170 rpm at 30°C. As the system reaches equilibrium, liquid samples of surfactant solution were collected and centrifuged. The supernatant liquid was analyzed for surfactant concentration in the bulk solution (Ahmadi and Shadizadeh, 2015; Arabloo et al., 2015; Barati-Harooni et al., 2016). The experiments were performed for PKA and SDS using similar procedures as above using PKA and SDS solutions at concentrations in the ranges 0.162-15.6 mmol/L and 1.734-15.6 mmol/L, respectively. The relationship of bulk surfactant concentration to the initial surfactant concentration was fit with Langmuir and Freundlich adsorption isotherm models.

2.3 Crude oil solubilization study

A 25-mL sample of crude oil and 25-mL of surfactant solution with a concentration of 1 CMC were mixed in 100-mL sample bottle. In addition, several similar sample bottles but without surfactant were prepared as controls. The sample bottles were shaken in an incubator shaker with a shaking rate of 170 rpm at 50°C. Then, the liquid phase was sampled every 2 h and analyzed for crude oil concentration using the COD technique (Siddiqui et al., 2014). The effects of salinity on crude oil solubilization were evaluated using distilled water and 0.1 mol/L NaCl solution (Spildo et al., 2014). No silica was added to the sample bottles to avoid surfactant loss from adsorption. The crude oil concentration was assessed using COD technique. Samples prepared without adding a surfactant were conducted and determined for unsolubilized crude oil concentration. A blank solution of surfactant was also prepared for baseline data. The equilibrium time for both systems was observed within 24 h.

2.4 Comparing surfactant adsorption and crude oil solubilization behaviors of PKA with selected commercial nonionic surfactants

The surfactant adsorption and crude oil solubilization of PKA were compared with Tergitol 15-S-9 and Tergitol TMN-6. The experimental procedures were as in section 2.2 above, except that the initial concentration was controlled to 1 CMC for each individual surfactant. Since the CMCs of tested nonionic surfactants were quite low, and present in similar range. The concentration of a nonionic surfactant was analyzed by the COD method. For crude oil solubilization, the experimental procedures are similar to those in section 2.3, except that the initial concentration of surfactants was controlled to 1 CMC in 0.1 mol/L NaCl solution, in all cases. The sample bottles were shaken for 24 h.

The experiments were randomized and performed in triplicate, and the standard deviation was less than 5%. The error bars of results are shown in the figures.

2.5 Data analysis

The amount of surfactant adsorption (q, mol/g adsorbent) was calculated as shown in Equation (1):

$$q = \frac{(C_i - C_e) \times V}{m_{silica}} \times 10^{-3} \quad (1)$$

Here, C_i (mol/g) and C_e (mol/g), respectively, are the initial concentration and the free surfactant concentration in bulk aqueous solution, V (mL) is the volume of the surfactant solution, and m_{silica} (g) is mass of silica (Bera et al., 2013).

Then, the surfactant adsorption was fit with pseudo-first order and pseudo-second order models, presented in Equations (2) and (3), respectively:

$$\ln (q_e - q_t) = \ln q_e - k_1 t \quad (2)$$

$$\frac{t}{q_t} = \frac{1}{k_2 q_e^2} + \frac{1}{q_e} t \quad (3)$$

Here, q_e (mol/L) and q_t (mol/L) are the amounts of adsorbed surfactants on silica at equilibrium, and that at time t (h^{-1}), respectively. k_1 (h^{-1}) is the rate constant of pseudo-first order. k_2 (g/mol/h) is the rate constant of pseudo-second order (Ahmadi and Shadizadeh, 2015).

The adsorption of surfactant at equilibrium was modeled with the Langmuir and Freundlich adsorption isotherms, according to Equations (4) and (5), respectively:

$$\frac{C_e}{q_e} = \frac{1}{K_L q_m} + \frac{C_e}{q_m} \quad (4)$$

$$\log q_e = \log K_F + \frac{1}{n} \log C_e \quad (5)$$

Here, q_e (mol/L) is the amount of adsorbed surfactant on silica at equilibrium; q_m (mol/L) is maximum adsorption of surfactant; C_e (mol/g) is free surfactant concentration in bulk aqueous solution at equilibrium; K_L (L/mol) is Langmuir constant indicating the strength of the adsorption force; K_F (mol/g) is Freundlich constant related to adsorption capacity; and n is Freundlich exponent accounting for adsorption intensity (Bera et al., 2013).

The surfactants present in a reservoir can lower the interfacial tension of crude oil/water or crude oil/rock, mobilizing the oil from reservoir rocks. Then crude oil tends to partition into surfactant micelles due to hydrophobic attraction forces. The micelles are subsequently mobilized from source rock by water flooding. Therefore, this experiment observes the crude oil solubility with each surfactant using the solubilization equilibrium constant (K_s) that can be calculated from Equations (6) and (7).

$$X_0 = \frac{C_{sol}}{C_m + C_{sol}} \quad (6)$$

$$K_s = \frac{x_0}{C_0} \quad (7)$$

Here, X_0 is the mole fraction of crude oil in micelles, C_{sol} (mol/L) is the solubilized crude oil concentration, C_m (mol/L) is the surfactant concentration in micellar form, K_s (mL/g) is solubilization equilibrium constant, and C_0 (mol/L) is the unsolubilized crude oil concentration (Rosen, 1989).

3. RESULTS AND DISCUSSION

3.1 Surfactant adsorption

3.1.1 Adsorption equilibrium time

The amount of an individual surfactant adsorbed on silica was determined as a function of time, and is shown in Figure 1. As time progresses the amount of adsorbed surfactant on silica rapidly increases, and then tends to become constant within 12 h for PKA, 15 h for SDS, and 20 h for CTAB, respectively. The maximum adsorption quantity was observed as 27.48 µmol/g for CTAB, 25.08 µmol/g for SDS, and 15.20 µmol/g for PKA.

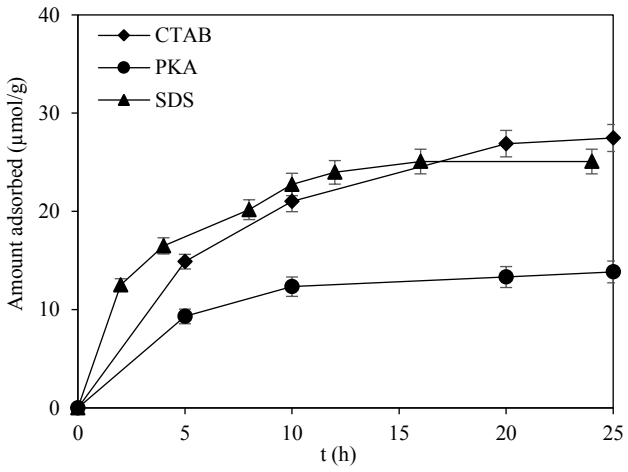

Figure 1. Adsorption kinetics of surfactants on silica in water at 30°C.

It can be seen that CTAB is adsorbed on silica more than SDS or PKA. Typically, the bare surface charge of silica is negative (Lee et al., 2007). The head group of CTAB exhibits a positive charge and is adsorbed on silica surface by ion pairing (Paria and Khilar, 2004). On the other hand, SDS has negatively-charged head group with repulsion from the silica surface. The adsorption of SDS on silica might be induced by weak ionic interactions. However, the SDS

adsorption is slightly below that of CTAB and higher than of PKA. Possibly SDS could form a second layer by tail-tail hydrophobic interactions. Similar results for anionic adsorption have been reported by Park et al. (2015). They observed that high adsorption of anionic surfactant could be brought by the alkyl-alkyl hydrophobic interactions at high surfactant concentrations. Additionally, PKA was less adsorbed on silica than CTAB and SDS. PKA has no charge on its head group and tends to adsorb on silica by van der Waals forces between the hydrophilic head group and the silica site, having the weakest adsorption on silica surface (Paria and Khilar, 2004). The order of adsorption by surfactant type is consistent with prior reports (Rabiu et al., 2016; Bera et al., 2017).

3.1.2 Kinetics of surfactant adsorption

The adsorption data for each surfactant were fitted with pseudo-first order and pseudo-second order models, and the kinetic parameters of adsorption are shown in Table 2.

Table 2. Kinetic parameters of selected surfactants adsorption in water at 30°C

Surfactant	Pseudo-first order			Pseudo-second order		
	k_1 (h^{-1})	q_e (µmol/g)	R^2	k_2 (g/µmol/h)	q_e (µmol/g)	R^2
CTAB	0.194	32.6	0.981	0.004	35.3	0.997
PKA	0.162	10.9	0.961	0.021	15.5	0.999
SDS	0.238	23.7	0.971	0.035	28.2	0.994

The coefficient of determination R^2 indicates that the pseudo-second order model is preferable for modeling the adsorption of CTAB, PKA and SDS. The predicted amount of adsorbed surfactant (q_e) reveals that CTAB adsorption is the highest, followed by SDS and PKA in this order. This rank order of surfactant adsorption matches well the adsorption equilibrium profiles shown in Figure 1. Besides, the k_2 values indicating the adsorption speed reveal that the adsorption rate of SDS is higher than those of PKA or CTAB. The adsorption rate increases inversely with the surfactant molecular weight (Table 1); SDS has the lowest molecular weight and a comparatively high rate constant (Liu, 2008).

3.1.3 Adsorption isotherm

The equilibrium data of adsorbed surfactant and free surfactant concentration were fitted with Langmuir or Freundlich isotherm models and the identified parameters are listed in Table 3.

Table 3. Identified parameters in Langmuir and Freundlich equilibrium isotherm models for the selected surfactants

Surfactant	Langmuir			Freundlich		
	q_{max} (µmol/g)	K_L (L/µmol)	R^2	K_F (µmol/g)	n	R^2
CTAB	30.4	7.98E-04	0.9984	0.291	1.938	0.9085
PKA	17.6	5.72E-04	0.9879	0.140	1.892	0.8875
SDS	76.9	5.77E-05	0.9163	0.014	1.198	0.9961

The R^2 values reveal that the adsorption isotherms of CTAB and PKA are well fitted with Langmuir isotherm, indicating monolayer coverage on silica. The maximum amount of the adsorbed surfactant (q_{max}) demonstrates that CTAB is more adsorbed on silica than PKA is. The data are consistent with the q_e values predicted from the pseudo-second order models earlier. In addition, K_L indicates the energy of adsorption or the strength of adsorption forces between silica sites and surfactants. A greater K_L represents stronger interactions between the silica sites and adsorbed surfactant molecules (Markandeya et al., 2017). This is consistent with the fact that the interactions by van der Waals forces observed for PKA-silica adsorption are weaker than that those by ion-pairing in oppositely-charged CTAB-silica adsorption (Atkin et al., 2003; Eriksson et al., 2002; Somasundaran et al., 1964). Moreover, the R^2 value indicates that the adsorption of SDS should be fitted with the Freundlich isotherm, indicating multilayer adsorption of SDS on silica and that possibly the silica surface is heterogeneous (Mi et al., 2016). This is consistent with the fact that multilayer adsorption has

been established in prior literature, especially at high SDS concentrations (Park et al., 2015).

3.1.4 Effect of NaCl on surfactant adsorption

The influence of salinity on surfactant adsorption behaviors was examined in 0.1 mol/L NaCl solution. The results were compared with those in water system and are illustrated in Figure 2. Adding NaCl to the system causes competitive adsorption of positively-charged sodium (Na^+) and CTAB on silica, and also increases the electrical repulsion for CTAB. This decreases the CTAB adsorption (Rabiu et al., 2016). On the other hand, the increase in the positive charge from Na^+ ions on silica surfaces could reduce the negatively-charged repulsion arising between SDS and silica, contributing to SDS adsorption on silica surfaces (Bera et al., 2013). Moreover, NaCl has no effect on PKA because it contains no charge and adsorbs on silica with hydrophobic attraction forces. The results match well other reports indicating that nonionic surfactants are relatively stable in electrolyte or high salinity solutions (Bera et al., 2013; Belhaj et al., 2020; Rabiu et al., 2016).

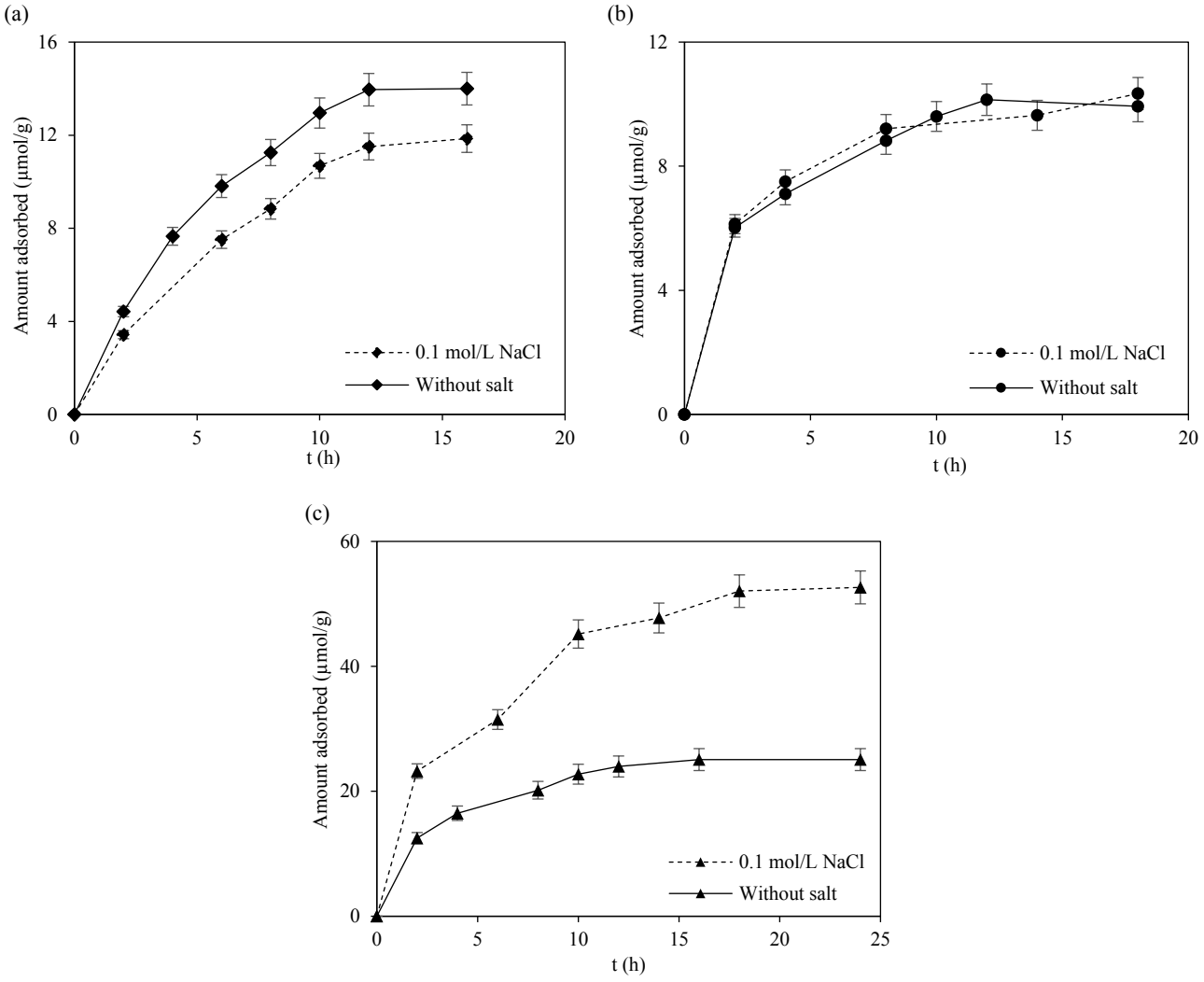

Figure 2 . Surfactant adsorption profiles on silica in 0.1 mol/L NaCl solution and water at 30°C for (a) CTAB, (b) PKA, and (c) SDS.

3.1.5 Effect of temperature on surfactant adsorption

The influences of temperature on adsorption behaviors of the surfactants in reservoir rocks are demonstrated in Figure 3. It was found that the adsorption of all surfactants decreased with temperature. The dominant impacts were observed for CTAB and SDS, while a minor effect was noted on the absorption of PKA. As the temperature increases, the kinetic energy of surfactant molecules increases, and this possibly facilitates surfactant diffusion from the surfaces, leading to lesser surfactant adsorption on silica (Wiśniewska, 2012).

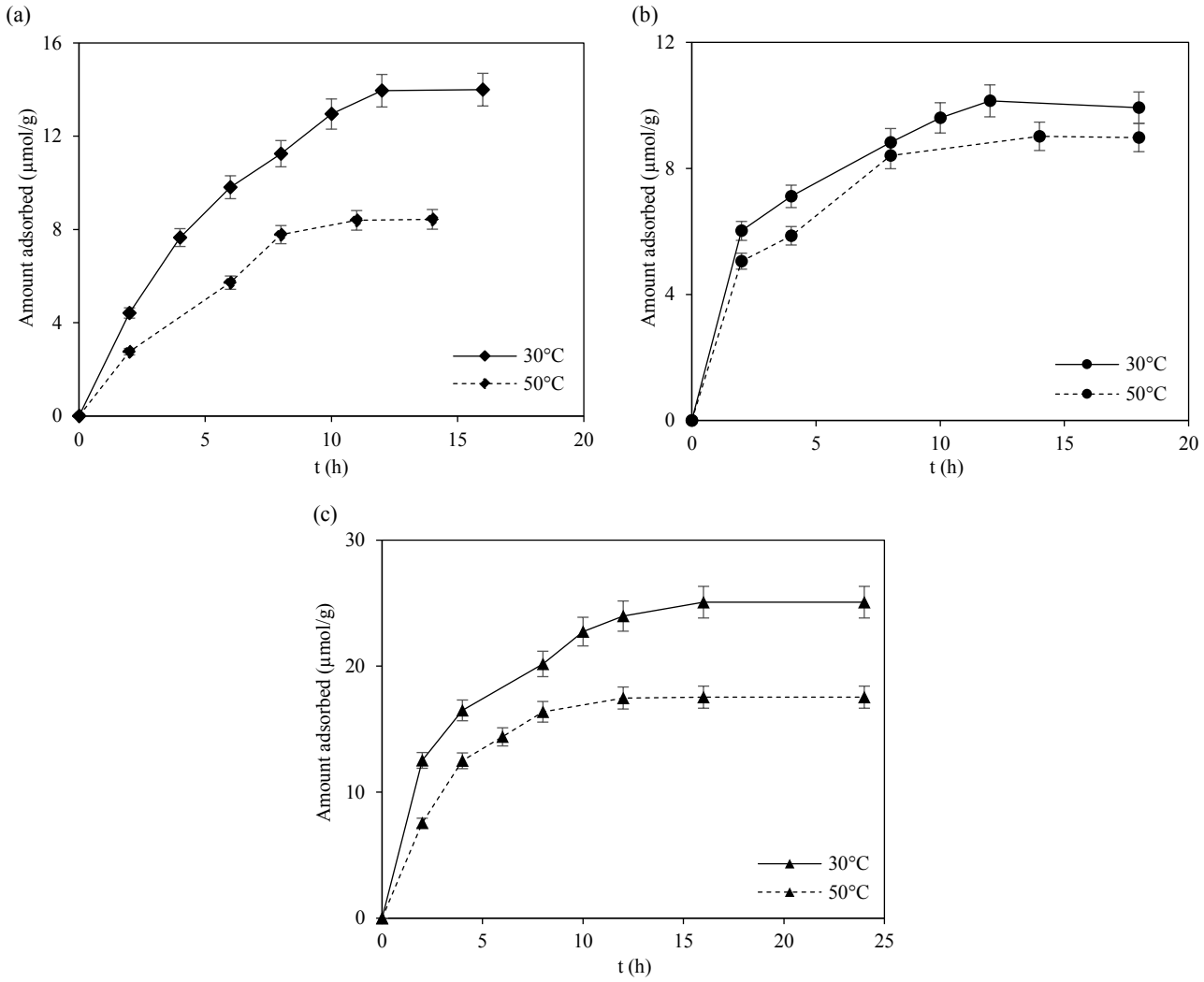

Figure 3. Effect of temperature on surfactant adsorption profiles for (a) CTAB, (b) PKA, and (c) SDS.

Additionally, the change of surfactant adsorption with temperature could be described by thermodynamics, including the changes in enthalpy (ΔH°, KJ/mol), entropy (ΔS°, KJ/mol/K), and standard Gibbs free energy (ΔG°, KJ/mol) (Bera et al., 2013). The ΔH° refers to the amount of heat that passes in or out of the system at constant pressure. The ΔS° indicates the disorder of the system, and the feasibility of the adsorption is clarified by ΔG°. The correlation of parameters was determined according to the Van't hoff equation in Equation (8).

$$\ln K_L = -\frac{\Delta H^0}{RT} + \frac{\Delta S^0}{R} \quad (8)$$

Here, R (8.314 J/K/mol) is the gas constant, T (K) is the temperature, and K_L (L/mol) is the Langmuir constant at controlled temperature (Juang et al., 2006). The data for K_L estimates from Langmuir isotherm were for 30°C and 50°C. Table 4 is a summary of K_L values for individual surfactant's equilibrium adsorption at these temperatures.

Table 4. The K_L values for individual surfactant's equilibrium adsorption at two tested temperatures.

Temperature (°C)	K_L (L/mol)		
	CTAB	PKA	SDS
30	797.98	572.39	57.70
50	323.00	191.00	32.90

Then, the data were plotted for 1/T versus ln K_L, so that the intercept and slope of correlation represent the values of ΔS° and ΔH°, respectively. Then, ΔG° for each temperature was determined using Equation (9). All these thermodynamic parameters are reported in Table 5.

$$\Delta G° = \Delta H° - T\Delta S° \quad (9)$$

Table 5. Thermodynamic parameters of surfactant adsorption on silica surface.

Surfactant	Temperature (°C)	Thermodynamic parameter		
		ΔG° (KJ/mol)	ΔH° (KJ/mol)	ΔS° (KJ/mol/K)
CTAB	30	-16.83	-36.80	-0.07
	50	-15.52		
PKA	30	-16.00	-44.65	-0.09
	50	-14.10		
SDS	30	-10.22	-22.85	-0.04
	50	-9.32		

A negative ΔG° indicates that the surfactant adsorption on silica surface occurs simultaneously. The ΔS° is negative, and this demonstrates that surfactant molecules tend to uniformly adsorb on the water/silica interfaces rather than stay disorganized in water above the surface. Furthermore, the negative ΔH° reveals that the adsorption process for all these surfactants is exothermic. Thus, the adsorption of surfactant decreases with increasing temperature. The calculated thermodynamic parameters agree well with the aforementioned experimental results and are consistent with prior studies (Ijagbemi et al., 2009; Juang et al., 2006; Wiśniewska, 2012).

3.2 The study of oil solubilization

The amount of crude oil partitioned into the surfactant solution at 1 CMC, 50°C, and 0 mol/L NaCl is shown in Figure 4. It can be seen that the largest amount of crude oil dissolved in surfactant solution was observed for SDS, followed by PKA, and CTAB in this order. SDS has the highest CMC and the largest amount of monomer in the bulk solution. This phenomenon means it has the most surfactant molecules available for adsorption at crude oil and surfactant solution interfaces, and facilitates the reduction of interfacial tension between crude oil and surfactant solution, treating the most crude oil (Tehrani-Bagha and Holmberg, 2013). The results agree well with the fact that anionic surfactants have commonly been suggested as effective for reducing interfacial tension between seawater and crude oil (Negin et al., 2017; Belhaj et al., 2020). In addition, it can be seen that PKA slightly outperformed CTAB.

Moreover, from Figure 4, it should be noted that adding NaCl could increase crude oil partitioning in the PKA, CTAB and SDS systems. Typically, adding salt reduces electrical repulsion of ionic heads, or steric repulsion of nonionic heads, resulting in closer packing at air-water interfaces and facilitating low interfacial tension enabling crude oil partitioning to increase (Karnanda et al., 2013; Rostami et al., 2019). Moreover, adding electrolyte in solution could reduce the repulsion forces between the similarly charged head groups, and consequently decrease the CMC (data shown in Table 6), increasing surfactant aggregation numbers and micelle volume. This facilitates the extent of micelle formation and solubilization of crude oil into micelles (Rosen, 1989; Dutkiewicz and Jakubowska, 2002; Qazi et al., 2017).

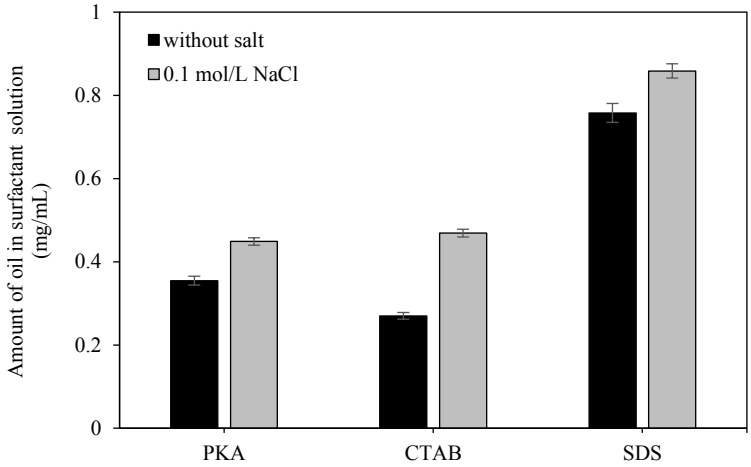

Figure 4. The effect of salinity on crude oil partitioning into the surfactant solution at 1 CMC and 50°C.

Table 6. The K_s values for crude oil solubilization in selected surfactant solutions at 0.1 mol/L NaCl and 50°C.

Surfactant	CMC (mmol/L)		K_s (mL/mg)
	without salt	0.1 mol/L NaCl	0.1 mol/L NaCl
PKA	0.23	0.19	10.33
CTAB	1	0.27	7.94
SDS	8.2	2.6	6.90

At controlled salinity, the results in Table 6 reveal that K_s has the rank order PKA>CTAB>SDS. This trend is reversed from the order of CMC for these surfactants. Theoretically, a nonionic surfactant has greater solubilizing performance than cationic or anionic surfactants, due to its lower CMC. Additionally, the greater solubilization of cationic over anionic might be due to looser packing of surfactant aggregation in micelles (Rosen, 1989). Thus, PKA has the lowest CMC and the highest K_s indicating the highest crude oil accessibility to the micellar core.

3.3 Comparison of PKA performance with commercial nonionic surfactants adsorption on silica and crude oil solubilization

The behaviors of PKA adsorption on silica surface and crude oil solubilization were compared with the secondary alcohol ethoxylates Tergitol 15-S-9 and Tergitol TMN-6. Both are widely considered good candidate nonionic surfactants in EOR studies (Bera et al., 2017; Shaw, 1984; Worthen et al., 2012). These surfactants are remarkably stable in high salinity or elevated temperature and show good oil recovery performance (Sharma and Mohanty, 2013; Mohan, 2009; Mandal et al., 2012). The results of surfactant adsorption and crude oil solubilization are shown in Figures 5 and 6, respectively. Figure 5 reveals that Tergitol 15-S-9 is adsorbed on silica better than Tergitol TMN-6 or PKA. The van der Waals interactions dominate in the adsorption of a nonionic surfactant on silica surfaces, and these forces increase with molecular mass of the surfactant (Paria and Khilar, 2004). Tergitol 15-S-9 has the highest molecular weight (see Table 1), resulting in the highest adsorption among these three surfactants.

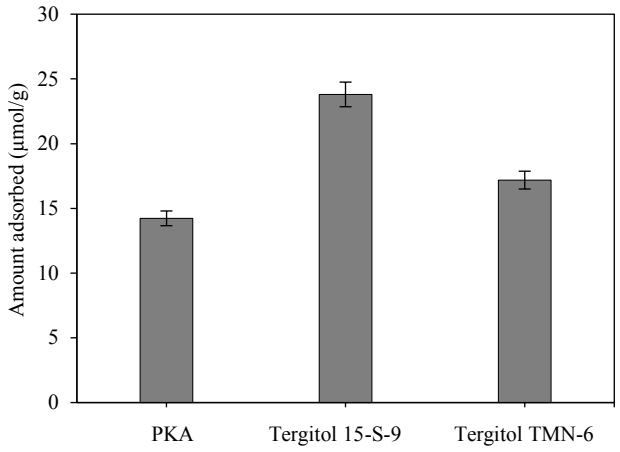

Figure 5. Amounts of nonionic surfactants adsorbed on silica at 1 CMC and 30°C.

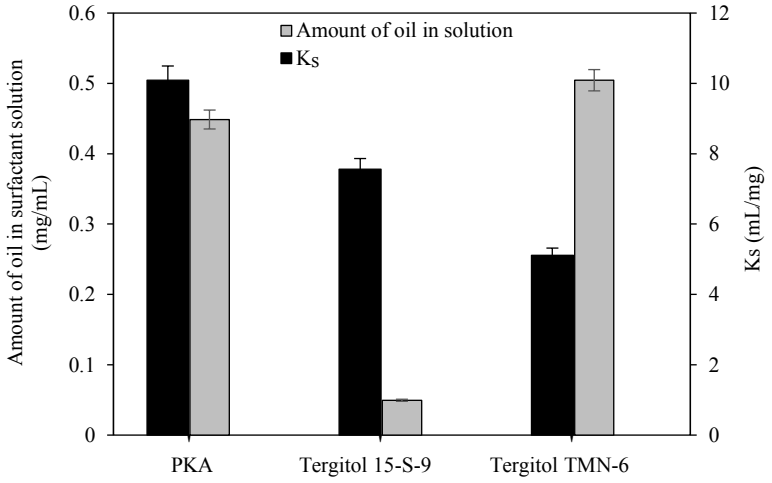

Figure 6. Amount of crude oil partitioning into nonionic surfactant solution and the K_s values in 0.1 mol/L NaCl solution at 1 CMC, 50°C.

Moreover, Figure 6 reveals that crude oil partitioning into surfactant solutions had the rank order Tergitol TMN-6>PKA>Tergitol 15-S-9. This is consistent with the rank order of CMC. As Tergitol TMN-6 has the highest CMC, its amount as monomer in bulk solution is greater than those of PKA or Tergitol 15-S-9. This leads to the most surfactant molecules available at crude oil/ surfactant solution interfaces, giving the highest crude oil partitioning in the surfactant solution (Rosen, 1989).

Additionally, the results in Figure 6 show that K_s had the rank order PKA>Tergitol 15-S-9>Tergitol TMN-6. Theoretically, this trend is consistent with micelle size. From the data listed in Table 1, Tergitol TMN-6 has a higher CMC than Tergitol 15-S-9, indicating smaller micellar size. Additionally, Tergitol 15-S-9 has similar hydrocarbon chain length as PKA, but its hydrophilic moiety is larger (Parnthong et al., 2018; Wetchakul, 2013). This causes greater repulsion between Tergitol 15-S-9 head groups and decreases aggregation number as well as size of micelles. As a result, less crude oil could be encapsulated in Tergitol 15-S-9 micelles than with PKA surfactant. Thus, it could be possible that the size of micelles for selected surfactants had the rank order PKA>Tergitol 15-S-9>Tergitol TMN-6. PKA possibly has the largest micelles and illustrates the most crude oil solubilization among the three nonionic surfactants (Rosen, 1989).

From the results above on surfactant adsorption and crude oil solubilization, it can be seen that PKA shows good potential for use in EOR when compared with these commercial surfactants. Typically, the natural surfactant loss due to adsorption in reservoir rocks has been reported as 3-15 mg/g (Seethepalli et al., 2014; Ahmadi et al., 2012; Ahmadi and Shadizadeh, 2015). In this work, the adsorption of PKA at initial concentration of 1 CMC was found to be around 4.4 mg/g, which is within the common range. Additionally, PKA shows good crude oil solubilization performance similar to the commercial surfactants tested. Thus, PKA is an interesting nonionic surfactant in terms of its potential for EOR, and is a promising natural product.

4. CONCLUSION

Based on our studies, palm kernel derivative surfactant PKA shows the lowest adsorption on silica among the tested surfactants, suggesting low surfactant losses in reservoirs. Additionally, the adsorption of PKA on silica is insignificantly affected by added salt or increased temperature. The adsorption kinetics of PKA follows pseudo-second order kinetics and Langmuir adsorption isotherm, indicating chemical adsorption and monolayer formation on silica surfaces. The thermodynamic parameters reveal that the surfactant adsorption on silica surface occurs simultaneously and uniformly on the water/silica interfaces. The adsorption process for PKA, SDS, and CTAB is exothermic. Moreover, PKA shows high performance in crude oil solubilization in comparison to the tested commercial ionic and nonionic surfactants.

ACKNOWLEDGEMENTS

We gratefully acknowledge the financial assistance provided by Faculty of Engineering's Graduate Study Scholarship, the Graduate school of Prince of Songkla University (PSU), and for facility support from the Department of Chemical Engineering, Faculty of Engineering, PSU. In addition, we would like to thank Assoc. Prof. Dr. Seppo Karrila for reviewing the draft manuscript.

REFERENCES

Ahmadi MA, Shadizadeh SR. Experimental investigation of a natural surfactant adsorption on shale- sandstone reservoir rocks: Static and dynamic conditions. Fuel 2015;159:15-26.

Ahmadi MA, Zendehboudi S, Shafiei A, James L. Nonionic surfactant for enhanced oil recovery from carbonates: Adsorption kinetics and equilibrium. Industrial and Engineering Chemistry Research 2012;51(29):9894-905.

Arabloo M, Ghazanfari MH, Rashtchian D. Spotlight on kinetic and equilibrium adsorption of a new surfactant onto sandstone minerals: A comparative study. Journal of the Taiwan Institute of Chemical Engineers 2015;50:12-23.

Atia AA, Radwan NRE. Adsorption of different surfactants on kaolinite. Adsorption Science and Technology 1997;15(8): 619-26.

Atkin R, Craig VSJ, Wanless EJ, Biggs S. Mechanism of cationic surfactant adsorption at the solid-aqueous interface. Advances in Colloid and Interface Science 2003;103(3):219-304.

Barati-Harooni A, Najafi-Marghmaleki A, Tatar A, Mohammadi AH. Experimental and modeling studies on adsorption of a nonionic surfactant on sandstone minerals in enhanced oil recovery process with surfactant flooding. Journal of Molecular Liquids 2016;220:1022-32.

Belhaj AF, Elraies KA, Alnarabiji MS, Shuhli JABM, Mahmood SM, Ern LW. Experimental investigation of surfactant partitioning in Pre-CMC and Post-CMC regimes for enhanced oil recovery application. Energies 2019;12(12):1-15.

Belhaj AF, Elraies KA, Mahmood SM, Zulkifli NN, Akbari S, Hussien OS. The effect of surfactant concentration, salinity, temperature, and pH on surfactant adsorption for chemical enhanced oil recovery: A review. Journal of Petroleum Exploration and Production Technology 2020;10(1):125-37.

Bera A, Kumar T, Ojha K, Mandal A. Adsorption of surfactants

on sand surface in enhanced oil recovery: Isotherms, kinetics and thermodynamic studies. Applied Surface Science 2013;284:87-99.

Bera A, Mandal A, Belhaj H, Kumar T. Enhanced oil recovery by nonionic surfactants considering micellization, surface, and foaming properties. Petroleum Science 2017;14(2):362-71.

Dutkiewicz E, Jakubowska A. Effect of electrolytes on the physicochemical behaviour of sodium dodecyl sulphate micelles. Colloid and Polymer Science 2002;208(11):1009-14.

Emadi S, Shadizadeh SR, Manshad AK, Rahimi AM, Mohammadi AH. Effect of nano silica particles on Interfacial Tension (IFT) and mobility control of natural surfactant (Cedr Extraction) solution in enhanced oil recovery process with nano-surfactant flooding. Journal of Molecular Liquids 2017;248:163-7.

Eriksson T, Börjesson J, Tjerneld F. Mechanism of surfactant effect in enzymatic hydrolysis of lignocellulose. Enzyme and Microbial Technology 2002;31(3):353-64.

Iglauer S, Wu Y, Shuler P, Tang Y, Goddard WA. New surfactant classes for enhanced oil recovery and their tertiary oil recovery potential. Journal of Petroleum Science and Engineering 2010;71(1-2):23-9.

Ijagbemi CO, Baek MH, Kim DS. Montmorillonite surface properties and sorption characteristics for heavy metal removal from aqueous solutions. Journal of Hazardous Materials 2009;166(1):538-46.

Juang LC, Wang CC, Lee CK. Adsorption of basic dyes onto MCM-41. Chemosphere 2006;64(11):1920-8.

Karnanda W, Benzagouta MS, AlQuraishi A, Amro MM. Effect of temperature, pressure, salinity, and surfactant concentration on IFT for surfactant flooding optimization. Arabian Journal of Geosciences 2013;6(9):3535-44.

Lee SH, Roichman Y, Yi GR, Kim SH, Yang SM, Van Blaaderen A, Van Oostrum P, Grier DG. Characterizing and tracking single colloidal particles with video holographic microscopy. Optics Express 2007;15(26):18275-82.

Liu Y. New insights into pseudo-second-order kinetic equation for adsorption. Colloids and Surfaces A: Physicochemical and Engineering Aspects 2008;320(1-3):275-8.

Mandal A, Bera A, Ojha K, Kumar T. Characterization of surfactant stabilized nanoemulsion and its use in enhanced oil recovery. Proceedings of the 1st Society of Petroleum Engineers International Oilfield Nanotechnology Conference and Exhibition; 2012 Jun 12-14; Palace Hotel, Noordwijk: Netherlands; 2012.

Markandeya, Shukla SP, Dhiman N. Characterization and adsorption of disperse dyes from wastewater onto cenospheres activated carbon composites. Environmental Earth Sciences 2017;76(20):1-12.

Mi X, Li G, Zhu W, Liu L. Enhanced adsorption of orange II using cationic surfactant modified biochar pyrolyzed from cornstalk. Journal of Chemistry 2016;2016:1-7.

Mohan K. Alkaline surfactant flooding for tight carbonate reservoirs. Proceedings of the 1st Society of Petroleum Engineers Annual Technical Conference and Exhibition; 2009 Oct 4-7; New Orleans Ernest N. Morial Convention Center, Louisiana: USA; 2009.

Mukherjee I, Sovacool BK. Palm oil-based biofuels and sustainability in southeast Asia: A review of Indonesia, Malaysia, and Thailand. Renewable and Sustainable Energy Reviews 2014;37:1-12.

National Center for Biotechnology Information (NCBI). PubChem Compound Database; CID= 3423265 [Internet]. 2005 [cite 2020 Jan 13]. Available from: https://pubchem.ncbi.nlm.nih.gov/compound/3423265.

National Center for Biotechnology Information (NCBI). PubChem Compound Database; CID=5974 [Internet]. 2004 [cite 2020 Jan 13]. Available from: https://pubchem.ncbi.nlm.nih.gov/compound/5974.

Negin C, Ali S, Xie Q. Most common surfactants employed in chemical enhanced oil recovery. Petroleum 2017;3(2):197-211.

Paria S, Khilar KC. A review on experimental studies of surfactant adsorption at the hydrophilic solid-water interface. Advances in Colloid and Interface Science 2004;110(3):75-95.

Park S, Lee ES, Sulaiman WRW. Adsorption behaviors of surfactants for chemical flooding in enhanced oil recovery. Journal of Industrial and Engineering Chemistry 2015;21:1239-45.

Parnthong J, Kungsanant S, Chavadej S. The influence of nonionic surfactant adsorption on enzymatic hydrolysis of oil palm fruit bunch. Applied Biochemistry and Biotechnology 2018; 186(4):895-908.

Qazi MJ, Liefferink RW, Schlegel SJ, Backus EH, Bonn D, Shahidzadeh N. Influence of surfactants on sodium chloride crystallization in confinement. Langmuir 2017;33(17):4260-8.

Rabiu AM, Elias S, Oyekola O. Evaluation of surfactant synthesized from waste vegetable oil to enhance oil recovery from petroleum reservoirs. Energy Procedia 2016;100:188-92.

Rosen MJ. Surfactants and Interfacial Phenomena. New York, USA: Wiley; 1989.

Rostami P, Mehraban MF, Sharifi M, Dejam M, Ayatollahi S. Effect of water salinity on oil/brine interfacial behaviour during low salinity waterflooding: A mechanistic study. Petroleum 2019;5(4):367-74.

Seethepalli A, Adibhatla B, Mohanty KK. Physicochemical interactions during surfactant flooding of fractured carbonate reservoirs. Society of Petroleum Engineers 2004;9(4):411-8.

Sharma G, Mohanty K. Wettability alteration in high-temperature and high-salinity carbonate reservoirs. Society of Petroleum Engineers 2013;18(4):646-55.

Shaw JE. Carboxylate surfactant systems exhibiting phase behavior suitable for enhanced oil recovery. Journal of the American Oil Chemists' Society 1984;61(8):1395-9.

Siddiqui MA, Kungsanant S, Chaiprapat S. Oil solubilization using surfactant for biohydrogen production. Advanced Materials Research 2014;931:183-7.

Somasundaran P, Healy TW, Fuerstenau DW. Surfactant adsorption at the solid-liquid interface - Dependence of mechanism on chain length. Journal of Physical Chemistry 1964;68(12):3562-6.

Spildo K, Sun L, Djurhuus K, Skauge A. A strategy for low cost, effective surfactant injection. Journal of Petroleum Science and Engineering 2014;117:8-14.

Tehrani-Bagha AR, Holmberg K. Solubilization of hydrophobic dyes in surfactant solutions. Materials 2013;6(2):580-608.

Wetchakul W. Production of Palm Kernel-Diethanolamide in a Stirred-tank Reactor [dissertation]. Songkhla, Prince of Songkla University; 2013.

Wiśniewska M. The temperature effect on the adsorption mechanism of polyacrylamide on the silica surface and its stability. Applied Surface Science 2012;258(7):3094-101.

Worthen A, Bagaria H, Chen Y, Bryant SL, Huh C, Johnston KP. Nanoparticle stabilized carbon dioxide in water foams for enhanced oil recovery. Proceedings of the 18th Society of Petroleum Engineers SPE Improved Oil Recovery Symposium; 2012 Apr 14-18; Cox Business Convention Center, Oklahoma: USA; 2012.

Model Based Change Detection of Water Body Using Landsat Imagery: A Case Study of Rajshahi Bangladesh

Tofayel Ahammad*, Hafizur Rahaman, B.M. Refat Faisal, and Nasrin Sultana

Bangladesh Space Research and Remote Sensing Organization (SPARRSO), Sher-e-Bangla Nagar, Agargaon, Dhaka-1207, Bangladesh

ARTICLE INFO

Received: 2 Jan 2020
Received in revised: 12 Jul 2020
Accepted: 17 Jul 2020
Published online: 30 Jul 2020
DOI: 10.32526/ennrj.18.4.2020.33

Keywords:
Water bodies/ Model/ Mosaic/ Pixel/ Binary image

*** Corresponding author:**
E-mail: tofayel.cu.phy@gmail.com

ABSTRACT

This study detected water bodies which included ponds, lakes, rivers, canals, irrigation land, etc. from Landsat TM (Thematic Mapper) and OLI (Operational Land Imager) data by Pixel Based Model (PBM) for the years 2000 to 2018 and identified the change in area of water body. Rajshahi Division of Bangladesh was selected as the study area for this case study. Landsat 5 data acquired in December 18th, 2000, January 12th, 2001, November 14th, 2005, January 26th, 2006, December 23rd, 2010, and December 14th, 2010 along with Landsat 8 data acquired in December 28th, 2015, January 6th, 2016, December 29th, 2018, and November 18th, 2018 were used as satellite imagery for this analysis. Two images of each month were taken to cover study area. The lowest and highest pixel value of the water body for each band was investigated. Then, a Pixel Based Model (PBM) was formed by using the entire Landsat band and run. The output of the model was shown as a binary image which includes water bodies and non-water bodies. The goal of this study is to verify the accuracy in finding common areas, accreted areas and abolished areas of the water bodies using the PBM model. The results show that overall accuracy of the model is 97% for the year 2000 with Kappa 0.94, 97% for the year 2005 with Kappa 0.94, 99% for the year 2010 with Kappa 0.98, 95% for the year 2015 and 2018 with Kappa 0.90. Also, it was observed that there have been significant changes in the water bodies during the chosen time periods.

1. INTRODUCTION

There are many forms of water bodies on the earth surface, such as surface water, lakes, ponds, rivers, reservoirs, transition water (irrigated water), etc. and is an essential component of the hydrological cycle, human beings and other forms of life (Jawak et al., 2015; Chave, 2001; Acharya et al., 2016). Identification of water bodies can be useful in many ways, such as estimation of water areas (Acharya et al., 2016; Rover et al., 2012; Alsdorf et al., 2007), flood area assessment (Acharya et al., 2016; Jain et al., 2005; Chignell et al., 2015), wetland inventories (Acharya et al., 2016; Rebelo et al., 2009; Ozesmi and Bauer, 2014), change detection (Acharya et al., 2016; Rokni et al., 2014; Du et al., 2012), managing and monitoring natural resources (Hassan et al., 2016), environmental monitoring, resource survey and drought detection. Since growing population and increasing socioeconomic necessities creates pressure on land area, the amount and location of water bodies change over time and space (Reis, 2008; Hassan et al., 2016). Changes in the amount and location of water bodies can indicate agricultural and environmental problems and affect human socioeconomic development (Hassan et al., 2016). Accurate estimation of water bodies is essential for both science and engineering research and policy making (Jiang et al., 2014; Selim, 2018; Jaafari and Nazarisamani, 2013; Hassan et al., 2016; Acharya et al., 2016). Satellite based remote sensing is a powerful tool to identify water bodies and detect changes over large areas because it provides continuous snapshots of earth surface over long periods (Reis, 2008). Among other satellite imagery, Landsat satellite imagery is very useful for such study because Landsat TM (Thematic Mapper), OLI (Operational Land Imager) imagery has a high spatial resolution (30 m), provides multispectral images (seven or eleven

Citation: Ahammad T, Rahaman H, Faisal BMR, Sultana N. Model based change detection of water body using Landsat imagery: A case study of Rajshahi Bangladesh. Environ. Nat. Resour. J. 2020;18(4):345-355. (https://doi.org/10.32526/ennrj.18.4.2020.33)

bands), short revisit interval (16 days), decades of records (almost 30 years) and is freely available (Jiang et al., 2014). Thus change detection analysis by using Landsat imagery is no longer cost- prohibitive (Jiang et al., 2014; Nicholas et al., 2013; Verpoorter et al., 2012). In order to detect water bodies, at present, different satellite-derived indices were used. The indices are described in the methodology section.

In this paper, we introduce a Pixel Based Model (PBM) to identify the changed area and identical area of water bodies automatically. The PBM method is more convenient than the water index method in the sense that the PBM method does not need a threshold value to identify water whereas every water index needs a threshold value to identify water. To identify water bodies, the PBM model needs to explore only the highest and lowest pixel value of water bodies. This method is not only useful for water detection but also helpful to detect the changed areas of crops, irrigated land, settlements, forests, etc. Using the PBM model, we detect the water bodies and area changes for the years 2000 to 2018 in the Rajshahi Division of Bangladesh.

2. METHODOLOGY

2.1 Study area

Rajshahi Division is one of the eight administrative divisions of Bangladesh. Geographically, Rajshahi Division is located between 23°48' and 25°16' north latitudes and between 88°01' and 89°48' east longitudes and is situated 23 m above sea level. It has an area of 18,174.4 km² (Miah, 2006). Rajshahi Division is in the central western region of Bangladesh. It consists of eight districts: Bogura, Chapainawabganj, Joypurhat, Naogaon, Natore, Pabna, Rajshahi and Sirajgonj. The famous Padma River borders Rajshahi Division on the south and another famous river, Jamuna River, lies across the eastern border. In the west, Rajshahi Division shares a border with India. This region was chosen because of the wide variety of demographic changes in the region (Miah, 2006). The study area is shown in Figure 1.

2.2. Data acquisition and image processing

To cover the study area, two images are required (path/row-138/43,139/43). Since two images taken on the same date could not be found, two images from the two closest days in December were used. Images were from the years 2000 to 2018 at approximately five year intervals. Landsat 5 TM and Landsat 8 OLI (path 138, row 043 and path 139, row 043) were used in this study. The Landsat 5 TM and Landsat 8 OLI Images were downloaded from USGS Earth Resources Observation Systems Data Centre (Rokni et al., 2014; Sekertekin et al., 2017). The dates of both images of same month were chosen to be as close as possible in the same vegetation season. All visible and infrared bands (except the thermal infrared) were included in the analysis. All the images were projected in UTM Zone 45N. Landsat image processing was performed using ERDAS Imagine 14 (Sekertekin et al., 2017).

Figure 1. Study area

In this paper, Thematic Mapper (TM) and Operational Land Imager (OLI) sensors are used for studying water body's detection for Rajshahi region of Bangladesh. Here, we have used band 1 to 5 for thematic mapper (TM) sensor and band 2 to 7 for Operational Land Imager (OLI) sensor (Rokni et al., 2014; Sekertekin et al., 2017). The data acquisition date and spatial resolution of the satellites sensors used in this paper are shown in Table 1.

2.3. Reference data

For the accuracy assessment of this study, we have used true water pixels which were manually digitized from the Landsat images for the respective years.

2.4. Water index methods

At present to identify water bodies, different water indices have been used. The indices are described in Table 2.

Table 1. Dates of Landsat TM and Landsat OLI satellite image with spatial resolution

Sensor name	Path/Row	Spatial resolution (m)	Image date	Total No. of bands	Number of bands used
Landsat TM	138/043	30	12 Jan 2001	7	6
Landsat TM	139/043	30	18 Dec 2000	7	6
Landsat TM	138/043	30	26 Jan 2006	7	6
Landsat TM	139/043	30	14 Nov 2005	7	6
Landsat TM	138/043	30	23 Dec 2010	7	6
Landsat TM	139/043	30	14 Dec 2010	7	6
Landsat OLI	138/043	30	06 Jan 2016	11	6
Landsat OLI	139/043	30	28 Dec 2015	11	6
Landsat OLI	138/043	30	29 Dec 2018	11	6
Landsat OLI	139/043	30	18 Nov 2018	11	6

Table 2. Satellite derived water index currently used for water detection

Water index	Formula	Threshold	Band information	Reference
Normalized-Difference Water Index (NDWI)	NDWI = (Green − NIR)/(Green + NIR)	There is no fixed threshold value. But it has positive value	For Landsat 5 TM, Band 1=Blue, Band 2=Green, Band 3=Red, Band 4=NIR, Band 5=MIR, Band 7= SWIR For Landsat 8 OLI, Band 2=Blue, Band 3=Green, Band 4=Red, Band 5=NIR, Band 6= MIR, Band 7= SWIR (Rokni et al., 2014).	Mcfeeters (1996); Rokni et al. (2014); Yang et al. (2015); Zhou et al. (2016); Kaplan and Avdan (2017)
Modified Normalized-Difference Water Index (MNDWI)	MNDWI = (Green − MIR)/(Green + MIR)	There is no fixed threshold value. But it has positive value		Xu (2006); Rokni et al. (2014); Yang et al. (2015)
Normalized Difference Moisture Index (NDMI)	NDMI = (NIR − MIR)/(NIR + MIR)	There is no fixed threshold value. But it has positive value		Wilson and Sader (2002); Rokni et al. (2014)
Water Ratio Index (WRI)	WRI = (Green + Red)/ (NIR + MIR)	There is no fixed threshold value. But value of water is greater than 1		Shen and Li (2010); Rokni et al. (2014)
Normalized Difference Vegetation Index (NDVI)	NDVI = (NIR − Red)/ (NIR + Red)	There is no fixed threshold value. But it has negative value		Trishchenko et al. (2001); Hatfield and Prueger 2010); Zoran and Stefan (2006)
Automated Water Extraction Index (AWEI)	AWEI = 4 × (Green-MIR) − (0.25 × NIR + 2.75 × SWIR)	There is no fixed threshold value. But value of water is greater than 1		Feyisa et al. (2014); Rokni et al. (2014)

2.5. Pixel based model for water detection

At first, all the obtained images were converted to spectral radiance using ERDAS IMAGINE 14 model maker. The required information including data acquisition date, Gain (Radiance_Multi_Band_x) and Bias (Radiance_Add_Band_x) was obtained from Landsat header files (Rokni et al., 2014). The lowest and highest pixel value (radiance value) of the water body for each band of the remotely sensed image 2000, 2005, 2010, 2015, and 2018 was identified by the selection of minimum and maximum value of each image band. The lowest and highest pixel value of water body for the images from 2000, 2005, 2010, 2015, and 2018 is shown in Table 3, Table 4, Table 5, Table 6, and Table 7, respectively. Then a Pixel Based Model (PBM) was formed indicating lowest and highest pixel value for each band for the year 2000. The result shows a binary image which includes only a water body and a non-water body.

Table 3. Lowest and highest pixel value of the water body for the image 2000

Band number	Lowest pixel value (radiance value)	Highest pixel value (radiance value)
1	48	64
2	33	54
3	25	42
4	5	24
5	1	6
7	1	2

Table 4. Lowest and highest pixel value of the water body for the image 2005

Band number	Lowest pixel value (radiance value)	Highest pixel value (radiance value)
1	51	72
2	39	60
3	21	47
4	15	29
5	1	5
7	1	2

Table 5. Lowest and highest pixel value of the water body for the image 2010

Band number	Lowest pixel value (radiance value)	Highest pixel value (radiance value)
1	58	74
2	44	63
3	29	53
4	16	29
5	1	11
7	1	3

Table 6. Lowest and highest pixel value of the water body for the image 2015

Band number	Lowest pixel value (radiance value)	Highest pixel value (radiance value)
2	63	73
3	44	57
4	29	44
5	12	31
6	1	6
7	1	2

Table 7. Lowest and highest pixel value of the water body for the image 2018

Band number	Lowest pixel value (radiance value)	Highest pixel value (radiance value)
2	58	75
3	42	62
4	28	47
5	11	33
6	1	11
7	1	3

The same procedure was repeated for remotely sensed images from 2005, 2010, 2015, and 2018. The results from the above five model identify water bodies for the years 2000, 2005, 2010, 2015, and 2018 respectively. Then a new model was made to detect the water bodies that were present in 2000 but abolished in 2005 by subtracting the binary image of 2005 from that of 2000. Another model was made to detect the accreted area of water bodies in 2005 but absent in 2000 by subtracting binary image of 2000 from that of 2005.

The PBM used for detecting water bodies is shown below using the pseudo-code defined by ERDAS software:

```
EITHER 1 IF (
(Band 1 >= lowest pixel value AND
Band 1 <= highest pixel value) AND
(Band 2 >= lowest pixel value AND
Band 2 <= highest pixel value) AND
(Band 3 >= lowest pixel value AND
Band 3 <= highest pixel value) AND
(Band 4 >= lowest pixel value AND
Band 4 <= highest pixel value) AND
(Band 5 >= lowest pixel value AND
Band 5 <= highest pixel value) AND
(Band 6 >= lowest pixel value AND
Band 6 <= highest pixel value) AND
) OR 0 OTHERWISE
```

Lastly, a model was made to detect the identical area of water bodies which are present both in 2000 and 2005 by subtracting the last two binary images from any of the binary image of water body. A flow chart of the work is shown in Figure 2. The model used in the whole work has been shown in the following:

Model for detecting abolished area in 2005 (Model-3 in the flowchart): Model for water bodies 2000 - Model for water bodies 2005

Model for detecting accreted area in 2005 (Model-4 in the flowchart): Model for water bodies 2005 - Model for water bodies 2000

Model for Identical water body which is present both in 2000 and 2005 (Model-5 in the flowchart): Water bodies' 2000 or Water bodies 2005 - abolished area in 2005 - accreted area in 2005

Model for detecting abolished area in 2010 (Model-3 in the flowchart): Model for water bodies 2005 - Model for water bodies 2010

Model for detecting accreted area in 2010 (Model-4 in the flowchart): Model for water bodies 2010 - Model for water bodies 2005

Model for Identical water body which is present both in 2005 and 2010 (Model-5 in the flowchart): Water bodies' 2000 or Water bodies 2010 - abolished area in 2010 - accreted area in 2010

Model for detecting abolished area in 2015 (Model-3 in the flowchart): Model for water bodies 2010 - Model for water bodies 2015

Model for detecting accreted area in 2015 (Model-4 in the flowchart): Model for water bodies 2015 - Model for water bodies 2010

Model for Identical water body which is present both in 2010 and 2015 (Model-5 in the flowchart): Water bodies' 2010 or Water bodies 2015 - abolished area in 2015 - accreted area in 2015

Model for detecting abolished area in 2018 (Model-3 in the flowchart): Model for water bodies 2015 - Model for water bodies 2018

Model for detecting accreted area in 2018 (Model-4 in the flowchart): Model for water bodies 2015 - Model for water bodies 2018

Model for Identical water body which is present both in 2015 and 2018 (Model-5 in the flowchart): Water bodies' 2015 or Water bodies 2018 - abolished area in 2018 - accreted area in 2018

Model for Identical water body which is present from 2000 to 2018 (Model-5 in the flowchart): Water bodies' 2000 or Water bodies 2005 or Water bodies 2010 or Water bodies 2015 or Water bodies 2018 - abolished area in 2005 - accreted area in 2005 - abolished area in 2010 - accreted area in 2010 - abolished area in 2015 - accreted area in 2015 - abolished area in 2018 - accreted area in 2018

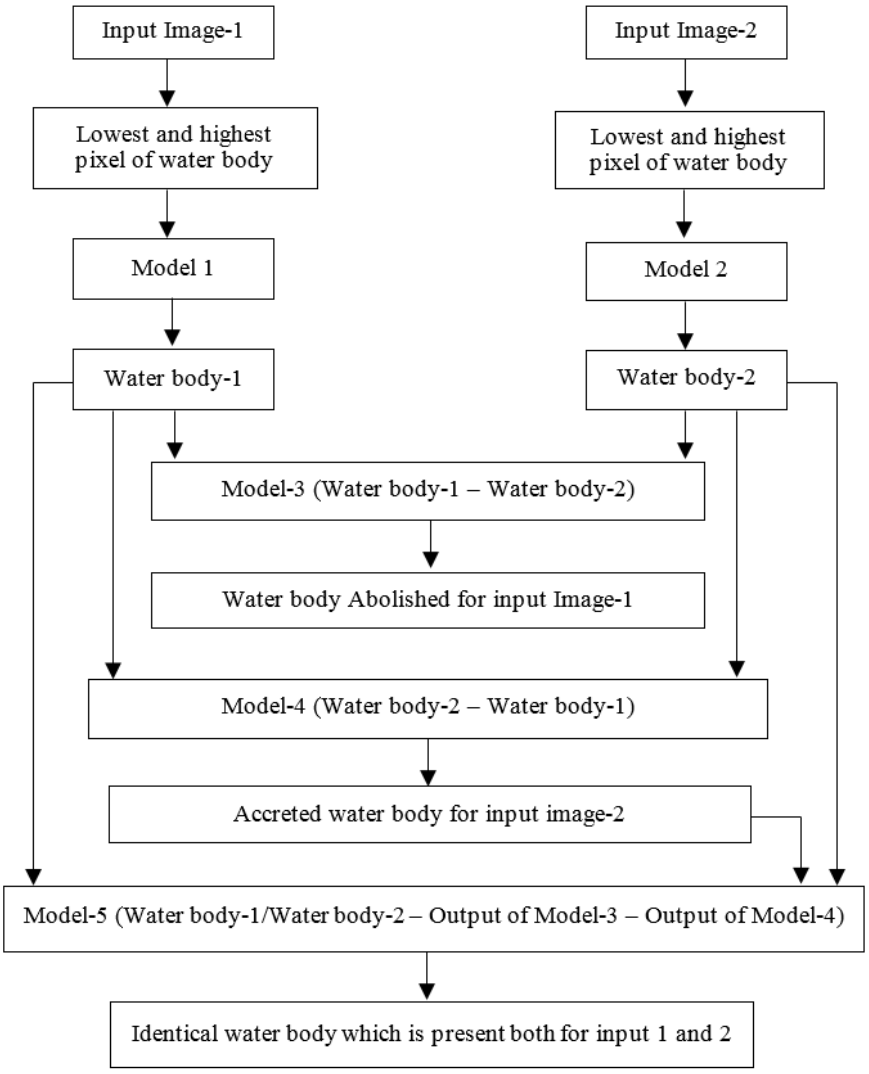

Figure 2. Overall flowchart adopted in this study

3. RESULTS AND DISCUSSION

Landsat TM (2010) and Landsat OLI (2017) images were used in this study. In this paper, a Pixel Based Model was investigated to detect the water bodies and its changes from the year 2000 to 2018 with five year interval. Figure 3(a), Figure 3(b), Figure 3(c), Figure 3(d), and Figure 3(e) show the false color composite (543) images of Rajshahi division for the year 2000, 2005, 2010, 2015 and 2018, respectively. Figure 3(f), Figure 3(g), Figure 3(h), Figure 3(i), and Figure 3(j) show the water body area for the year 2000, 2005, 2010, 2015, and 2018, respectively.

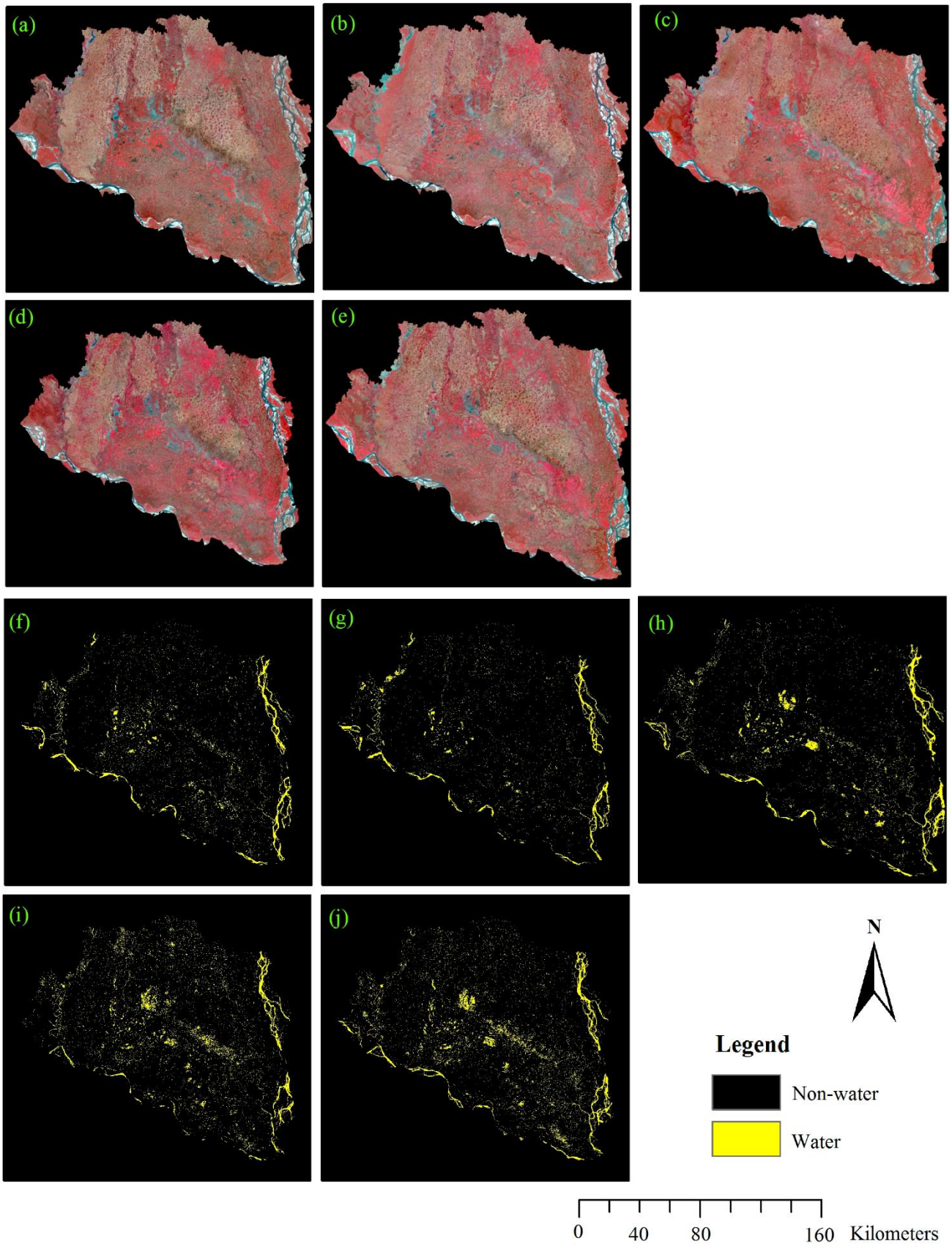

Figure 3. (a) Input satellite image 2000; (b) Input satellite image 2005; (c) Input satellite image 2010; (d) Input satellite image 2015; (e) Input satellite image 2018; (f) Detected water body 2000; (g) Detected water body 2005; (h) Detected water body 2010; (i) Detected water body 2015; (j) Detected water body 2018.

The accuracy of the PBM model was tested for the whole study period. The overall accuracy of the model is 97% for the year 2000 with Kappa 0.94. Similarly overall accuracy of the model is 97% for the year 2005 with Kappa 0.94, 99% for the year 2010 with Kappa 0.98, 95% for the year 2015 and 2018 with Kappa 0.90. The accuracy of the PBM model is shown in Table 8.

Table 8. Accuracy of the PBM model

Accuracy (%)				
Year	User	Producer	Overall	Kappa
2000	96.08	98	97	0.94
2005	94.34	100	97	0.94
2010	100.00	98	99	0.98
2015	94.12	96	95	0.90
2018	94.12	96	95	0.90

The increment and decreases of the water body is due to the erosion, accretion and net gain/loss of land in the Coastal Areas, formation of new houses, and formation of new fishing zones in the study area. The area which is eroded creates millions of environmental refuges whereas the area which is accreted give shelter to millions of environmental refuges (Alam and Uddin, 2013). The statistics revealed that water body and non-water body types were consistent in their direction of change from 2000 to 2018. The total area of water bodies was 808.59 km^2 in 2005 which is least during the study period and the highest (1373.77 km^2) is in 2018, showing continuous increment of water body from 2000 to 2018 (shown in Table 9).

In 2000, water body covers 5.35% of the total study area. In 2005, water body has been decreased to 4.45% of the total area with a net change of 0.90% (163.44 km^2) from the year 2000. From 2010, there was a continuous increase of water body up to 2018.

In 2010, water body increased to 5.55% of the total area with a net change of 1.10 % (199.55 km^2) from the year 2005. In 2015, water body increased to 6.74% of the total area with a net change of 1.19% from the year 2010. In 2018, water body increased to 7.56% of the total area with a net change of 0.82% from the year 2015. In comparison with the base year 2000, water bodies increased to 2.21% in 2018. The percentage of water body and non-water body from year 2000 to 2018 and variation of water body from year 2000 to 2018 has been shown in Figure 4 and Figure 5, respectively.

Table 9. Area of water body and its change from the year 2000 to 2018

Year	Area of water body (km^2)	Abolished area of water body (km^2)	Accreted area of water body (km^2)	Net Change (km^2)
2000	972.03	-	-	-
2005	808.59	559.98	396.53	-163.45
2010	1008.14	401.07	600.62	199.55
2015	1225.42	546.55	763.83	217.28
2018	1373.77	553.75	702.10	148.35

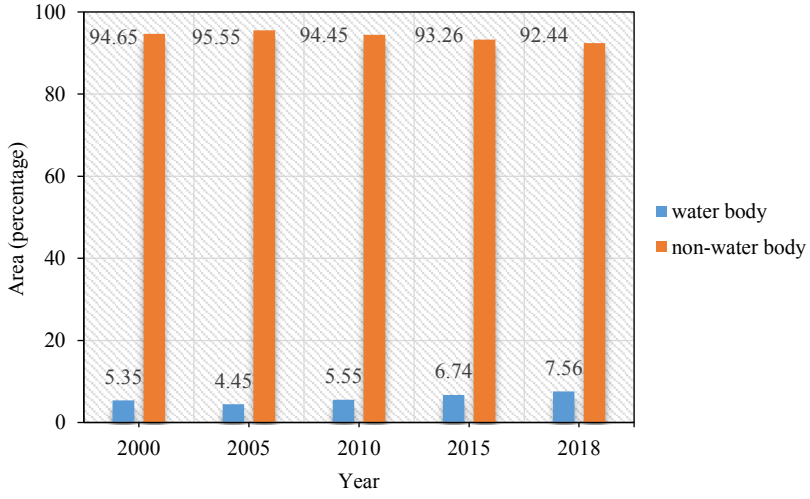

Figure 4. Percentage of water body and non-water body from 2000 to 2018

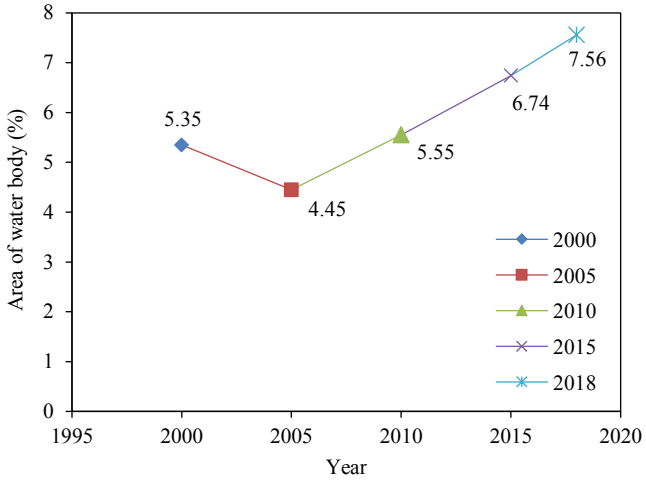

Figure 5. Variation of water body from 2000 to 2018

In 2005, 559.98 km^2 of water body had been abolished and 396.53 km^2 new areas has been added to water body with a net decrease of 163.45 km^2 water body. In 2010, 401.07 km^2 area of water body had been abolished and 600.62 km^2 of new areas was added to water body with a net increase of 199.55 km^2 water body. In 2015, 546.55 km^2 of water body had been abolished and 763.83 km^2 of new areas was added to water body with a net increase of 217.28 km^2 water body. In 2018, 553.75 km^2 area of water body had been abolished and 702.10 km^2 of new areas was added to water body with a net increase of 148.35 km^2 water body. From the above discussion it is clear that accreted area of water body has been increased every year except 2005 which implies that erosion has been increased every year after 2005. Due to erosion there is a huge probability to create new environmental refuges. Area of water body and its change from the year 2000 to 2018 has been shown in Table 9. Figure 6(a), Figure 6(c), Figure 6(e), and Figure 6(g) show the abolished area of water body for the years 2005, 2010, 2015 and 2018, respectively. Figure 6(b), Figure 6(d), Figure 6(f), and Figure 6(h) show the accreted area of water body for the years 2005, 2010, 2015, and 2018, respectively.

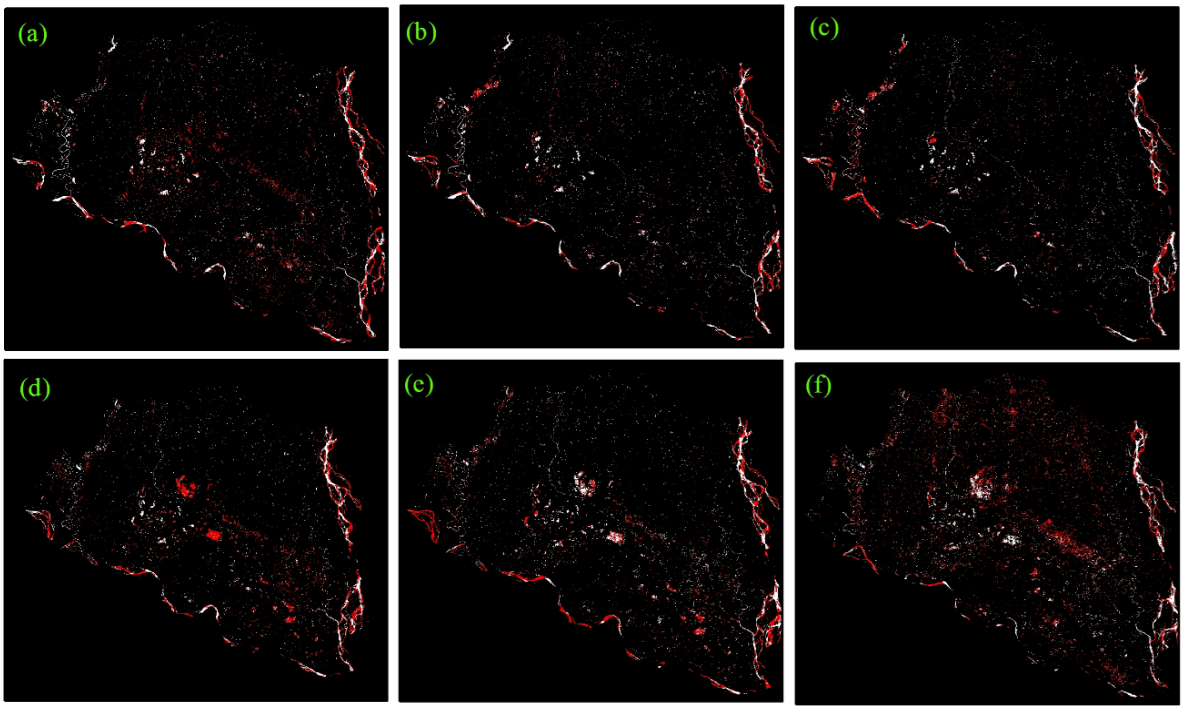

Figure 6. (a) Abolished area of water body 2005; (b) Accreted area of water body 2005; (c) Abolished area of water body 2010; (d) Accreted area of water body 2010; (e) Abolished area of water body 2015; (f) Accreted area of water body 2015; (g) Abolished area of water body 2018; (h) Accreted area of water body 2018

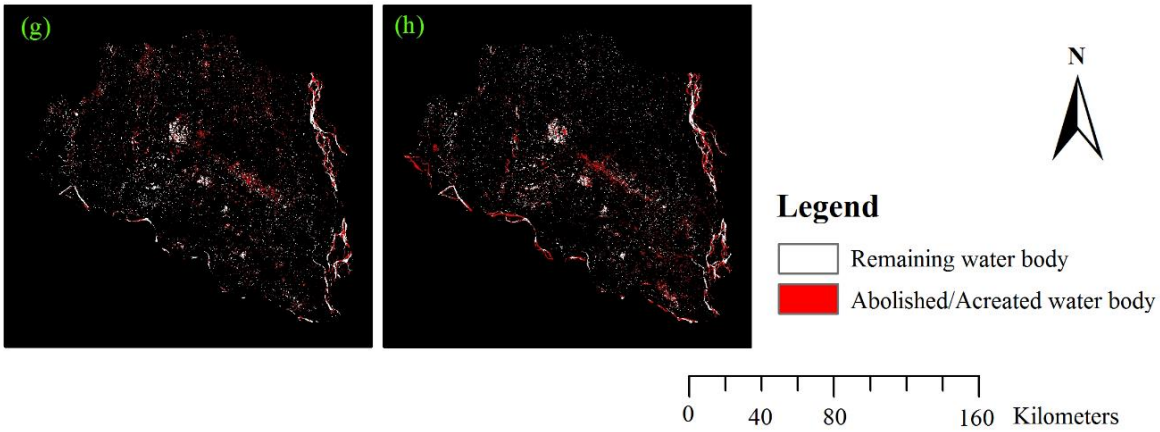

Figure 6. (a) Abolished area of water body 2005; (b) Accreted area of water body 2005; (c) Abolished area of water body 2010; (d) Accreted area of water body 2010; (e) Abolished area of water body 2015; (f) Accreted area of water body 2015; (g) Abolished area of water body 2018; (h) Accreted area of water body 2018 (cont.).

The identical areas of water body from year 2000 to 2005, 2005 to 2010, 2010 to 2015, and 2015 to 2018 are 412.06, 407.52, 461.59 and 671.67 km^2 respectively (Table 10). But in comparison with the base year 2000, only 78.21 km^2 of water body was identical with 2018 which shows that erosion and accretion are common hazards in this region. Figure 7(a), Figure 7(b), Figure 7(c), Figure 7(d), and Figure 7(e) show the identical area of water body for the range of year 2000 to 2005, 2005 to 2010, 2010 to 2015, 2015, to 2018, and 2000 to 2018, respectively.

Table 10. Identical area of water body from the year 2000 to 2018

Year range	Identical area (ha)	Identical area (km^2)
2000 to 2005	41,205.7	412.06
2005 to 2010	40,751.6	407.52
2010 to 2015	46,159.2	461.59
2015 to 2018	67,167.1	671.67
2000 to 2018	7,821.09	78.21

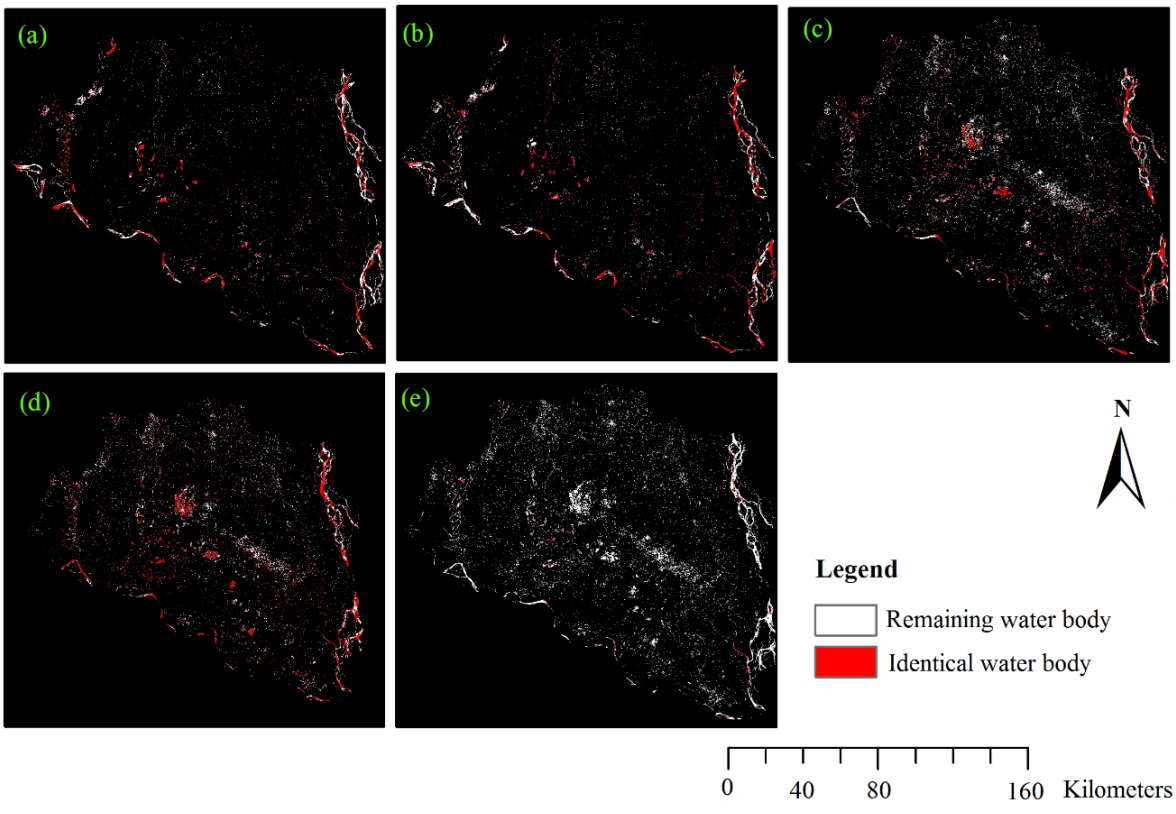

Figure 7. (a) Identical water body present 2000 and 2005; (b) Identical water body present 2005 and 2010; (c) Identical water body present 2010 and 2015; (d) Identical water body present 2015 and 2018; (e) Identical water body from 2000 to 2018

4. CONCLUSION

The present study demonstrates a Pixel Based Model technique to detect water bodies using Landsat satellite imagery for the years 2000 to 2018. This study also finds abolished area, accreted area and identical area of water body using PBM method for the study period. The PBM model has high accuracy for this analysis and it is very convenient to detect water body, abolished area, accreted area and identical area in relatively short time. This method is also very useful in the sense that this model needs to explore lowest and highest pixel value (radiance value) of the water body for each band of the remotely sensed image by the selection of minimum and maximum value of each image band. The result showed that the accreted area of water body in Rajshahi Division of Bangladesh has increased every year except 2005 which implies that erosion is a dominant phenomenon is this region. Due to erosion, there is a huge probability to create new environmental refuges. Regular analysis is required to get the exact condition of this area. If the government gets the real information about the erosion and accretion, it will be very helpful for the government to take immediate proper steps to resolve the problems. This method is not only useful for water detection but also helpful to detect crops, irrigated land, settlement, forest, etc.

REFERENCES

Alam MS, Uddin K. A Study of morphological changes in the coastal areas and Offshore Islands of Bangladesh using remote sensing. Scientific and Academic Publishing 2013;2(1):15-8.

Alsdorf DE, Rodríguez E, Lettenmaier DP. Measuring surface water from space. Reviews of Geophysics 2007;45(2): RG2002(1-24).

Acharya TD, Lee DH, Yang IT, Lee JK. Identification of water bodies in a Landsat 8 OLI image using a J48 decision tree. Sensors 2016;16:1075.

Chave P. The EU water framework directive: An introduction. IWA Publishing; 2001. p. 208.

Chignell SM, Anderson RS, Evangelista PH, Laituri MJ, Merritt DM. Multi-temporal independent component analysis and Landsat 8 for delineating maximum extent of the 2013. Colorado Front Range Flood. Remote Sensing 2015;7:9822-43.

Du Z, Linghu B, Ling F, Li W, Tian W, Wang H, Gui Y, Sun B, Zhang X. Estimating surface water area changes using time-series Landsat data in the Qingjiang River Basin, China. Journal of Appllied Remote Sensing 2012;6:063609.

Feyisa GL, Meilby H, Fensholt R, Proud SR. Automated water extraction index: A new technique for surface water mapping using Landsat imagery. Remote Sensing of Environment 2014;140:23-35.

Hatfield JL, Prueger JH. Value of using different vegetation indices to quantify agricultural crop characteristics at different growth stages under varying management practices. Remote Sensing 2010;2:562-78.

Hassan Z, Shabbir R, Ahmad SS, Malik AH, Aziz N, Buttand A, Erum S. Dynamics of land use and land cover change (LULCC) using geospatial techniques: A case study of Islamabad Pakistan. Springer Plus 2016;5,812(1-11).

Jiang H, Feng M, Zhu Y, Lu N, Huang J, Xiao T. An automated method for extracting rivers and lakes from Landsat imagery. Remote Sensing 2014;6:5067-89.

Jain S, Singh RD, Jain MK, Lohani AK. Delineation of flood-prone areas using remote sensing techniques. Water Resource Management 2005;19:333-47.

Jaafari S, Nazarisamani A. comparison between land use/land cover mapping through Landsat and Google Earth Imagery. American-Eurasian Journal of Agricultural and Environmental Sciences 2013;13(6):763-68.

Jawak SD, Kulkarni K, Luis AJ. A review on extraction of lakes from remotely sensed optical satellite data with a special focus on Cryospheric Lakes. Advances in Remote Sensing 2015;4:196-213.

Kaplan G, Avdan U. Object-based water body extraction model using Sentinel-2 satellite imagery. European Journal of Remote Sensing 2017;50:137-43.

Mcfeeters SK. The use of the normalized difference water index (NDWI) in the delineation of open water features. International Journal of Remote Sensing 1996;17:1425-32.

Miah S. Rajshahi Division [internet]. 2006 Available from: http://en.banglapedia.org/index.php?title=Rajshahi_Division.

Nicholas R, Goodwin, Lisa JC, Robert JD, Flood N, Tindall D. Cloud and cloud shadow screening across Queensland, Australia: An automated method for Landsat TM/ETM+ time series. Remote Sensing of Environment 2013;134:50-65.

Ozesmi SL, Bauer ME. Satellite remote sensing of wetlands. Wetlands Ecological Management 2014;10:381-402.

Reis S. Analyzing land use/land cover changes using remote sensing and GIS in Rize, North-East Turkey. Sensors 2008;8:6188-202.

Rokni K, Ahmad A, Selamat A, Hazini S. Water feature extraction and change detection using Multitemporal Landsat Imagery. Remote Sensing 2014;6:4173-89.

Rover J, Ji L, Wylie BK, Tieszen LL. Establishing water body areal extent trends in interior Alaska from multi-temporal Landsat data. Remote Sensing Letters 2012;3:595-604.

Rebelo LM, Finlayson CM, Nagabhatla N. Remote sensing and GIS for wetland inventory, mapping and change analysis. Journal of Environmental Management 2009;90:2144-53.

Shen L, Li C. Water Body Extraction from Landsat ETM+ Imagery Using Adaboost Algorithm. Proceedings of 18th International Conference on Geoinformatics; Beijing: China; 2010. p. 1-4.

Selim M. Change Detection Analysis using new nano satellite imagery. International Journal of Engineering and Advanced Technology 2018;7:1-10.

Sekertekin A, Marangoz AM, Akcin H. Pixel-based classification analysis of land use land cover using Sentinel-2 and Landsat-8 data. International Archives of the Photogrammetry, Remote Sensing and Spatial Information Sciences 2017;XLII-4/W6: 91-3.

Trishchenko AP, Cihlar J, Zhanqing Li. Effects of spectral response function on surface reflectance and NDVI measured with moderate resolution satellite sensors. Remote Sensing of Environment 2001;81:1-18.

Verpoorter C, Kutser T, Tranvik L. Automated mapping of water bodies using Landsat multispectral data. Limnology and Oceanography: Methods 2012;10:1037-50.

Wilson EH, Sader SA. Detection of forest harvest type using multiple dates of Landsat TM imagery. Remote Sensing of Environment 2002;80:385-96.

Xu H. Modification of normalised difference water index (NDWI) to enhance open water features in remotely sensed imagery. International Journal of Remote Sensing 2006;27:3025-33.

Yang L, Tian S, Yu L, Ye F, Qian J, Qian Y. Deep learning for extracting water body from Landsat imagery. International Journal of Innovative Computing, Information and Control 2015;11:1913-29.

Zoran M, Stefan S. Climatic Changes Effects on Spectral Vegetation Indices for Forested Areas Analysis from Satellite Data. Proceedings of the 2nd Environmental Physics Conference; Alexandria: Egypt; 2006. p. 73-83.

Zhou ZG, Tang P, Zhou M. Detecting anomaly regions in satellite image time series based on seasonal autocorrelation analysis. ISPRS Annals of the Photogrammetry, Remote Sensing and Spatial Information Sciences 2016;III-3:303-10.

Study of Ribulose 1, 5-Bisphosphate Carboxylase from S*ulfobacillus acidophilus* Strain NY-1 Isolated from Lignite Mines

Jenny Angel Stanislaus[1*] and Dhandapani Ramamoorthy[2]

[1]*Department of Biochemistry, Holy Cross College, Tiruchirappalli, Tamilnadu, India*
[2]*Department of Microbiology, Periyar University, Salem, Tamilnadu, India*

ARTICLE INFO

Received: 2 Feb 2020
Received in revised: 11 Jul 2020
Accepted: 20 Jul 2020
Published online: 18 Aug 2020
DOI: 10.32526/ennrj.18.4.2020.34

Keywords:
Sulfobacillus/ Mines/ RuBisCo/ Ion exchange chromatography/ Global warming

*** Corresponding author:**
E-mail: jennyangelbiochem @hcctrichy.ac.in

ABSTRACT

One of the key compounds engaged in the carbon dioxide fixation cycle (Calvin-Benson-Bassham cycle) is Ribulose 1, 5-Bisphosphate Carboxylase/ Oxygenase (RuBisCo). These are known to act as a carbon sink thus leading to decrease of the carbon level in the atmosphere. This unique property of RuBisCo can therefore help in diminishing an Earth-wide global warming problem, a noteworthy risk in the present world. In the present study, presence of RuBisCo in *Sulfobacillus acidophilus* strain NY-1 was studied. This strain was isolated from Neyveli lignite mines and their growth parameters such as pH and temperature wereoptimized. The ideal pH and temperature for *S. acidophilus* was at pH 1.7 and at 45°C respectively. The correlation of growth of *S. acidophilus* with light, carbon dioxide and aeration was investigated by enumerating the number of cells/mL using a hemocytometer. The cell count was highest in light condition whereas no growth was observed in dark condition. At the 60th hour of incubation, a cell density of 1.60×10^6 cells/mL was observed. Similarly, in the presence of carbon dioxide the maximum cell count was 2.72×10^6 at the 40th hour of incubation with aeration. The presence of RuBisCo in *S. acidophilus* was affirmed by ion exchange chromatography technique.

1. INTRODUCTION

In the carbon cycle, the predominant part of terrestrial carbon is stored in soil, whereas only a minor part is seen in the vegetation. During the process of biomass formation and decomposition sequestration of carbon dioxide (greenhouse gas) occurs. As a result, soil organic carbon may influence and counteract global warming. Atmospheric carbon dioxide is absorbed by the enzyme RuBisCo which is one of the prominent enzymes in the Calvin-Benson-Bassham (CBB) cycle. This cycle includes three main enzymes: Ribulose Bisphosphate Carboxylase/Oxygenase, sedoheptulose-bisphosphatase and phosphoribulokinase (Sage et al., 2008). The Ribulose 1, 5-Bisphosphate Carboxylase/ Oxygenase (RuBisCo) is the most significant enzyme among the three enzymes as it acts as a carbon dioxide sink. Hence, it plays an imperative part in decreasing the carbon dioxide level which in turn will reduce global warming.

The RuBisCo plays two main roles depending on the availability of carbon dioxide/oxygen sources. One function is known as the Carboxylase activity. In this reaction, the addition of molecular carbondioxide to Ribulose 1, 5-bisphosphate (RuBP) forms two molecules of 3-phosphoglyceate (3-PGA) catalyzed by RuBisCo. This provides an opportunity for conversion of atmospheric inorganic carbon to organic carbon in our biosphere (Meenakshi and Srisudha, 2012; Ke-Quing et al., 2014). Another important function is the Oxygenase process which is considered as a competitive negative side reaction. The addition of oxygen to RuBP, forms one molecule of 3-PGA and one molecule of 2-phosphoglycolate (Ken et al., 2001; Tominaga et al., 2020). Subsequently enhancing RuBisCo's carbon-dioxide-fixing capability will thus lead to increase in carbondioxide entrapment (Fischer and Edmeades, 2010; Erb and Zarzycki, 2018).

Citation: Stanislaus JA, Ramamoorthy D. Study of ribulose 1, 5-bisphosphate carboxylase from S*ulfobacillus acidophilus* strain NY-1 isolated from lignite mines. Environ. Nat. Resour. J. 2020;18(4):356-362. (https://doi.org/10.32526/ennrj.18.4.2020.34)

A wide variety of RuBisCo forms are reported in both prokaryotes and eukaryotes. RuBisCo are classified into two types-Form I and Form II-based on amino acid sequences. Form I is further classified into two groups, the Green-like group and the Red-like group. The examples for green-like include proteobacteria, cyanobacteria, green algae and plants. Red-like examples include eukaryotic non-green algae and bacteria such as *A. eutrophus* (Delwiche and Palmer, 1996; Watson and Tabita, 1997). The three-dimensional structures of RuBisCo from microorganisms such as *Sulfobacillus* (Caldwell et al., 2007); *Synechococcus* sp. strain PCC 6301 (Newman and Gutteridge, 1994); *Chromatiumvinosum* (Nakagawa et al., 1986); *Rhodospirillum rubrum* (Schneider et al., 1990); *Galdieria partita* (Shibata et al., 1996); and plants like spinach (Andersson et al., 1989) and tobacco (Chapman et al., 1988) have been investigated in detail. The complete key observations of this enzyme from the year 1947 up to 2006 was presented by Portis and Parry (2007) and will be helpful in utilization of this enzyme in a holistic way. Caldwell et al. (2007) also studied the enzymes involved in CBB cycle in *Sulfobacillus* and the genes encoding RuBisCo.

In 2007, the Intergovernmental Panel on Climate Change (a United Nations Body) published a report in which it stated that the average global atmospheric temperature is rapidly increasing. This is mainly due to greenhouse gases such as carbondioxide whose level has increased since the start of the industrial revolution. Much advancement in technology has been implemented to capture the atmospheric carbondioxide as in the case of the carbon capture and storage (CCS) system. Using this system it is possible to trap 90% of existing carbon dioxide emission underground, but environmentalists fear that entrapping could lead to earthquakes in the future (Liben et al., 2012).

Research on another aspect of trapping carbon dioxide using RuBisCo was also reported as this enzyme plays a key role in photosynthesis. This is one of the most abundant enzymes present in nature but the main limitation is that it is heat labile and inefficient. Ways have been considered in improving the efficiency of this enzyme so that it can absorb more atmospheric carbon dioxide. In this present study, an attempt was made to detect the presence of RuBisCo protein from mining bacteria, as it has been proven that such bacteria can produce heat stable proteins. Therefore, the assay of RuBisCo was assessed by ion exchange chromatography from *Sulfobacillus* sp. under optimized condition. This study may help in further manipulation of bacterial RuBisCo for effective utilization to reduce the carbon dioxide level in the atmosphere which is a significant factor in global warming.

2. METHODOLOGY

2.1 Culture conditions

Most of the acidophilic bacteria cannot be cultivated in ordinary culture media as the agar used as solidifying agent in media becomes liquefied at lower pH. Therefore, in the present work *S. acidophilus* strain NY-1 was cultivated in liquid medium (ferrous sulfate tryptone soy broth) at pH 3.0 at 37ºC for 5 days. The culture was inoculated at 5 day intervals thrice in fresh medium for adaptation in new environment. This culture was maintained as pre-cultured strain and used for further studies.

2.2 Optimization of growth parameters

In order to study the effect of various growth parameters on the growth of the organism as well to optimize the parameters the culture was grown in liquid media. Enumeration of *S. acidophilus* can be done by cell count method and spectrophotometric method, as it is difficult to cultivate in solid media.

2.2.1 Effect of temperature and pH

To ferrous sulfate tryptone soy broth, 2% (v/v) of pre-cultured strain was inoculated. It was incubated at different temperatures of 37, 45, 55 and 65ºC and shaken at 150 rpm for 5 days (Watling et al., 2008). For every 24 h, a cell count using a Neubauer chamber was performed. To study the effect of initial pH, the medium pH was adjusted with 2.0 N sulphuric acid to pH 1.7, 2.2, and 3.0 respectively and shaken at 150 rpm at 45ºC for 5 days. Every 24 h for 5 days, a cell count estimation was done. Simultaneously the turbidity was measured at 700 nm in a Systronic double beam spectrophotometer.

2.2.2 Effect of light and dark condition

The pre-cultured strain 2% (v/v) was inoculated in 100 mL ferrous sulfate tryptone soy broth and incubated under light in a shaker for 150 rpm at 45ºC for 5 days. At regular intervals the culture was subjected to cell count using a Neubauer chamber. Likewise another set of inoculated medium were grown under dark conditions and similarly the culture

was subjected to cell count by using a Neubauer chamber for 5 days (Wedel and Soll, 1998).

2.2.3 Presence and absence of carbon dioxide

The pre-cultured strain 2% (v/v) was inoculated in 100 mL ferrous sulfate tryptone soy broth supplemented with 2% sodium bicarbonate for carbon utilization as a substitute for atmospheric CO_2 and another without carbon dioxide (Maryshamya et al., 2019). The medium was incubated at 45°C for 5 days and the cultures were subjected to cell count. Aeration was provided to the culture media through a sterile tube which was connected to a motor. Air bubbles were seen to arise from the bottom of the liquid media thus providing aeration.

2.3 Determination of cell count by hemocytometer

A uniform cell suspension of 10 µL was mixed with 10 µL of 0.4 % trypan blue solution (fresh and filtered) in phosphate buffered saline. It was gently vortexed and allowed to stand for 10 min. The preparation was then observed in hemocytometer under 100X magnification. The cells that take up the stain and those that do not take were counted and expressed in terms of percentage of cell viability

$$\% \text{ Cell viability} = (\text{Total viable cells (Unstained)} / \text{Total cells (Viable + Dead)}) \times 100$$

2.4 Protein characterization

Partial purification of protein was carried out by ammonium sulfate precipitation method. The supernatant was obtained by centrifugation at 5,000 rpm for 20 min to which 80% ammonium sulfate was added and kept overnight (O'Donnelly et al., 2014). It was again centrifuged at 13,000 rpm for 20 min and the pellet was suspended in 20 mM Tris-HCL buffer (pH 7.0). The pellet was later subjected to dialysis overnight at 4°C with dialysis membrane-150 (cut off MW 5,000 to 10,000).

2.4.1 Ion exchange chromatography

The dialysate was subjected to ion exchange chromatography using DEAE cellulose column. The DEAE cellulose column was thoroughly washed with equilibrated buffer (10 mM Tris-H_2SO_4, pH-7.4). 1.0 gm of DEAE cellulose was mixed with 10 mL of 0.05 M equilibrated buffer and added to the column of 8.0 cm height. The column was packed tightly and allowed to settle well. The column was washed with equilibrated buffer once before loading the sample (Robinson et al., 1988).Care should be taken that the column remains wet throughout the experiment. One mL of the dialyzed sample was loaded and the column was washed with 10 mL of linear gradient of 0.2 to 0.5 M $(NH_4)_2SO_4$ salt (equilibrium buffer). Fractions of 3 mL of eluent were collected in a series of test tubes. The optical density of the collected eluent was measured at OD_{280} nm using Cystronics double beam spectrophotometer.

3. RESULTS AND DISCUSSION

There are many reports on RuBisCo enzymes availability in plants and it has been extensively studied. The role of this enzyme in lower form of organisms like algae, cyanobacteria and proteobacteria are also studied recently. But only a few reports are available for gram positive bacteria. Isolation of RuBisCo from Gram positive bacteria (*Sulfobacillus acidophilus*) from harsh environments will further help in manipulating this enzyme for various applications. RuBisCo is the key enzyme of the Calvin-Benson-Bassham (CBB) cycle which may be the principal route of carbon-fixing pathway for acidophiles. In the present investigation *S. acidophilus* strain NY-1 was isolated from soil in Neyveli Lignite mines (data not shown). This soil is rich in lignite fragments, pyrite, and total carbon content and secondary minerals such as gypsum. The top layers are usually of neutral pH but the subsoil remains acidic (pH 2.5-2.9). This may be due to oxidation of pyrite, soil leaching and minerals precipitation. All the above factors contribute to the isolation of *Sulfobacillus* sp. in such mining sites.

3.1 Optimization of growth parameters

Standardization of growth parameters is very essential for all microorganisms as these conditions may lead to maximum growth.

3.1.1 Effect of temperature and pH

The most predominant factors such as temperature and pH optima for the growth of *S. acidophilus* strain NY-1 were studied. The effect of temperature was studied and it was observed that the bacterium was able to tolerate temperatures up to 65°C, but maximum growth was observed at 45°C (Figure. 1). Most acidophilic organisms grow well between 28-62°C, the strain *S. acidophilus* is therefore considered as a moderately thermophilic acidophile. There are many reports on the thermophilic nature of *Sulfobacillus* sp. such as *S. thermosulfidooxidans*

which was able grow in batch culture at 45°C (Kaneda, 1991), *Sulfobacillus* sp. strain VKMB at 50°C (Tsaplina et al., 1991), *S. acidophilus* at 48°C (Norris et al., 1996), *S. thermosulfidooxidans* DSM 9293 at 45°C and *S. thermosulfidooxidans* VKM B-1269 at 50-55°C (Golovacheva and Karavaiko, 1978).

The effect of acidic pH such as 1.7, 2.2, and 3.0 was also studied and maximum growth was observed at pH 1.7 (Figure 2). The optimum pH for *S. thermosulfidooxidans* was observed between pH 1.9-2.4 as reported by Golovacheva and Karavaiko (1978). A similar report was described previously by Norris et al. (1996) about the presence of RuBisCo in *S. acidophilus* that were grown autotrophically at 45ºC on ferrous iron (50 mM) at pH 1.6. The acidic pH and high temperature tolerance seen in this strain contribute to the prevention of bacterial contamination when grown at an industrial scale.

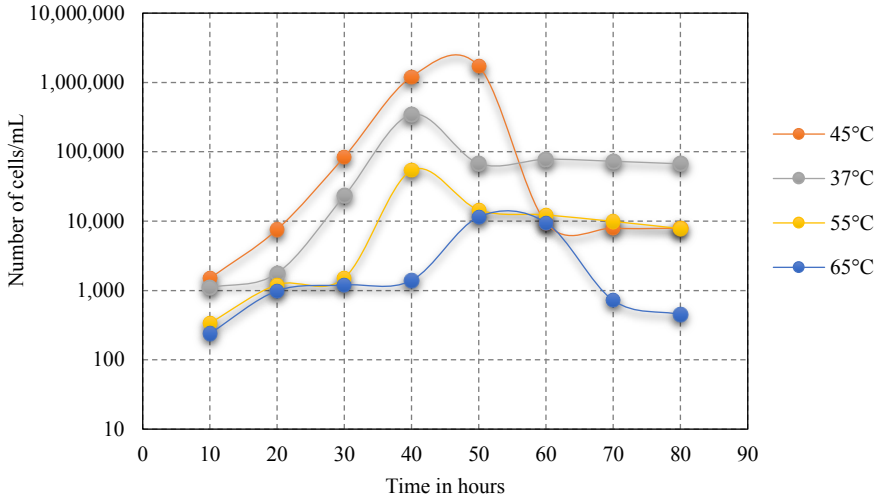

Figure 1. Growth of *Sulfobacillus acidophilus* strain NY-1in varying temperature

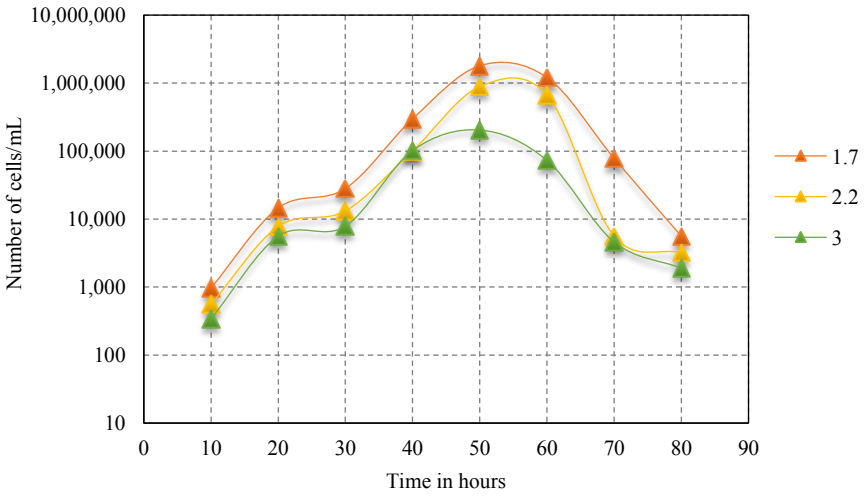

Figure 2. Growth of *Sulfobacillus acidophilus* strain NY-1 in varying pH of 1.7, 2.2, and 3.0

3.1.2 Effect of light and dark condition

The effect of light and dark condition on the growth of the strain was also studied. The maximum cell density was observed as 1.60×10^6 at the 60th hour of incubation for the strain NY-1 (Table 1). No growth was observed in dark condition which indicates that autotrophs require light for its growth. Light is also essential for RuBisCo activity as it was higher in light conditions than in dark conditions as reported by Wedel and Soll (1998). In contrast, in the absence of light *Ralstonia eutropha* was able to grow with CO_2 as its carbon source by utilizing the energy from H_2 oxidation.

3.1.3 Presence and absence of carbon dioxide

Environments where the oxygen concentration keeps changing are mainly dominated by chemolithotrophic sulphur and iron oxidizing bacteria. In acidic media enriched with metal ions, the solubility

of oxygen significantly reduces with increasing temperature. Therefore, the influence of carbon dioxide along with aeration was studied. An increase in the cell number was observed in the presence of carbon dioxide and the deposition of insoluble precipitates also increased. Comparative studies of the data showed that the cell density was higher, reaching a maximum of 2.72×10^6 cells/mL, in the presence of carbon dioxide than in its absence.

Table 1. Cell count enumeration in different conditions

Isolate	Growth rate at different conditions (number of cells/mL)	20 h	40 h	60 h	80 h	100 h	Growth rate at dark Condition
NY-1	Light condition	1.45×10^4	1.71×10^5	1.60×10^6	1.21×10^6	1.67×10^3	Nil-Absence of cells
	Presence of carbon dioxide	1.35×10^5	2.72×10^6	1.33×10^6	1.21×10^6	1.89×10^4	
	Absence of carbon dioxide	7.60×10^3	6.50×10^4	1.70×10^6	9.91×10^4	7.80×10^3	

3.2 Determination of cell count

One of main limitations in solid media cultivation of acidophiles such as *Sulfobacillus* sp. is that it cannot be cultivated in agar medium. Therefore, assessment of cell growth can be elucidated by cell count and spectrophotometric method. The FeSYE media is the most preferred media as it contains potassium tetrathionate and ferrous sulphate which areutilized as energy sources. The iron sulphur precipitate formation due to acidic pH was also reduced due to the buffering effect of this medium. In the spectrometric method, there is a possibility of enumerating both viable and non-viable cells. Moreover, the precipitate formed may also interfere with the results. In the case of cell counts, this limitation can be overcome by differentiating between viable and non-viable cells. Therefore, in the present study, cell count enumeration was also performed, even though it is a tedious process, by using the microscopic technique-Neubauer cell counter. (Table 2) In the microscopic method, trypan staining was carried out to differentiate viable cells from non-viable cells. Viable cells do not take up the stain and thus appear colourless, whereas dead cells take up the stain and appear blue in colour.

Table 2. Cell count determination by hemocytometeric and spectrophotometeric method

Sample name	Cell count by hemocytometer	Optical density at 478 nm	Cell viability (%)
NY-1	2.80×10^6	1.816	75.3

3.3 Assay of RuBisCo by ion exchange chromatography

After partial purification by dialysis overnight at 4°C the sample was loaded in Ion exchange chromatography column. This method was followed as it is a simple and cheaper method used to separate RuBisCo from the sample (Robinson et al., 1988). The equilibrium buffer $(NH_4)_2SO_4$ are generally used in ion exchange chromatography as it is capable of removing the endogenous inhibitors. In this chromatographic technique large volume protein samples can be used compared to other methods. Hence in the present study ion exchange chromatography was followed using ammonium sulphate buffer after dialysis of the crude extract.

The fractions were collected at regular time interval and absorbance was read at 280 nm. About 4 peaks were observed at 5th, 9th, 12th and 14th fraction. The curve obtained from ion exchange chromatography was compared with the RuBisCo obtained from spinach leaves. Out of these a highest peak was seen at the 9th fraction which was found to be RuBisCo on comparison with the standard. This was eluted at about 0.1 M of $(NH_4)_2SO_4$ with an A_{280} of 0.154 (Figure 3). The ratio of the absorbance at 280 nm and 260 nm was found to be 2.40 confirming the presence of proteins.

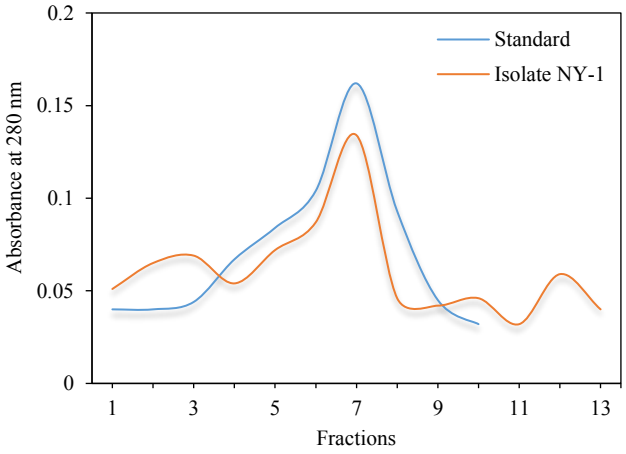

Figure 3. Ion exchange chromatogram of standard RuBisCo obtained from spinach and from the *Sulfobacillus acidophilus* strain NY-1

4. CONCLUSION

Due to global warming, the atmospheric temperature is constantly increasing, which is contributed by the rapid increase in carbon dioxide level. Scientists have been working to limit the increase in global temperature by not only diminishing the amount of carbon released into the environment, but also by disposing it. In this aspect, new findings such as carbon capture and sequestration have been followed. Carbon capture is a simple method in which the carbon emissions generated by many industries are trapped underground. The major drawback of this method is the chance of leakage in carbon pipes that may cause lethal damage to the environment. Carbon sequestration in biological systems is therefore becoming a suitable alternative. RuBisCo is an effective enzyme that sequesters carbon dioxide, but has low efficiency and is a heat labile protein. This protein is to a great degree a slow catalyst whose activity is mainly dependent on temperature. Therefore, in the present study, RuBisCo was extracted from the wild strain *Sulfobacillus acidophilus* NY-1 which has heat stable properties. Only a few reports on the presence of RuBisCo in gram positive acidophiles are available, hence this study may establish a framework for future studies to improve RuBisCo carbon sequestering efficiency.

ACKNOWLEDGEMENTS

The authors are grateful to Maulanaazad fellowship University grant Commission for financial support to carry out the research work.

REFERENCES

Andersson I, Knight S, Schneider G, Lindqvist Y, Lundqvist T, BraÈndeÂn CI, Lorimer GH. Crystal structure of the active site of Ribulose-Bisphosphate Carboxylase. Nature 1989; 337:229-34.

Caldwell PE, MacLean MR, Norris PR. Ribulose bisphosphate carboxylase activity and a Calvin cycle gene cluster in *Sulfobacillus* species. Microbiology 2007;153:2231-40.

Chakrabarty S, Bhattacharya S, Bhattacharya K. A nonradioactive assay method for determination of enzymatic activity of D-ribulose-1, 5-bisphosphate Carboxylase/Oxygenase (RuBisCo). Journal of Biochemical and Biophysical Methods 2002;52;179-87.

Chapman MS, Suh SW, Curmi PM, Cascio D, Smith WW, Eisenberg DS. Tertiary structure of plant RuBisCo: Domains and their contacts. Science 1988;241:71-4.

Delwiche CF, Palmer JD. Rampant horizontal transfer and duplication of RuBisCo genes in eubacteria and plastids. Molecular Biology and Evolution 1996;13:873-82.

Erb TJ, Zarzycki J. A short history of RuBisCo: the rise and fall of Nature's predominant CO_2 fixing enzyme. Current Opinion in Biotechnology 2018;49:100-7.

Fischer RA, Edmeades GO. Breeding and cereal yield progress. Crop Science 2010;50:85-98.

Golovacheva RS, Karavaiko GI. Sulfobacillus, a new genus of thermophilic sporulating bacteria. Mikrobiologiia 1978; 47(5):815-22.

Kaneda T. Iso- and ante-isofatty acids in bacteria: Biosynthesis, function, and taxonomic significance. Microbiological Reviews 1991;5:288-302.

Ken K, Norihiro M, Toshiaki F, Haruyuki A, Tadayuki I, Kunio M. Crystal structure of a novel-type archaeal RuBisCo with pentagonal symmetry. Structure 2001;9(6):473-81.

Ke-Quing X, Peng B, Qiong-Li B, Yan J, Fu-Yi H, Jian-Qiang S, Yong-Guan Z. Quantitative analyses of ribulose-1, 5-bisphosphate Carboxylase/Oxygenase (RuBisCo) large-subunit genes (cbbL) in typical paddy soils. Federation of European Microbiological Societies Microbiology Ecology 2014;87:89-101.

Liben J, Andrew SP, Craig TW, Rusdy H. Current development of carbon capture and storage in the UK: A non-technical review. International Journal of Low-Carbon Technologies 2012; 8(4):225-9.

Maryshamya A, Rajasekar T, Rengasamy R. Carbon sequestration potential of *Scenedesmus quadricauda* (Turpin) and evaluation on Zebrafish (*Danio rerio*). Aquaculture Reports 2019;13:178-84.

Meenakshi S, Srisudha S. *In silico* characterization and homology modeling of cyanobacterial RuBisCo (LS) with computational tools and bioinformatic servers. Helix 2012;4:185-91.

Nakagawa H, Sugimoto M, Kai Y, Harada S, Miki K, Kasai N. Preliminary crystallographic study of a ribulose-1, 5-bisphosphate Carboxylase Oxygenase from *Chromatium vinosum*. Journal of Molecular Biology 1986;191:577-8.

Newman J, Gutteridge S. Structure of an effector-induced inactivated state of ribulose-1, 5-bisphosphate Carboxylase/ Oxygenase: the binary complex between enzyme and xylulose 1, 5-bisphosphate. Structure 1994;2:495-502.

Norris PA, Clark DA, Owen JP, Waterhouse S. Characteristics of *Sulfobacillus acidophilus* sp. nov. and other moderately thermophilic mineral-sulphide-oxidizing bacteria. Microbiology 1996;142:775-83.

O'Donnelly K, Zhao G, Patel P, Butt MS, Mak LH, Kretschmer S, et al. Isolation and kinetic characterisation of hydrophobically distinct populations of form I Rubisco. Plant Methods 2014;10:17.

Portis A, Parry M. Discoveries in RuBisCo (Ribulose 1, 5-bisphosphate Carboxylase/Oxygenase): A historical perspective. Photosynthesis Research 2007;94:121-43.

Robinson SP, Streusand VJ, Chatfield JM, Portis AR. Purification and assay of rubisco activase from leaves. Plant Physiology 1988;88(4):1008-14.

Sage RF, Way DA, Kubien DS. Rubisco, Rubisco activase, and global climate change. Journal of Experimental Botany 2008;59(7):1581-95.

Schneider G, Lindqvist Y, Lundqvist T. Crystallographic renement and structure of Ribulose-1,5-bisphosphate Carboxylase from *Rhodospirillum rubrum* at 1.7 Å resolution. Journal of Molecular Biology 1990;211(4):989-1008.

Shibata N, Yamamoto H, Inoue T, Uemura K, Yokota A, Kai Y. Crystallization and preliminary crystallographic studies of ribulose-1,5-bisphosphate Carboxylase/Oxygenase from a red

alga, *Galdieria partita*, with a high specificity factor. Journal of Biochemistry 1996;120:1064-6.

Tominaga J, Takahashi S, Sakamoto A, Shimada H. Arabidopsis BSD2 reveals a novel redox regulation of RuBisCo physiology *in vivo*. Plant Signaling and Behavior 2020;15(4):873-6.

Tsaplina IA, Bogdanova TI, Sayakin DD, Karavaiko GI. Effects of organic substances on the growth of *Sulfobacillus thermosulfidooxidans* and pyrite oxidation. Mikrobiologiya 1991;60:686-92.

Watling HR, Perrot FA, Shiers DW. Comparison of selected characteristics of *Sulfobacillus* species and review of their occurrence in acidic and bioleaching environments. Hydrometallurgy 2008;93:57-65.

Watson GM, Tabita FR. Microbial Ribulose 1, 5-bisphosphate Carboxylase/Oxygenase: A molecule for phylogenetic and enzymological investigation. Federation of European Microbiological Societies Microbiology Letters 1997;146: 13-22.

Wedel N, Soll J. Evolutionary conserved light regulation of Calvin cycle activity by NADPH-mediated reversible phosphoribulokinase/CP12/glyceraldehyde-3-phosphate dehydrogenase complex dissociation. Proceedings of the National Academy of Sciences of the United States of America 1998;95(16):9699-704.

Preliminary Assessment of Air During COVID-19 Lockdown: An Unintended Benefit to Environment

Shazia Pervaiz[1*], Kanwal Javid[2], Filza Zafar Khan[3], Younis Zahid[1], and Muhammad Ameer Nawaz Akram[4]

[1]Environmental Protection Agency, Punjab, Pakistan
[2]Department of Geography, University of the Punjab, Lahore, Pakistan
[3]Pakistan Council of Scientific and Industrial Research Laboratories Complex, Lahore, Pakistan
[4]Laboratory of Information Engineering in Surveying, Mapping and Remote Sensing, Wuhan University, China

ARTICLE INFO

Received: 14 May 2020
Received in revised: 12 Jul 2020
Accepted: 22 Jul 2020
Published online: 11 Aug 2020
DOI: 10.32526/ennrj.18.4.2020.35

Keywords:
Air SDGs/ Coronavirus and air pollution/ COVID-19 and SDGs/ Lahore air quality index

*** Corresponding author:**
E-mail: shaziapervaiz@gmail.com

ABSTRACT

The death rate of people is increasing globally during the current outbreak of coronavirus. To combat with COVID-19 havoc, the world has adopted lockdown policies, including Pakistan. Ironically, the invisible virus is suffocating humans at a fast rate but on the other side, there is a visible monster in the world gobbling up human health, i.e., air pollution. Therefore, the main rationale of the present research is to visualize the air quality during the 'Lockdown' period in Lahore, Pakistan by mapping via online tools and techniques using a geospatial system. According to the present findings, the concentrations of air pollutants, such as particulate matters (PM_{10} and $PM_{2.5}$), nitrogen oxides as NO and NO_2, and sulphur dioxide, are below the maximum permissible levels of the Punjab Environmental Quality standards (PEQs), although ozone exceeds its PEQs. So in light of the results, once this COVID-19 crisis is over, the government should speed up measures to lessen air pollution to achieve targets of sustainable development goals (SDGs). Moreover, the present results of air assessment during COVID-19 would serve as a useful reminder for the government of Punjab to cut down air emission levels after the pandemic.

1. INTRODUCTION

In Pakistan, the first coronavirus case was reported in Lahore on 26th February, 2020 (Badshah et al., 2020) and cases spurted rapidly all over Pakistan within a short span of time (Saqlain et al., 2020). All provinces of Pakistan were affected by COVID-19 (Ahmad et al., 2020) and amongst them Sindh was the most vulnerable province reported with the largest number of coronavirus cases initially (Waris et al., 2020). In the meantime, the wide spread of deadly disease suspended all the religious, academic, social, and administrative activities at international levels (Chauhan and Singh, 2020).

During COVID-19 pandemic, the world faced its highest mortality rate, but on the other side, it proved to be a significant factor in the reduction of air emissions by altering anthropogenic activities. It is the one and only virus that demonstrated a new era to get rid of all the preceding impossible environmental problems in a possible way. As per early published statistics, Pakistan's neighboring country China reported the highest death rate (Saqlain et al., 2020). Meanwhile, a significant reduction in nitrogen dioxide was also reported during COVID-19 in China (Wang et al., 2020). Similarly, a decline in air pollution was also reported in Italy, which is one of the countries in the world most affected by COVID-19 (Gatto et al., 2020).

Hence, air pollution is one of the serious threats (Gupta et al., 2013) to life diversity and is reported as a factor for the high fatality due to COVID-19 in Italy (Ogen, 2020). Its destructive nature has detrimental effects on humans, animals (Camargo and Alonso, 2006) and plants (Najjar, 2011). Ecologically, it damages the quality of water and soil (Mellouki et al., 2016). Further, its toxicology is one of the causes of

Citation: Pervaiz S, Javid K, Khan FZ, Zahid Y, Akram MAN. Preliminary assessment of air during COVID-19 lockdown: An unintended benefit to environment. Environ. Nat. Resour. J. 2020;18(4):363-375. (https://doi.org/10.32526/ennrj.18.4.2020.35)

acid rain and temperature inversion (Singh and Agrawal, 2007). Likewise, the escalating global concern is one of the largest environmental problems in Pakistan (Ali and Athar, 2008; Colbeck et al., 2011). In 2018, Pakistan ranked 169 out of 180 countries in the Environmental Performance Index (EPI) (Pakistan Today, 2020), even though its environmental sector is highly prioritized to achieve SDGs (Elder and Olsen, 2019).

Given above the planetary scenario of air pollution, the highest concentration of atmospheric pollutants (Mansha et al., 2012) were reported at an alarming level in Lahore (Colbeck et al., 2019), namely particulate matter $PM_{2.5}$ (Rasheed et al., 2015) and PM_{10} (Stone et al., 2010). As a result, the consequences of air pollution have led to poor health issues (Ashraf et al., 2019) in the city. Despite the fact that environmental legislations, rules and regulations have been formulated in Punjab, Pakistan to control the air pollution, the environmental development is at a noticeably poor level under EPI.

So with respect to the COVID-19 lockdown plan to overcome the pandemic in the city, the contingency plan altered the existing air quality of Lahore. Considering the above scenario, the aim of the present study is to provide a bird's eye view of air quality during COVID-19 lockdown. So, the objectives of the present study are three fold: (1) to map the air pollution level in Lahore during lockdown of COVID-19; (2) to review the air pollution level in 2019 and compare its concentration with the lockdown period of 2020; (3) to evaluate the key air pollutant concentrations in the lockdown period. Thus, findings of the present study provide updated information of air quality during the COVID-19 lockdown. Further, this information can be used to prepare alternative strategies to mitigate the air pollutants to improve the environment of urban areas.

2. METHODOLOGY

2.1 Site description

Lahore, a well-known historical and cultural city of gardens (Ghaffar, 2015; Pervaiz et al., 2019), was chosen to carry out the present study. Lahore is located in the north-east of Punjab. Neighboring country, India lies on the east of Lahore (Lodhi et al., 2009; Akhtar et al., 2015) and linked with the Indian state of Punjab (Tariq and Ali, 2016). District Sheikhupura is located on the North West of the city, Kasur on the south and River Ravi flows in the north (Riaz, 2010). Geo-spatially, the city is situated between 31°15′-31°45′ North, 74°01′74°39′ East (Colbeck et al., 2011) and consists of 1,172 km^2 land surface area (Figure 1).

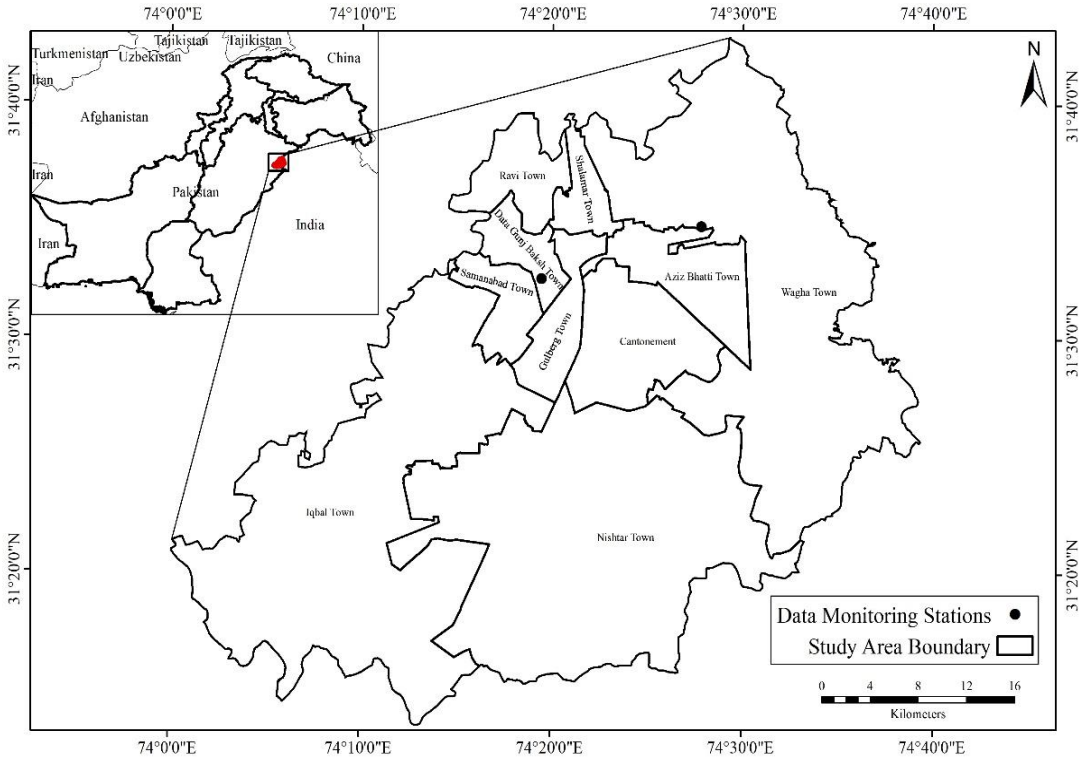

Figure 1. Map of the study area

2.2 Demography

Lahore (Nawaz et al., 2015) is among the mega cities of the world and the second largest metropolis of the country. The population of the city has grown very rapidly during the past decades (Jan and Iqbal, 2008; Aziz et al., 2015) and having 11 million dwellers (Ali et al., 2020) in 2017 (Pakistan Bureau of Statistics, 2017).

2.3 Climate

Lahore has a semi-arid climate (Batool and Ch, 2009; Ali et al., 2020) where extreme and intense weather conditions are observed during different seasons. Lahore experiences summer (April to June with the average temperature above 40°C (Rana and Bhatti, 2018). Whereas, monsoon season (July to September) is associated with heavy rainfalls. December to February is the months of winter with dense fog when temperature falls at low level i.e., 0°C (Alam et al., 2013). Moreover, metrological variables (Kinney, 2008) vary seasonally such as precipitation, temperature, humidity, wind velocity and speed (Sadiq and Qureshi, 2010) which determine the quality of air (Table 1).

Table 1. Metrology of study area in March 2019 and March 2020

March	Wind speed (knot) 300 UTC		Wind speed (knot) 1,200 UTC		Rain (mm)		Min. Temp. (°C)		Max. Temp (°C)		Humidity (%) 300 UTC		Humidity (%) 1,200 UTC	
	2019	2020	2019	2020	2019	2020	2019	2020	2019	2020	2019	2020	2019	2020
20	11	0	7	3	0	0	14	15	29	29	74	78	47	41
21	3	11	8	4	TR	TR	14	16	26	29	74	76	39	54
22	5	0	9	3	0	0	14	14	27	26	71	75	29	42
23	7	0	14	0	0	0	16	15	28	29	55	63	36	25
24	4	0	7	4	TR	TR	14	18	25	31	70	61	59	61
25	5	4	6	3	0	4	14	14	26	22	84	77	38	51
26	5	6	13	4	0	0	13	13	29	26	68	51	27	51
27	0	5	4	12	0	6.4	15	16	29	28	80	95	33	85
28	0	6	5	5	0	14	17	14	31	20	65	89	32	57
29	3	4	4	3	0	0	18	14	32	26	82	81	41	38
30	6	5	12	9	0	0	19	15	33	29	82	60	40	37
31	0	8	10	3	0	0	17	17	32	27	68	63	31	86
Max.	11	11	14	12	-	14	19	18	33	31	84	95	59	86
Min.	0	0	4	0	-	0	13	13	25	20	55	51	27	25
Avg.	4.1	4.1	8.3	4.4	-	2.4	15	15	29	27	73	72	38	52

*TR=0.01 mm

2.4 Environmental overview

Environmentally, the city of gardens 'Lahore' has been converted into the city of concrete in the past three decades. Urban sprawl (Liaqat et al., 2017; Sabir and Anjum, 2017), economic development (Pervaiz et al., 2019), industrial expansion (Raja et al., 2010; Rehman et al., 2019) vehicular emissions (Ilyas, 2007; Shirwani et al., 2019; Ali et al., 2020) and biomass burnings (Sidra et al., 2015; Abas et al., 2019) are the variety of sources deteriorating the natural environment (Pervaiz et al., 2019) of the city. On the top, semi-arid climate of the city strongly supports to accumulate the air pollutants in the atmosphere (Shahid et al., 2013). Thus, the city is vulnerable by having air borne diseases (Aziz and Bajwa, 2007; Raja et al., 2010) caused by the combination of multiple pollutants. Besides, the pernicious air pollution has been also reported to elevate the death rate during the outbreak of COVID-19 (Wang et al., 2020). On the basis of above discussion, Table 2 lists the air pollutants defined in PEQs, their prescribed limit and the impacts on the environment of Lahore.

2.5 Data

The present study relied on the data derived from the official website of Environment Protection Department (EPD), Punjab to examine and compare the pollutant concentrations of the study site in March 2019 and during the COVID-19 lockdown (Figure 2 and Figure 3), (EPD, 2020a). Further, the Punjab Environmental Quality Standards (PEQs) for air

(Table 2) were also obtained from the official source of EPD, Punjab (EPD, 2020b).

In addition, considering that meteorological elements are closely associated with air pollution (Yen et al., 2013) the city level data of weather consisting of wind speed (300 and 1,200 Knot), rain (millimeter per hour), temperature (degree Celsius), and humidity (300 UTC and 1,200 UTC) (Bao and Zhang, 2020) was obtained from Pakistan Meteorological Department for the analysis (Table 1).

Table 2. Air pollutants source, environmental effects and PEQs

Sr. No.	Pollutant	Source	Environmental effect	PEQs
1	Particulate matter (PM_{10})	Diesel-powered vehicles; Factories; Power plants; Industries; Incinerators; Construction activities; Windblown dust. (Mabahwi et al., 2014).	Major source of haze; Damages buildings and other materials.	150 µg/m^3
2	Particulate matter ($PM_{2.5}$)	Transportation; Combustion of fossil fuels; Biomass and waste burnings; Construction sites. (Malashock et al., 2018).	Same effects as PM_{10}. (Zha et al., 2013).	35 µg/m^3
3	Nitrogen oxides as (NO)	Motor vehicles; Emissions from the industrial and domestic fossil fuels; (Cheng et al., 2012).	Acid rain; Smog; Damages buildings; Destroys vegetation growth. (Najjar, 2011).	40 µg/m^3
4	Nitrogen oxides as (NO_2)	Fuel combustion (gasoline, coal or oil); Automobile emissions. (Barone-Adesi et al., 2015)	Acid rain; Smog; Deleterious to the cell membrane of plants; Deplete soil fertility. (Chen et al., 2007).	80 µg/m^3
5	Sulphur dioxide (SO_2)	Mining and quarrying; Manufacturing of chemicals; Petroleum refineries; Metal industries; Power generation; Transportation; Community services; Industries;Brick kilns; Combustion of coal and oil. (Haider et al., 2017)	Haze; Formation of acid rain; Damages vegetative growth; Deteriorates surface water and soil by increasing acidification; Corrodes buildings and monuments.	120 µg/m^3
6	Ozone (O_3)	Secondary pollutant formed by chemical reaction of VOCs and NOx in the presence of sunlight. (Guo et al., 2019).	Smog; Damages rubber, fabric and other materials; Reduces plants growth and yield (Munzi et al., 2017).	130 µg/m^3

2.6 Air quality index (AQI)

AQI (Tiwari and Ali, 1987) is based on the concentration values using six key pollutants including Nitrogen Oxides as NO_2 and NO, O_3, $PM_{2.5}$, PM_{10} and SO_2 (Table 2) and calculated according to the following Equation:

$$AQI = NO_2+NO+O_3+PM_{2.5}+PM_{10}+SO_2/6$$

2.7 Data analysis

In order to determine the results, the geospatial technique (Javid et al., 2020) is adopted to analyze and compare the AQI (Chattopadhyay et al., 2010) using six key criteria pollutants. Moreover, the metrological factors were also evaluated by using the minimum, maximum and average criteria.

3. RESULTS AND DISCUSSION

3.1 Air quality index and metrology of Lahore in March 2019 and March 2020

In order to achieve objectives of the study, the AQI was encompassed and classified on six criteria pollutants to analyze the air pollution level during COVID-19 lockdown and compared with the period of March, 2019. Table 2 describes the PEQs level and the Figures 2 and 3 summarizes the results and supports the similar findings which were observed in India (Gautam, 2020). According to Table 2 and Figure 3, the concentration levels of air pollutants in the study area

were below the maximum permissible levels of PEQs in March, 2020, except the northwestern part of Lahore. Moreover, the overall air quality of other towns has also improved significantly during lockdown like other neighboring countries of Pakistan such as India (Mitra et al., 2020) and China (Xu et al., 2020).

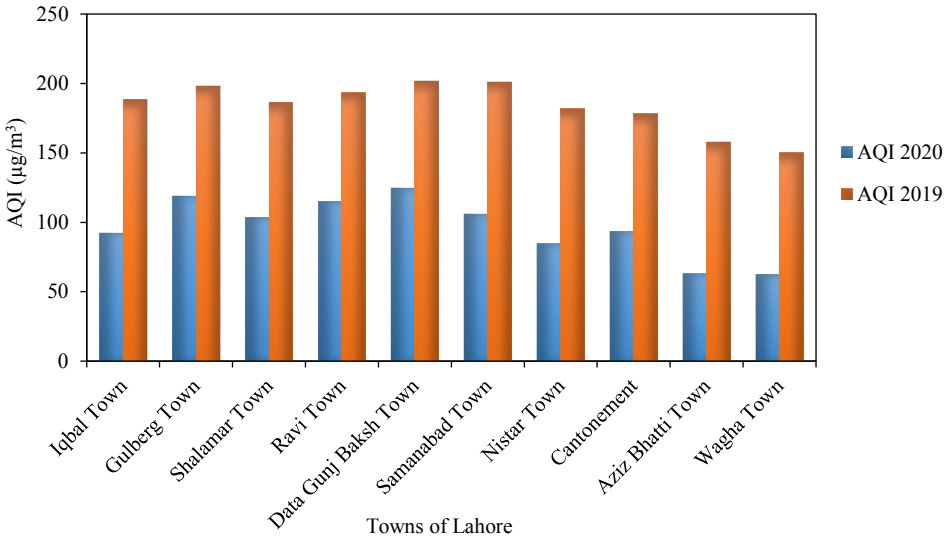

Figure 2. Air quality index level of Lahore in March 2019 and March 2020

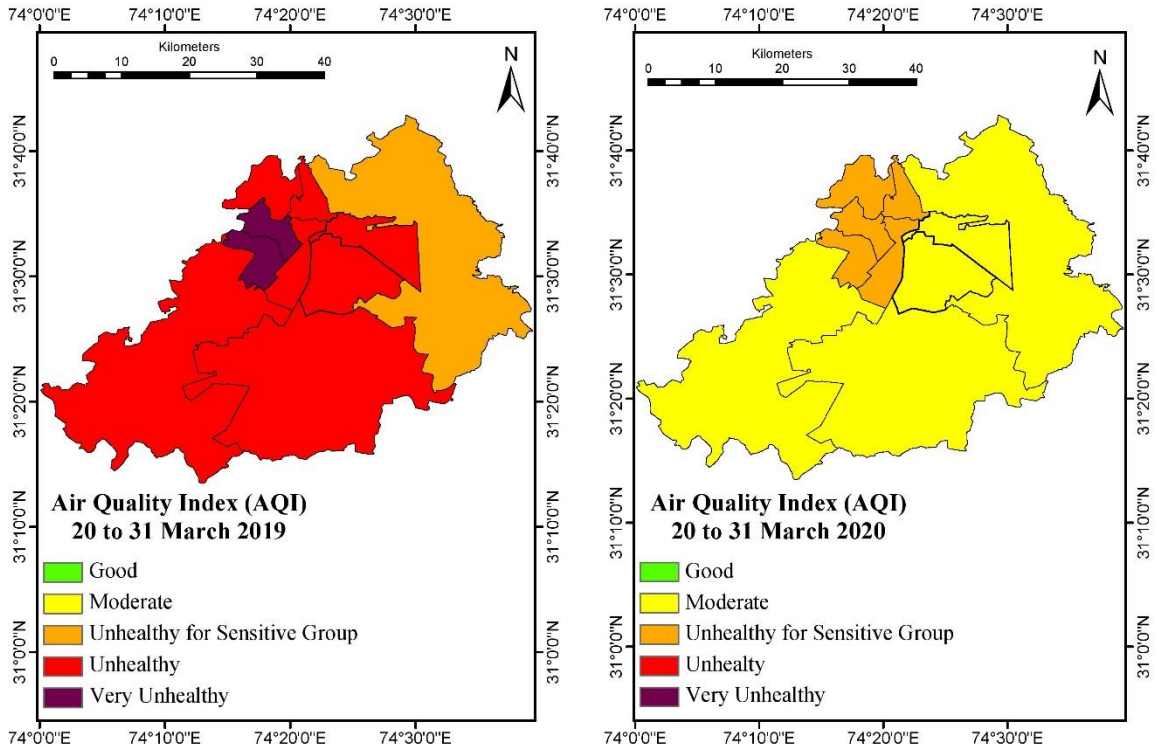

Figure 3. Air quality index of Lahore in March 2019 and March 2020
(The studies conducted by Kambalagere (2020), Ramasamy (2020), Isaifan (2020), Zambrano-Monserrate et al. (2020) supported the above results globally during COVID-19.)

On the other hand, rain showers reduced the concentration of air pollutants during the lockdown. So, the recorded 22ºC average temperature (Bao and Zhang, 2020) and the average rainfall (2.4 mm) had a strong influence on the state of air in March 2020 (Table 1).

Furthermore, analyzing the results (Figure 3), it is recorded that the air quality index has dropped from

188 to 92 in Iqbal Town (IT), 198 to 118 in Gulberg Town (GT), 186 to 103 in Shalamar Town (ST), 193 to 114 in Ravi Town (RT), 201 to 124 in Data Gunj Baksh Town (GBT), 200 to 105 in Samanabad Town (SBT), 181 to 84 in Nishtar Town (NT), 157 to 63 in Aziz Bhatti Town (ABT) and 194 to 62 in Wagha Town (WT) and 178.25 to 93.50 in Cantonment (Cantt) area. In contrast, the ground based measurements of air pollutants exhibited on the south-eastern and north-western side of Lahore experienced the highest concentrations of air pollution and did not meet PEQs in March 2019. Extraordinarily high concentrations of air pollution in these parts of Lahore are mainly due to the industrial estates, small and medium industrial units, vehicular fumes and burning trash.

3.2 NO_2 assessment in March 2019 and March 2020

Based upon the results of NO_2 level in March 2019 and 2020 (Figure 4) it was reflected that the highest trends of air pollutant in terms of NO_2 were found in Ravi Town (RT), Shalamar Town (ST), Data Gunj Baksh Town (DGBT) and Samanabad Town (SBT). This is attributed to the industrial and population density in all towns that have increased the levels of toxic air pollution. On the other side, during lockdown a huge demand of home delivery has suddenly increased for groceries, food, household and medical items which accelerates the NO_2 values. Furthermore, in crowded areas stay-at-home policy was not followed strictly. So, the high concentration of NO_2 can be attributed due to the non-seriousness of the people towards social distancing which is also reported in the study of Dantas et al. (2020). Similarly, another reason is the operational movement of heavy duty vehicles (HDV) used to transport food in the market during lockdown. Additionally, the combustion of fuels in industries may also have increased the trend of NO_2 as the towns of Lahore have big industrial network and diesel based vehicles are common in the city. Apart from that, the nitrogen in the air compresses at high temperature and reacts with oxygen in the combustion chambers of gasoline and diesel driven vehicles and emits NOx. That is why no significant drop in NO_2 emissions has been recorded and supports the similar results of a previous study (Goyal et al., 2006). Moreover, the previous study of Jafary and Faridi (2006) has also reported the highest concentration of NO_2 in one of the crowded towns of Lahore i.e., Samanabad. Moreover, the similar result of the present study is also reported during the lockdown period in the capital city of Iran (Bauwens et al., 2020). Additionally, considering the results of other towns the NO_2 values has declined during lockdown and presents the improvement in air quality. Therefore, in support of this result, several studies have been reported globally (Aloi et al., 2020; Bao and Zhang, 2020; Bashir et al., 2020; Kerimray et al., 2020; Kaplan and Avdan, 2020; İban, 2020).

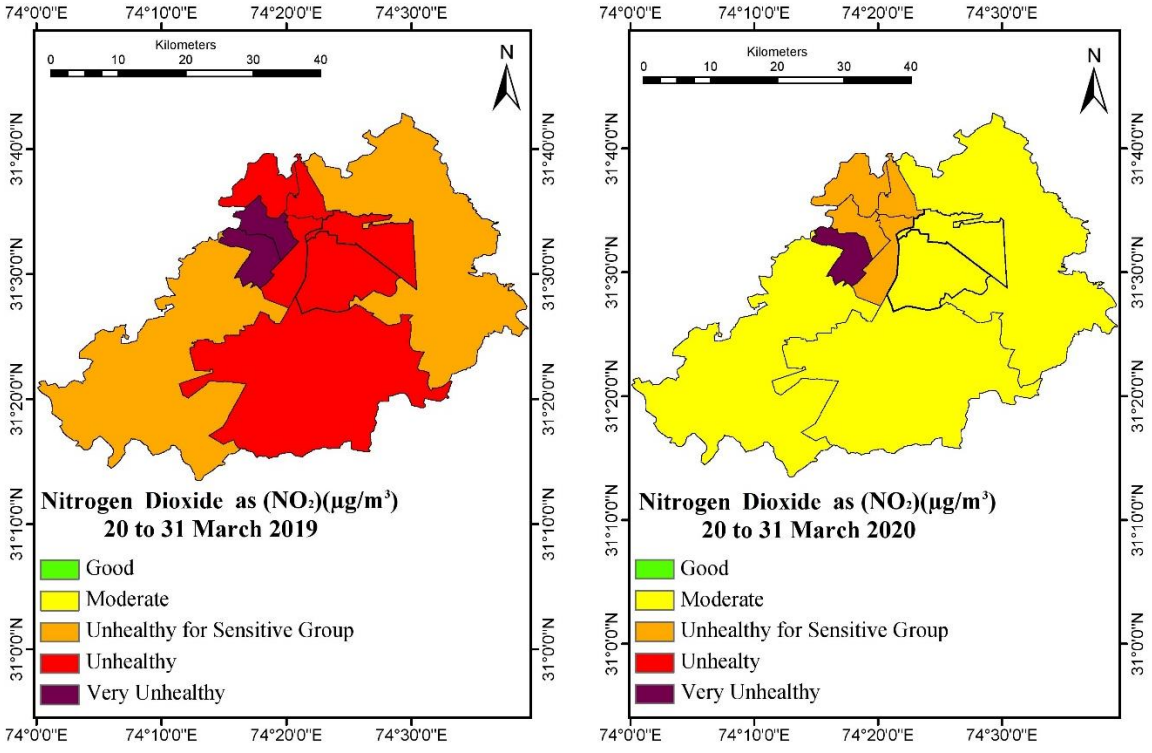

Figure 4. NO_2 level of Lahore in March 2019 and March 2020

3.3 NO assessment in March 2019 and March 2020

According to Figure 5, the air quality index classes have shown reduction in the NO level during March 2020 when the lockdown came into effect. Based on the results of Figure 5, the urban air quality of Lahore has exhibited good air quality index level in Nishtar Town (NT), Iqbal Town (IT), Samanabad Town (SBT). While in Wagha Town (WT), air quality index was recorded as moderate under and displayed similar trends as in 2019. Moreover, Gulberg Town (GT) showed an unhealthy air quality index which is one of the largest hubs of industrial estates of Lahore and located in the north-western part of the city. Further, the highest values of air quality index (hazardous) have been recorded in the Ravi and Data Gunj buksh Towns. Basically, the hazardous level of air quality index is associated with the burning of substandard fuel commercially. In addition, the Lahore's air pollutants are the compound results of industrial and vehicular emissions with the inclusion of metrological elements (Table 2). So, the concentration level of NO is relatively unhealthy for sensitive group in 2019 and supports the similar findings of earlier study (Gorai et al., 2015). However, the overall results indicate that air quality index has improved in few towns of Lahore due to the closure of anthropogenic activities.

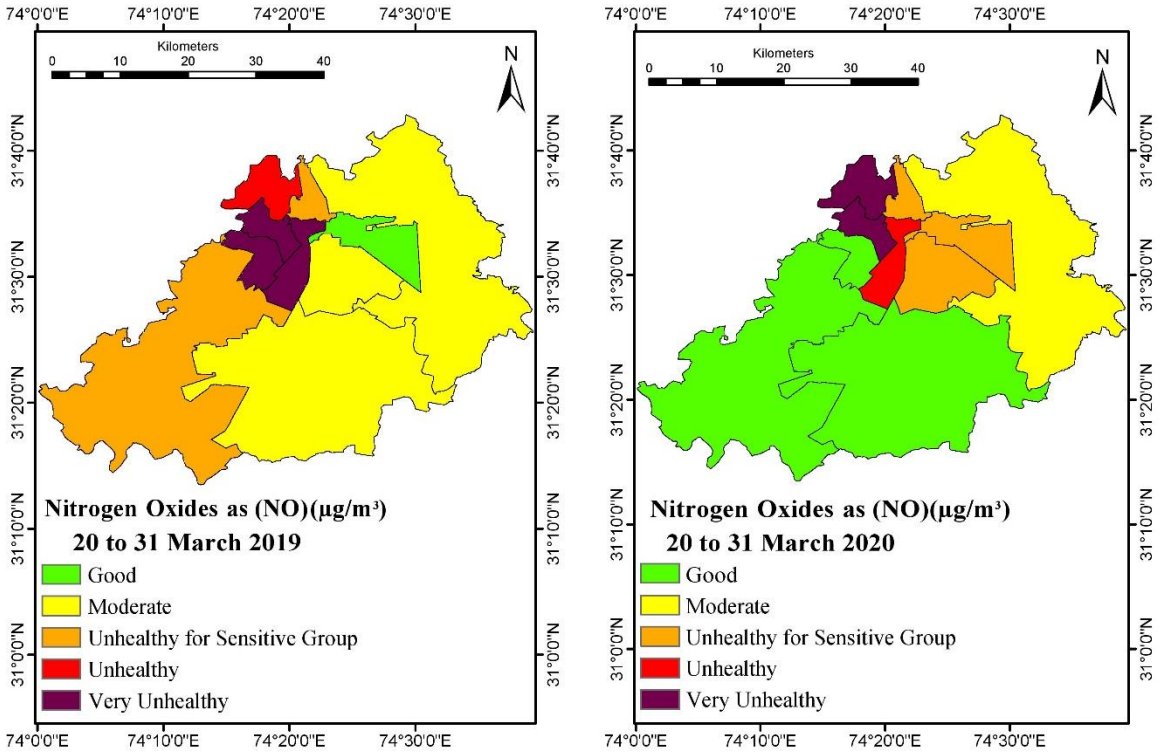

Figure 5. NO level of Lahore in March 2019 and March 2020

3.4 O_3 assessment in March 2019 and March 2020

Figure 6 exhibits the mean concentration level of O_3 in Lahore in March 2019 and the lockdown period of March 2020. In comparison with the results of 2019, the overall situation in terms of O_3 in 2020 was recorded at unhealthy to hazardous levels. Basically, a rise in O_3 usually occurs when the NO level decreases (Quan et al., 2014). In the present case of COVID-19 lockdown, the O_3 mean concentration level rose compared to 2019, which supports the findings of the study conducted by Dantas et al. (2020). Thus, in the current lockdown, the highest concentration of O_3 (unhealthy) was recorded in Iqbal Town (IT) and Shalamar Town (ST). Moreover, the hazardous level of ozone has been recorded in Gulberg Town (GT), Samanabad Town (SBT) and Data Gunj Buksh Town (DBT). Thus analyzing Figure 5, the lower NO concentration helped to increase the concentration of O_3 and supported the results of the study conducted in Italy during lockdown (Collivignarelli et al., 2020).

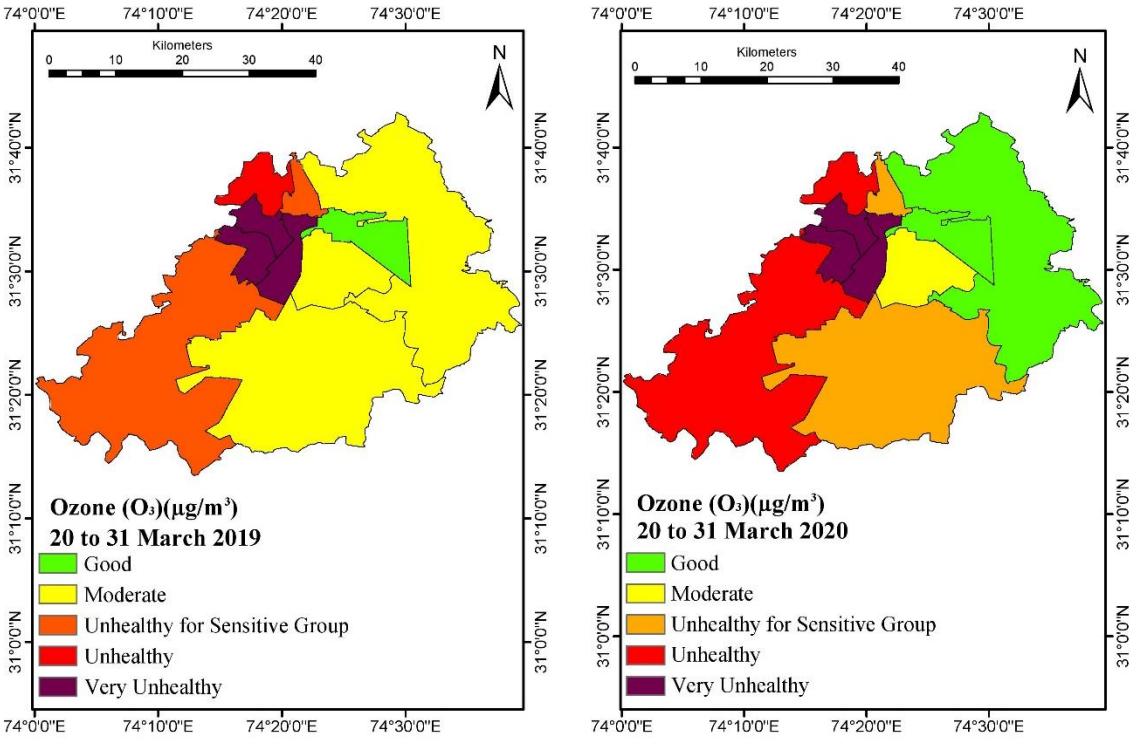

Figure 6. O_3 level of Lahore in March 2019 and 2020

3.5 $PM_{2.5}$ assessment in March 2019 and March 2020

According to Figure 7, $PM_{2.5}$ mean concentration level has dropped from unhealthy to moderate level during lockdown as compared to the last year data. Further, it is evident from results that eight out of nine towns have a moderate range of $PM_{2.5}$. This is because the main social and economic restrictions were enforced during the lockdown period. Similarly, not only the noticeable fall of $PM_{2.5}$ concentration was witnessed in Lahore, but also recorded in the several cities of India during the precautionary measures of COVID-19 (Sharma et al., 2020). Further, the results of Figure 7 also state that $PM_{2.5}$ concentration is inconsistent all over the Lahore in 2019 due to the operational sources of air pollutants such as commercial, industrial and transportation. On the other side, metrological variables of 2019 were also the leading cause to elevate the concentration of air pollution which is documented in the study of EEA (2020). Hence, the significant reduction in $PM_{2.5}$ encourages and motivates us to mitigate unnecessary social activities to avoid the havoc of air pollution and get a chance to breathe in the clean air.

3.6 PM_{10} assessment in March 2019 and March 2020

PM_{10} is well documented for the disastrous health effects on urban dwellers. In addition, with the combination of coronavirus, the pollutant became adverse for human life in metropolitan cities. Similarly, Lahore is the leading city of Pakistan which experiences the worst air pollution level and also choked in pandemic. But the adopted control measures of COVID-19 have improved the air quality of Lahore within a short period. Conversely from $PM_{2.5}$, notable reduction was recorded in PM_{10} during lockdown period (Figure 8). Moreover, the similar results of PM_{10} reduction are also reported in the current study conducted in Delhi, India during lockdown (Mahato et al., 2020). Nevertheless, the basic reasons behind the moderate tendency of PM_{10} levels are the closure of construction sites, economic and social activities during the pandemic. Closing these dominant sources of air pollutants in towns such as Lahore improved the AQI, i.e., good to moderate. In addition, another study of Otmani et al. (2020) also reported the similar results in the wake of lockdown. Overall, after comparison with 2019, it is exhibited that the moderate level of PM_{10} is measured throughout the study period which is also attributed with the metrological conditions. Thus, the minimal level of PM_{10} is clear evidence that Lahore can achieve its emissions reduction targets by adopting concrete measures to avoid air borne diseases.

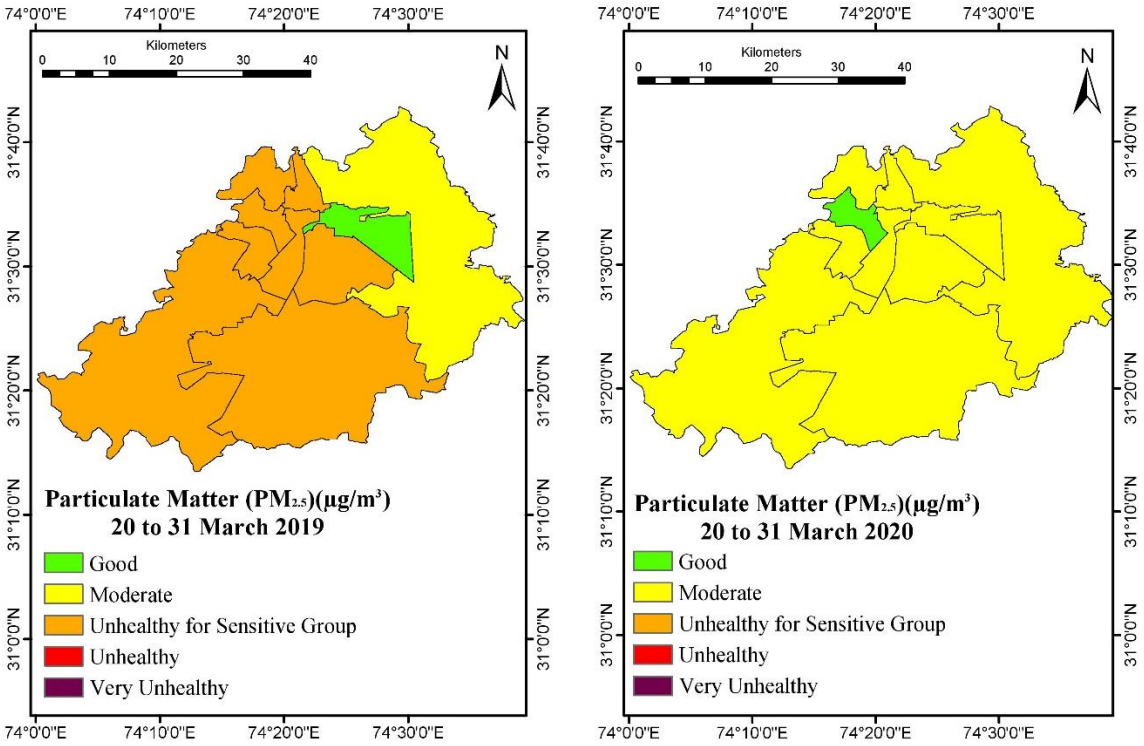

Figure 7. $PM_{2.5}$ level of Lahore in March 2019 and 2020

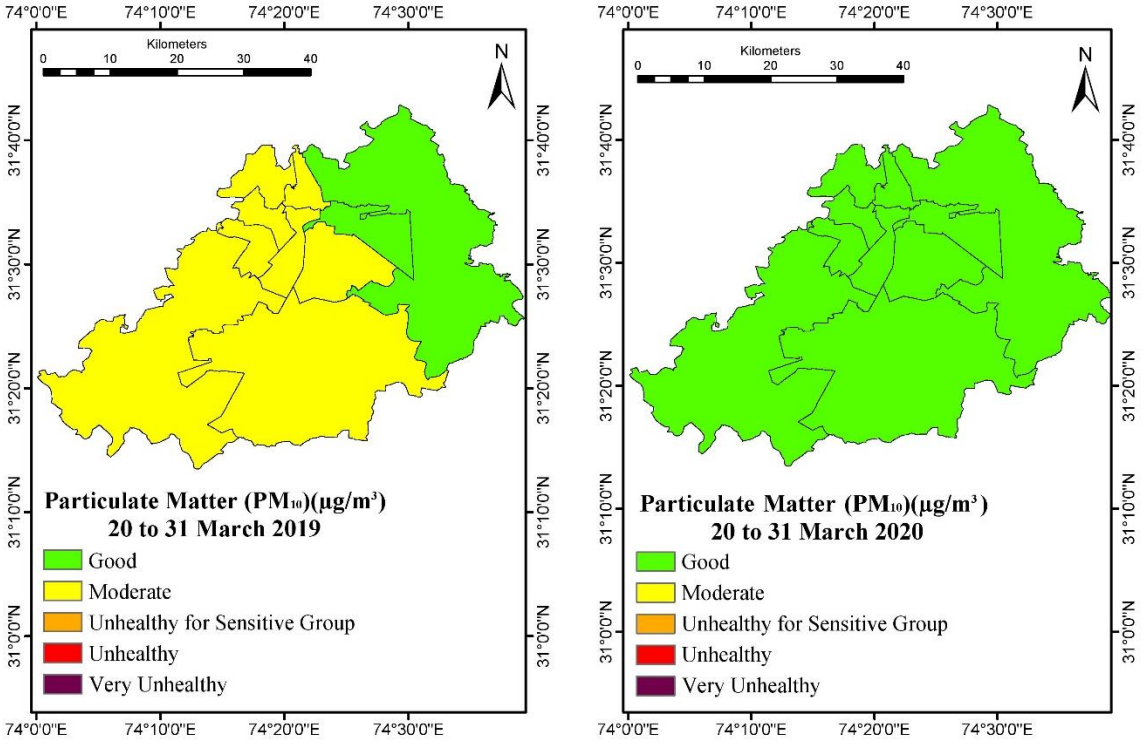

Figure 8. PM_{10} Level of Lahore in March 2019 and March 2020

3.7 SO_2 assessment in March 2019 and March 2020

SO_2 is one of the leading pollutants that are infamous for smog and their presence in the air is highly poisonous for the respiratory system of humans. Notably, since 2016 Lahore is experiencing its worst episode of smog during October to February. During February, when the city was facing the havoc of smog, the fatal pandemic broke out. In this regard, the adopted contingency measures to overcome pandemic has altered the concentration level of air pollutants and resulted in a significant reduction of SO_2 range in Lahore. Thus, according to the present

findings (Figure 9), the concentration level of SO_2 is recorded under the maximum prescribed limit of PEQs. This may be attributed to major SO_2 emitting industries being non-functional during the pandemic lockdown. Besides, the metrological aspect in terms of scattered rains has also improved the quality of air in a short span of time (Table 1). So, the overall air quality index in all towns of Lahore is remarkably visible under the category of 'Good'. Further, comparing results with 2019, the SO_2 levels were also under the permissible level of Punjab's ambient air quality standards and categorized in good to moderate in all towns. But in 2020, the AQI range of SO_2 is improved and associated with the suspension of industrial activities (Otmani et al., 2020) and attributed with the frequent rainfall which cleaned the air during coronavirus lockdown (Kapil, 2020).

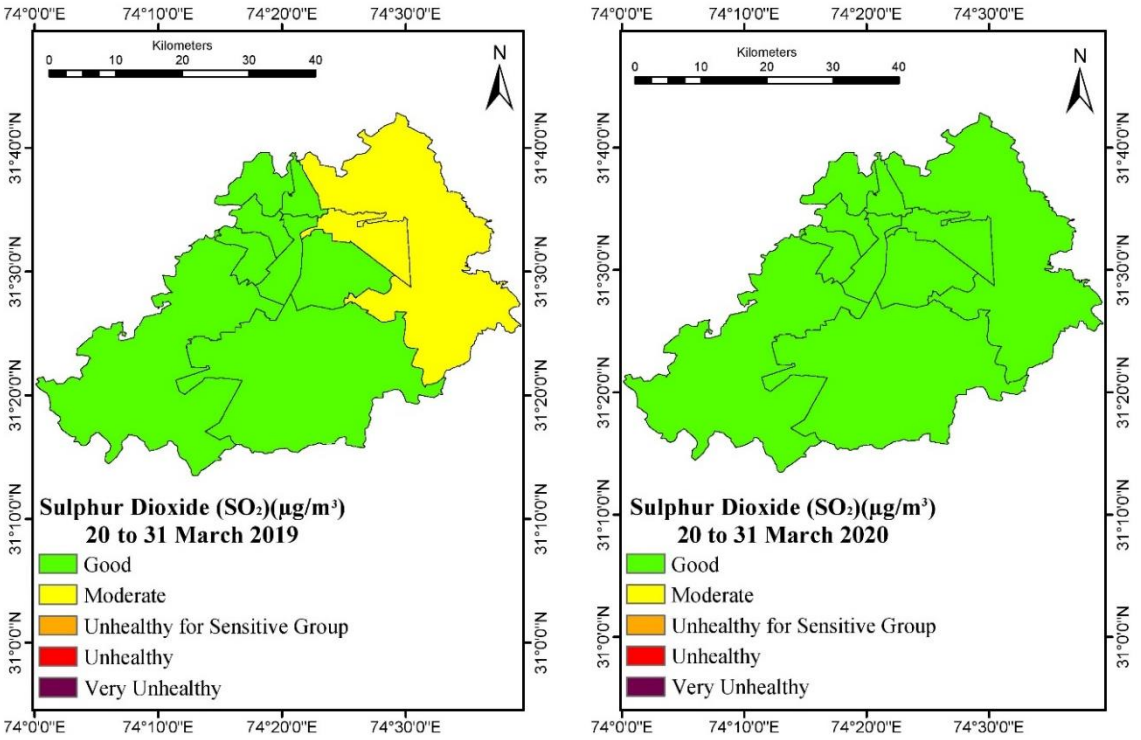

Figure 9. SO_2 level in March 2019 and 2020

4. CONCLUSION

The findings of the present study infer that quarantine and metrological factors strongly influence the air quality. Thus, the cohesive situation of the pandemic lockdown combining with the weather influence has benefitted the air by lowering the magnitude of NO, PM_{10}, $PM_{2.5}$ and SO_2 in the study area. Although the diffusion of air pollutants is diminishing for a short span of time due to control measures of COVID-19, this practice cannot be carried out on a long term basis when the pandemic will be over. Therefore, the regulatory authorities should take necessary measures to reconsider the existing mechanism and redevelop strategies to combat deteriorated air. Moreover for the time being, the air quality can be maintained using the same steps which are initiated during lockdown such as to promote remote working, expand online dealings, and discourage unnecessary travelling. Moreover, the new technologies should be introduced in the industrial sector like zig zag technology in the brick kiln industry to overcome the air pollution level.

REFERENCES

Abas N, Saleem MS, Kalair E, Khan N. Cooperative control of regional transboundary air pollutants. Environmental Systems Research 2019;8(1):10.

Alam K, us Sahar N, Iqbal Y. Aerosol characteristics and radiative forcing during pre-monsoon and post-monsoon seasons in an urban environment. Aerosol and Air Quality Research 2013;14(1):99-107.

Ali M, Athar M. Air pollution due to traffic, air quality monitoring along three sections of National Highway N-5, Pakistan. Environmental Monitoring and Assessment 2008;136(1-3):219-26.

Ali G, Bao Y, Ullah W, Ullah S, Guan Q, Liu X, et al. Spatiotemporal trends of aerosols over urban regions in Pakistan and their possible links to meteorological parameters. Atmosphere 2020;11(3):306.

Aloi A, Alonso B, Benavente J, Cordera R, Echániz E, González F, et al. Effects of the COVID-19 Lockdown on urban mobility: Empirical evidence from the city of Santander (Spain). Sustainability 2020;12(9):3870.

Ahmad T, Khan M, Khan FM, Hui J. Are we ready for the new fatal Coronavirus: scenario of Pakistan? Human Vaccines and Immunotherapeutics 2020;16(3):736-38.

Akhtar MM, Zhonghua T, Sissou Z, Mohamadi B. Assess arsenic distribution in groundwater applying GIS in capital of Punjab, Pakistan. Natural Hazards and Earth System Sciences Discussions 2015;3(3):2119-47.

Ashraf A, Butt A, Khalid I, Alam RU, Ahmad SR. Smog analysis and its effect on reported ocular surface diseases: A case study of 2016 smog event of Lahore. Atmospheric Environment 2019;198:257-64.

Aziz A, Bajwa IU. Minimizing human health effects of urban air pollution through quantification and control of motor vehicular carbon monoxide (CO) in Lahore. Environmental Monitoring and Assessment 2007;135(1-3):459-64.

Aziz A, Ahmad I, Mayo SM, Hameed R, Nadeem O. Urbanization and its impacts on founded areas of big cities in Pakistan: Case studies of "Ichra" and "Sanda" areas in Lahore. University of Engineering and Technology Taxila Technical Journal 2015;20(1):71-75.

Badshah SL, Ullah A, Badshah SH, Ahmad I. Spread of novel coronavirus by returning pilgrims from Iran to Pakistan. Journal of Travel Medicine 2020;27(3):1-3.

Bao R, Zhang A. Does lockdown reduce air pollution? Evidence from 44 cities in northern China. Science of the Total Environment 2020;29:139052.

Bashir MF, Bilal BM, Komal B. Correlation between environmental pollution indicators and COVID-19 pandemic: A brief study in Californian context. Environmental Research 2020;13:109652.

Barone-Adesi F, Dent JE, Dajnak D, Beevers S, Anderson HR, Kelly FJ, et al. Long-term exposure to primary traffic pollutants and lung function in children: Cross-sectional study and meta-analysis. PloS One 2015;10(11):1-16.

Batool SA, Ch MN. Municipal solid waste management in Lahore city district, Pakistan. Waste Management 2009;29(6):1971-81.

Bauwens M, Compernolle S, Stavrakou T, Müller JF, van Gent J, Eskes H, et al. Impact of coronavirus outbreak on NO_2 pollution assessed using TROPOMI and OMI observations. Geophysical Research Letters 2020;3:1-9.

Camargo JA, Alonso Á. Ecological and toxicological effects of inorganic nitrogen pollution in aquatic ecosystems: A global assessment. Environment International 2006;32(6):831-49.

Chattopadhyay S, Gupta S, Saha RN. Spatial and temporal variation of urban air quality: A GIS approach. Journal of Environmental Protection 2010;27;1(03):264-77.

Chauhan A, Singh RP. Decline in $PM_{2.5}$ concentrations over major cities around the world associated with COVID-19. Environmental Research 2020:187;109634.

Chen TM, Kuschner WG, Gokhale J, Shofer S. Outdoor air pollution: Nitrogen dioxide, sulfur dioxide, and carbon monoxide health effects. American Journal of the Medical Sciences 2007;333(4):249-56.

Cheng M, Jiang H, Guo Z. Evaluation of long-term tropospheric NO_2 columns and the effect of different ecosystem in Yangtze River Delta. Procedia Environmental Sciences 2012;13: 1045-56.

Colbeck I, Nasir ZA, Ahmad S, Ali Z. Exposure to PM_{10}, $PM_{2.5}$, PM_1 and carbon monoxide on roads in Lahore, Pakistan. Aerosol and Air Quality Research 2011;11:689-95.

Colbeck I, Sidra S, Ali Z, Ahmed S, Nasir ZA. Spatial and temporal variations in indoor air quality in Lahore, Pakistan. International Journal of Environmental Science and Technology 2019;16(6):2565-72.

Collivignarelli MC, Abbà A, Bertanza G, Pedrazzani R, Ricciardi P, Miino MC. Lockdown for COVID-2019 in Milan: What are the effects on air quality? Science of the Total Environment 2020;732:139280.

Dantas G, Siciliano B, França BB, da Silva CM, Arbilla G. The impact of COVID-19 partial lockdown on the air quality of the city of Rio de Janeiro, Brazil. Science of the Total Environment 2020;729:139085.

European Environment Agency (EEA). Air quality and COVID-19 [Internet]. 2020. [cited 2020 April 11]. Available from: https://www.eea.europa.eu/themes/air/air-quality-and-covid19 /air-quality-and-covid19.

Elder M, Olsen SH. The design of environmental priorities in the SDGs. Global Policy 2019;10:70-82.

Environment Protection Department (EPD). Air quality monitoring; Government of the Punjab, Pakistan [Internet]. 2020a [cited 2020 March 20]. Available from: https://epd.punjab.gov.pk/air_quality.

Environment Protection Department (EPD). Rules and regulations; Government of the Punjab, Pakistan [Internet]. 2020b [cited 2020 March 20]. Available from: https://epd.punjab.gov.pk/rules_regulations.

Gatto M, Bertuzzo E, Mari L, Miccoli S, Carraro L, Casagrandi R, et al. Spread and dynamics of the COVID-19 epidemic in Italy: Effects of emergency containment measures. Proceedings of the National Academy of Sciences 2020;117(19):10484-91.

Gautam S. The influence of COVID-19 on air quality in India: A boon or inutile. Bulletin of Environmental Contamination and Toxicology 2020;11:1-3.

Ghaffar A. Use of geospatial techniques in monitoring urban expansion and land use change analysis: A case of Lahore, Pakistan. Journal of Basic and Applied Sciences 2015;11: 265-73.

Gorai AK, Tuluri F, Tchounwou PB, Ambinakudige S. Influence of local meteorology and NO_2 conditions on ground-level ozone concentrations in the eastern part of Texas, USA. Air Quality, Atmosphere and Health 2015;8(1):81-96.

Goyal SK, Ghatge SV, Nema PS, Tamhane SM. Understanding urban vehicular pollution problem vis-a-vis ambient air quality-case study of a megacity (Delhi, India). Environmental Monitoring and Assessment 2006;119(1-3):557-69.

Guo H, Gu X, Ma G, Shi S, Wang W, Zuo X, et al. Spatial and temporal variations of air quality and six air pollutants in China during 2015-2017. Scientific Reports 2019;9(1):1-11.

Gupta P, Khan MN, da Silva A, Patadia F. MODIS aerosol optical depth observations over urban areas in Pakistan: Quantity and quality of the data for air quality monitoring. Atmospheric Pollution Research 2013;4(1):43-52.

Haider R, Yasar A, Tabinda AB. Urban emission patterns at a semi-arid site in Lahore, Pakistan. Polish Journal of Environmental Studies 2017;26(1):59-68.

İban MC. Geospatial data science response to COVID-19 crisis and pandemic isolation tracking. Turkish Journal of Geosciences 2020;1(1):1-7.

Ilyas SZ. A review of transport and urban air pollution in Pakistan. Journal of Applied Sciences and Environmental Management 2007;11(2):113-21.

Isaifan RJ. The dramatic impact of Coronavirus outbreak on air quality: Has it saved as much as it has killed so far? Global Journal of Environmental Science and Management 2020; 6(3):275-88.

Jan B, Iqbal M. Urbanization trend and urban population projections of Pakistan using weighted approach. Sarhad Journal of Agriculture 2008;24(1):173-80.

Jafary ZA, Faridi IA. Air pollution by roadside dust and automobile exhaust at busy road-crossings of Lahore. Pakistan Journal of Physiology 2006;2(2):20-3.

Javid K, Akram MA, Ranjha MM, Pervaiz S. GIS-based assessment of aridity over Punjab Province, Pakistan, by using climatic indices. Arabian Journal of Geosciences 2020; 13(7):1-12.

Kambalagere Y. A study on air quality index (AQI) of Bengaluru, Karnataka during lockdown period to combat coronavirus disease (Covid-19): Air quality turns 'better' from 'hazardous'. Studies in Indian Place Names 2020;40(69):59-66.

Kapil S. 78% cities recorded 'good', 'satisfactory' AQI during COVID-19 lockdown: CPCB [Internet]. 2020 [cited 2020 April 22]. Available from: https://www.downtoearth.org.in /news/air/78-cities-recorded-good-satisfactory-aqi-during-covid-19-lockdown-cpcb-70621.

Kaplan G, Avdan ZY. COVID-19: Spaceborne nitrogen dioxide over Turkey. Eskişehir Technical University Journal of Science and Technology A-Applied Sciences and Engineering 2020;21(2):251-5.

Kerimray A, Baimatova N, Ibragimova OP, Bukenov B, Kenessov B, Plotitsyn P, et al. Assessing air quality changes in large cities during COVID-19 lockdowns: The impacts of traffic-free urban conditions in Almaty, Kazakhstan. Science of the Total Environment 2020:730;139179.

Kinney PL. Climate change, air quality, and human health. American Journal of Preventive Medicine 2008;35(5):459-67.

Liaqat H, Waheed A, Malik NA, Vohra IA. Measuring urban sustainability through compact city approach: A case study of Lahore. Journal of Sustainable Development Studies 2017; 10(2):61-81.

Lodhi A, Ghauri B, Khan MR, Rahman S, Shafique S. Particulate matter ($PM_{2.5}$) concentration and source apportionment in Lahore. Journal of the Brazilian Chemical Society 2009; 20(10):1811-20.

Mabahwi NA, Leh OL, Omar D. Human health and wellbeing: Human health effect of air pollution. Procedia-Social and Behavioral Sciences 2014;153:221-9.

Mahato S, Pal S, Ghosh KG. Effect of lockdown amid COVID-19 pandemic on air quality of the megacity Delhi, India. Science of the Total Environment 2020:730;139086.

Malashock D, Khwaja HA, Fatmi Z, Siddique A, Lu Y, Lin S, Carpenter D. Short-term association between black carbon exposure and cardiovascular diseases in Pakistan's largest megacity. Atmosphere 2018;9(11):420.

Mansha M, Ghauri B, Rahman S, Amman A. Characterization and source apportionment of ambient air particulate matter ($PM_{2.5}$) in Karachi. Science of the Total Environment 2012;425: 176-83.

Mellouki A, George C, Chai F, Mu Y, Chen J, Li H. Sources, chemistry, impacts and regulations of complex air pollution: Preface. Journal of Environmental Science (China) 2016; 40:1-2.

Mitra A, Ray Chadhuri T, Mitra A, Pramanick P, Zaman S. Impact of COVID-19 related shutdown on atmospheric carbon dioxide level in the city of Kolkata. Parana Journal of Science and Education 2020;6(3):84-92.

Munzi S, Ochoa-Hueso R, Gerosa G, Marzuoli R. (E)merging directions on air pollution and climate change research in Mediterranean Basin ecosystems. Environmental Science and Pollution Research 2017;24(34):26155-9.

Najjar YS. Gaseous pollutants formation and their harmful effects on health and environment. Innovative Energy Policies 2011;1:1-9.

Nawaz A, Shahbaz MA, Javed M. Management of organic content in municipal solid waste: A case study of Lahore. International Journal of Environment and Waste Management 2015; 15(1):15-23.

Ogen Y. Assessing nitrogen dioxide (NO_2) levels as a contributing factor to the coronavirus (COVID-19) fatality rate. Science of the Total Environment 2020;726:138605.

Otmani A, Benchrif A, Tahri M, Bounakhla M, El Bouch M, Krombi MH. Impact of Covid-19 lockdown on PM_{10}, SO_2 and NO_2 concentrations in Salé City (Morocco). Science of the Total Environment 2020;735:139541.

Pakistan Bureau of Statistics. Provisional summary results of 6th population and housing census 2017. Islamabad [Internet]. 2017 [cited 2020 March 22]. Available from http://www.pbscensus.gov.pk/.

Pakistan Today. Pakistan among 12 worst countries in environmental pollution: EPI report [Internet]. 2020 [cited 2020 March 28]. Available from: https://www.pakistantoday.com.pk/2018/01/24/pakistan-among-12-worst-countries-in-environmental-pollution-epi-report/.

Pervaiz S, Javid K, Khan FZ, Talib B, Siddiqui R, Ranjha MM, Akram MA. Spatial analysis of vegetation cover in urban green space under new government agenda of clean and green Pakistan to tackle climate change. Journal of Ecological Engineering 2019;20(4):245-55.

Quan J, Tie X, Zhang Q, Liu Q, Li X, Gao Y, et al. Characteristics of heavy aerosol pollution during the 2012-2013 winter in Beijing, China. Atmospheric Environment 2014;88:83-9.

Raja S, Biswas KF, Husain L, Hopke PK. Source apportionment of the atmospheric aerosol in Lahore, Pakistan. Water, Air, and Soil Pollution. 2010;208(1-4):43-57.

Ramasamy D. Enchanted improvements in air quality across India: A study from COVID-19 lockdown perspective. Adalya Journal 2020;9(5):101-25.

Rana IA, Bhatti SS. Lahore, Pakistan-Urbanization challenges and opportunities. Cities 2018;72(1):348-55.

Rasheed A, Aneja VP, Aiyyer A, Rafique U. Measurement and analysis of fine particulate matter ($PM_{2.5}$) in urban areas of Pakistan. Aerosol and Air Quality Research 2015;15(2):426-39.

Rehman SA, Cai Y, Siyal ZA, Mirjat NH, Fazal R, Kashif SU. Cleaner and sustainable energy production in Pakistan: Lessons learnt from the Pak-Times model. Energies 2019; 13(1):1-21.

Riaz O. Impact of Population Growth on Urban Expansion in Lahore, 1951-1998 [dissertation]. University of the Punjab; Lahore, Pakistan: 2010.

Sabir S, Anjum GA. Problems and prospects of curbside parking in Lahore: Policy implications for effective management.

Mehran University Research Journal of Engineering and Technology 2017;4:867-80.

Sadiq N, Qureshi MS. Climatic variability and linear trend models for the five major cities of Pakistan. Journal of Geography and Geology 2010;2(1):83-92.

Saqlain M, Munir MM, Ahmed A, Tahir AH, Kamran S. Is Pakistan prepared to tackle the coronavirus epidemic? Drugsand Therapy Perspectives 2020;36:213-4.

Shahid MA, Ahmad N, Hussain K, Naseem S. Compound phase analysis of solid aerosols collected from different locations of Faisalabad and Lahore (Pakistan) using matrix-flushing method. Peak Journal of Physical and Environmental Science Research 2013;1:54-65.

Sharma S, Zhang M, Gao J, Zhang H, Kota SH. Effect of restricted emissions during COVID-19 on air quality in India. Science of the Total Environment 2020;728:138878.

Shirwani R, Gulzar S, Asim M, Umair M, Al-Rashid MA. Control of vehicular emission using innovative energy solutions comprising of hydrogen for transportation sector in Pakistan: A case study of Lahore City. International Journal of Hydrogen Energy 2019;45(32):16287-97.

Sidra S, Ali Z, Nasir ZA, Colbeck I. Seasonal variation of fine particulate matter in residential micro-environments of Lahore, Pakistan. Atmospheric Pollution Research 2015; 6(5):797-804.

Singh A, Agrawal M. Acid rain and its ecological consequences. Journal of Environmental Biology 2007;29(1):15-24.

Stone E, Schauer J, Quraishi TA, Mahmood A. Chemical characterization and source apportionment of fine and coarse particulate matter in Lahore, Pakistan. Atmospheric Environment 2010;44(8):1062-70.

Tariq S, Ali M. Satellite and ground-based remote sensing of aerosols during intense haze event of October 2013 over Lahore, Pakistan. Asia-Pacific Journal of Atmospheric Sciences 2016;52(1):25-33.

Tiwari TN, Ali M. Air quality index for Calcutta and its monthly variation for various localities. Indian Journal of Environmental Protection 1987;7:172-6.

Wang P, Chen K, Zhu S, Wang P, Zhang H. Severe air pollution events not avoided by reduced anthropogenic activities during COVID-19 outbreak. Resources, Conservation and Recycling 2020;158:104814.

Waris A, Khan AU, Ali M, Ali A, Baset A. COVID-19 outbreak: Current scenario of Pakistan. New Microbes and New Infections 2020;35:100681.

Xu K, Cui K, Young LH, Wang YF, Hsieh YK, Wan S, et al. Air quality index, indicatory air pollutants and impact of COVID-19 event on the air quality near central China. Aerosol and Air Quality Research 2020;20:1204-21.

Yen MC, Peng CM, Chen TC, Chen CS, Lin NH, Tzeng RY, et al. Climate and weather characteristics in association with the active fires in northern Southeast Asia and spring air pollution in Taiwan during 2010 7-SEAS/Dongsha Experiment. Atmospheric Environment 2013;78:35-50.

Zambrano-Monserrate MA, Ruano MA, Sanchez-Alcalde L. Indirect effects of COVID-19 on the environment. Science of the Total Environment 2020;728:138813.

Zha S, Zhang S, Cheng T, Chen J, Huang G, Li X, et al. Agricultural fires and their potential impacts on regional air quality over China. Aerosol and Air Quality Research 2013;13(3):992-1001.

Estimation of Cadmium Contamination in Different Restoration Scenarios by RUSLE Model

Arisara Charoenpanyanet[1*] and Panlop Huttagosol[2]

[1]*Department of Geography, Faculty of Social Sciences, Chiang Mai University, Chiang Mai 50200, Thailand*
[2]*Department of Mining and Petroleum Engineering, Faculty of Engineering, Chiang Mai University, Chiang Mai 50200, Thailand*

ARTICLE INFO

Received: 9 May 2020
Received in revised: 27 Jul 2020
Accepted: 31 Jul 2020
Published online: 25 Aug 2020
DOI: 10.32526/ennrj.18.4.2020.36

Keywords:
RUSLE model/ Soil loss/ Cadmium contamination/ Forest restoration/ Mae Tao watershed

*** Corresponding author:**
E-mail: arisara.cmu@gmail.com

ABSTRACT

The Mae Tao watershed of Thailand faced cadmium (Cd) contamination problems from zinc mining for a long time until the mining area was closed to decrease the level of Cd concentration. This study reproduced the possible scenarios of Cd contamination due to soil loss. Four scenarios of forest restoration were implemented in this study, all of which were calculated with the Revised Universal Soil Loss Equation (RUSLE) integrated with satellite imagery and Geographic Information Systems (GIS). Landsat 8-OLI was acquired and land use/land cover (LULC) was classified in each scenario. Soil loss maps were created. An inverse distance weighting (IDW) technique was used to estimate the concentration of Cd based on the field data consisting of 101 points of measured Cd concentration. Results from RUSLE model and IDW technique were combined to calculate Cd contamination due to soil loss for all four scenarios. Results showed that the restoration of Scenario 3, forest restoration in old and new mining areas in cooperation with reservoir construction, helped decrease Cd contamination the most. The lowest level of Cd contamination from soil loss was found in this scenario by about 156 ha (total of Cd contamination by 165,924.32 ton/year).

1. INTRODUCTION

Mae Tao watershed, Mae Sot District, Tak Province has faced a cadmium contamination problem for a very long time. The largest zinc deposit of Thailand is located in this area (DPIM, 2009a). The zinc was excavated by surface mining which was a broad category of mining in which soil and rock overlaying the mineral deposit are removed (Suppakarn et al., 2016). During the years 1969-1975, the mine was first operated by a private company. However, there were no mine operations during the years 1976-1983 and this area was abandoned. Zinc mining then continued again from 1984-2017. In the first period of the zinc mine operation, in 1974, there was a dispute involving the problem of Cd contamination in Mae Tao Creek (Suppakarn et al., 2016). A high level of Cd contamination in paddy fields and rice seeds in Mae Tao watershed was first reported by the International Water Management Institute (IWMI) in 1998. In addition, studies on Cd contamination were performed by sampling rice seeds, paddy soil and bed load sediments continuously from the irrigation water of the Mae Tao River (DPIM, 2009b; Simmons and Pongsakul, 2002; Simmons et al., 2003; Simmons et al., 2005; Thamjedsada and Chaiwiwatworakul, 2012). It found that Cd from mining waste contaminating the groundwater can cause pollution of downstream paddy fields (Sriprachote et al., 2012). Also, the study of Unhalekhaka and Kositanont (2008) indicated that the level of Cd contamination has affected the health and livelihood of the farmers. Moreover, the Pollution Control Department (PCD) (2013) found that Cd paddy field soil with a depth of less than 30 centimeters had a high level of contamination (more than 30 mg Cd/kg soil) within a total area of 40 ha, and had a medium level of contamination (3-30 mg Cd/kg soil) within a total area of 570 ha. The PCD and other agencies furthermore suggested soil management guidelines from academic sources in which there would be surface dredging specifically in an area with high Cd contamination.

Citation: Charoenpanyanet A, Huttagosol P. Estimation of cadmium contamination in different restoration scenarios by RUSLE Model. Environ. Nat. Resour. J. 2020;18(4):376-386. (https://doi.org/10.32526/ennrj.18.4.2020.36)

As a problem mentioned above, four scenarios of forest restoration were suggested by relevant sectors (Royal Forest Department, Department of Primary Industries and Mines, and private company) for reducing Cd contamination due to soil loss in Mae Tao watershed. They were: 1) forest restoration in the old mining area; 2) forest restoration in both the old mining area and the new mining area; 3) forest restoration in both mining areas in cooperation with reservoir construction; and 4) forest restoration in both mining areas in cooperation with weir construction. Moreover, assessing the suitable scenario is an essential procedure to select the best measure to reduce Cd contamination and protect the Mae Tao watershed. Therefore, RUSLE model was applied to estimate soil loss (Atoma et al., 2020; Batista et al., 2017; Chuenchum et al., 2020; Farhan et al., 2013; Ganasri and Ramesh, 2016; Kassawmar et al., 2018; Kim, 2006; Lazzari et al., 2015; Lee and Lee, 2006; Millward and Mersey, 1999; Ostovari et al., 2017; Rammahi and Khassaf, 2018; Somprasong and Chaiwiwatworakul, 2015; Xu et al., 2012) and was integrated with IDW technique in GIS to estimate the spatial concentration of Cd (Mesnard, 2013; Somprasong and Chaiwiwatworakul, 2015). Soil loss with RUSLE model and Cd concentration with IDW were used as the parameters to estimate Cd contamination in soil loss in the last step (Somprasong and Chaiwiwatworakul, 2015). In the past, the studies on integration of RUSLE model to estimate soil pollution such as arsenic (As), copper (Cu), zinc (Zn), and lead (Pb) were limited. This study has therefore integrated RUSLE model with geoinformatics techniques to estimate Cd commination from soil loss.

The main goal of this study was to estimate which area restoration measure scenario would help decrease the accumulation of the Cd the most. This study was conducted to help provide better proof for policy makers in advancing the measures of area restoration for agencies concerned with environmental impact. This estimation used the RUSLE model, satellite image, and GIS with the following purposes: 1) to estimate soil loss with RUSLE model and reproduce scenarios of the Mae Tao watershed restoration; and 2) to estimate Cd contamination in the sediment from the Mae Tao watershed restoration scenario.

2. METHODOLOGY

2.1 Study area

The Mae Tao watershed in its general vicinity covers the areas of the Sub-districts of Pra Tat Pa Daeng, Mae Tao, and Mae Gu in the Mae Sot District, Tak Province, Thailand. It covers an area of about 6,000 ha. It is in Eastern Thailand at 16°45′ latitude and 98°35′ longitude (Figure 1). Most of the area is high mountainous with a high gradient and is covered by forest. The watershed is divided into three part: the lower, upper left and upper right. The zinc mine is located in the upper right watershed which has an area of approximately 2,996 ha.

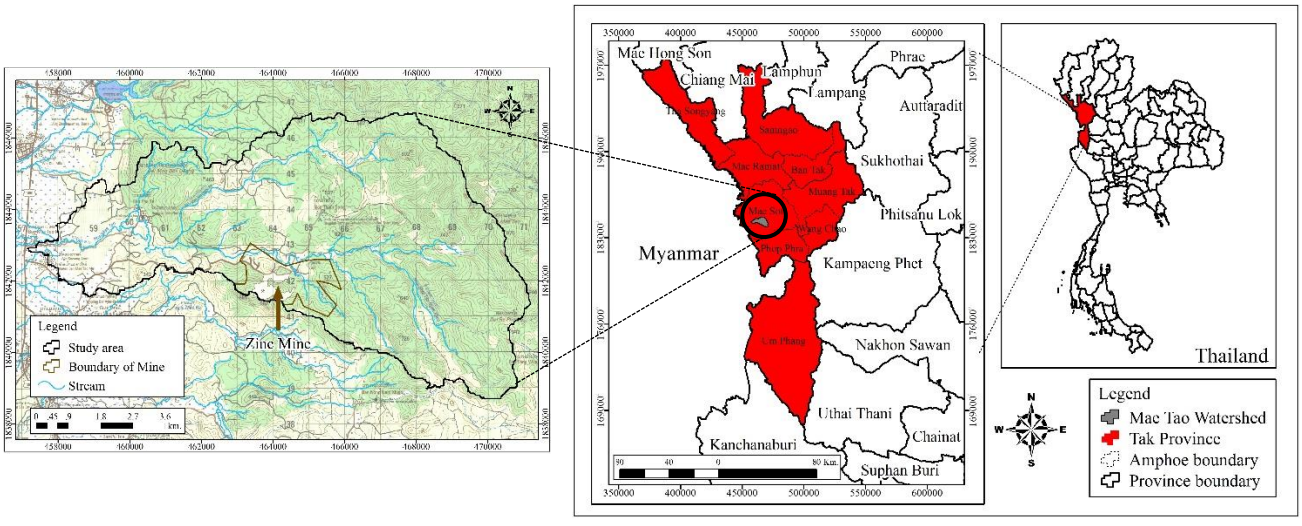

Figure 1. Study area: Mae Tao watershed, Thailand

2.2 Data to be used

1) Landsat 8-OLI with 30 m. spatial resolution captured on January 23rd, 2017 at 10:49 a.m. was used for analyzing the LULC of all four scenarios and for analyzing C-factor and P-factor in RUSLE model. Image selection was based on termination of zinc mine operations. The criterion on image selection for being used in differentiation were considered from the seasons of each compared scenario since the seasons affected farmers' planting in the area. LULC were decided based on Thailand's standard criterion (Land Development Department, 2000).

2) Annual average rainfall data of 10 years (2007-2016) in the study area was for analyzing R-factor in RUSLE model. Rainfall data derived from Mae Sot, Mae Ramad and Phawo meteorological stations, Tak Province.

3) Spatial data (.shp) of soil type from Land Development Department of Thailand was for analyzing K-factor in RUSLE model.

4) Contour line was for creating the data for the digital elevation model (DEM), input for analyzing LS-factor in RUSLE model. DEM resolution for this study was 30 m.

5) Field surveying data of LULC for examining the accuracy of LULC classification results from satellite imageries, and the 101 points of Cd concentration in the study area were for analyzing Cd contamination in sediment. The sampling points were chosen by random sampling along the Mae Tao River.

2.3 Scenarios

The scenarios of Cd contamination from mining restoration in the Mae Tao watershed were defined based on the mining restoration measures which were put into four scenarios (Figure 2). They are as follows:

Scenario 1: Forest restoration in old mining area

This scenario used Landsat 8-OLI satellite imageries captured in January 2017 (a period of non-operating mining) as representative in LULC. There were two areas of forest restoration in this scenario. The first area was the forest plantation areas of the Royal Forest Department (forest restoration 3). The second area was the plantation forest area in an area of the zinc mining project (forest restoration 4). Originally an empty area of land with parts of ground cover, there were plans to restore the forest in the majority of the area, and to adjust the landscape to allow for a learning center and a place for ecotourism.

Scenario 2: Forest restoration in old mining area and new mining area

In this scenario, forest would be planted following Scenario 1 while adding two more areas of forest planting in the outer mining area. They are designated the forest planting area, orchard planting area, and integrated farming area (outside of the areas which invoke land use rights) (forest restoration 1 and 2), where the original area was cultivated on an area of conserved forest with mono-cropping destroying the land's surface. This area was a unit filled with zinc and Cd; therefore, there should be an adjustment to the agricultural activity methods from mono-cropping, to integrated farming for land surface preservation.

Scenario 3: Forest restoration in old mining area and new mining area in cooperation with reservoir construction

This scenario was a forest planting determination following Scenario 2 in cooperation with the reservoir construction area.

Scenario 4: Forest restoration in old mining area and new mining area in cooperation with weir construction

This scenario was a forest planting determination following Scenario 2 in cooperation with the weir construction area.

The LULC classification results were examined by field surveying. The classification accuracy for the LULC classes was 83%, examined with 85 randomly distributed points.

2.4 RUSLE Model

RUSLE model is a very powerful method for estimation of soil erosion in specific situations such as dam construction, mining, typhoon, assessing land management measures, LULC change, and mountain areas (Atoma et al., 2020; Chuenchum et al., 2020; Kassawmar et al., 2018; Kim, 2006; Lazzari et al., 2015; Rammahi and Khassaf, 2018; Somprasong and Chaiwiwatworakul, 2015). RUSLE model integrates remote sensing techniques together with GIS for estimation of the quantity of lost sediment in the four scenarios as shown in Equation (1).

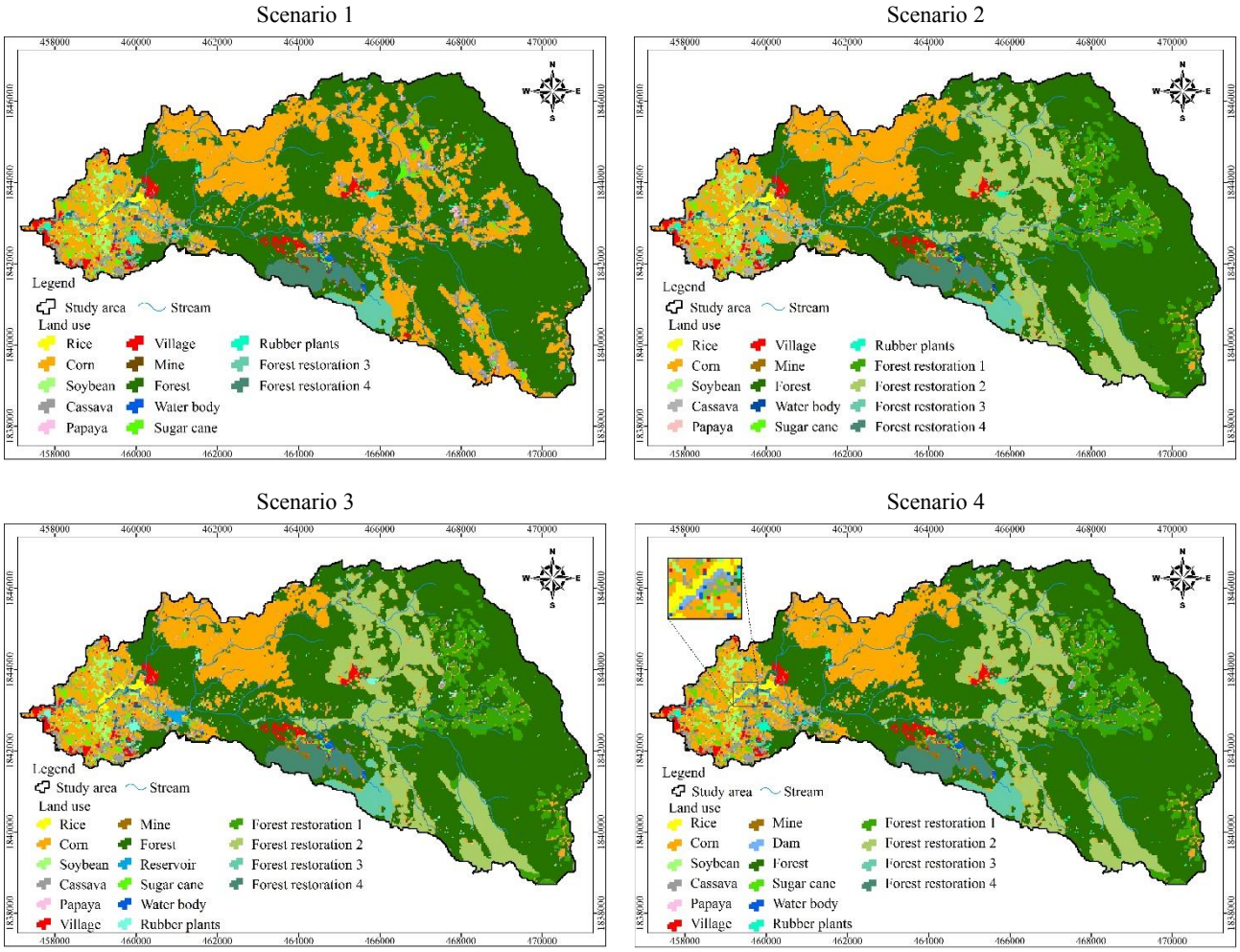

Figure 2. Land use/land cover classification of each scenario

$$A = R\ K\ C\ P\ L\ S \quad (1)$$

Where; A=the average of soil loss (ton/ha/year), R=the rainfall and runoff erosivity factor (mm/ha/year), K=the soil erodibility factor (no unit), C=the crop management factor) (no unit), P=a term representing the conservation practice factor (no unit), and LS=the slope length and steepness factor (no unit).

R-factor: The R-factor is an index of the runoff power of rain. It includes the factors of rainfall and runoff. These factors are different based on the area in which they occur (Oliveria et al., 2012). This equation relies on annual rainfall for calculation as shown in Equation (2) (Land Development Department, 2000).

$$R = 0.4669X - 12.1415 \quad (2)$$

Where; R=rainfall erosivity (mm/ha/year) and X=average annual rainfall (mm/year)

Annual rainfall data for the period from 2007-2016 (10 years) were collected from three stations: Mae Sot, Mae Ramad, and Phawo. This data was used to create spatial interpolation data and calculated with Equation (2) (Figure 3).

K-factor: This factor indicates soil erodibility of any type of soil. The Land Development Department (1983, stated in Land Development Department, 2000), assigned soil types by different sets of soil based on the property of the soil. The K-factor was calculated following the soil types and their geological units. The K-factor of Thailand is between 0.04 and 0.56. However, in the times period for which this study was conducted, the K-factor had little to no change (Figure 3).

LS-factor: This factor relates to geographical characteristics and is calculated from an analysis of the slope length index. The L-factor influences erosivity and is a 'no unit' number. The index of slope-steepness, or S-factor, is a gradient index and has no size or unit. Both factors can be greater than or less than 1. The LS-analyzing method can be completed by following Equation (3) (Ozcan et al., 2007).

$$LS = \left(\frac{xn}{22.13}\right)^{0.4} \times \left(\frac{\sin\theta}{0.0896}\right)^{1.3} \quad (3)$$

Where; LS=slope length and steepness of inclination, x=flow accumulation, n=cell size, and θ=steepness (degree).

The result of the LS-factor is presented in Figure 3. Because this factor had no change in a short period of time, the LS-factor of all four scenarios remained the same.

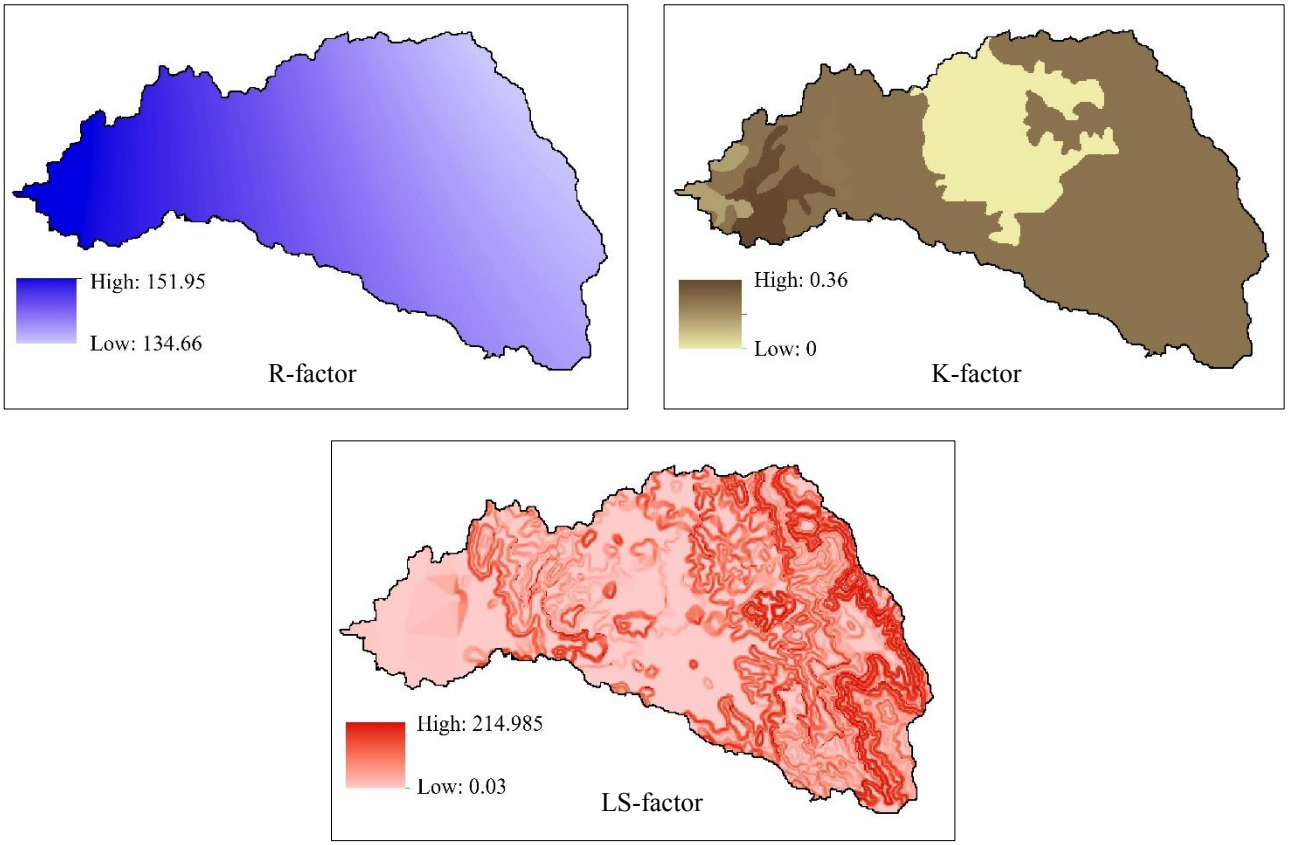

Figure 3. R-factor, K-factor, and LS-factor

C-factor: The cropping management factor of this study was an application of the Normalized Difference Vegetation Index (NDVI). NDVI is from calculations between reflectance in the near infrared band (NIR) and reflectance in the red band (RED). When NDVI is known, it can be converted into C-factor using Equation (4). Nevertheless, the C-factor is different based on each scenario (Figure 4).

$$C = \exp\left(-\alpha \frac{NDVI}{\beta - NDVI}\right) \quad (4)$$

Where, α is a constant of -2, β is a constant of 1 (European Commission, 2000), and exp is a constant of 2.71828.

P-factor: The practice management factor is a factor of erosion-control measure which is used in the management of soil erosion in different areas where preservation is practiced. This study used P-factor based on a LULC of the Land Development Department (2000). The values of cropping management factor were used to define P-factor which was have been different in each scenario as there were different land use types (Figure 4).

The criterion used in classifying the levels of sediment movement or average soil loss in this study was used from the criterion of the Land Development Department (2000) for organizing the level range (Table 1).

Table 1. Category of soil loss severity in Thailand

Severity level	Soil loss rate (ton/ha/year)	Status
Very low severity	0-12.5	Balance
Less severity	12.5-31.25	Monitor
Moderate severity	31.25-93.75	Monitor
High severity	93.75-125	Risk
Very High severity	>125	Crisis

Source: Adapted from Land Development Department (2000)

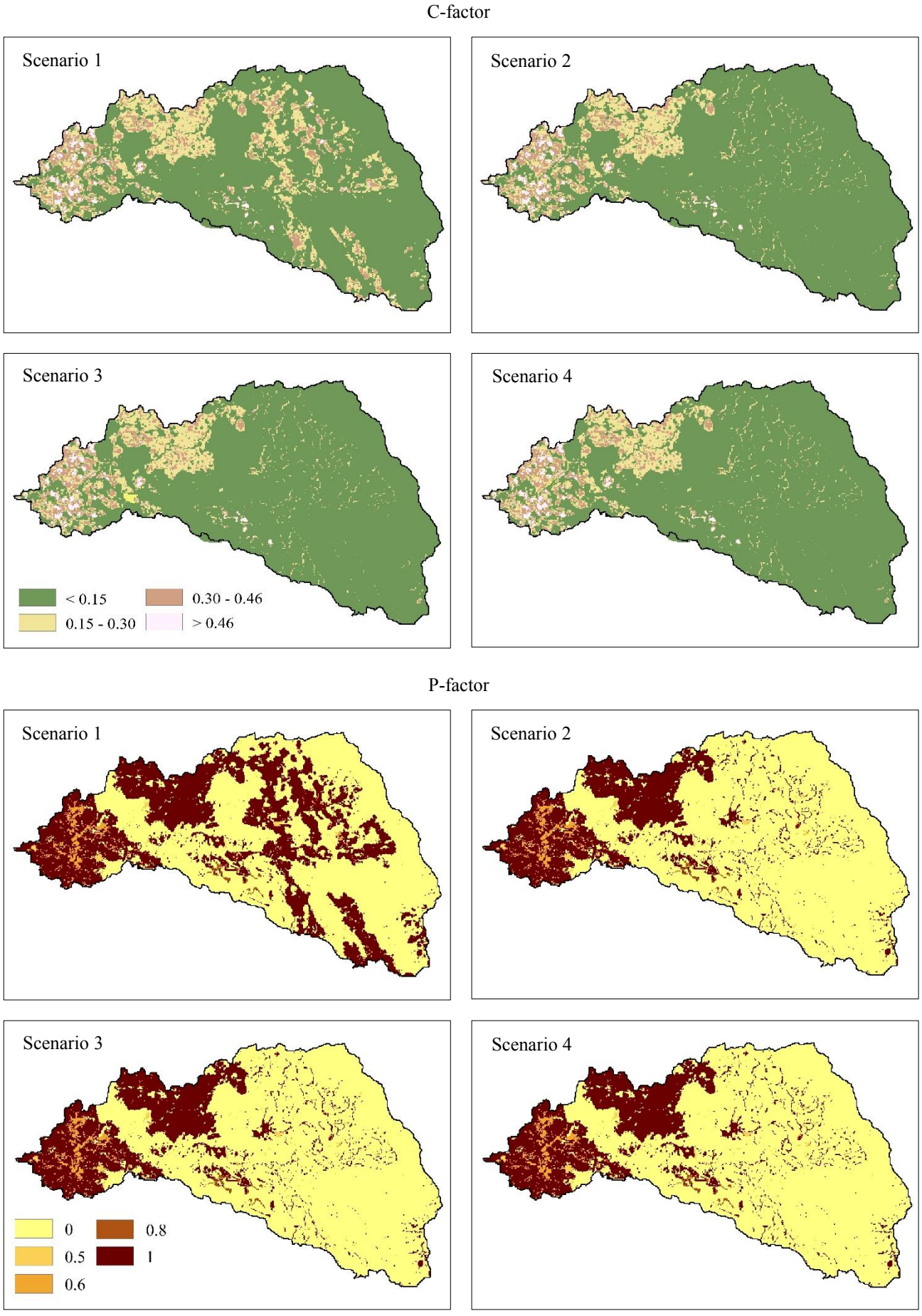

Figure 4. C-factor and P-factor

2.5 Inverse distance weight (IDW)

IDW is used to estimate the spatial concentration of Cd. The advantages of this method were for estimation of unknown values and it has a superior performance than other interpolation methods (Azpurua and Ramos, 2020). This study used data from actual Cd collection points in the Mae Tao watershed with 101 points in total collected on February 5th, 2017. Each sample was a collection of top soil (0-15 cm) from which the Cd concentration was determined. This existing data as shown in Equation (5) is considered as a means of prediction of the concentration of Cd in areas that have not yet been measured.

$$\mathrm{CdIDW} = \sum_{n}^{i=1} \mathrm{wifi} \quad (5)$$

Where; CdIDW=cadmium concentration (mg cadmium/kg soil), i=Cd concentration from field surveying (mg Cd/kg soil), w_i=weight value, and n=the amount of mg Cd collected from the points of collection in the study area.

2.6 Estimation of Cd contamination in soil loss

An analysis result of the average of soil loss from Equation (1) and Cd concentration calculated from IDW from Equation (5) were used as the parameter to estimate potential of Cd movement in soil loss. Potential of Cd movement in soil loss was calculated by the following Equation (6).

$$\mathrm{Pcd} = 0.16 \times \mathrm{A} \times \mathrm{CdIDW} \quad (6)$$

Where; Pcd=potential of Cd movement in soil loss (ton Cd/ha/year), A=average of soil loss (ton/ha/year), and CdIDW=Cd concentration calculated by IDW technique (mg Cd/kg soil).

The average of soil loss from RULSE model (parameter A) and Cd concentration from IDW technique (parameter CdIDW) were a spatial data. Both parameters and weighting value were applied by raster calculation to estimate the Cd contamination in soil loss.

3. RESULTS AND DISCUSSION

3.1 Soil loss estimation with RUSLE model

After analyzing five factors affecting sediment movement, each factor was then used to calculate the sediment movement of the Mae Tao watershed in all four scenarios with RUSLE model. The result of soil loss analysis with RUSLE model from four scenarios found a severe level of sediment movement (more than 125 ton/ha/year) as a critical level with high movement of soil and surface erosion affecting the ecosystem was found the most in Scenario 1 at 76.86 ha, which was the highest rate of erosion at 1,346.13 ton/ha/year. This was due to Scenario 1 covering the largest area of monoculture, namely corn, sugar cane, and soybean. C-factor and P-factor have been affected by LULC types therefore these factors were a high influence on the level of sediment movement. The second most critical was Scenario 3 at 21.04 ha. The least critical levels were found in Scenarios 2 and 4, both expressing the same numerical value of 19.16 ha (Figure 5). High levels of lost sediment occur in corn areas, including the middle of Mae Tao watershed, especially in Scenario 1. But some spatial soil erosion results differ in other areas, especially along the mainstreams (Somprasong and Chaiwiwatworakul, 2015). The different results can be identified by the computation of the C-factor and P-factor which are influenced by different LULC.

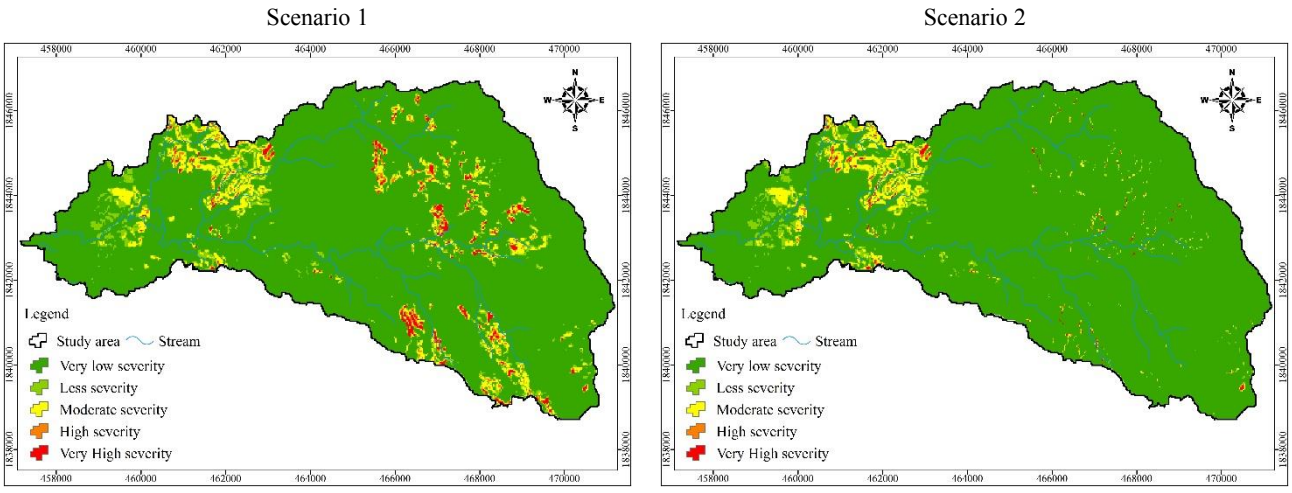

Figure 5. Soil loss estimation of each scenario

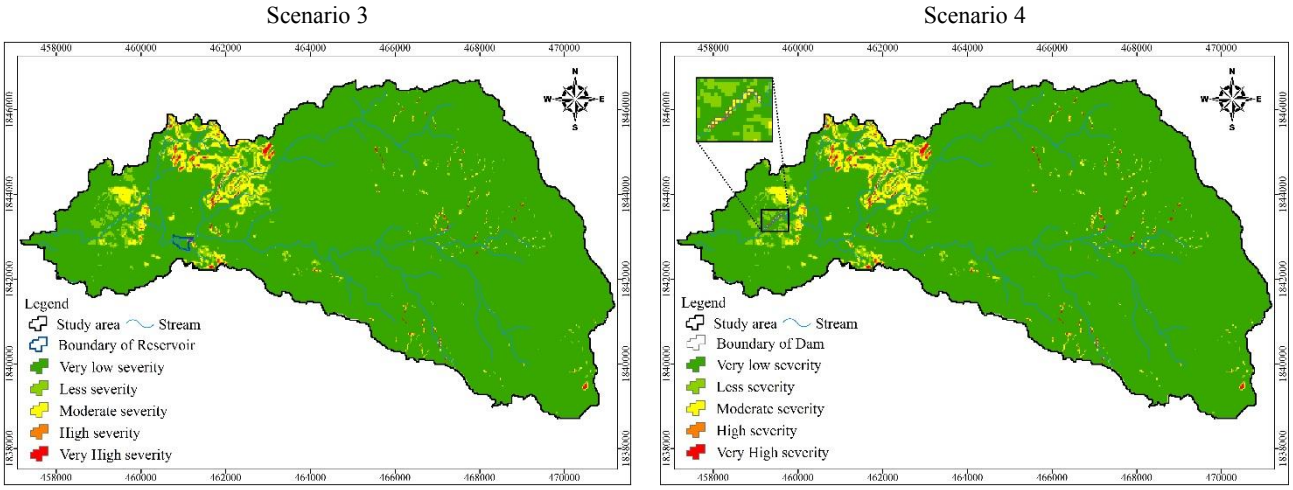

Figure 5. Soil loss estimation of each scenario (cont.)

For this study, observed soil sediment data from field surveying was not performed. However, the observed soil sediment data and the sediment yield results from RUSLE model simulation were well correlated with a correlation higher than 0.9 (Chuenchum et al., 2020).

3.2 Cadmium contamination estimation in the sediment

3.2.1 Spatial concentration of Cadmium

The field data of measured Cd concentration from the study areas found that 50.5% of total points had more than the regulatory standard concentration of 3 mg Cd/kg soil. All the data collected in this study was put into the function of the GIS for analyzing the spatial concentration of Cd. The results showed that an area that exceeds the European Economic Community's maximum permissible (EEC MP) level, was found west of the Mae Tao watershed covering about 2.12 ha. Cd concentration exceeding the standard set in place by the Enhancement and Conservation of National Environment Quality Act (more than 37 mg Cd/kg soil) was found in an area of about 640 ha located in the middle of the Mae Tao watershed-originally a mining area. Nonetheless, the average Cd concentration in the Mae Tao watershed was found to be 13.64 mg Cd/kg soil, which exceeds all of the standards according to the EEC MP criterion. The range with more than 60.01 mg Cd/kg soil had an average Cd concentration as high as 110.93 mg Cd/kg soil. This concentration of Cd is considered as an amount that could affect the ecosystem as well as the human residents living in the area (Figure 6). Moreover, rice field soil samples collected in the study area had Cd levels of 3.40-284 mg Cd/kg soil, 94 times the EEC MP concentration in soil (Simmons et al., 2005). In additional, high Cd concentration from IDW were found near the residential area west of the Mae Tao watershed, with a range of Cd concentrations from 0-200 mg/kg. (Somprasong and Chaiwiwatworakul, 2015).

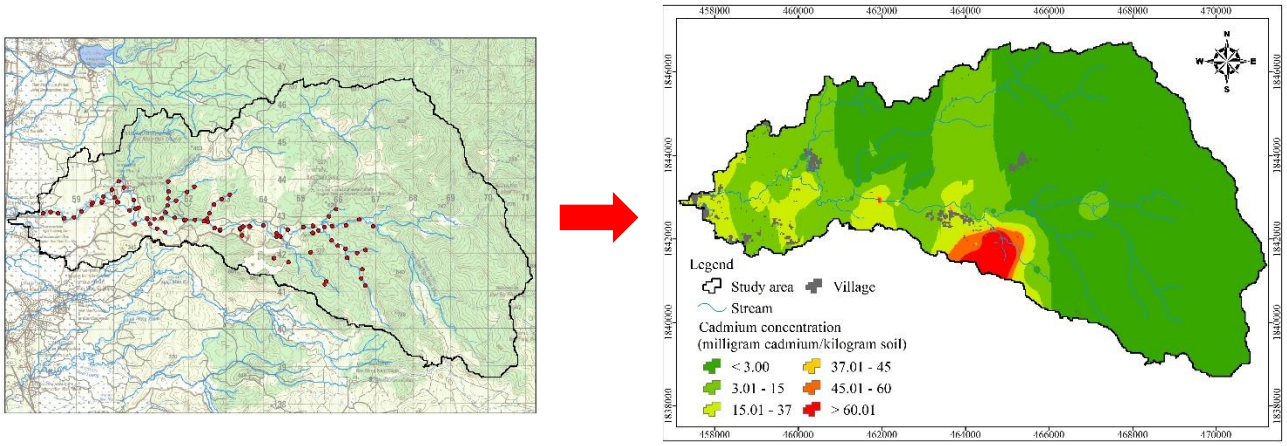

(a) 101 points of measured Cd concentration from the study areas

(b) spatial concentration of Cd from IDW

Figure 6. Locations of measured Cd concentration (a) and concentration of Cd from IDW (b)

3.2.2 Cadmium contamination from soil loss

After analyzing the spatial concentration of Cd with GIS, the criteria range was determined by separating the levels of Cd contamination from soil loss into three levels: 1) high level of Cd contamination with more than 30 ton/ha/year; 2) medium level of Cd contamination with 3-30 ton/ha/year; and 3) low level of Cd contamination with less than 3 ton/ha/year. These criteria were used for a determination of Cd contamination from the range of soil loss (Figure 7). Cd contamination estimates also due to erosion occurred in the mining production area. In addition, there is significant evidence that the upstream area of the basin has the potential to release Cd during incidents of erosion (Somprasong and Chaiwiwatworakul, 2015). The total Cd concentrations in sediment were increased when passing the zinc mines (Thamjedsada and Chaiwiwatworakul, 2012).

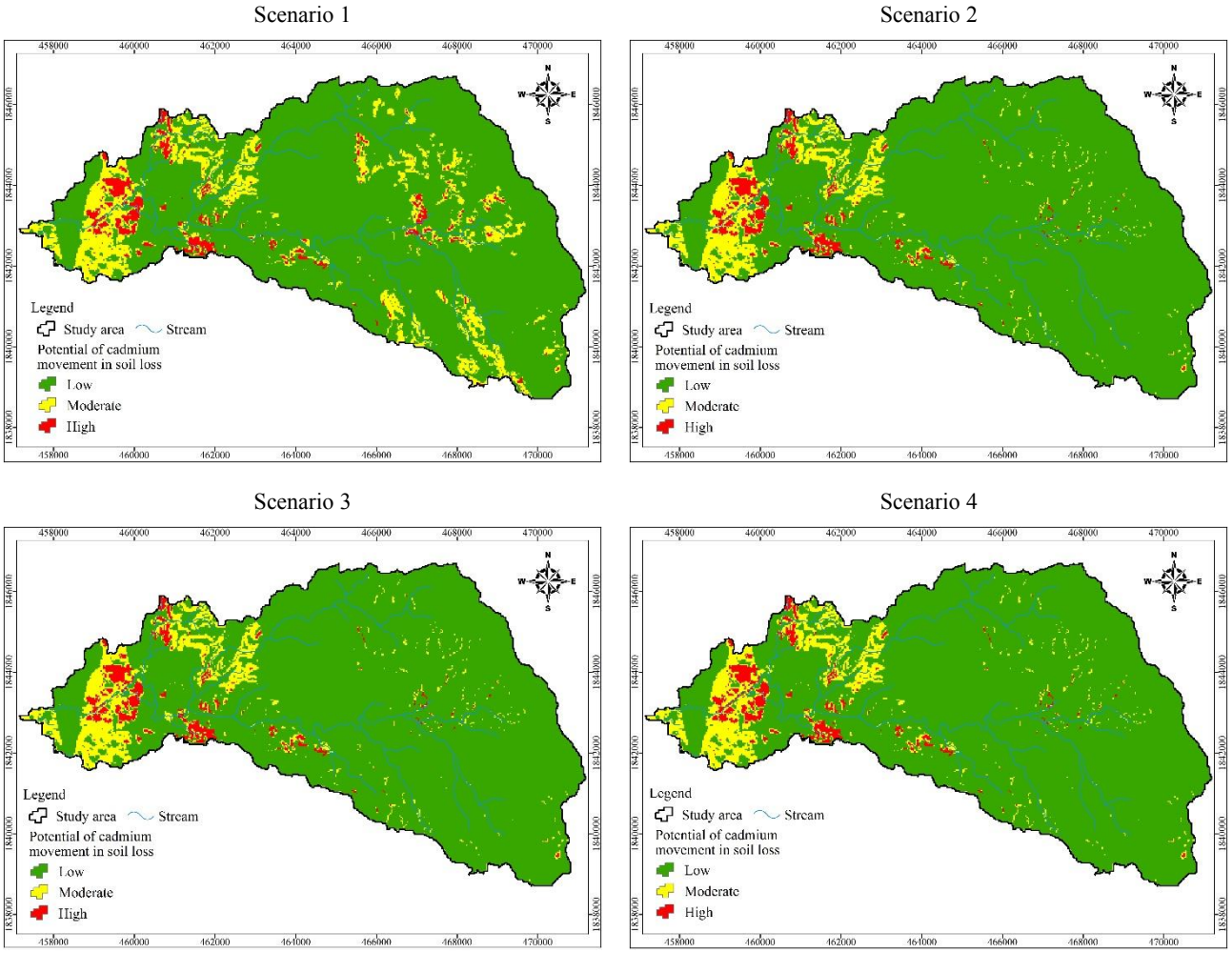

Figure 7. Cd contamination from soil loss of each scenario

A high level of Cd contamination from soil loss (more than 30 ton Cd/ha/year) was found mostly in the east and middle areas of the Mae Tao watershed. Scenario 1 had the highest Cd contamination from soil loss, which was about 187.20 ha. Scenario 4 was the second-most contaminated at about 158.40 ha, while Scenario 2 was contaminated at about 156.80 ha. Scenario 3 yielded the least contaminated at about 156.32 ha (Table 2). From this result, it can be concluded that Scenario 3 is the best measure to decrease Cd contamination of the soil loss in Mae Tao watershed. RUSLE model can certainly aid in implementation of soil management and conservation practices to reduce the soil erosion (Ganasri and Ramesh, 2016) and also help to locate the severe soil loss areas for suitable conservation practices (Ostovari et al., 2017).

Moreover, an area exceeding a high level of Cd contamination from soil loss (more than 30 ton Cd/ha/year), was analyzed with land used in the Mae Tao watershed. The results of the four scenarios of this study found that a high level of Cd contamination was

found mostly in the corn plantation area (104,995.63 ton/year in Scenario 3) (Table 2), as well as the sugar cane (13,758.86 ton/year in Scenario 3) and cassava plantation areas (11,977.18 ton/year in Scenario 3). This result revealed that soil loss and Cd Contamination problems were highly influenced by monoculture.

Table 2. High level of Cd contamination (CC) in each LULC

Land use/land cover	Scenario 1		Scenario 2		Scenario 3		Scenario 4	
	Area (ha)	Total of cc (ton/year)	Area (ha)	Total of cc (ton/year)	Area (ha)	Total of cc (ton/year)	Area (ha)	Total of cc (ton/year)
Corn	133.86	120,522.95	106.37	104,968.64	106.08	104,995.63	107.95	104,987.90
Sugar cane	10.09	11,453.11	8.81	13,758.86	8.81	13,758.86	8.81	13,758.86
Cassava	14.29	14,589.88	11.21	11,881.87	11.15	11,977.18	11.14	11,898.20
Soybean	6.65	7,315.42	7.46	9,358.64	7.39	6,606.22	7.39	6,606.22
Water body	5.67	11,569.15	4.72	5,892.86	4.72	5,892.86	4.65	5,928.45
Village	7.35	12,839.04	7.73	10,539.61	7.73	10,539.60	7.73	10,539.60
Mining area	1.54	2,138.39	1.81	2,537.99	1.81	2,537.99	1.81	2,537.99
Para rubber	0.09	70.69	-	-	0.02	35.79	0.02	21.52
Paddy field	7.11	8,817.81	7.73	9,065.96	7.73	9,065.96	7.65	9,175.93
Papaya	0.99	871.35	0.94	514.21	0.94	514.21	0.95	514.21
Total	187.65	190,187.80	156.78	168,518.64	156.33	165,924.32	158.11	165,968.89

4. CONCLUSION

The application of RUSLE model, satellite data, and GIS could be effective techniques to assess the suitable measures for environmental management, especially soil pollution. The results of this study demonstrated the pattern of Cd contamination from soil loss in the each LULC area and could explore Cd contamination in remote areas. The results highlight the advantage of the methods selected in this study. However, regarding the limitation of this study, it would be helpful if observed soil sediment data was collected by field surveying to examine the result from RUSLE model in further study.

ACKNOWLEDGEMENTS

We would like to express my deepest gratitude to Department of Primary Industries and Mines for supporting the research fund, Thai Meteorological Department (TMD) for supporting the meteorological data and also the United State Geological Survey (USGS) for available remotely sensed data.

REFERENCES

Atoma H, Suryabhagaven K, Balakrishnan M. Soil erosion assessment using RUSLE model and GIS in Huluka watershed, central Ethiopia. Sustainable Water Resources Management 2020;6:1-12.

Azpurua M, Ramos K. A comparison of spatial interpolation methods for estimation of average electromagnetic field magnitude. Progress in Electromagnetics Research 2020;14:135-45.

Batista G, Silva N, Silva C, Curi N, Bueno T, Junior A, et al. Modeling spatially distributed soil losses and sediment yield in the upper Grande River Basin-Brazil. Catena 2017;157:139-50.

Chuenchum P, Xu M, Tang W. Estimation of soil erosion and sediment yield in the Lancang-Mekong River using the modified revised universal soil loss equation and GIS techniques. Water 2020;12,135.

Department of Primary Industries and Mines (DPIM). Report of the Study on the Solution of Cd Contamination in the Mae Tao Basin, Mae Sot District, Tak Province. Bangkok, Thailand: Office of Primary Industries and Mines Khet3 (Northern part), Ministry of Industry; 2009a.

Department of Primary Industries and Mines (DPIM). Report of Water Quality and Stream Sediment Monitoring at Doi Padaeng zinc Mining in Mae Sot District, Tak Province. Bangkok, Thailand: Office of Primary Industries and Mines Khet3 (Northern part), Ministry of Industry; 2009b.

European Commission. Soil erosion risk assessment in Italy [Internet]. 2000 [cited 2020 Feb 24]. Available from: https://esdac.jrc.ec.europa.eu/ESDB_Archive/serae/GRIMM/italia/eritaly.pdf.

Farhan Y, Zregat D, Farhan I. Spatial estimation of soil erosion risk using RUSLE approach, RS, and GIS techniques: A case study of Kufranja watershed, Northern Jordan. Journal of Water Resource and Protection 2013;5:1247-61.

Ganasri P, Ramesh H. Assessment of soil erosion by RUSLE model using remote sensing and GIS-A case study of Nethravathi Basin. Geoscience Frontiers 2016;7:953-61.

Kassawmar T, Gessesse GD, Zeleke G, Subhatu A. Assessing the soil erosion control efficiency of land management practices implemented through free community labor mobilization in Ethiopia. International Soil and Water Conservation Research 2018;6:87-98.

Kim HS. Soil Erosion Modeling Using RUSLE and GIS on the IMHA Watershed, South Korea [dissertation]. USA: Colorado State University; 2006.

Land Development Department. Soil Loss in Thailand. Bangkok, Thailand: Ministry of Agriculture and Cooperatives; 2000.

Lazzari M, Gioia D, Piccarreta M, Daneses M, Lanorate A. Sediment yield and erosion rate estimation in the mountain catchments of the Camastra artificial reservoir (Southern Italy): A comparison between different empirical methods. Catena 2015;127:323-39.

Lee S, Lee H. Scaling effect for estimating soil loss in the RUSLE model using remotely sensed geospatial data in Korea. Journal of Hydrology and Earth System Science 2006;3:135-57.

Mesnard L. Pollution models and inverse distance weighting: Some critical remarks. Computer and Geosciences 2013;52:459-69.

Millward A, Mersey J. Adapting the RUSLE to model soil erosion potential in a mountainous tropical watershed. Catena 1999;38:109-29.

Oliveria S, Wendland E, Nearing A. Rainfall erosivity in Brazil: A review. Catena 2012;100:139-47.

Ostovari Y, Ghorbani-Dashtaki S, Bahrami H, Naderi M, Dematte A. Soil loss estimation using RUSLE model, GIS and remote sensing techniques: A case study from the Dembecha Watershed, Northwestern Ethiopia. Geoderma 2017;11:28-36.

Ozcan U, Erpul G, Basaran M, Erdogan E. Use of USLE/GIS technology integrated with geostatistics to assess soil erosion risk in different land uses of Indagi Mountain Pass-Cankırı, Turkey. Environment Geology 2007;53:1731-41.

Pollution Control Department (PCD). Annual Report 2013. Bangkok, Thailand: Ministry of Natural Resources and Environment; 2013.

Rammahi AH, Khassaf SI. Estimation of soil erodibility factor in RUSLE equation for Euphrates River watershed using GIS. International Journal of GEOMATE 2018;14:164-9.

Simmons RW, Pongsakul P. Towards the development of a sampling strategy to evaluate the spatial distribution of Cd in contaminated irrigated rice-based agricultural systems. Proceeding of the 17th World Congress of Soil Science; 2002 Aug 14-21; Bangkok: Thailand; 2002.

Simmons RW, Pongsakul P, Chaney RL, Saiyasipanich D, Klinphoklap S, Nobuntou W. The relative exclusion of zinc and iron from rice grain in relation to rice grain cadmium as compared to soybean: Implications for human health. Plant Soil 2003;257:163-70.

Simmons RW, Sukreeyaponge O, Noble AD, Chinabut N. Final Report of LDD-IWMI Land Zoning and Cd Risk Assessment Activities Undertaken in Phatat Pha Daeng and Mae Tao Mai Sub-district, Mae Sot, Tak Province, Thailand. SEA Regional Office, Kasetsart University, Thailand: International Water Management Institute; 2005.

Somprasong K, Chaiwiwatworakul P. Estimation of potential cadmium contamination using an integrated RUSLE, GIS and remote sensing technique in a remote watershed: A case study of the Mae Tao Basin, Thailand. Environmental Earth Sciences 2015;73:4805-18.

Sriprachote A, Kanyawongha P, Ochiai K, Matoh T. Current situation of cadmium-polluted paddy soil, rice and soybean in the Mae Sot District, Tak Province, Thailand. Soil Science and Plant Nutrition 2012;58:349-59.

Suppakarn T, Waragorn S, Pirat J. Application of vegetation and soil indices for monitoring the reclamation area at Phadeng zinc mine in Tak Province, Northern Thailand. Proceeding of the Asia-Pacific Conference on Engineering and Applied Science; 2016 Aug 25-27; Tokyo: Japan; 2016.

Thamjedsada T, Chaiwiwatworakul P. Evaluation of cadmium contamination in the Mae Tao Creek sediment. Proceeding of the 2012 International Conference on Sustainable Environmental Technologies (ICSET); 2012 Apr 26-27; Century Park Hotel, Bangkok: Thailand; 2012.

Unhalekhaka U, Kositanont C. Distribution of cadmium in soil around zinc mining area. Thai Journal of Toxicology 2008;23:170-4.

Xu L, Xu X, Meng X. Risk assessment of soil erosion in different rainfall scenarios by RUSLE model coupled with information diffusion model: A case study of Bohai Rim, China. Catena 2012;100:74-82.

Landslide Hazard Mapping in Panchase Mountain of Central Nepal

Padam Bahadur Budha[1,2,*], Pawan Rai[2,3], Prem Katel[2], and Anu Khadka[4]

[1]*Nepal Environmental Resources Organization, Kathmandu, Nepal*
[2]*Xavier International College, Department of Environmental Science, Kathmandu, Nepal*
[3]*Goldengate International College, Environmental Science Program, Kathmandu, Nepal*
[4]*Southern Illinois University Edwardsville, Faculty of Environmental Sciences, Illinois, USA*

ARTICLE INFO

Received: 15 May 2020
Received in revised: 29 Jul 2020
Accepted: 19 Aug 2020
Published online: 9 Sep 2020
DOI: 10.32526/ennrj.18.4.2020.37

Keywords:
Hazard zonation/ Landslide inventory/ Nepal Himalaya/ Panchase Forest/ Risk reduction/ Slope failures

*** Corresponding author:**
E-mail: padambudha88@gmail.com

ABSTRACT

Numerous slope failures have been noticed in the Panchase region of central Nepal posing threats to people and biodiversity. Considering the need to reduce landslide risks, this research determined the spatial extent of landslide hazard degrees in the Panchase area. The research site, with an area of 278.324 km^2, consists of parts of the Kaski, Parbat, and Syangja Districts. A Statistical Index Method was used for hazard analysis that produced weights. Positive weight values for each factor class represented a higher hazard and vice versa. An inventory of the study area identified 556 landslides measuring 1.511 km^2 indicating a landslide density of 2 per km^2 area. Thirteen percent (36.18 km^2) of the total experimental area was rated as a very high hazard zone. Similarly, the area occupied by high hazard and moderate hazard zones were 77.66 km^2 (28%), and 81.83 km^2 (29%) respectively. The validation showed that the method can produce results with of accuracy of 82.8%. This indicated the hazard assessment process is acceptable and replicable. The factor classes having greater influence for higher landslide hazard are: near the streams, near the roads, barren or grassland, land with phyllite bedrocks, land receiving rainfalls greater than 4,000 mm, lands with an elevation range from 1,000 m to 1,500 m, slopes steeper than 30°, and south-facing slope. During risk management work by local authorities, considerations should be given to these factors and areas with higher hazards.

1. INTRODUCTION

Varnes (1984) defined landslides as 'almost all varieties of mass movements on slope including rock falls, topples and debris flow that involves little or no true sliding'. There is the influence of gravity beside natural and human-induced factors that initiate slope forming materials to move outward and downward along a definite plane of failure. This process has been described as a landslide. Landslides are the product of a complex interplay of various triggering and conditioning factors. Landslides, when combined with human interferences, become complex and hazardous. The landslides and erosion induced geomorphic events bring disaster and land degradation, which in turn aggravates poverty and seriously impairs development efforts. This necessitates the identification of the locations where landslide incidents can occur in the future, quantification of probable loss, and proposal of measures to mitigate the impacts. Landslide risk mapping can be a useful tool (Maes et al., 2017) which includes landslide inventory, hazard zonation, and vulnerability estimation. A hazard can be defined as "a dangerous phenomenon, substance, human activity or condition that may cause loss of life, injury or other health impacts, property damage, loss of livelihoods and services, social and economic disruption, or environmental damage" (UNISDR, 2009). The determining factors for landslide hazards are altitude, slope angle, aspect, vertical curvature (Alkhasawneh et al., 2013), landforms, lithological characteristics, tectonic units, illumination coefficient (Ghimire, 2010), intense rainfall, and the hill slope alteration (Bhusan and Goswami, 2013). When triggering factors like extreme rainfall or zones of tectonic movements are used then results are explained as hazard maps.

Citation: Budha PB, Rai P, Katel P, Khadka A. Landslide hazard mapping in Panchase Mountain of central Nepal. Environ. Nat. Resour. J. 2020;18(4):387-399. (https://doi.org/10.32526/ennrj.18.4.2020.37)

Landslide hazard is one of the most lethal geological hazards in Nepal in terms of the frequency of its occurrence and cumulative loss and damage. In Nepal, most landslides hazards can be observed occurring in the hilly and mountainous regions. Such mountains are active and fragile (Upreti, 2001), and have high relief which makes them landslide-prone during high-intensity monsoon rainfall, and earth tremors (Kayastha et al., 2013). During monsoon, the orographic effect is activated as clouds can't cross the Himalayas forcing greater rainfall in Central and Eastern Nepal, and this, in turn, triggers many landslide related disasters (Dahal, 2012). In the hazard-prone country like Nepal, landslide risk mapping is an essential tool that helps planners to decide the suitable sites for the construction of roads, bridges, hydropower plants, and so on. Landslide hazard and risk studies imply the assessment of various scenarios according to the type and intensity of the triggering mechanism, in which local and regional developments of landslide mechanisms must be considered, as well as their direct and indirect consequences (Cascini et al., 2004). Landslide losses can be avoided if problems are recognized before the happening of a landslide event. Some studies have been previously carried out (Budha et al., 2016; Ghimire, 2010; Kayastha et al., 2013) on landslide hazard assessment in Nepal Himalaya.

This research was carried out in an ecologically important Panchase Mountain Ecological Region (PMER) of central Nepal, which is an essential element of the corridor linking the middle mountain species to that of higher mountains as a part of the Chitwan-Annapurna Landscape. Threatened and endangered species like *Cyathea spinulosa*, *Michealia champaca*, and *Taxus wallichiana* have been noticed in this area during field visits. Thirty seven ecosystem services were identified in PMER ranging from provisional services, regulating services, cultural services, to supporting services (Adhikari et al., 2018) and the services are beneficial to local and national economies along with global impacts (Bhandari et al., 2018). Such services are at higher risk of being diminished by the occurrence of landslides. The current approach of constructing rural roads in PMER had caused many shallow landslides and debris flows (Leibundgut et al., 2016). In addition, there are natural triggering factors of landslide occurrences like rainfall and earthquakes. Such landslides carry debris and deposit heavily in forest areas, cultivated lands, and settlements (Dhakal, 2016). This process reduces the benefits of ecosystem services. Phewa Lake is shrinking due to landslides and soil erosion as there is heavy sedimentation in the lake area (Watson et al., 2019). Ramsar Sites Information Service (RSIS) mentioned that the wetlands in Kaski district were incorporated in Ramsar sites (RSIS, 2016) as Lake Cluster of Pokhara Valley which also included Phewa Lake (Figure 1) and its watershed. Streams flowing from PMER carries a huge amount of debris that causes sedimentation in Phewa Lake which in turn destroys the biodiversity of the area. It seems that there occurs a chain of impacts starting from landslides and erosion, to sedimentation in river and lake to loss of biodiversity of the lake. The losses incurred by nature in this area are intangible.

It can be seen that PMER is an ecologically important area that forms the corridor for north-south connection, inhabited by endangered species, and providing water storage for Phewa Lake. In the meantime, many landslides observed in PMER are deteriorating the natural habitat of wild flora and fauna which necessitate the mapping of landslides and preparation of hazard maps. Thus, the objective of this research was to conduct a landslide inventory of the PMER and prepare hazard zonation for landslides with the application of remote sensing and Geographical Information System (GIS) for effective landslide hazard mapping.

2. METHODOLOGY

2.1 Experimental site

The study area for this research is part of the PMER, a protected forest area presented in Figure 1, and will be referred to as Panchase hereafter. Panchase occupies portions of the Kaski, Parbat and Syangja Districts covering an area of 278.324 km^2. With the changed administrative structure of Nepal as Rural Municipality (RMP) and Municipalities (MP), there are now six administrative units, as illustrated by Figure 1, as local units. These are Pokhara and Annapurna of Kaski District, Modi and Kushma of Parbat District, and Aandhikhola and Phedikhola of Syngja District. Altogether, there are 20 wards in this area.

The altitude of Panchase ranges from 715 m to 2,504 m above mean sea level and the highest point is the Panchase peak. Topographically, the area ranges from moderate to steep terrain. As one ascends towards higher altitudes from Phewa Lake the slopes become steeper. The Panchase Mountain comprises the headwater of three river systems, one end to the Phewa Lake, and forms the most important source of

water for the lake. The area surrounding the peak is a dense forest with *Alnus-Schima*, *Castanopsis-Pinus*, *Daphniphyllum*, and *Rhododendron-Quercus* the major tree types (Phuyal et al., 2015). These trees are representative of lower subtropical, upper subtropical, and lower temperate bioclimatic zones, respectively. Temperatures in the Pancahse region range from a mean minimum of 5.3°C to a mean maximum of 29°C and it is located in a region of Nepal that receives the highest amount of annual average rainfall of 3,882 mm. This climatic information was obtained from the Department of Hydrology and Meteorology, Government of Nepal.

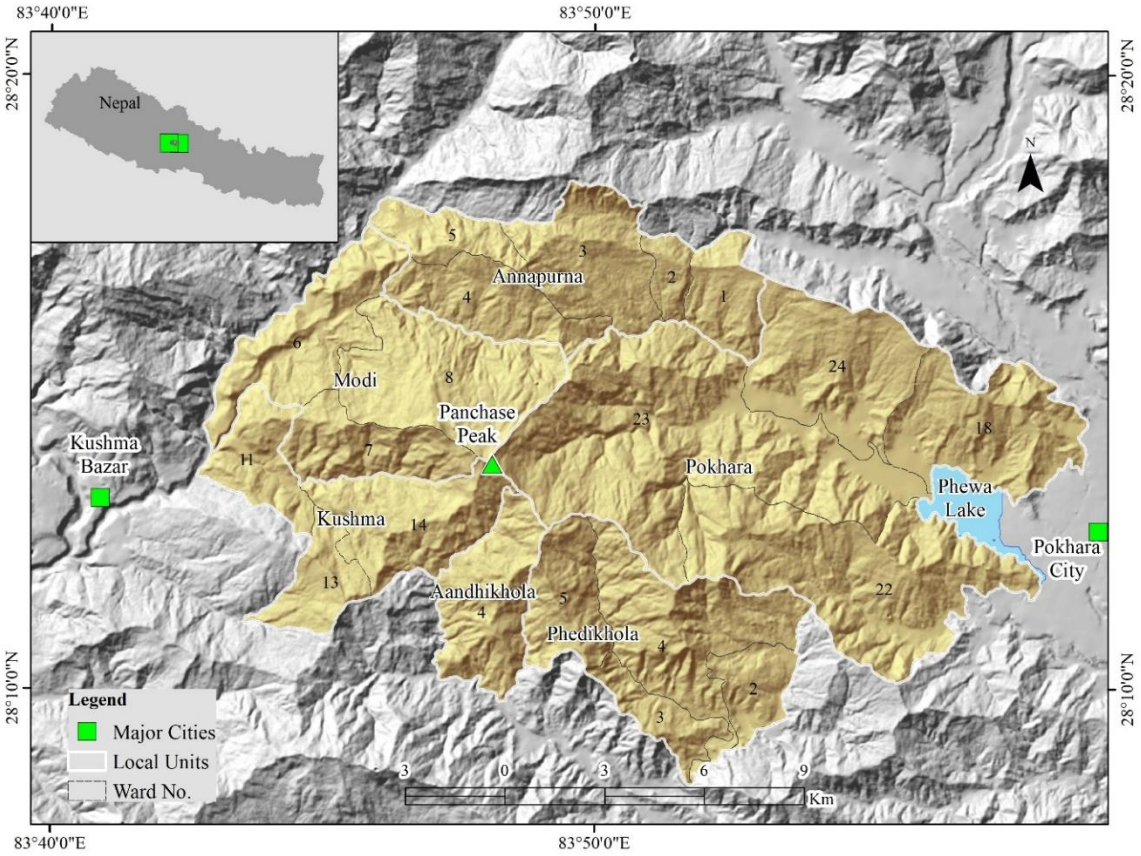

Figure 1. Panchase showing local units and ward numbers (inset; location in central Nepal)

2.2 Data and sources

The data used in this study are composed of both primary and secondary sources. Table 1 lists all the data used in this research and their sources. The inventory of landslides was done from Google Earth and updated after the fieldwork. Some of the secondary data used in this research were digital data of topographic maps, rainfall readings, and geological maps. Open Street maps were also explored to obtain the data of roads. Digitization was done over Google Earth for drawing major rivers.

2.3 Hazard assessment process

The technique of hazard mapping includes analysis of landslides inventoried and development of some relations with factors associated with the process of land-sliding so that hazard status of specific area can be estimated. Figure 2 represents the elaborated form of the landslide hazard mapping process. Landslides were located on Google Earth and digitized as polygons to estimate their coverage. The inventory was divided into two groups consisting of 70 and 30 percentages (Nachappa et al., 2020) of landslides to be used in hazard mapping and validation processes respectively.

Table 1. List of data and the sources used in this research

Data	Sources
Landslides	Google Earth
Topographic data	Department of Survey
Geological maps	Department Mines and Geology
Rainfall data	Department of Hydrology and Meteorology
Roads	Open street maps, Google Earth
Streams	Department of Survey, Google Earth

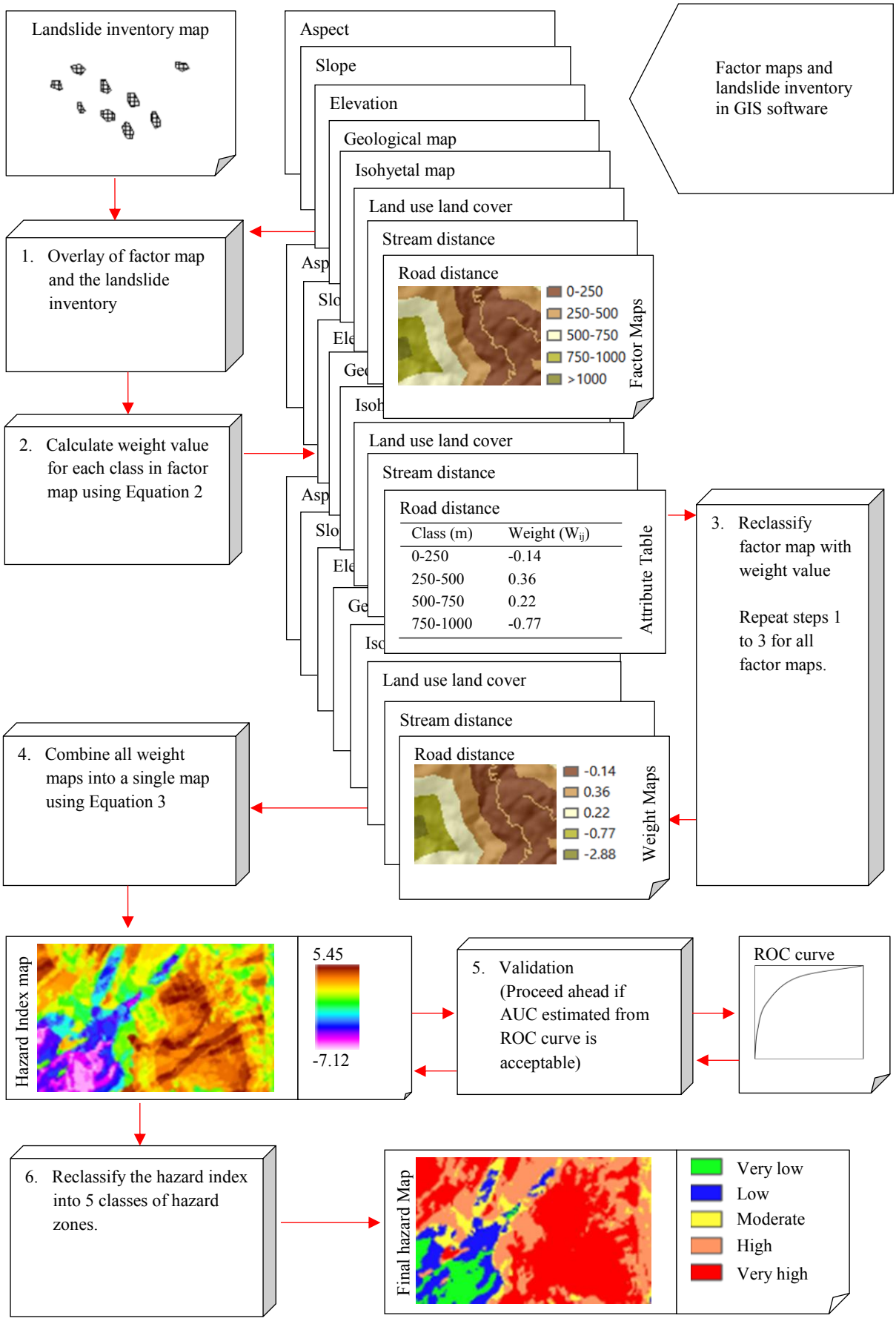

Figure 2. Flowchart of the method used in the hazard mapping process (modified after van Western et al., 1997)

2.3.1 Landslide inflicting factors

There were eight factors considered for landslide hazard mapping in this research with assumptions that they influenced the formation of landslides. These factors are listed in Table 2 and shown in Figure 3. Three topography based factors (elevation, aspect, and slope gradient) were derived from Digital Elevation Model (DEM) produced from contours of 20 m interval. Two distance-based maps were created: the distance from streams and the distance from roads. Other factors used were land use map from topographic sheet modified with recent satellite imagery in GIS, geological maps digitized from a scanned copy of geological maps, and isohyetal map produced from the interpolation of rainfall data of 14 rainfall stations.

Table 2. The factors and their derivation techniques

Factor	Derivation of factors
Aspect	DEM processing
Slope	DEM processing
Elevation	DEM processing
Stream distance	Stream buffering
Road distance	Road buffering
Land use and land cover	Topographic sheet digitization and update
Geology	Digitization of geological map
Isohyetal map	Interpolation of rainfall data

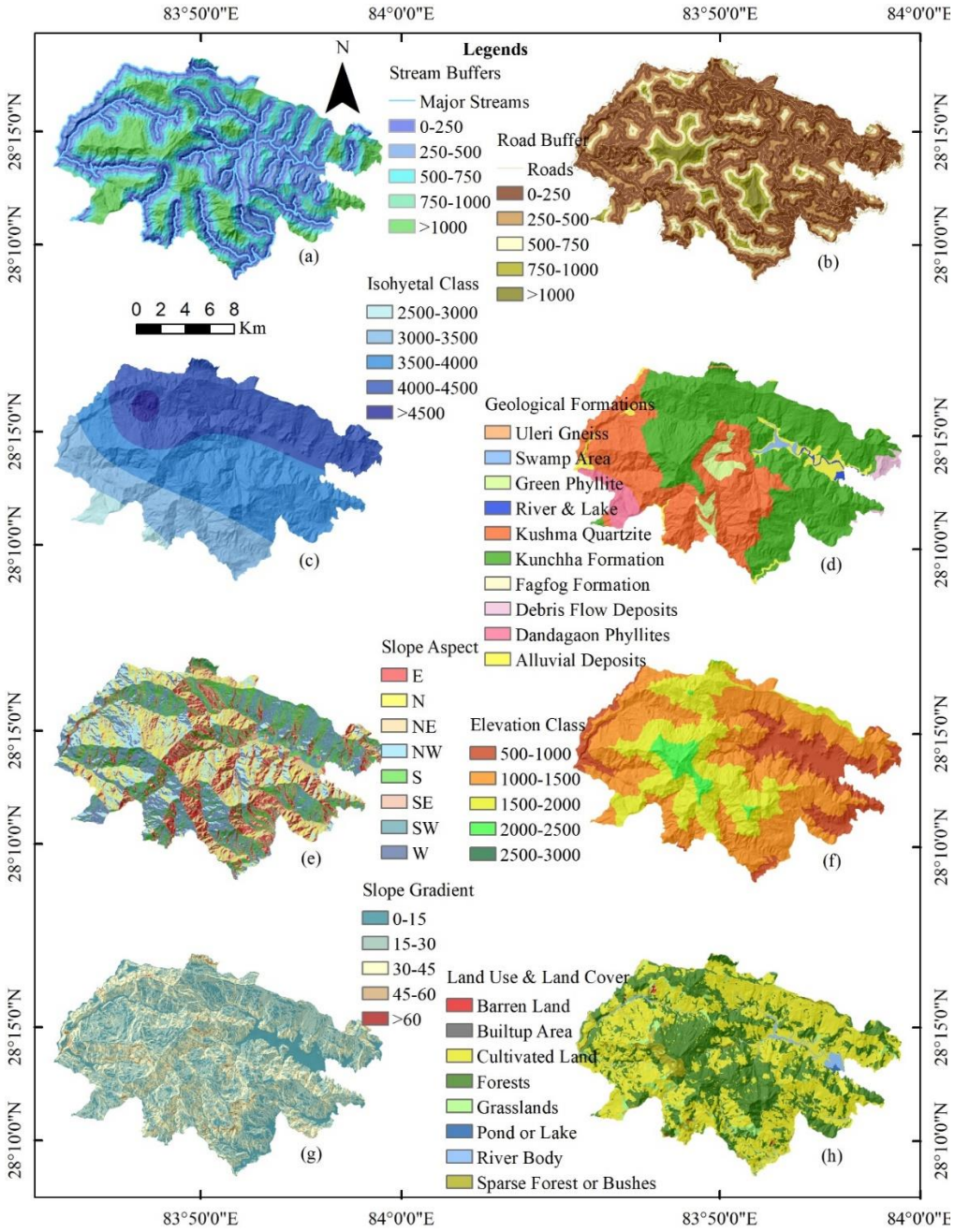

Figure 3. Map of Panchase showing (a) stream buffers in meters; (b) road buffers in meters; (c) isohyetal classes in millimeter; (d) geological formations; (e) aspect showing eight directions; (f) elevation in meters; (g) slope in degrees; and (h) land use land cover

2.3.2 Landslide inventory

Landslide inventory includes an enumeration of location, date of occurrence, and type of movement (Guzzetti, 2005) of landslide incidents which can be extracted satellite imageries, topographic sheets, or field surveys. The inventory of landslides was done from the digitization of landslides scars observed on Google Earth imageries of different times. The inventory was verified in the subsequent field visits and updated thereafter. In the field study data regarding the surrounding conditions, impacted areas, and elements were also recorded.

2.3.3 Hazard zonation and validation

Statistical index method or bivariate analysis was used in this research for the process of hazard mapping. This method was first introduced by van Westen et al. (1997) for landslide hazard analysis. In this method, a weight value for a factor class, such as a certain land-use type or a certain slope class is defined. A weight value is the natural logarithm of the ratio of landslide densities. Ratio being landslide density (f_{ij}) in a certain class (i) of factor (j) divided by the landslide density (f) in the entire map as depicted by the following equations (van Westen et al., 1997):

$$W_{ij} = \mathrm{Ln}\left[\frac{f_{ij}}{f}\right] = \mathrm{Ln}\left[\frac{\left(\frac{A^*_{ij}}{A_{ij}}\right)}{\left(\frac{A^*}{A}\right)}\right] \quad (1)$$

$$W_{ij} = \mathrm{Ln}\left[\left(\frac{A^*_{ij}}{A_{ij}}\right) \times \left(\frac{A}{A^*}\right)\right] \quad (2)$$

Where; W_{ij}=weight given to class i of factor j, A_{ij}^*=area of the landslide in class i of factor j, A_{ij}=area of class i of factor j, A^*=total area of landslides in the entire map, A=area of the entire map.

Each factor maps are classified according to their weight values. Overlaying factor maps using their weight values in the GIS environment produce the hazard map. The process used for overlaying was the weighted sum method and equal importance was given to all parameters. Thus, this summing method can be represented by the following equation:

$$HI = \sum_{j=n}^{n} W_{ij} \quad (3)$$

Where; HI=Hazard Index of landslides, W_{ij}=weight of class i of parameter j, n=number of parameters.

The validation process includes the preparation of the Receiver Operational Characteristics (ROC) curve and estimating the area under the curve (AUC). The AUC varies between 0 (worse-than-random model), 0.5 (random model), and 1 (best discriminating model) (Hirzel et al., 2006). The AUC greater than 0.6 are generally accepted models but higher accuracies are preferred.

3. RESULTS AND DISCUSSION

3.1 Landslide inventory

In Panchase, there were altogether 556 landslides inventoried covering 1.51 km^2 in total area. Five hundred landslides were marked from the Google Earth that had a measured area of 1.176 km^2. Fifty six landslides were updated via field visits adding an area of 0.335 km^2. The landslide density thus became 1.99 per km^2 in this research area. Figure 4 represents the landslide inventory map of Panchase.

Size of the smallest landslide recorded was 40.253 m^2 and the largest one measured 105,722.156 m^2. The largest landslide was located in Annapurna RMP, ward number 3. Table 3 lists the landslides according to the wards of six local administrative units. The highest numbers of landslides were seen in ward 3 of Annapurna RMP. There were 108 landslides in this ward that also measured the highest coverage in the area. There were 281 landslides in Annapurna RMP alone, which is almost half of the entire landslide's inventories. This probably plays a crucial role in hazard mapping. On the other hand, a portion of Kushma MP had the least number of landslides which was 14.

Table 3. Number and area of landslides according to ward numbers of municipality and rural municipality in Panchase

Municipality/rural municipality	Ward number	No. of landslides	Area of landslides (m^2)
Aandhikhola	4	24	98,549.04
Annapurna	1	28	35,900.91
Annapurna	2	32	46,045.57
Annapurna	3	108	327,401.65
Annapurna	4	99	200,778.07
Annapurna	5	14	53,418.38
Kushma	11	5	16,894.98

Table 3. Number and area of landslides according to ward numbers of municipality and rural municipality in Panchase (cont.)

Municipality/rural municipality	Ward number	No. of landslides	Area of landslides (m^2)
Kushma	14	9	17,323.08
Modi	6	24	55,775.86
Modi	7	6	24,149.09
Modi	8	28	29,093.46
Phedikhola	2	8	41,722.18
Phedikhola	4	21	146,026.86
Pokhara	18	17	32,793.83
Pokhara	22	15	33,440.51
Pokhara	23	105	283,565.88
Pokhara	24	13	67,185.67
		556	1,510,260.06

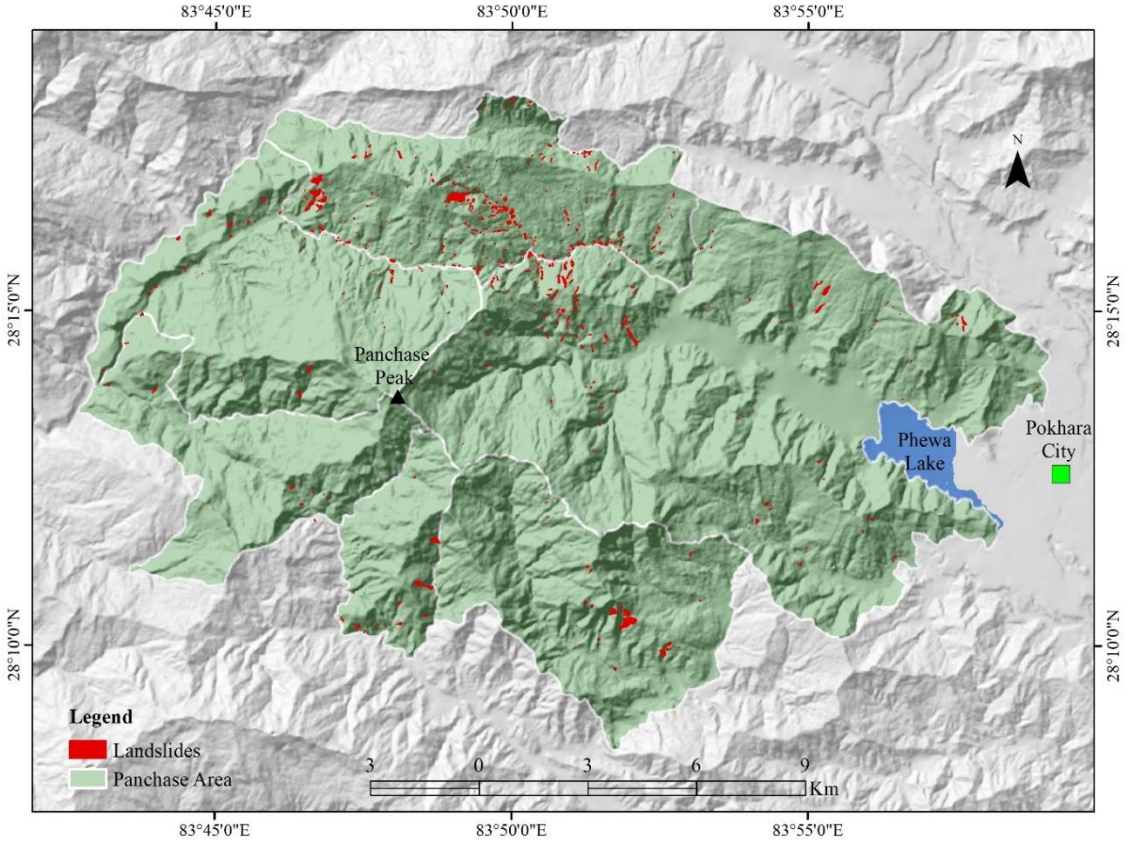

Figure 4. Landslides inventory of Panchase area

3.2 Hazard zonation and validation

A set of 388 landslides were separated by random selection to be used for hazard mapping. The remaining landslides were kept for the validation of the results. In Table 4, we can see the area of landslides occurred in different factor classes and weight values. The total area of landslides (A) is 1.51 km^2. Nearest buffers for stream and road buffers categories, forests for land use land cover classes, and Kunchha Formation for geological formations, respectively, bear higher landslide areas. Parts with 4,000-4,500 mm rainfall, 1,000-1,500 m elevation and south-southwest slope faces with gradients of 15°-45° covered more area of landslides than other classes in respective factors.

From Table 4, it can be said which factor class played a key role in hazard output by looking at their weight values. As the weight values of each pixel in a factor class are added to produce a hazard map, pixels with positive weight values produce higher hazard zones. Thus, factor classes such as near the streams, near the roads, in barren lands or grasslands, with phyllite rocks, having rainfall greater than 4,000 mm, 1,000 m to 1,500 m of elevation, south-facing and

steeper than 30^o slope, are liable for developing higher hazard. On the contrary, negative values of pixels are summed in the process of hazard map production and result in lower hazard categories.

Table 4. Calculation of weight value for each factor class for hazard analysis

Factor	Factor class	Factor area (A_{ij})	Landslide area (A_l)	Landslide area modeled (A_{ij}*)	A_{ij}*/A_{ij}	Weight (W_{ij})
Stream buffer (m)	0-250	79.5780	0.612	0.374	0.005	0.22
	250-500	69.5536	0.317	0.237	0.003	-0.10
	500-750	53.0668	0.247	0.177	0.003	-0.12
	750-1,000	35.2868	0.140	0.116	0.003	-0.14
	>1,000	41.2488	0.185	0.147	0.004	-0.06
Road buffer (m)	0-250	165.554	0.752	0.540	0.003	-0.14
	250-500	65.3872	0.558	0.355	0.005	0.36
	500-750	28.6172	0.170	0.134	0.005	0.22
	750-1,000	11.6452	0.020	0.020	0.002	-0.77
	>1,000	7.5304	0.001	0.002	0.000	-2.88
Land use land cover classes	Cultivated land	143.1240	0.358	0.277	0.002	-0.67
	Bushes	10.4216	0.042	0.032	0.003	-0.21
	River body	6.1456	0.016	0.005	0.001	-1.57
	Forests	109.7008	0.762	0.474	0.004	0.14
	Grasslands	8.4980	0.177	0.132	0.015	1.41
	Barren land	0.4272	0.145	0.132	0.309	4.41
	Pond or lake	0.4136	0.000	0.000	0.000	0
	Builtup area	0.0032	0.000	0.000	0.000	0
Geological formations	Fagfog formation	0.0264	0.000	0.000	0.000	0
	Alluvial deposits	11.3288	0.011	0.008	0.001	-1.68
	Dandagaon phyllites	8.8050	0.000	0.000	0.000	0
	Sidhane green phyllite	8.9136	0.011	0.004	0.000	-2.13
	Kunchha formation	147.2744	1.071	0.772	0.005	0.33
	Kushma quartzite	95.4952	0.400	0.264	0.003	-0.31
	Debris flow deposits	3.5012	0.001	0.001	0.000	-2.40
	Swamp area	1.7812	0.000	0.000	0.000	0
	Uleri gneiss	0.3390	0.006	0.001	0.004	-0.06
Isoheytal map (mm)	2,500-3,000	7.8312	0.019	0.013	0.002	-0.84
	3,000-3,500	58.2320	0.296	0.211	0.004	-0.04
	3,500-4,000	106.4440	0.207	0.152	0.001	-0.97
	4,000-4,500	101.4888	0.930	0.644	0.006	0.52
	>4,500	4.7380	0.048	0.031	0.007	0.54
Elevation range (m)	500-1,000	47.6520	0.109	0.077	0.002	-0.84
	1,000-1,500	138.8040	0.984	0.735	0.005	0.34
	1,500-2,000	81.5628	0.406	0.237	0.003	-0.26
	2,000-2,500	10.7092	0.001	0.002	0.000	-2.82
	>2,500	0.0060	0.000	0.000	0.000	0
Aspect (Slope directions)	N	37.6744	0.132	0.085	0.002	-0.51
	NE	33.6220	0.180	0.106	0.003	-0.18
	E	29.8532	0.175	0.116	0.004	0.03
	SE	30.8232	0.260	0.148	0.005	0.24
	S	41.1036	0.318	0.264	0.006	0.53
	SW	43.0896	0.319	0.244	0.006	0.40
	W	30.0888	0.070	0.049	0.002	-0.84
	NW	32.4792	0.046	0.038	0.001	-1.16
Slope (degree)	0-15	59.4276	0.059	0.041	0.001	-1.69
	15-30	145.6352	0.718	0.500	0.003	-0.09
	30-45	66.6100	0.656	0.457	0.007	0.60
	45-60	7.0156	0.067	0.052	0.007	0.67
	>60	0.0456	0.001	0.001	0.018	1.54

Figure 5 shows the hazard map overlaid by the boundary of the RMP/MP. The research observed that the flood plain area of Harpan Khola which is upstream of Phewa Lake and areas surrounding the Panchase peak have low hazard categories. A higher hazard can be observed in most areas of the Annapurna and northern part of Pokhara. Also, the lower or southern portion of Aandhikhola and Phedikhola RMP have an area of high hazard.

Looking at the overall map, the moderate hazard was found occupying a large area of about 81.83 km^2 which makes 29% of the experimental site. High and very high hazard zones occupy the area up to 77.66 km^2 and 36.18 km^2, respectively. The percentage of area covered by these categories is shown in the legend of Figure 5. Similarly, low and very low hazard zones measure 58.8 km^2 and 24.27 km^2 respectively together forming 30% of the total area.

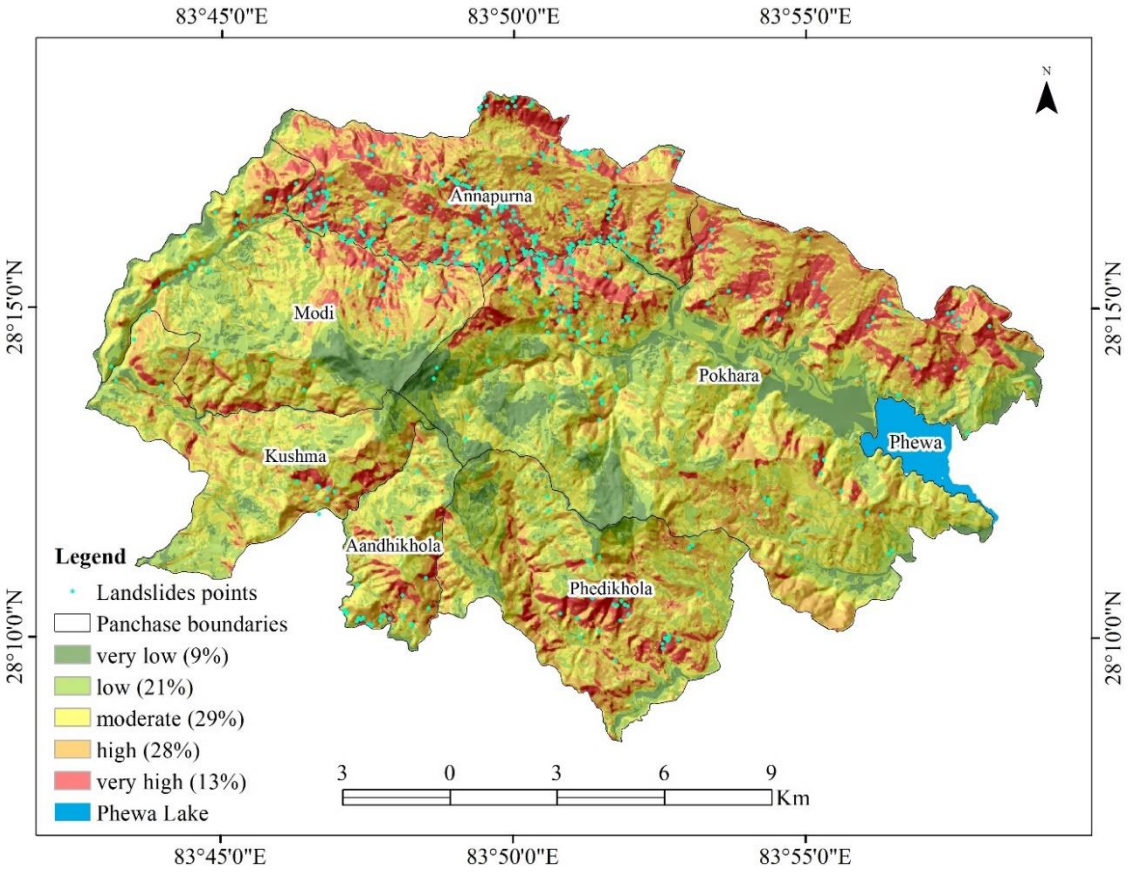

Figure 5. Hazard zonation map of PMER with municipalities and rural-municipalities

The validation for the hazard map showed 0.828 part of AUC as indicated by Figure 6. This means the model's predictability is 82.8% in this experimental site. Also, this implies the results of hazard assessment are acceptable and can be used in similar research in other areas of similar topography. The AUC showed 0.762 for higher Himalayas (Budha et al., 2016) and was 0.758 near Mahabharata Range (Kayastha et al., 2013), as both used the same statistical index method as used in this research. This specifies higher accuracy in the middle mountains of Nepal.

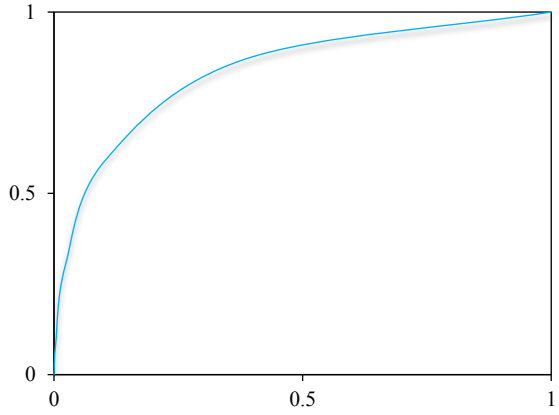

Figure 6. ROC curve for validation of results (AUC=0.828)

When we standardize the raster values of hazard from zero to one most of the local units seem to have a mean value around 0.5 as shown in Figure 7. We can see that the average hazard value of Annapurna RMP is higher than the others. This indicates the area of Panchase that belonged to Annapurna RMP is more prone to landslide hazards. Similarly, the average hazard value of Aandhikhola and Phedikhola RMP is greater than 0.5. Modi RMP and Kushma MP have relatively lower hazard from landslides than other areas. This average score can be linked to the occurrence of landslides from Table 3, which revealed that Annapurna RMP has a greater hazard score as well as a higher number of landslides.

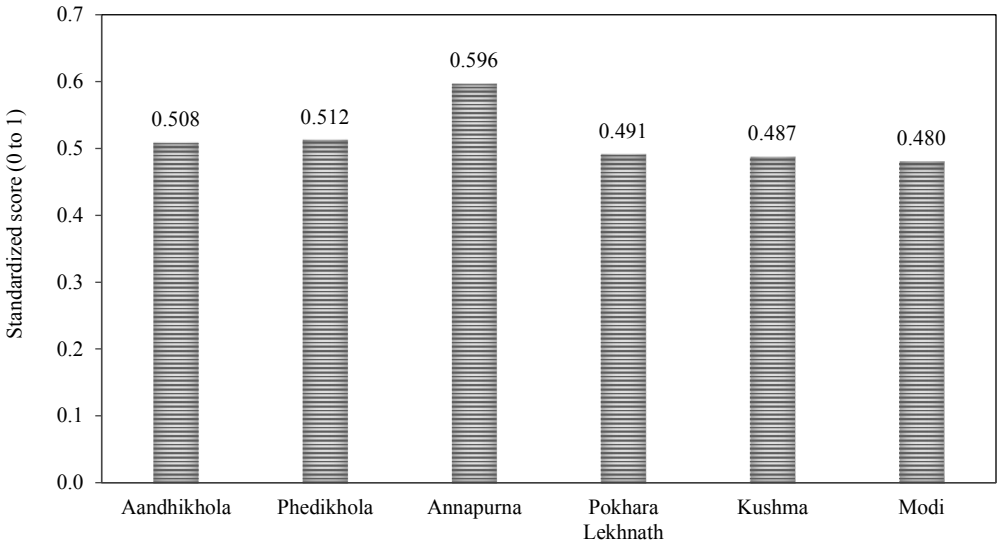

Figure 7. The average hazard value of each municipality/rural municipality

4. DISCUSSIONS

4.1 Landslide inventory

With 556 landslides, the landslide density in the Panchase area was found to be 1.99 per km^2. In research conducted at a location nearby this experimental site, landslide densities of 0.44 per km^2 (Basnet et al., 2006) and 0.571 per km^2 (Bhatt et al., 2013) were found in Phewa and Rupa watersheds, respectively. Phewa watershed is a part of the present study area. The landslide densities had increased by four folds since 2006 when the first research was carried out in Phewa watershed. Only 16 landslides recorded by Basnet et al. (2006), in Sarangkot and Kaskikot which are now ward number 18 and 24 of Pokhara respectively, had now increased to 30. The landslide susceptibility mapping done in 2016 used 80 landslides (Pradhan and Kim, 2016) which had increased to 260 during the time of this research. Thus in Phewa watershed of 123 km^2 landslide density had increased from 0.65 per km^2 to 2.1 per km^2. Above figures indicates that numbers of landslides are increasing annually in Phewa watershed and in larger difference. These results can be the outcome of haphazard road construction without considering fragile geology of the area besides natural triggers of highly saturated slopes and excess rainfall.

4.2 Factors influencing landslide hazard

In Table 4, there can be noticed the spatial coverage of different factor classes along with the area of landslides occurred in the respective class. The total area of landslides (A) is 1.51 km^2. While we consider stream as a factor 0.612 km^2 of landslide area had occurred in 0m to 250 m factor class. It was observed that there were higher occurrences of landslides in the buffers nearer to the streams. Saturation of the slopes near the streams is altered by the excess amount of water available which promotes the instability in the slopes. The higher the instability, the higher the chances of landslide occurrences. Similar situations prevail in road buffers as well, as we can observe in Table 4 there is a higher frequency of landslides occupied. Fifty percent of the total landslide area was found within 250 m distance from the road. The occurrence of landslides within 100m from the roadside was more than twice as likely as that triggered by an earthquake (McAdoo et al., 2018). In mountain regions, roads are closely connected with

landslide risk as they destabilize slopes and often lead to the expansion of settlements into hazard zones (Lennartz, 2013). This phenomenon of landslide occurrence due to fresh road cuttings had happened in some parts of Panchase as well. The current style of road construction is inducing soil erosion and shallow landslides which is in turn affecting the road structures as well as downslope land-use types (Leibundgut et al., 2016). Field observation reflected that some households are under threat due to the openings of new tracks. Those households were mainly located at the down-slope of road cuts.

In the case of land use, we can observe a higher amount of landslide area in forests and cultivated lands which are 0.762 km^2 and 0.358 km^2 respectively which together accounted for 75% of the total landslide area. A study in Phewa watershed had also found higher landslides among forests (Basnet et al., 2006) whereas cultivation lands had higher landslides in a study at Mugu District (Budha et al., 2016). Bhatt et al. (2013) also found higher landslides in cultivated lands than in forests. Landslides in cultivated lands may be attributed to the regular disturbance of the soil and the surface but in the case of forested areas, landslides can be related to steep topography, less surface cover, and weak geology.

Among geological types, the highest landslide occurrence was observed in Kunchha formation as it is formed of phyllite rocks that get weathered easily. This formation had landslides of 1.071 km^2 which is almost 70% of the total landslide area. In a study by Budha et al. (2016), landslides were observed more often in geology with rock combinations of phyllite with gneiss and schists. Rocks along with road cuts in the field were observed as highly weathered which may be responsible for landslides. In some weathered rocks, the occurrence of clay mineralization further influences landslides. Clay mineralization in phyllite and quartzite rocks were responsible for Dumre landslides due to rainfall which was a major triggering agent (Regmi et al., 2013). Such processes are slow and prolonged which enhances the weathering of rocks.

In the case of the isohyetal factor, landslides were observed highly occurring in the class having 4,000 mm to 4,500 mm of annual average rainfall as shown in Table 4. In this category 0.93 km^2 of landslides were observed that accounted for 60%. The occurrence of landslides decreased in other classes of the isohyetal factor. Here, landslide occurrence was seen higher in areas with greater rainfall. The orographic effect of the Himalayan range is responsible for extreme rainfall in central and eastern Nepal causing higher landslide incidents in these regions (Dahal, 2012). The rainfall in Panchase area is generally greater as the orographic effect is onset by the Annapurna and Machhapuchhre Mountains. This may be responsible for triggering the landslides in the hilly region. In the Himalayas, up to 53 mm of continuous rainfall for 24 h can trigger landslides (Dikshit et al., 2019). On average, a rainfall of 10 h or less requires a rainfall intensity above 12 mm/h to trigger failure, but a rainfall duration of 100 h or longer with an average intensity of 2 mm/h can also trigger landslides in the Himalaya (Dahal and Hasegawa, 2008).

We can see most landslides occurring in mid-elevations of 1,000-2,000 m. Factor class 1,000-15,000 m of elevation occupied 0.984 km^2 of the landslide area. The elevation is taken as a factor in landslide hazard assessment. The elevation of the place can reflect certain type of climatic conditions because temperature decreases as height is increased. A climatic character such as temperature change and rainfall distribution is dependent upon the elevation (Dawadi, 2017). Also, in areas with weak rocks, relative relief is an important factor to determine the landslide hazard (Ghimire, 2010). Again, when we consider the aspect of the slopes, most landslides were observed in south-facing slopes whether they may be southeast, southwest, or just south. This is similar to the results of Bhatt et al. (2013) in a study of Phewa watershed, where the south and east face of slopes had higher landslide occurrences. There is differential solar input in different aspects and the rainfall amount also varies for various aspects. This, in turn, affects slope stability. South and east slopes generally receive higher solar radiation and a higher amount of rainfall. Similarly, in the case of the slope, gradients with 15° to 45° have a higher area of landslides. Together they occupy 1.374 km^2.

5. CONCLUSION

In the Panchase area, 556 landslides were inventoried that showed landslide density had increased by four-fold since 2006. This should be a key concern for organizations working in disaster risk management of districts in Panchase. Likewise, hazard zonation showed 41% of the total study area under high and very high hazard of landslides. Major contributing factors to the landslide hazard were southern and eastern slopes, with gradients greater

than 30°, barren lands and forests, having geology of Kunchha Formation with phyllites as major rock type, areas with annual average rainfall greater than 4,000 mm, and streams and roads proximities. Thus, the hazard analysis of Panchase revealed the whole area of Annapurna and the northern part of Pokhara in the Panchase area being located in higher hazard category along with half the area of the ecologically important Phewa Lake watershed. Still, very fewer tasks are being done to reduce landslide happenings: rather, more anthropogenic disturbances are increasing its frequency. The research findings can be key insights for local administrative units of Kaski, Syangja, and Parbat district to manage the landslide hazard and inclusion in the annual plans of disaster risk management.

ACKNOWLEDGEMENTS

We would like to acknowledge the Ministry of Science and Technology, Government of Nepal for providing funds through Research and Innovative Grants Program 2017-18 that make it possible to conduct this research. We would also like to give our sincere thanks to all the respondents, key informants for their active and cordial participation during the questionnaire part of the research.

REFERENCES

Adhikari S, Baral H, Nitschke CR. Identification, prioritization and mapping of ecosystem services in the Panchase Mountain Ecological Region of Western Nepal. Forests 2018;9:Article ID 554.

Alkhasawneh MS, Ngah UK, Tay LT, Mat Isa NA, Al-Batch MS. Determination of important topographic factors for landslide mapping analysis using MLP network. The Scientific World Journal 2013;2013:Article ID 415023.

Basnet P, Balla MK, Pradhan BM. Landslide hazard zonation, mapping and investigation of triggering factors in Phewa lake watershed, Nepal. Banko Janakari 2006;22:43-52.

Bhandari AR, Khadka UR, Kanel KR. Ecosystem services in the mid-hill forests of western Nepal: A case of Panchase Protected Forest. Journal of Institute of Science and Technology 2018;23(1):10-7.

Bhatt BP, Awasthi KD, Heyojoo BP, Silwal T, Kafle G. Using geographic information system and analytical hierarchy process in landslide hazard zonation. Applied Ecology and Environmental Sciences 2013;1(2):14-22.

Bhusan K, Goswami DC. Triggering factors of landslides and determination of rainfall threshold: A case study from northeast India. In: Margottini C, Canuti P, Sassa K, editors. Landslide Science and Practice, Volume 4: Global Environmental Changes. Heidelberg, Germany: Springer; 2013. p. 87-92.

Budha PB, Paudyal K, Ghimire M. Landslide susceptibility mapping in eastern hills of Rara Lake, western Nepal. Journal of Nepal Geological Society 2016;50:125-31.

Cascini L, Bonnard C, Jibson R, Montero-Olarte J. Landslide hazard and risk zoning for urban planning and development. Proceedings of the International Conference on Landslide Risk Management; 2005 May 31-Jun 3; Vancouver: Canada; 2004.

Dahal RK. Rainfall-induced landslides in Nepal. International Journal of Erosion Control Engineering 2012;5(1):1-8.

Dahal RK, Hasegawa S. Representative rainfall thresholds for landslides in the Nepal Himalaya. Geomorphology 2008; 100:429-43.

Dawadi B. Climatic records and linkage along an altitudinal gradient in the southern slope of Nepal Himalaya. Journal of Nepal Geological Society 2017;53:47-56.

Dhakal S. The Role of Landslides on the Sediment Budget in Upper Phewa Watershed, Western Nepal [dissertation]. Eschede, Faculty of Geo-Information Science and Earth Observation, University of Twente; 2016.

Dikshit A, Sarkar R, Pradhan B, Acharya S, Dorji K. Estimating rainfall thresholds for landslide occurrence in the Bhutan Himalayas. Water 2019;11:Article ID 1616.

Ghimire M. Landslide occurrence and its relation with terrain factors in the Siwalik Hills, Nepal: Case study of susceptibility assessment in three basins. Natural Hazards 2010;56(1):299-320.

Guzzetti F. Landslide Hazard and Risk Assessment [dissertation]. Germany, University of Bonn; 2005.

Hirzel AH, Le Lay G, Helfer V, Randin C, Guisan A. Evaluating the ability of habitat suitability models to predict species presences. Ecological Modelling 2006;199(2):142-5.

Kayastha P, Dhital MR, De Smedt F. Evaluation and comparison of GIS based landslide susceptibility mapping procedures in Kulekhani Watershed, Nepal. Journal of the Geological Society of India 2013;81(2):219-31.

Leibundgut G, Sudmeier-Rieux K, Devkota S, Jaboyedoff M, Derron M-H, Penna I, et al. Rural earthen roads impacts assessment in Phewa watershed, Western Region, Nepal. Geoenvironmental Disasters 2016;3(13):1-25.

Lennartz T. Constructing Roads - Constructing risks? Settlement decisions in view of landslide risk and economic opportunities in western Nepal. Mountain Research and Development 2013;33(4):364-71.

Maes J, Kervyn M, de Hontheim A, Dewitte O, Jacobs L, Mertens K, et al. Landslide risk reduction measures: A review of practices and challenges for the tropics. Progress in Physical Geography: Earth and Environment 2017;41(2):191-221.

McAdoo BG, Quak M, Gnyawali KR, Adhikari BR, Devkota S, Rajbhandari PL, et al. Roads and landslides in Nepal: how development affects environmental risk. Natural Hazards and Earth System Sciences 2018;18:3203-10.

Nachappa TG, Kienberger S, Meena SR, Hölbling D, Blaschke T. Comparison and validation of per-pixel and object-based approaches for landslide susceptibility mapping. Geomatics, Natural Hazards and Risk 2020;11(1):572-600.

Phuyal P, Koirala M, Dhakal S. Comparative study of carbon stock in different forest types of Panchase. In: Bhuju DR, Rijal KR, editors. Building EbA knowledge in Nepal (Compilation of EbA research studies in Panchase, EbA Pilot Site). Kathmandu: Central Department of Environmental Science, Tribhuvan University; 2015. p. 62-5.

Pradhan AMS, Kim Y-T. Landslide susceptibility mapping of Phewa catchment using multilayer perceptron artificial neural network. Nepal Journal of Environmental Science 2016;4:1-9.

Regmi AD, Yoshida K, Dhital MR, Devkota K. Effect of rock weathering, clay mineralogy, and geological structures in the formation of large landslide, a case study from Dumre Besei landslide, Lesser Himalaya Nepal. Landslides 2013;10(1):1-13.

Ramsar Sites Information Service (RSIS). Lake cluster of Pokhara Valley [Internet]. 2016 [cited 2017 Dec 4]. Available from: https://rsis.ramsar.org/ris/2257?language=en.

United Nations International Strategy for Disaster Reduction (UNISDR). 2009 UNISDR Terminology on Disaster Risk Reduction. Geneva: United Nations International Strategy for Disaster Reduction; 2009.

Upreti BN. The physiography and geology of Nepal and their bearing on the landslide problem. In: Tainchi L, Chalise SR., Upreti BN, editors. Landslide Hazard Mitigation in the Hindu Kush-Himalayas. Kathmandu: International Centre for Integrated Mountain Development (ICIMOD); 2001. p. 30-50.

van Westen CJ, Rengers N, Terlien MTJ, Soeters R. Prediction of the occurrence of slope instability phenomena through GIS-based hazard zonation. Geologische Rundschau. 1997;86:404-14.

Varnes DJ. Landslide Hazard Zonation: A Review of Principles and Practices. United Nations Educational, Scientific and Cultural Organization; 1984.

Watson CS, Kargel JS, Regmi D, Rupper S, Maurer JM, Karki A. Shrinkage of Nepal's second largest lake (Phewa Tal) due to watershed degradation and increased sediment influx. Remote Sensing 2019;11:Article ID 444.

Spatial Variations of Surface Water Quality in Hau Giang Province, Vietnam Using Multivariate Statistical Techniques

Nguyen Thanh Giao*

College of Environment and Natural Resources, Can Tho University, Can Tho 900000, Vietnam

ARTICLE INFO

Received: 22 May 2020
Received in revised: 7 Aug 2020
Accepted: 24 Aug 2020
Published online: 10 Sep 2020
DOI: 10.32526/ennrj.18.4.2020.38

Keywords:
Hau Giang Province/ Monitoring/ Multivariate statistical techniques/ Total suspended solid/ Surface water

*** Corresponding author:**
E-mail: ntgiao@ctu.edu.vn

ABSTRACT

This study assessed the surface water monitoring system in Hau Giang Province in 2019. The monitoring data for pH, temperature, total suspended solids (TSS), dissolved oxygen (DO), biochemical oxygen demand (BOD), chemical oxygen demand (COD), ammonium (NH_4^+_N), nitrite (NO_2^-_N), nitrate (NO_3^-_N), orthophosphate (PO_4^{3-}_P), coliforms, and iron (Fe) were collected from the Department of Natural Resources and Environment, Hau Giang Province, Vietnam. The results were compared with the national technical regulation on surface water quality (QCVN 08-MT: 2015/BTNMT). Then, these parameters were used to determine the locations and parameters for water quality monitoring using multivariate analyses including cluster analysis (CA) and principal component analysis (PCA). The results indicated that the main concerns for the quality of water in the canal of Hau Giang Province were organic matter (high BOD and COD), nutrients (NH_4^+_N, NO_2^-_N, PO_4^{3-}_P), coliforms and iron. The CA results showed that 42 monitoring locations could be decreased to 26 locations, reducing monitoring costs by up to 32%. The PCA identified 12 sources of pollution, of which three main sources were PC1, PC2 and PC3 accounting for 75.6% of the variation in water quality. PCA findings showed that all the current water variables in the 2019 monitoring program were significant. The present study could help local environmental managers to reconsider the selected locations and parameters in the environmental monitoring program.

1. INTRODUCTION

Hau Giang Province is located in the sub-region of the Hau River in the Vietnamese Mekong Delta with an area of 160,058.69 ha and six main rivers (canals): Vam Mai Dam, Xa No Canal, Cai Lon Canal, Lai Hieu Canal, Quan Lo Phung Hiep, and Xang Nang Mau Canal. The province has a flat terrain and intertwined with interconnected river systems with a total length of approximately 2,300 km, predominantly, the Hau River along the Chau Thanh District with a length of about two km. The hydrological regime is mostly influenced by the Hau and Cai Lon Rivers. Along with the national development, Hau Giang Province has gradually shifted its economic structure towards industrialization and modernization combined with a strong urbanization process. Hau Giang can be considered as a province with mixed economic characteristics. In agriculture, rice cultivation plays a major role (rice fields (40%) as well as orchards (13%) and aquaculture, combined with urbanized and industrial agglomerations (German Aerospace Center, 2011). Agricultural farming can lead to accumulation of pesticides in water bodies causing exposure of humans and aquatic organisms (Toan et al., 2013). In addition, the terrain is low, sloping from the Northeast to the Southwest, and is influenced by the East and West Sea tides, so the saline intrusion situation is very serious and unpredictable, contributing to negative impacts in the water quality in the province (Hau Giang Department of Science and Technology, 2019). On the other hand, Hau Giang is also the province with predominantly acid sulphate soils; through soil erosion and runoff can cause high concentration of heavy metals (especially Fe and Al) in the surface water. Besides that, the rapid development of industrial area

Citation: Giao NT. Spatial variations of surface water quality in Hau Giang Province, Vietnam using multivariate statistical techniques. Environ. Nat. Resour. J. 2020;18(4):400-410. (https://doi.org/10.32526/ennrj.18.4.2020.38)

has increased the amount of wastes. This has put heavy pressure on the province's water environment. Therefore, the uncontrolled urbanization and economic development have posed many challenges to environmental issues, especially the water environment.

Water is very essential for life and various human activities. Hence, water quality monitoring has a crucial task to manage and maintain good water sources for socio-economic development. However, the choice of sampling locations, number of locations and analytical parameters in water quality monitoring is a difficult problem. Physicochemical and biological indicators are regularly selected to monitor the surface water quality in the Mekong Delta, Vietnam (Wilbers et al., 2014; Phung et al., 2015; Giao, 2019; Giao and Nhien, 2020). In particular, the physicochemical indicators mostly include temperature, pH, total suspended solids (TSS), turbidity, dissolved oxygen (DO), biological oxygen demand (BOD), chemical oxygen demand (COD), ammonium (NH_4^+_N), orthophosphate (PO_4^{3-}_P), heavy metals (Fe, Al, Mn, Cr, Cd), chloride (Cl^-), sulfate (SO_4^{2-}), pesticides, and antibiotics. The biological indicators commonly used are *E. coli* and coliforms (MPN/100 mL) (Wilbers et al., 2014; Phung et al., 2015). These indicators can be preliminary information to assess the level of pollution and suitability of water for a specific purpose (Gebreyohannes, 2015). In Vietnam, selecting indicators and locations for a monitoring program are mainly based on funding and factors affecting water quality. For example, sampling locations are often divided into impact factors such as agriculture, aquaculture, residential/urban areas, tourism, industrial areas, etc. (MONRE, 2012). Multivariate analysis is globally used to assess water quality (Hosseinimarandi et al., 2014; Venkatramanan et al., 2014), such as a measure of fluctuations in the river and lake water quality (Cho et al., 2009; Chounlamany et al., 2017). Moreover, some previous studies have also used effective multivariate techniques to identify pollution sources and evaluate the monitoring network (Vega et al., 1998; Singh et al., 2005; Hosseinimarandi et al., 2014; Giao, 2020). Therefore, to achieve this goal the system of canals in Hau Giang was selected to conduct surface water quality assessment in Hau Giang Province, effectiveness of 42 locations and 12 environmental parameters in identifying the main sources of pollution in surface water quality monitoring program. The research results will be pivotal information to improve the surface water quality monitoring system in the province.

2. METHODOLOGY

2.1 Data collection

Data were collected at 42 sampling sites representing the surface water quality in Hau Giang Province in 2019. Thirty six of the monitoring sites were on canals: Xa No Canal (from XN1 to XN7), Vinh Vien Market (VVM8), Xang Nang Mau Canal (from NM9 to NM13), Cai Dau Canal (CD14, CD15), Vam Cai Cui (CC16), Vam Mai Dam (MD17), Cai Con Canal (CCO18, CCO19, CCO20), Cai Lon Canal (CL21, CL22), Cua Ga Canal (CG23), Lai Hieu Canal (LH24, LH25), Bung Tau Canal (BT26), Mang Ca Canal (MC27), Xeo Mon Canal (XM28), Kinh Cung Market (KCM29), Ba Lang River (BL30, BL31, BL32), Tan Phu Thanh Industrial Zone Port (KCN33), Hau Giang 3 Canal (HG34, HG35), and Xeo Xu Canal (XX36). The remaining sampling sites were located on the Hau River section flowing through the province (SH37, SH38, SH39, SH40, SH41, and SH42). All of the canals, Xa No Canal, Xang Nang Mau Canal, Cai Con Canal, Vam Cai Cui, Ba Lang River, Cai Dau Canal, and Vam Mai Dam, connected to the Hau River. The location map of monitoring data collection is shown in Figure 1.

Surface water samples were determined in March (end of dry season), May (onset of rainy season), August (end of rainy season) and October (onset of dry season) at 42 sampling sites. Water samples were collected in accordance with the guide of Vietnam Environment Administration (2018)-Guidance on sampling of rivers and streams. The samples were collected in the middle of the river/ canal flow (depending on the width of the canals) with a depth of about 30 cm below the surface water. At each site, three samples were mixed to obtain a pooled sample representing the site. A 2-liter sample bottle with a cap was rinsed at least three times with the same water source before collecting sample. Particularly, microbiological analysis samples were taken in a glass bottle which has been sterilized at 175ºC for 2 h. A total of 12 indicators were analyzed to assess water quality: pH, temperature, TSS (mg/L), DO (mg/L), BOD (mg/L), COD (mg/L), NH_4^+_N (mg/L), NO_2^-_N (mg/L), NO_3^-_N (mg/L), PO_4^{3-}_P (mg/L), Fe (mg/L), and coliforms (MPN/100 mL). pH, temperature, and DO parameters were measured in-situ by pH meter (HANNA HI 8224, Rumani) and DO meter (Milwaukee SM 600, Rumani). The remaining

water quality indicators were properly preserved and analyzed at the laboratory of the Provincial Center for Natural Resources and Environment Monitoring Hau Giang Province by Standard methods (APHA, 1998).

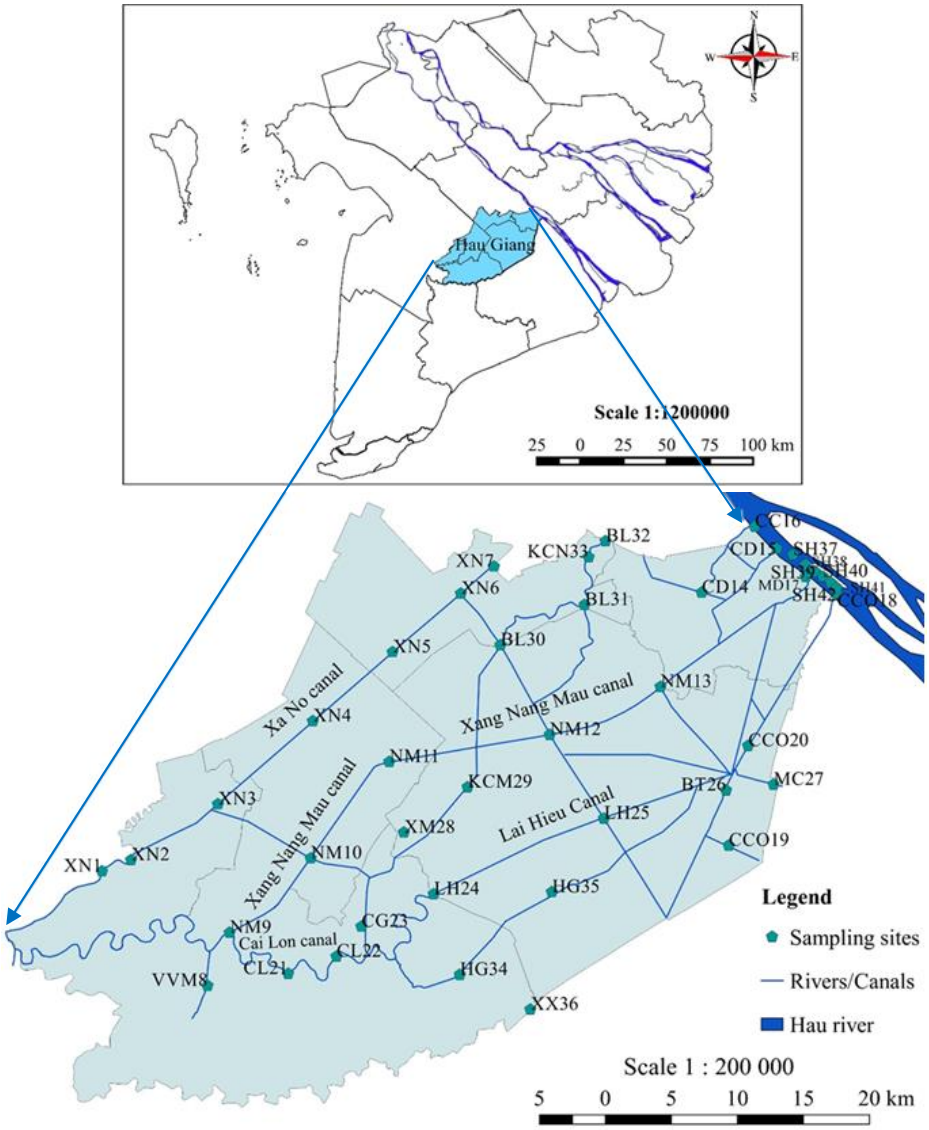

Figure 1. Water monitoring networks in Hau Giang Province

Cluster analysis (CA) is widely used to group water sources by spatio-temporal distribution (Feher et al., 2016; Chounlamany et al., 2017). Samples with similar pollution characteristics will be grouped into the same group, and different pollution properties will be classified into another group. In this study, cluster analysis was conducted by Ward's method (Salah et al., 2012) and presented in a dendrogram (Feher et al., 2016; Chounlamany et al., 2017). A dendrogram can help in determining the number of location groups which have similar characteristics. After identifying the location groups, the selection of effective sites to continue monitoring was based on two factors, the same group and the same river, because the survey of multiple locations on the same canal may not bring large fluctuations and is costly during periodic monitoring.

Principal Component Analysis (PCA) is used to extract important information from the original dataset (Feher et al., 2016; Chounlamany et al., 2017). The axis rotation method performed in PCA is Varimax. Each of the original variables will be classified as one principal component (PC) and each PC is a linear combination of the original variables (Feher et al., 2016). The purpose of the PCA is to reduce the initial variables that do not contribute significantly to data variability. The correlation between PCs and original variables were exhibited by weighing factors (loading)

(Feher et al., 2016). The absolute values of weighing factors (WF) have a strong correlation between PCs and parameters when WF>0.75, average (0.75> WF>0.5) and weak (0.5>WF>0.3) (Liu et al., 2003). Both CA and PCA analyses were computed using the copyrighted software Primer 5.2 for Windows (PRIMER-E Ltd, Plymouth, UK).

3. RESULTS AND DISCUSSION

3.1 Surface water quality in Hau Giang Province in 2019

Surface water quality in Hau Giang Province in 2019 was summarized in Figure 2. It can be seen that the average value of pH and temperature at the sampling sites during the year did not have large fluctuations. pH measured on-sites ranged from 6.8±0.0 to 7.1±0.3 and the annual average was about 7±0.1, which was within permitted limits of QCVN 08-MT: 2015/BTNMT (Table 1). Previous studies showed that the surface water pH in An Giang, Can Tho and Soc Trang also fluctuated in the neutral range (Lien et al., 2016; Ly and Giao, 2018; Tuan et al., 2019; Giao, 2020). Temperature varied from 28.6±0.2°C to 29.6±0.9°C, averaging at 29.4±0.38°C and within the permitted limits of WHO (2008) (<40°C). In addition, the temperature on Hau River ranged from 28.9±0.4°C to 29±0.5°C in 2019, which was lower than the temperature in the Hau Giang River. On the other hands, the temperature on Hau Giang Rivers and canals were similar to the in-field canals of An Giang Province ranging from 28.1±0.9°C to 31.3±2.0°C (Ly and Giao, 2018).

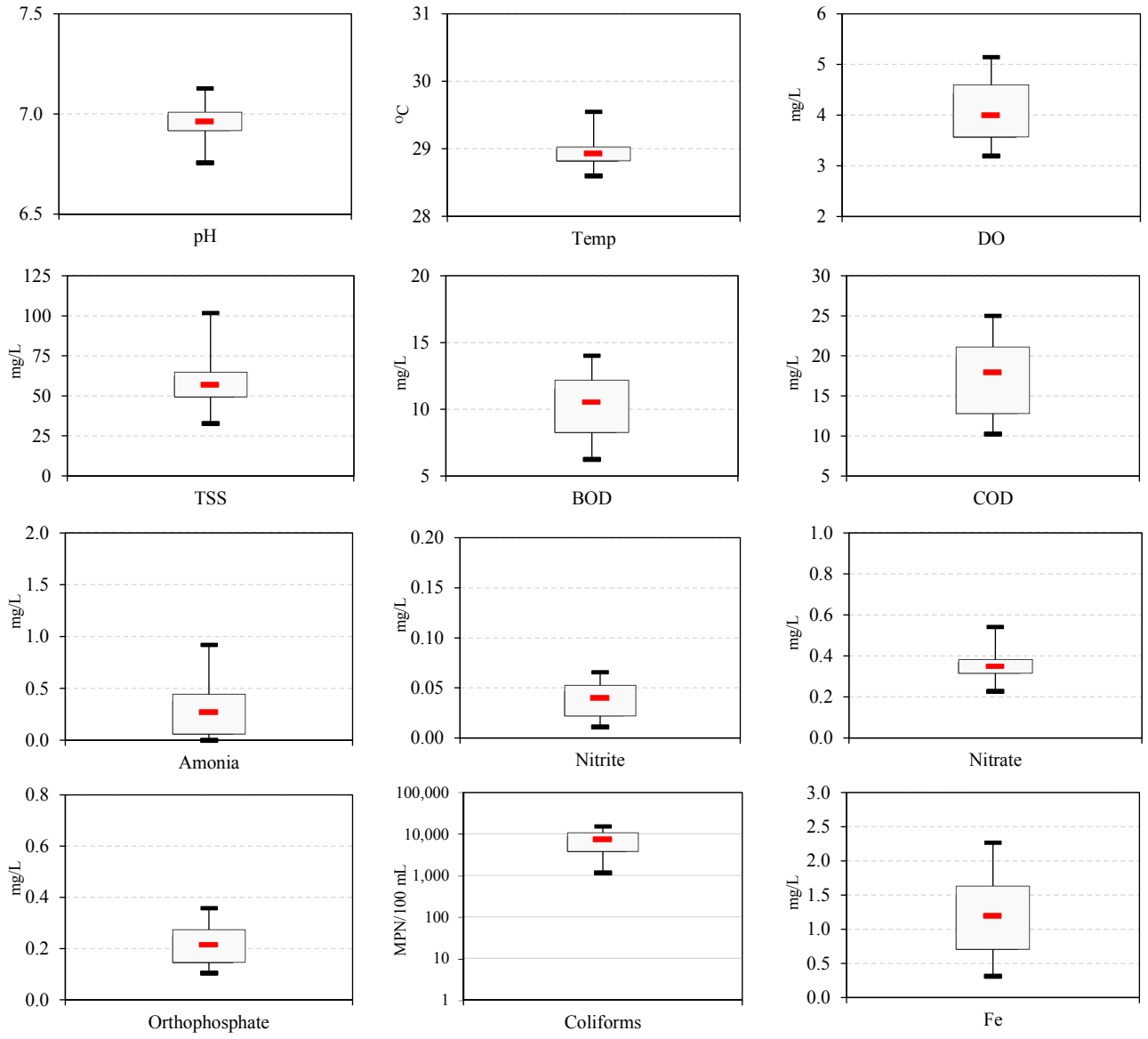

Figure 2. Physisco-chemical, biological characteristics of water quality in Hau Giang in 2019

The mean of TSS concentration in Hau Giang Province in 2019 was 57±22.6 mg/L ranging from 32.8±6.4 to 101.8±40.9 mg/L. In particular, the average TSS concentration in Hau River and in-field canals varied from 34.8±22.6 to 50.8±26.6 mg/L and 32.8±6.4 to 101.8±40.9 mg/L, respectively; this indicated that the water quality in Hau River was less polluted by TSS than those of the canals in Hau Giang Province. The high TSS concentration was due to rainwater runoff, erosion and the presence of phytoplankton in the environment (MONRE, 2012; Giao and Nhien, 2020). The concentration of TSS in Hau River in 2016 was higher than the current study (51.5±31.37 mg/L) (Lien et al., 2016); however, this concentration tended to be similar in 2018 (Giao, 2020). In the in-field canals of An Giang Province, TSS was recorded between 25.0-93.7 mg/L in the period from 2009-2016 (Ly and Giao, 2018). Meanwhile, in the canals of Soc Trang Province, TSS ranged from 16-176 mg/L (Tuan et al., 2019). Thus, TSS concentration in the surface water in Hau Giang was higher than that in canals in An Giang and lower than that in canals in Soc Trang. This may be because Soc Trang is a coastal province, heavily influenced by mudflats and estuaries. According to Akan et al. (2008) and Gebreyohannes et al. (2015), the concentrations of TSS in the canals in Hau Giang Province in 2019 can be comparable to wastewater (TSS concentration is less than 100 mg/L).

The DO value on the in-field canal in the current study was relatively large ranging from 3.2±0.1-5.2±0.8 mg/L and in Hau River ranged from 4.6±0.2-4.7±0.1 mg/L, the annual average was 4.0±0.3 mg/L, there may be negative effects on aquatic ecosystem life (Gebreyohannes et al., 2015). DO concentration in the canals had a tendency of being lower than in Hau River, because the concentration of DO depends on the air diffusion into the water, turbulence in rivers, the presence of biodegradable organic matters and the photosynthesis of phytoplankton (Giao and Nhien, 2020). DO concentration in Soc Trang Canals was 1.7 to 6.2 mg/L (Tuan et al., 2019); in the in-field canals of An Giang was in the range of 4.9-5.5 mg/L in the period from 2009-2016 (Ly and Giao, 2018). DO concentration in the canals in Hau Giang Province was similar to that in Soc Trang and An Giang Canals.

In Hau River, concentrations of BOD and COD were in the ranges of 7.3±3.9-8.3±3.4 mg/L and 12±7.1-12.8±8.9 mg/L, respectively. The concentrations of BOD and COD in the in-field canals were 6.3±0.5-14±4.5 mg/L and 14±4.5-25±8.9 mg/L, respectively. This indicated that the water quality in the canals and Hau River was organically polluted and the pollution level in the infield canals tended to be higher. Some previous studies have also concluded that the canals in the Mekong Delta have been organically polluted. For example, the period of 8 years from 2009-2016 in An Giang Province, BOD concentration in the canals ranged from 4.7±2.3-12.3±9.2 mg/L (Ly and Giao, 2018); BOD and COD values in canals locating in Soc Trang Province were 2.2-22.4 and 6.0-44.9 mg/L, respectively (Tuan et al., 2019); and COD value on Hau River was in the range of 10.4±1.2-16.5±4.1 mg/L (Giao, 2020). This can be explained by the influence of socio-economic activities such as agriculture, industry, services, residential and urban areas (MONRE, 2012; Zeinalzadeh and Rezaei, 2017).

The average concentration of NH_4^+_N, NO_2^-_N and NO_3^-_N compounds in the year 2019 had the average concentrations of 0.27±0.16, 0.04±0.017, and 0.35±0.20 mg/L, respectively. Specifically, the concentration of NH_4^+_N in Hau River and the in-field canals in Hau Giang Province fluctuated from 0±0-0.1±0 mg/L and 0±0-0.92±0.56 mg/L, respectively. NH_4^+_N concentration in surface water in Soc Trang ranged from 0.02 to 4.15 mg/L (Tuan et al., 2019), which was higher than that of Hau Giang Province. Besides that, NO_2^-_N concentration was in the range of 0.011±0.006-0.066±0.049 mg/L (in-field canals) and 0.011±0.007-0.017±0.009 mg/L (Hau River). The NO_2^-_N concentrations in the canals in Hau Giang Province were much lower than those of NO_2^-_N (0.001-0.56 mg/L) in the canals in Soc Trang Province (Tuan et al., 2019). This showed that the water environment was lacking oxygen and could be toxic to aquatic life, consistent with the low DO value in the above discussion. In addition, NO_3^-_N concentrations in the canals in An Giang Province ranged from 0.03 to 1.76 mg/L in the period from 2009 and 2016 (Ly and Giao, 2018). Meanwhile, NO_3^-_N concentration in the canals in Soc Trang Province varied from 0.05 to 1.14 mg/L (Tuan et al., 2019). The concentration of NO_3^-_N in the canals in Hau Giang Province in 2019 (0.23±0.05-0.54±0.44 mg/L) did not differ from the concentrations recorded in An Giang and Soc Trang Provinces. In Hau River, NO_3^-_N concentration was recorded in the range of 0.34±0.15-0.38±0.13 mg/L, which tended to be higher than those in 2018. The difference between the research results and the current study can be a result of oxidation of organic debris, human and animal wastes (DWAF, 1996). From the

above discussion, the levels of NH_4^+_N, NO_2^-_N and NO_3^-_N in the in-field canals had the tendency of being higher in Hau River. However, according to DWAF (1996) and Boyd and Green (2002), the nitrogen concentrations found in natural surface water sources range from <0.2 mg/L ($N\text{-}NH_4^+$), <<5 mg/L ($N\text{-}NO_3^-$). Thus, nitrate concentration was not an important environmental issue in Hau Giang Province, but NH_4^+_N concentration in the in-field canals should be paid more attention.

Orthophosphate concentration ranged from 0.1±0.02-0.36±0.26 mg/L. The average was 0.23±0.07 mg/L (in-field canals) and 0.1±0.05-0.23±0.26 mg/L (Hau River) with 0.13±0.05 mg/L the mean concentration. It can be seen that the orthophosphate concentration in Hau River was lower than in the canals in Hau Giang Province. On the other hand, the PO_4^{3-}_P concentration in the canals was reported ranging from 0-0.9 mg/L in Soc Trang Province (Tuan et al., 2019) and the mean concentration of 0.16±0.12 mg/L in An Giang province (Ly and Giao, 2018), which were lower than the in-field canals of Hau Giang Province in the current study. The sources of orthophosphate in the water environment are agricultural runoff, livestock, domestic and industrial wastes (Barakat et al., 2016).

Coliforms densities ranged from 1,156.3±500 to 1,657.5±612.6 MPN/100 mL in Hau River and 3,225±1,913.8 to 15,275±15,244.8 MPN/100 mL in the in-field canals; the densities of coliform in Hau River was significantly lower than that in the in-field canals. In addition, it can be recognized that coliforms were a problem that needs more attention in the canals in Hau Giang Province than in Hau Rivers. Coliforms were detected in An Giang, Soc Trang Provinces, and Hau River with the fluctuation of 2,260-155,000 MPN/100 mL, 2,300-89,000 MPN/100 mL, and 1,346±915-2,126±1,741 MPN/100 mL, respectively (Ly and Giao, 2018; Tuan et al., 2019; Giao, 2020). This indicated that the densities of coliforms in the in-field canals in Hau Giang Province were lower than those in An Giang and Soc Trang Provinces, which could mean that water quality was less polluted by fecal materials. The origin of coliforms can be from human and animal feces (Bolstad and Swank, 1997; UNICEF, 2008).

The average iron concentration was 1.2±0.6 mg/L in 2019 ranging from 0.3±0.1-0.47±0.2 mg/L (Hau River) and 0.50±0.2-2.26±0.5 (in-field canals). Due to acid sulfate soil property, it has resulted in the release of iron into surface water leading to aesthetic issues, disposal costs, and human health. In Soc Trang, the iron concentration in surface water ranges from 0.30-3.75 mg/L (Tuan et al., 2019), tended to higer than that in the canals in Hau Giang Province. In addition to the geographical conditions, human activities (e.g., washing acidic soil, intensive agricultural production) are responsible for the iron-contaminated water.

Table 1 illustrates the limit values of surface water quality parameters that are regulated in Vietnam. The limits are applied to assess and manage surface water quality and provide a basis for appropriate protection and use of water resources. All in all, the mean values of the monitoring indicators were greater than the national technical regulation on surface water quality (QCVN 08-MT: 2015/BTNMT), with the exception of nitrogen compounds and pH (Table 1). Although the nitrogen concentration in the water was in accordance with the permitted standard, the surface water environment is facing the risk of eutrophication due to the higher concentration of dissolved phosphorus (Li and Liao, 2003). Thus, it could be implied that artificial activities such as rainwater runoff, industrial and agricultural cultivation, acid sulfate soil washing exert an adverse impact on water quality in the province. The water quality in the canals in Hau Giang fields tended to be more polluted than that in Hau River. For example, the density of coliforms and Fe in Hau River were within limits regulated by QCVN 08-MT: 2015/BTNMT, while the coliform densities and Fe concentrations on the in-field canals of Hau Giang exceeded the limits at all sampling sites.

Table 1. Limited value of surface water quality parameters

Parameter	Units	Limit values	
		QCVN*A1	QCVN*A2
pH	-	6-8.5	6-8.5
Temperature	°C	-	-
TSS	mg/L	20	30
DO	mg/L	≥6	≥5
BOD	mg/L	4	6
COD	mg/L	10	15
NH_4^+-N	mg/L	0.3	0.3
NO_2^--N	mg/L	0.05	0.05
NO_3^--N	mg/L	2	5
PO_4^{3-}-P	mg/L	0.1	0.2
Coliforms	MPN/100 mL	2,500	5,000
Fe	mg/L	0.5	1

*National technical regulation on surface water quality (QCVN 08-MT: 2015/BTNMT); A1 means water quality used for domestic purposes (after normal treatment has been applied), conservation of aquatic plants and animals and other purposes; A2 is used for domestic purposes but treatment technology must be applied.

3.2 Assessment of water quality monitoring locations in Hau Giang Province in 2019

The average value of each water quality monitoring indicator was used as input data to group water quality by the sampling location. To optimize the monitoring locations, the sampling sites that were within the same group and in the same river can be reduced. For example, if a group has 3 sites located in the same canal, one of the three sites can be selected for monitoring. Besides that, if they are in the same group but in different rivers, the monitoring points are still selected for the coming year monitoring.

The results of cluster analysis showed that 42 locations of surface water sampling in Hau Giang Province were classified into nine groups denoted from 1 to 9 (Figure 3), in which group 9 represented the lowest pollution level and group 1 was the highest pollution level. The XM28, KCM29, and HG35 sites in groups 2, 4, and 8 were found to be less similar than the other sampling sites and belonging to different canals that are surely remained for monitoring. In the case of a group with multiple monitoring points in the same area, one representative location can be selected for the remaining positions.

Particularly, group 1, including XN5, XN6, and XN7 points on Xa No Canal, have similar data, hence, it is possible to choose one of these points to monitor water quality in this area. Group 3 consisted of 6 locations belonging to 3 areas such as Xa No Canal (XN2, XN3, XN4), Nang Mau Canal (NM10, NM11), and Vinh Vien Market (VVM8). Among the sampling points in the group 3, only one sampling point per river was chosen to collect water samples. XN1, XN3, XN4 and NM10, NM11 sites were located in Xa No and Xang Nang Mau Canals, respectively. Therefore, only one location is selected in each canal. On the other hand, the VVM8 site was in a separate canal; thus, this location was retained for monitoring. Similarly, the number of sampling locations in groups 5, 6, 7 and 9 can be reduced from 8 to 6, 3 to 2, 8 to 6, and 11 to 5 locations (Figure 3). Thus, the total number of 42 locations could be reduced to 26 locations but still ensuring the accuracy of the monitoring process, resulting in a 32% reduction in the total cost of monitoring. In one case, 26 sampling locations that could be selected to monitor the water quality in Hau Giang Province is shown in Figure 4. In this case, the external locations which border between Can Tho city, Soc Trang and Kien Giang Provinces were given the priority to be selected so that they can assess the water input and output of the area. Previous studies have also shown that the application of CA in grouping water quality by sampling location would help reduce the number of sampling locations and therefore significantly diminish costs (Feher et al., 2016; Chounlamany et al., 2017; Giao, 2020).

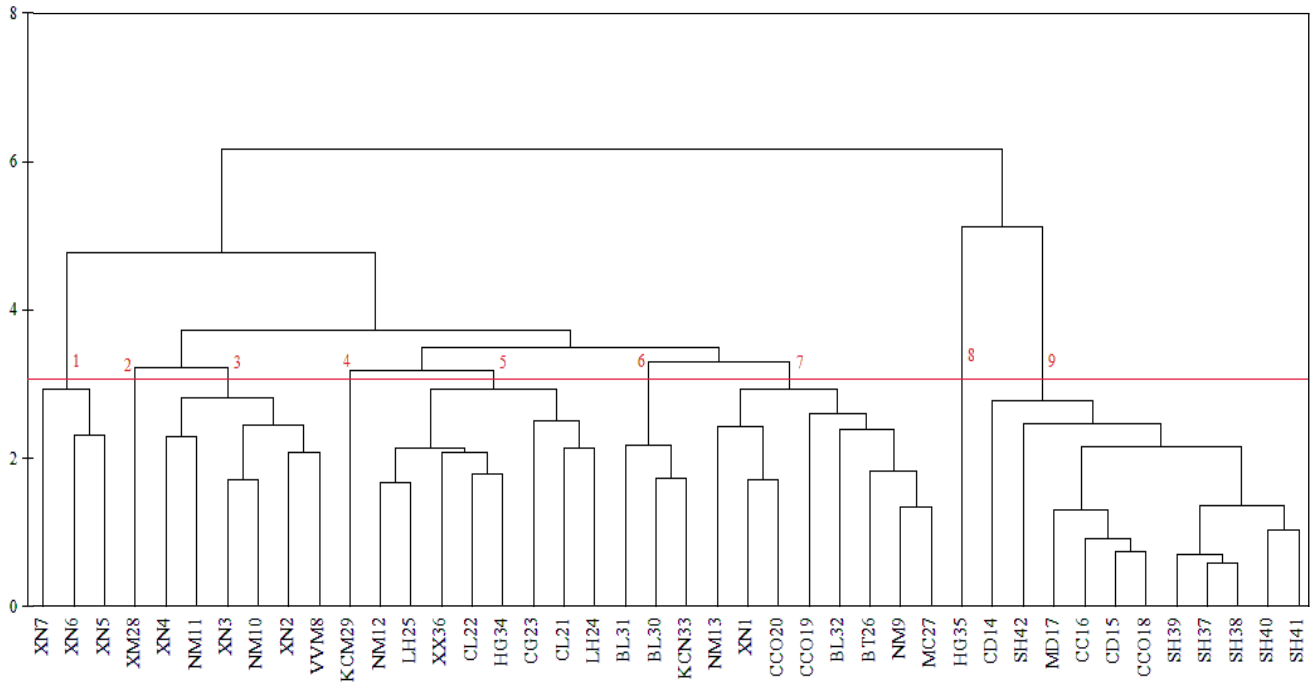

Figure 3. Spatial variations of surface water quality in Hau Giang Province in 2019

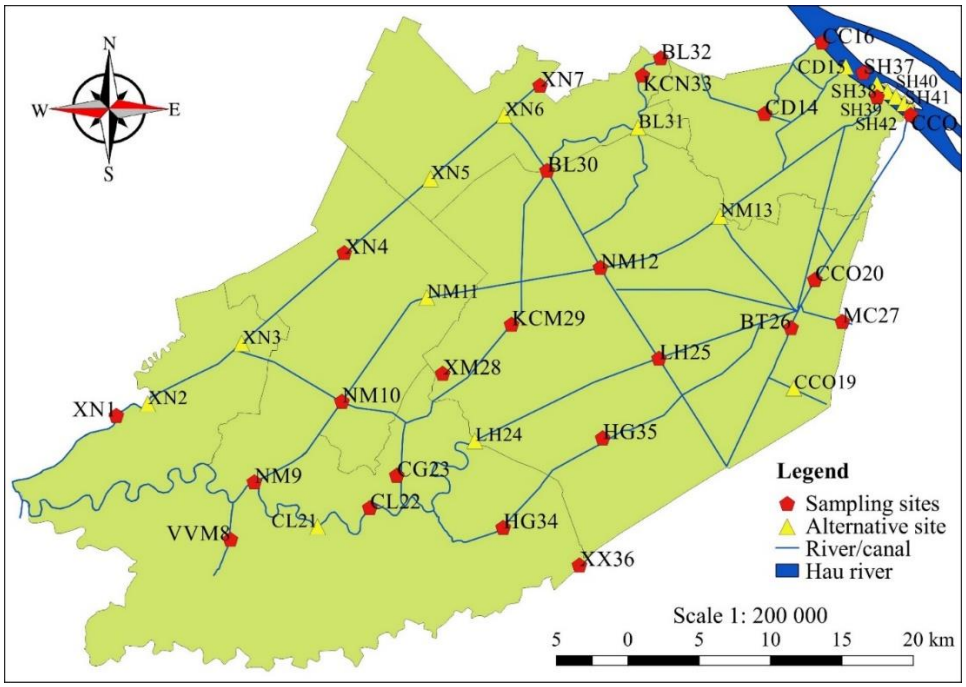

Figure 4. The recommended sampling sites after performing cluster analysis (Note: XN7 or XN5 or XN6; XN4 or XN2 or XN3; NM10 or NM11; NM9 or NM13; CL22 or CL21; LH25 or LH24; BL32 or BL31; CCO20 or CCO19; CD14 or CD15; SH37 or SH38 or SH39 or SH40 or SH41 or SH42)

3.3 Identification of water quality monitoring parameters

Table 2 presents the results of PCA, sources of pollution and water quality indicators showing the impact of pollution sources. Regarding pollution sources, the results of PCA demonstrated that there were 12 pollution sources. The main sources included PC1, PC2, and PC3 with their eigenvalue values greater than 1 (Shrestha and Kazama, 2007), which was responsible for 75.6% of the variation in water quality. Meanwhile, sources from PC4 to PC12 were subsidiary sources contributing 24.4% to the variation in water quality of Hau Giang Province.

PC1 could be considered as a non-point source explaining 52.5% of the variation in water quality data since there was a weak correlation (from 0.313 to 0.356) between PC1 and the water monitoring parameters (e.g., TSS, DO, BOD, COD, NH_4^+_N, NO_2^-_N, NO_3^-_N, PO_4^{3-}_P, and Fe). Hence, some non-point sources were typical in Hau Giang such as flows from agricultural areas, markets, and the sources of pollution by the riparian population. Besides that, Hau Giang has an inter-water transport road of Can Tho-Hau Giang Province (Xa No Canal, Ba Lang Canal). Therefore, this can also be considered as a non-point source that significantly affected the water quality in the study area.

The pH and temperature were mainly explained by PC2, PC3, and PC4 which represent weather (the amount of light reaching the water bodies), hydrological regime (water depth, volume, flow), and buffering capacity of water in the acidic water environment. Besides, it can be seen that coliform values at PC1, PC2, PC3, and PC4 did not contribute significantly to the explanation of water quality pollution. Nevertheless, the coliform value at PC1 was asymptotic to 0.3, which was weakly correlated. This indicated that coliform was not the main parameter influenced on PC1. The correlation of PC5 and PC8 to TSS were positively and negatively correlated by 0.500 and -0.514, respectively. Two possible sources causing high TSS were storm runoff and riverbank erosion (Giao, 2020).

Dissolved oxygen concentration was inversely correlated with PC8 (-0.514), PC10 (-0.490) and PC11 (-0.362) affected by many factors such as temperature, air diffusion, presence of aquatic plants and organic matter (Galal-Gorchev et al., 1993; Kazi et al., 2009; Chounlamany et al., 2017). Both BOD and COD were explained by PC12 with correlation coefficients of 0.693 and -0.707, respectively. These parameters were good indicators for organically polluted environments (Siwiec et al., 2018); therefore, it is reasonable to have the same origin. The sources of organic pollution possibly were human activities such as urban-residential, services and tourism, industrial production and agriculture (Zeinalzadeh and Rezaei, 2017).

Table 2. Principal component analysis for surface water quality monitoring data

Parameters	PC1	PC2	PC3	PC4	PC5	PC6	PC7	PC8	PC9	PC10	PC11	PC12
pH	0.088	-0.256	**0.731**	**-0.521**	-0.004	-0.021	0.106	-0.169	0.137	0.234	0.084	-0.006
Temperature	0.037	**0.606**	-0.250	**-0.473**	-0.112	0.342	-0.099	-0.172	0.342	0.183	-0.160	-0.012
TSS	**-0.313**	0.192	-0.126	-0.099	**0.500**	-0.347	0.067	**-0.514**	-0.357	0.254	0.090	0.016
DO	**0.344**	-0.178	-0.060	-0.096	-0.138	-0.182	-0.294	**-0.568**	-0.039	**-0.490**	**-0.362**	0.054
BOD	**-0.354**	-0.053	0.157	0.283	-0.181	0.363	0.093	-0.276	0.002	0.083	-0.176	**0.693**
COD	**-0.356**	-0.059	0.143	0.283	-0.191	0.312	0.009	-0.357	0.050	-0.001	-0.051	**-0.707**
NH_4^+-N	**-0.321**	-0.213	0.027	0.037	**0.507**	-0.064	**-0.443**	0.147	**0.542**	-0.020	-0.277	0.013
NO_2-N	**-0.336**	0.162	0.051	0.165	0.167	-0.263	**0.634**	0.089	0.218	-0.506	-0.223	-0.017
NO_3-N	**-0.318**	-0.172	**0.539**	**-0.433**	-0.031	0.064	-0.321	0.105	-0.202	**-0.376**	0.119	0.029
PO_4^{3-}-P	**-0.318**	-0.172	-0.049	**-0.433**	-0.031	0.246	-0.172	0.304	**-0.584**	-0.082	**-0.380**	-0.066
Coliforms	-0.298	0.157	0.080	0.027	**-0.584**	**-0.597**	-0.314	0.094	0.035	0.253	-0.094	0.016
Fe	**-0.342**	-0.167	-0.189	-0.282	-0.146	0.077	-0.224	-0.095	0.095	**-0.363**	**0.708**	0.108
Eigenvalue	6.30	1.70	1.08	0.88	0.54	0.46	0.31	0.24	0.21	0.19	0.10	0.01
%Variation	52.5	14.2	9.0	7.4	4.5	3.8	2.6	2.0	1.7	1.6	0.8	0.1
Cum.%var.	52.5	66.7	75.6	83.0	87.4	91.2	93.8	95.8	97.5	99.1	99.9	100.0

Note: Bold values indicate weak, moderate and strong correlation between PCs and original variables

PC1, PC5, PC7, and PC9 were correlated with the fluctuations of NH_4^+_N by -0.321, 0.507, -0.443, and 0.542, respectively. This could mean that there were many sources of NH_4^+_N release such as fertilizer application, biodegradation of organic matters, and natural factors that affect these two processes (Zeinalzadeh and Rezaei, 2017).

NO_2^-_N had a moderate correlation with PC7 (0.634), however NO_2^-_N was formed mainly due to the effect of microorganisms in the presence of NH_4^+_N and DO (Giao et al., 2017). PCA results also showed that NO_3^-_N had a weak relationship with PC3 (0.539), PC4 (-0.433), and PC10 (-0.376) impling that the source of NO_3^-_N in water environment is quite a diversity including agricultural fertilizers and the presence of NH_4^+_N metabolites under aerobic conditions. Previous research has shown that the presence of NO_3^-_N in river water was greatly influenced by human activities (Zeinalzadeh and Rezaei, 2017). PO_4^{3-}_P had a weak relationship with PC4 (-0.433), PC9 (-0.584), and PC11 (-0.380). It could mean that there were many factors leading to the fluctuation of orthophosphate concentration in the surface water environment in Hau Giang Province such as fertilizers, washing powders, and the decomposition of wastes and plant and animal residues (Bolstad and Swank, 1997; Barakat et al., 2016; Zeinalzadeh and Rezaei, 2017; Chounlamany et al., 2017). The major sources of the presence of coliforms in surface water in Hau Giang Province were PC5 (-0.584) and PC6 (-0.597). These sources might be from humans and animals through excretion that is not well-managed (Bolstad and Swank, 1997; UNICEF, 2008). Iron (Fe) was an important contribution by the PC11 source with a correlation coefficient of 0.708. Hau Giang is a heavy acid sulfate soil so this PC11 was a great source represents the natural conditions of the acid sulphate soils. In addition, PC10 also contributed weakly (-0.363) in explaining the fluctuation of iron concentration in the surface water environment of Hau Giang Province in 2019.

PCA results showed that all indicators (pH, temperature, TSS, DO, BOD, COD, NH_4^+_N, NO_2^-_N, NO_3^-_N, PO_4^{3-}_P, coliforms, and Fe) have significant impacts on surface water quality in Hau Giang Province. Thus, it is necessary to continue monitoring these water quality parameters in surface water monitoring program. However, NO_2^-_N might not be needed because they could be predicted by

the concentration of NH_4^+_N, NO_3^-_N, and DO. The COD/BOD ratio ranged from 1.5-1.8 (averaged at 1.7), so it is possible to choose one of the two indicators for analysis and reduce cost savings. This is entirely appropriate under condition that the province has a limit of funding for environmental monitoring.

4. CONCLUSION

The water quality in Hau Giang Province in 2019 was assessed to be contaminated by organic matters, nutrients, coliforms, and iron. Most of the monitoring parameters were over the national standard (QCVN 08-MT: 2015/BTNMT). The Hau River section flowing through Hau Giang Province was less polluted than the other canals and rivers in the study. The CA results determined that it is highly possible to monitor 26 locations instead of the current 42 locations while ensuring representative for the water monitoring of the study area. This new monitoring program possibly saves monitoring costs by up to 32%. The PCA results demonstrated that there were 12 PCs contributing to the change in water quality in Hau Giang Province. In which, PC1, PC2, and PC3 were the three main sources explaining up to 75.6% of the water quality variation leading to water pollution. The results also showed that all the water quality parameters significantly influenced the surface water quality in Hau Giang Province in 2019. To reach cost efficiency, NO_2^-_N, and BOD or COD indicators are considered for reductions because it could be predicted by the concentrations of the other available related parameters. Subsequent studies will need to investigate specifically for each different source of pollution in different canals that facilitate appropriate management strategies to improve surface water quality in Hau Giang Province.

ACKNOWLEDGEMENTS

The author would like to thank the Department of Natural Resources and Environment Hau Giang Province for providing water monitoring data. All opinions expressed in this paper represent the scientific and personal views of the authors and do not necessarily reflect the views of the data provider.

REFERENCES

Akan JC, Abdulrahman FI, Dimari GA, Ogugbuaja VO. Physicochemical determination of pollutants in wastewater and vegetable samples along the Jakara wastewater Channelin Kano metropolis, Kano State, Nigeria. European Journal of Scientific Research 2008;23(1):122-33.

American Public Health Association (APHA). Standard Methods for the Examination of Water and Wastewater. 20th ed. Washington D.C., USA: APHA; 1998.

Barakat A, Baghdadi ME, Rais J, Aghezzaf B, Slassi M. Assessment of spatial and seasonal water quality variation of Oum Er Rbia River (Morocco) using multivariate statistical techniques. International Soil and Water Conservation Research 2016;4(4):284-92.

Bolstad PV, Swank WT. Cumulative impacts of land-use on water quality in a southern Appalachian watershed. Journal of the American Water Resources Association 1997;33(3):519-33.

Boyd CE, Green BW. Water quality monitoring in shrimp farming areas: An example from Honduras, Shrimp Farming and the Environment. Auburn: USA: The World Bank, NACA, WWF and FAO Consortium Program on Shrimp Farming and the Environment; 2002.

Cho KH, Park Y, Kang JH, Ki SJ, Cha S, Lee SW, et al. Interpretation of seasonal water quality variation in the Yeongsan Reservoir, Korea using multivariate statistical analyses. Water Science and Technology 2009;59(11):2219-26.

Chounlamany V, Tanchuling MA, Inoue T. Spatial and temporal variation of water quality of a segment of Marikina River using multivariate statistical methods. Water Science and Technology 2017;66(6):1510-22.

Department of Water Affairs and Forestry (DWAF). South African Water Quality Guidelines (2nd ed): Volume 1; Pretoria: DWAF; 1996.

Enkatramanan S, Chung SY, Lee SY, Park N. Assessment of river water quality via environmentric multivariate statistical tools and water quality index: A case study of Nakdong river basin, Korea. Journal of Earth and Environmental Sciences 2014;9(2):125-32.

Feher IC, Zaharie M, Oprean I. Spatial and seasonal variation of organic pollutants in surface water using multivariate statistical techniques. Water Science and Technology 2016;74:1726-35.

Galal-Gorchev H, Ozolins G, Bonnefoy X. Revision of the WHO guidelines for drinking water quality. Annali dell'Istituto Superiore di Sanità 1993;29:335-45.

Gebreyohannes F, Gebrekidan A, Hadera A, Estifanos S. Investigations of physico-chemical parameters and its pollution implications of Elala River, Mekelle, Tigray, Ethiopia. Momona Ethiopian Journal of Science 2015; 7(2):240-57.

German Aerospace Center. Land Cover Classification for Part of the Provinces Can Tho, Dong Thap, Vinh Long (Rapid Eye 2011). Germany: German Aerospace Center, German Remote Sensing Data Center; 2011.

Giao NT, Limpiyakorn T, Kunapongkiti P, Thuptimdang P, Siripattanakul-Ratpukdi S. Influence of silver nanoparticles and liberated silver ions on nitrifying sludge: Ammonia oxidation inhibitory kinetics and mechanism. Environmental Science and Pollution Research 2017;24:9229-40.

Giao NT, Nhien HTH. Phytoplankton-water quality relationship in water bodies in the Mekong Delta, Viet Nam. Journal of Applied Environmental Research 2020;42(2):1-12.

Giao NT. Evaluating current water quality monitoring system on Hau River, Mekong Delta, Vietnam using multivariate

statistical technique. Journal of Applied Environmental Research 2020;42(1):14-25.

Giao NT. The use of zoobenthos for the assessment of water quality in canals influenced by landfilling and agricultural activity. Journal of Vietnamese Environment 2019;11(1):21-31.

Hau Giang Department of Science and Technology. Assess the situation and build a model to improve household livelihoods in areas affected by saline intrusion and climate change in Hau Giang Province. Hau Giang, Vietnam: Department of Science and Technology; 2019.

Hosseinimarandi H, Mahdavi M, Ahmadi H, Motamedvaziri B, Adelpur A. Asessment of groundwater quality monitoring network using cluster analysis, Shib-Kuh Plain, Shur Watershed, Iran. Journal of Water Resource and Protection 2014;6:618-24.

Kazi TG, Arain MB, Jamali MK, Jalbani N, Afridi HI, Sarfraz RA, et al. Assessment of water quality of polluted reservoir using multivariate statistical techniques: A case study. Ecotoxicology and Environmental Safety 2009;72(20):301-9.

Li JX, Liao WG. An analysis on the possibilities of eutrophication in the Three Gorges Reservoir. Science and Technology Review 2003;9:49-52.

Lien NTK, Huy LQ, Oanh DTH, Phu TQ, Ut VN. Water quality in mainstream and tributaries of Hau River. Journal of Science Can Tho University 2016;43:68-79.

Liu CW, Lin KH, Kuo YM. Application of factor analysis in the assessment of groundwater quality in a Blackfoot disease area in Taiwan. Science of the Total Environment 2003;313:77-89.

Ly NHT, Giao NT. Surface water quality in canals in An Giang Province, Viet Nam, from 2009 to 2016. Journal of Vietnamese Environment 2018;10(2):113-9.

Ministry of Natural Resources and Environment (MONRE). National Technical Regulation on Surface Water Quality (QCVN 08-MT: 2015/BTNMT). Hanoi, Vietnam: MONRE; 2015.

Ministry of Natural Resources and Environment (MONRE). National State of Environment-Surface Water Quality. Hanoi, Vietnam: MONRE; 2012.

Phung D, Huang C, Rutherford S, Dwirahmadi F, Chu C, Wang X, et al. Temporal and spatial assessment of river surface water quality using multivariate statistical techniques: A study in Can Tho City, a Mekong Delta area, Vietnam. Environmental Monitoring Assessment 2015;187:229-41.

Salah EAM, Turki AM, Othman EMA. Assessment of water quality of Euphrates River using cluster analysis. Journal of Environmental Protection 2012;3:1629-33.

Shrestha S, Kazama F. Assessment of surface water quality using multivariate statistical techniques: A case study of the Fuji River Basin. Japan Environmental Modelling and Software 2007;22:464-75.

Singh KP, Malik A, Sinha S. Water quality assessment and apportionment of pollution sources of Gomti River (India) using multivariate statistical techniques: A case study. Analytica Chimica Acta 2005;538:355-74.

Siwiec T, Reczek L, Michel MM, Gut B, Hawer-Strojek P, Czajkowska J, et al. Correlations between organic pollution indicators in municipal wastewater. Archives of Environmental Protection 2018;44(4):50-7.

Toan PV, Sebesvari Z, Bläsing M, Rosendahl I, Renaud FG. Pesticide management and their residues in sediments and surface and drinking water in the Mekong Delta, Vietnam. Science of the Total Environment 2013;452-453:28-39.

Tuan DDA, Thu BA, Trung NH. Assessing quality of surface water for urban water supply source for Soc Trang City. Scientific Journal of Can Tho University 2019;4A:61-70. (in Vietnamese)

United Nations Children's Fund (UNICEF). UNICEF Handbook on Water Quality. New York, USA: UNICEF; 2008.

Vega M, Pardo R, Barrado E, Debán L. Assessment of seasonal and polluting effects on the quality of river water by exploratory data analysis. Water Research 1998;32:3581-92.

Vietnam Environment Administration (VEA). Guidance on Sampling of Rivers and Streams (TCVN 6663-6:2018). Hanoi, Vietnam: Ministry of Science and Technology; 2018.

Wilbers GJ, Becker M, Nga LT, Sebesvari Z, Renaud FG. Spatial and temporal variability of surface water pollution in the Mekong Delta, Vietnam. Science of the Total Environment 2014;485-486:653-65.

World Health Organization (WHO). Guidelines for drinking-water quality, 3rd edition: Volume 1 Recommendations, Incorporating First and Second Addenda. Geneva, Italy: WHO; 2008.

Zeinalzadeh K, Rezaei E. Determining spatial and temporal changes of surface water quality using principal component analysis. Journal of Hydrology: Regional Studies 2017;13:1-10.

Response of Streamflow and Soil Erosion to Climate Change and Human Activities in Nam Rom River Basin, Northwest of Vietnam

Hoang Le Huong[1,2] and Ngo Thanh Son[1,3*]

[1]*Consulting Center of Technological Sciences for Natural Resources and Environment, Gia Lam, Ha Noi, Vietnam*
[2]*College of Forestry and Natural Resources, University of the Philippines Los Banos, Laguna 4031, Philippines*
[3]*Faculty of Land Management, Vietnam National University of Agriculture, Trau Quy, Gia Lam, Ha Noi, Vietnam*

ARTICLE INFO

Received: 15 May 2020
Received in revised: 17 Aug 2020
Accepted: 26 Aug 2020
Published online: 10 Sep 2020
DOI: 10.32526/ennrj.18.4.2020.39

Keywords:
Climate change/ Land use land cover (LULC)/ Streamflow/ Soil erosion/ SWAT model/ Nam Rom Watershed/ River Basin

*** Corresponding author:**
E-mail: ntson@vnua.edu.vn

ABSTRACT

Change in climate and land use is the main cause of increasing streamflow and soil erosion. However, very few studies have investigated these changes on a basin scale. Thus, this study used the Soil and Water Assessment Tool (SWAT) method to evaluate the effects of both land use and climate change effects on streamflow, sediment yield, and soil loss in the Nam Rom River Basin, Northwest of Vietnam. The outputs of the SWAT model demonstrated it to be a strong tool in predicting catchment hydrology, sediment transport, and soil loss. Meanwhile, based on SWAT model simulation, it was found that reforestation and management practices executed between 1992 and 2015 strongly contributed to the decreased sediment yield. The potential for climate change clearly leads to an increase to sediment yield and significantly more soil loss. The combined climate and land use change analysis indicated that land use planning could be adopted to mitigate streamflow (16.9%) and sediment load (4.9%) in the future, in conjunction with the projected direct impact of climate change. In conclusion, the findings in the present study contribute useful knowledge, methods, and techniques that could be reapplied to other regions in Vietnam and the world in terms of land and water conservation.

1. INTRODUCTION

Global climate change in temperature and precipitation patterns are expected to alter water resource availability, sediment transport, and pollutants over the world (Duan et al., 2020; Krysanova and White, 2015; Ngo et al., 2015; Wu et al., 2012). Land use and land cover (LULC) change have disturbed overland flow generation and resulted in changing hydrological processes and the transport of pollutants (Van and Cochard, 2017; Van, 2007). LULC and climate change are recognized as the main elements in controlling the catchment hydrology, sediment yield and soil erosion (Boru et al., 2019; Shrestha et al., 2016; Alansi et al., 2009). Therefore, understanding hydrological responses, sediment transport, and soil loss plays a key role in developing long term LULC and water conservation and sustainable watershed preservation.

Recently, several studies have reported the impacts of LULC and climate change on hydrology and soil erosion in different spatial and temporal scale (Ziegler et al., 2007; Nie et al., 2011; Phan et al., 2011; Khoi and Suetsugi, 2014; Ngo et al., 2015; Uniyal et al., 2015). Results of previous studies found that the increase in precipitation would likely increase changes of erosion by approximately 12% to 45% (Son and Binh, 2020; Van, 2007). In addition, change in climate and forest types has a significant impact on streamflow and sediment transport, however, no clear distinction was made between individual and combined effects of LULC and climate change on streamflow and sediment yield. Few research undertakings have also been conducted using the remote sensing (RS) and Soil and Water Assessment Tool (SWAT) to evaluate and predict hydrological responses and soil erosion in Southeast Asia due to a lack of data sharing and limited temporal and spatial data (Ngo et al., 2015).

The Nam Rom Watershed is a typical watershed located in Dien Bien Province which plays an important role in supplying freshwater for its locality. Forests and crops like rubber, rice, maize, and cassava are dominant in this area; however, under the pressure

Citation: Huong HL, Son NT. Response of streamflow and soil erosion to climate change and human activities in Nam Rom River Basin, Northwest of Vietnam. Environ. Nat. Resour. J. 2020;18(4):411-423. (https://doi.org/10.32526/ennrj.18.4.2020.39)

impacts of population growth a dramatic decline in forest areas and increased cash crop (maize and cassava) and built-up areas have taken place since the last few decades (Huong et al., 2017; Do and Son, 2017). Aside from this, the Nam Rom Watershed is considered as one of the most disaster-prone regions, suffering from tropical storms, landslides, drought, soil erosion, and degradation (Do and Son, 2017). Therefore, a question needs to be explored, and is the motivation for the current study: Are human activities or climate variability the main causes of the increased streamflow and sediment load?

Currently, many hydrological models, such as LISEM (Jetten et al., 2003), ANSWERS (Bouraoui et al., 1996), AGNPS (Young et al., 1985), MIKE-SHE (Thompson et al., 2004), MMF (Morgan, 2001), WEPP (Flanagan et al., 2012), and SWAT (Arnold et al., 1998) are used to simulate the soil erosion and hydrological process involved in the hydrological cycle. Among these methods, the SWAT model was selected for the present study. SWAT represents the spatial distribution of hydrological properties using the fundamental concept of the hydrological response unit (HRU). SWAT is widely used to assess hydrological effects of environmental change around the world (see SWAT literature database: https://www.card.iastate.edu/swat_articles/). Besides, SWAT presents a user-friendly graphical interface facilitating the handling input data.

In addition, as we know so far, no clear distinction has been made between individual and combined effects of LUCCs and climate change on hydrology and sediment yield in previous studies (Son and Binh, 2020). Therefore, the present study aims at quantifying the historical and projected change in LULC and climate change on streamflow, sediment transport, and soil erosion in the Nam Rom Watershed. For doing this, we follow the spatially distributed hydrological model approach and implement the SWAT model using RS data and monthly hydrological data. The sub-objectives are: (1) to calibrate and validate the SWAT model in terms of flow and sediment yield; (2) to simulate responses of streamflow, sediment yield, and soil erosion to individual land-use change and climate variation; (3) to investigate the combined impact of land-use change and climate variation on streamflow and soil erosion; and (4) a deep understanding of hydrological processes can provide tools and methods that could be used to other river basins in Southeast Asia as well as long term soil conservation programs.

2. METHODOLOGY

The research content is distributed into two main parts corresponding to the past and future periods through the application of hydrological models (SWAT). The first part presents the steps in setting up the SWAT model, model running, model calibration and validation. Model application focuses on simulation of stream flow and sediment loads based on the variations in land use in the past. In addition, special attention is given to simulation streamflow for long term under projected land use and climate change scenarios. The principle impacts of hydrology are not only land use but also climate change. Therefore, the objective of this study is to assess individual and combined effects of land use and climate change on streamflow and soil erosion. It is very important to understand hydrology and soil erosion from these changes in order to develop strategies for land use planning and water management. The second part of the study is to predict land use scenarios based on the population growth and socio-economic development as well as land use demands and plans in the study area. SWAT modeling is selected to simulate the impacts of projected land use and climate scenarios in 2030 on streamflow and soil erosion considering the socioeconomic development and population growth in the study area. Figure 1 illustrates the detailed methodology applied in this research.

2.1 Study area

The study area is situated in the Nam Rom Watershed, Northwest of Vietnam (between 20°90' to 21°40' E and from 102°30' to 103°20' N). The drainage area of the Nam Rom Watershed covers 1,348 km^2 with elevation ranges from 2019 m to 436 m (Figure 2). Nam Rom is generally characterized by a tropical monsoon climate with high annual precipitation (1,600 mm), however, its precipitation is spatial and seasonal distributed unevenly with, rainy season accounting for 80% of total annual rainfall. Soils in this study area mostly located on slopes, and thus are major causes of severe soil erosion (Dien Bien People's Committee, 2015b).

LULC in the Nam Rom Watershed is predominantly forests (45.87% of the total area) and cash crop (35.23%). The major land use in the basin area includes lowland rice, rain-fed crops (upland rice, corn, bean, cassava, groundnuts, etc.) and perennial crops (10.57%) (fruit trees, acacia, rubber, etc.). The people's committee in Dien Bien Province indicated

that the characteristics of the study area are massive changes in LULC patterns and conservation practices in the last few decades (Dien Bien People's Committee, 2015a).

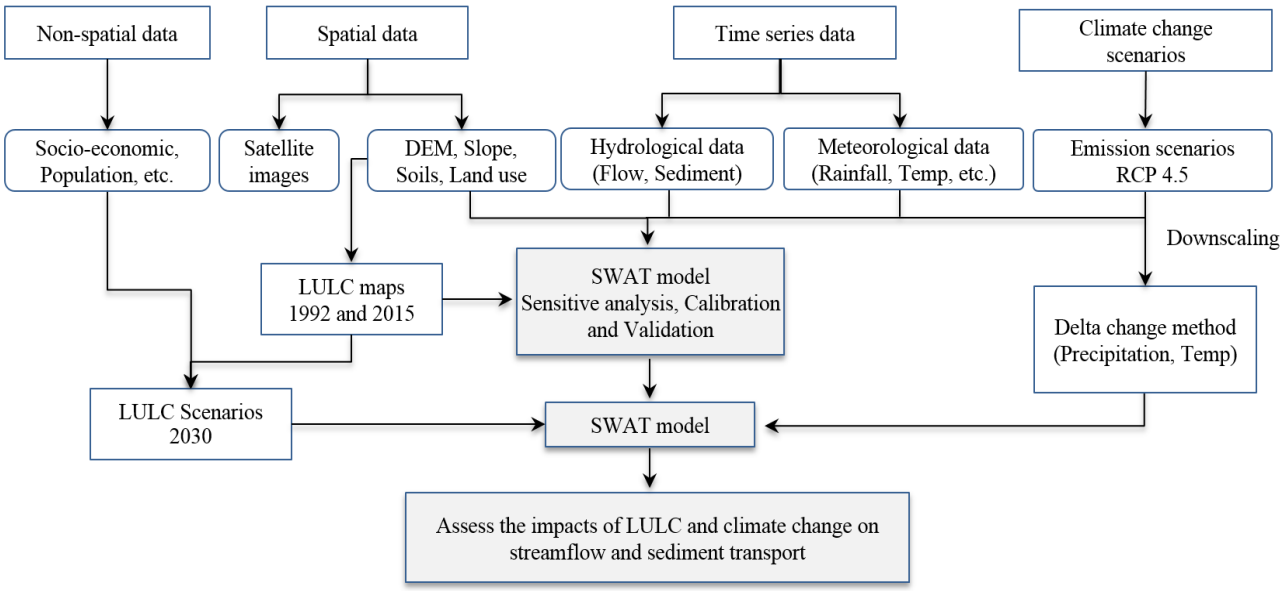

Figure 1. Research methodology applied for this study

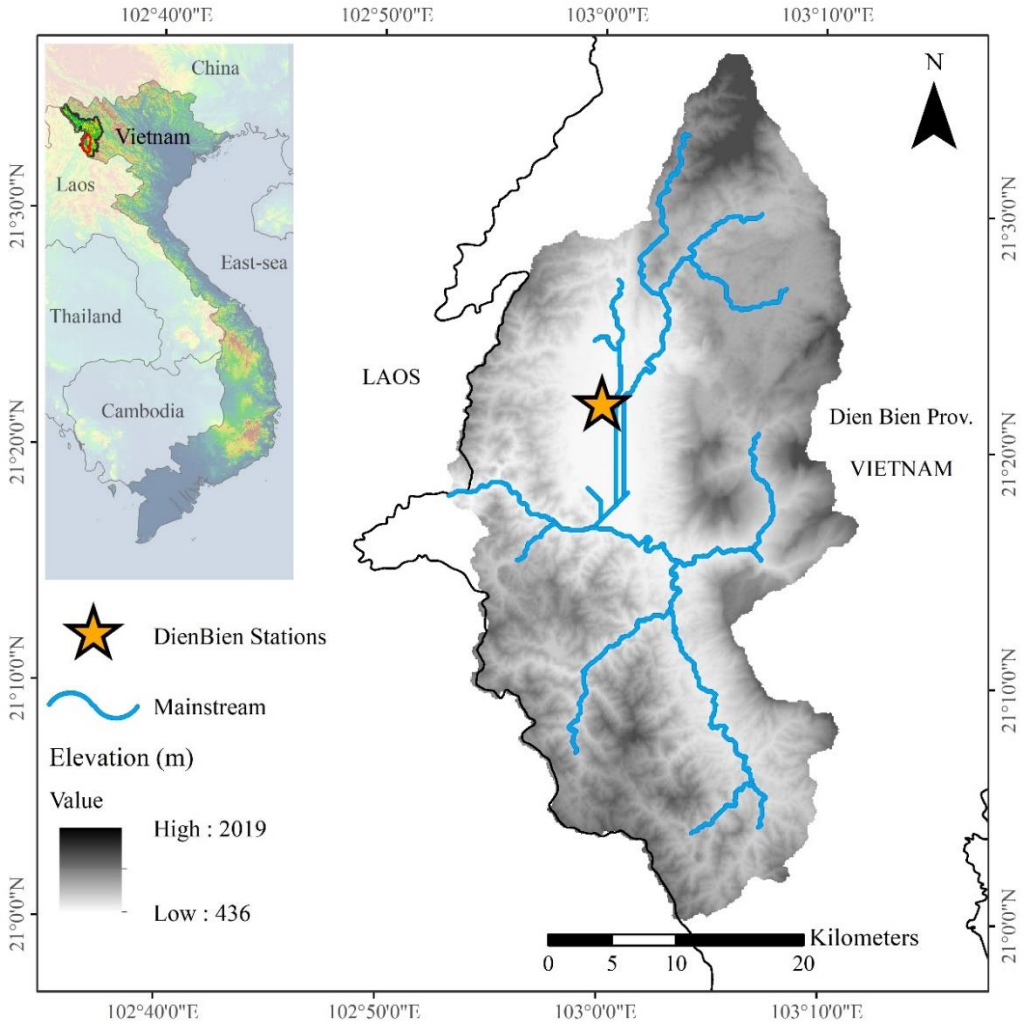

Figure 2. Study area

2.2 Data collection

Time series data including climate data (daily precipitation, temperature, evapotranspiration, and humidity) and hydrological data (flow and sediment yield) were collected from the station nearest to the center of each sub-basin in the Northwestern region.

Spatial data (Figure 3) include: (a) a 50 m-DEM covering Nam Rom Watershed obtained from Ministry of Natural Resources and Environment (MONRE); and (b) slope map was divided into five classes, 0°-3° (Very Gentle), 3°-8° (Gentle), 8°-15° (Moderate), 15°-35° (Moderate to Steep) and >35° (Very Steep) (MONRE, 2015); (c) Soil characteristics of 18 soil types inputted in the SWAT model collected from MONRE and Mekong River Commission (MRC); and (d) to (f) LULC: satellite images in digital format of the area in 1992 and 2015 produced using Landsat satellite images downloaded from the USGS website (http://glovis.usgs.gov) at Path/Row-128/55 and 129/45 in the respective year, the LULC maps have been performed through image classification using the maximum likelihood classification (MLC) algorithm.

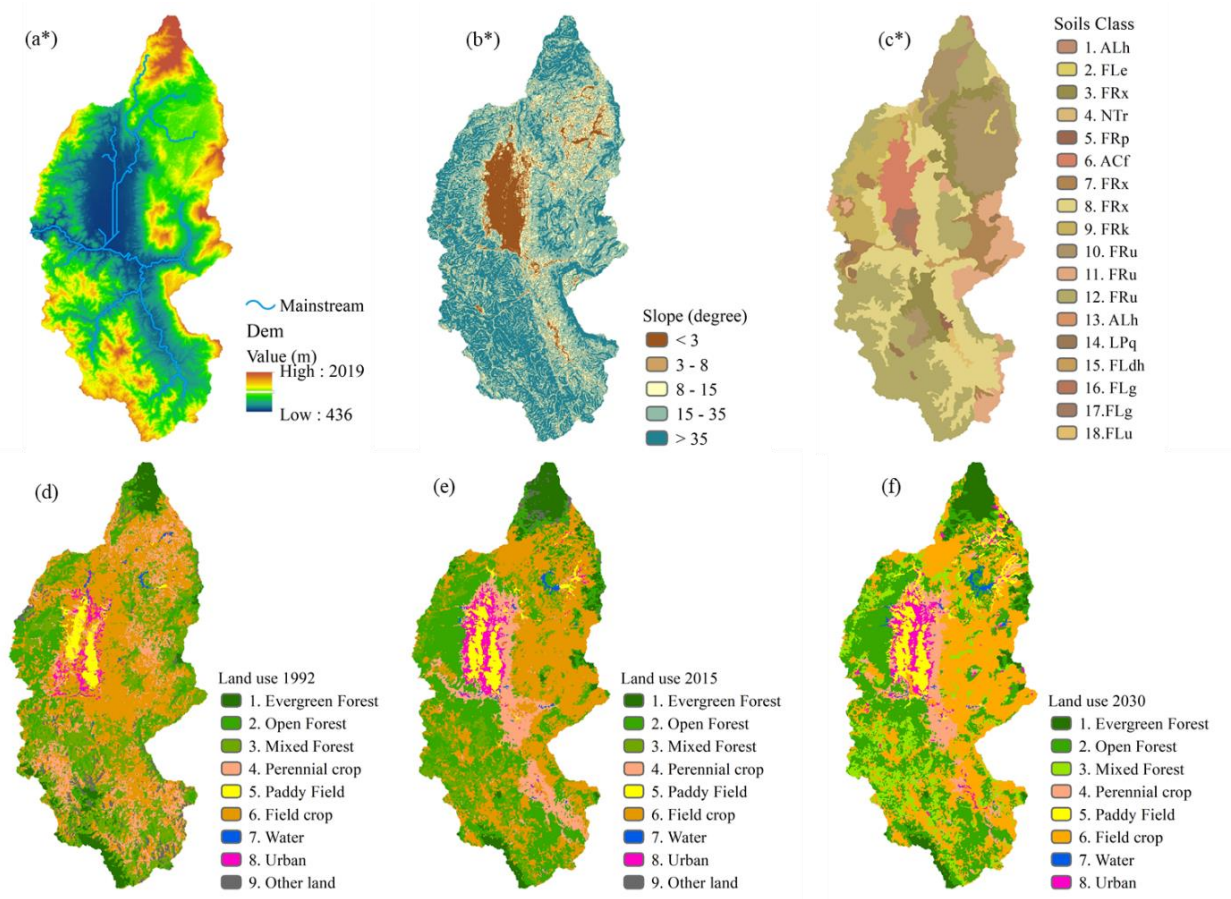

Figure 3. SWAT model inputs and delineated outputs [(a) DEM and meteorological station; (b) Slope; (c) Soil classes; (d) Land use in 1992; (e) Land use in 2015; and (f) Land use in 2030] *Sources: MONRE (2015)

2.3 Application hydrological model (SWAT)

2.3.1 SWAT model description

SWAT, a spatial and physical distributed model, is applied widely in the world for evaluating the environmental change of hydrology in large and complex watersheds over long term periods. In addition, SWAT has been examined in several climate conditions in the world from arid and semi-arid regions to humid and tropical areas (Ngo et al., 2015).

In this research, potential evapotranspiration (PET) was calculated by using the Penman-Monteith method, while surface runoff (overland flow) was calculated by Soil Conservation Services (SCS) curve number method. The water balance was likewise used in the SWAT model to calculate the hydrological cycle which represents as follows (Neitsch et al., 2011):
which represents as follows (Neitsch et al., 2011):

$$SW_t = SW_0 + \sum_{i=1}^{t} (R_{day} - Q_{surf} - E_a - W_{seep} - Q_{gw}) \quad (1)$$

Where; SW_t is the: final soil-water content; SW_0 is the initial soil water content; R_{day} is the precipitation amount; Q_{surf} is the surface runoff amount; E_a is the amount of evapotranspiration; W_{seep} is the percolation; Q_{gw} (mm H_20) is the return flow; and t is time in days (Neitsch et al., 2011).

Modified Universal Soil Loss Equation (MUSLE) used for the simulation of soil erosion (Wischmeier and Smith, 1978) is computed as below:

$$Sed = 11.8(Q_{surf} \cdot q_{peak} \cdot area_{hru})^{0.56} \cdot K_{USLE} \cdot C_{USLE} \cdot P_{USLE} \cdot LS_{USLE} \cdot CFRG \quad (2)$$

Where; Sed (metric tons) is the sediment yield; q_{peak} (m^3/s) is the peak runoff rate; $area_{hru}$ (ha) is the hydrologic response unit (HRU); K_{USLE} is the soil erodibility factor; C_{USLE} is the cover and management factor; P_{USLE} is the practice factor; LS_{USLE} is the topographic factor; and CFRG is the coarse fragment factor (Wischmeier and Smith, 1978).

2.3.2 Model calibration and validation

The Sequential Uncertainty Fitting (SUFI-2) algorithm was applied to implement calibration and validation of the hydrological model in this study. According to Moriasi et al. (2007), to evaluate model performance, three (3) indicators Nash-Sutcliffe (NS); percent bias (PBIAS), Observation's standard deviation ratio (RSR) as shown in equations (3)-(5) respectively, must be used:

$$NS = 1 - \left[\sum_{i=1}^{n}(Q_{obs}^{i} - Q_{sim}^{i})^2\right] / \left[\sum_{i=1}^{n}\left(Q_{obs}^{i} - \overline{Q}_{obs}^{i}\right)^2\right] \quad (3)$$

$$RSR = \frac{RMSE}{STDEV_{obs}} = \frac{\sqrt{\sum_{i=1}^{n}\left((Q_{obs}^{i} - Q_{sim}^{i})^2\right)}}{\sqrt{\sum_{i=1}^{n}\left((Q_{obs}^{i} - \overline{Q}_{obs})^2\right)}} \quad (4)$$

$$PBIAS = \sum_{i=1}^{n}(Q_{obs}^{i} - Q_{sim}^{i}) \times 100 / \sum_{i=1}^{n} Q_{obs}^{i} \quad (5)$$

Where; n is the number of time steps; Q^i_{obs}, and Q^i_{sim} are the observation and simulation; on the i^{th} time step; and $\overline{Q_{obs}}$ is the mean of observation (Q^i_{obs}) across the n evaluation time steps.

2.3.3. Model applications

(1) Land use change analysis

Change analysis in LULC was performed by overlaying classified LULC maps of two-time periods (1992 vs 2015, and 2015 vs 2030). There were nine land use classes in the basin with the most common agricultural land use in the basin known to be the evergreen forest, open forest, mixed forest, perennial crop, paddy field, field crop, urban, water body and aquaculture, and other lands (Table 1). LULC in the Nam Rom Watershed was dominated by converting forests (FRST and ORCD) to the paddy field, open forest, and urban area. Five land use classes (open forest (FRSD), mixed forest (FRST), field-crop (FCRP), rice (PDDY), and urban (URBN)) turned out to significant effect LULC change. From 1992 to 2015, FSRD, URBN, and PDDY increased from 15,739.7 ha to 39,876.9 ha (18.1%), 2,175.3 ha to 4,196.9 ha (1.5%), and 3,292.7 ha to 4,939.0 ha (1.2%), respectively. In contrast, there was a significant decrease in the area of FRST, ORCD, and BARR from 34,849.4 to 14,084.8 ha (15.5%), 17,729.5 to 14,127.8 ha (2.7%), and 4,652.4 to 1,323.8 ha (2.5%), respectively.

The projected LULC scenario in 2030 was created following and in consideration of its baseline land use in 2015. The predication was done in order to settle the population growth rate estimated at 1.22 and maintain food security by increasing over 50% in the paddy field and 15% in urban land. Note that the following types of on-going changes in LULC were found in the Nam Rom Watershed: (1) vacant lots especially urban lands are utilized for all other purposes of land use; (2) inefficient upland fields were converted into forest land or orchard; (3) mixed forest or open forest to evergreen forest are converted, if possible; (4) lowland are transformed into paddy fields and expand existing residential neighborhoods are expanded nearby lands. These trends, as seen in Figure 3, are assumed to be maintained in the future.

Table 1. LULC change in the period of 1992-2015 and 2015-2030

No.	Land use classes	SWAT code	Area (ha)			Change (%)	
			1992	2015	2030	1992-2015	2015-2030
1	Evergreen forest	FRSE	6,320.52	7,367.31	7,349.76	16.56	-0.24
2	Open forest	FRSD	15,739.56	39,876.93	40,689.09	153.35	2.04
3	Mixed forest	FRST	34,849.35	14,084.55	14,802.84	-59.58	5.10
4	Perennial crop	ORCD	17,729.46	14,127.84	9,434.70	-20.31	-33.22

Table 1. LULC change in the period of 1992-2015 and 2015-2030 (cont.)

No.	Land use classes	SWAT Code	Area (ha)			Change (%)	
			1992	2015	2030	1992-2015	2015-2030
5	Paddy field	PDDY	3,292.74	4,939.02	7,456.32	50.00	50.97
6	Field crop	AGRR	48,290.31	47,110.32	48,090.33	-2.44	2.08
7	Water	WATR	659.52	682.47	1,014.48	3.48	48.65
8	Urban area	URBN	2,175.30	4,196.88	4,871.61	92.93	16.08
9	Other lands	BARR	4,652.37	1,323.81	0.00	-71.55	-100.00
	Total area (ha)		133,709.13	133,709.13	133,709.13		

(2) Climate change scenarios

In the northwestern provinces, AR5 scenarios were selected for the study site because it was downscaled by AOGCM, GCMs, RCM, Global Ocean model, and statistic downscaling techniques (Thuc et al., 2016). The PRECIS (Hadley Centre-UK) method was utilized for downscaled future climate change scenarios in the Northwest of Vietnam. Also, based on the climate change set for the Northwest regions in the future, RPC 4.5 (2016-2035) scenarios were used for evaluating LULC and CC effects on streamflow and soil erosion in the present study.

(3) SWAT applications

In this research, one factor such as land use or climate change was changed while others were kept constant. The influences of LULC and climate change were computed by comparing five scenarios: S1: 1992 LULC and 1992-2003 climate ; S2: 2015 LULC and 1992-2003 climate; S3: 1992 LULC and 2004-2015 climate; S4: 2015 LULC and 2004-2015 climate; S5: 2030 LULC and 2016-2030 climate (projected LULC and climate scenarios).

3. RESULTS AND DISCUSSION

3.1 Model calibration and validatin

Results of the SWAT model in Figure 4 and Table 2 indicated flow simulation in the following values at calibrated and validated periods for NS: 0.76 and 0.65; RSR: 0.49 and 0.60; and PBIAS: 6.76 and 8.37, respectively. In terms of sediment yield, respective values at calibrated and validated periods appeared at 0.82 and 0.81 for NS; 0.47 and 0.55 for RSR; and -16.06 and -18.95 for PBIAS (Table 3).

Table 2. Indicators for model performance

SWAT model performance	NS	PBIAS	RSR
Very good	0.75<NS≤1.00	PBIAS<±10	0.00≤RSR≤0.50
Good	0.65<NS≤0.75	±10≤NS≤±15	0.50<NS≤0.60
Satisfactory	0.50<NS≤0.65	±15≤NS≤±25	0.60<NS≤0.70
Unsatisfactory	NS≤0. 5	PBIAS≥±15	RSR>0.70

Sources: Yang et al. (2014)

Table 3. Model performances for the monthly simulated flow and sediment

Indicators	Flow		Sediment yield	
	Calibration (1992-2003)	Validation (2004-2015)	Calibration (1995-2003)	Validation (2004-2010)
RSR	0.49	0.60	0.47	0.55
NS	0.76	0.65	0.82	0.81
PBIAS (%)	6.76	8.37	-16.06	-18.95

In comparison with the guidelines set in Moriasi et al. (2007) the SWAT performance is from good to very good, meaning that the model can be applied to simulate LULC and climate change on streamflow and sediment transport in Nam Rom Watershed.

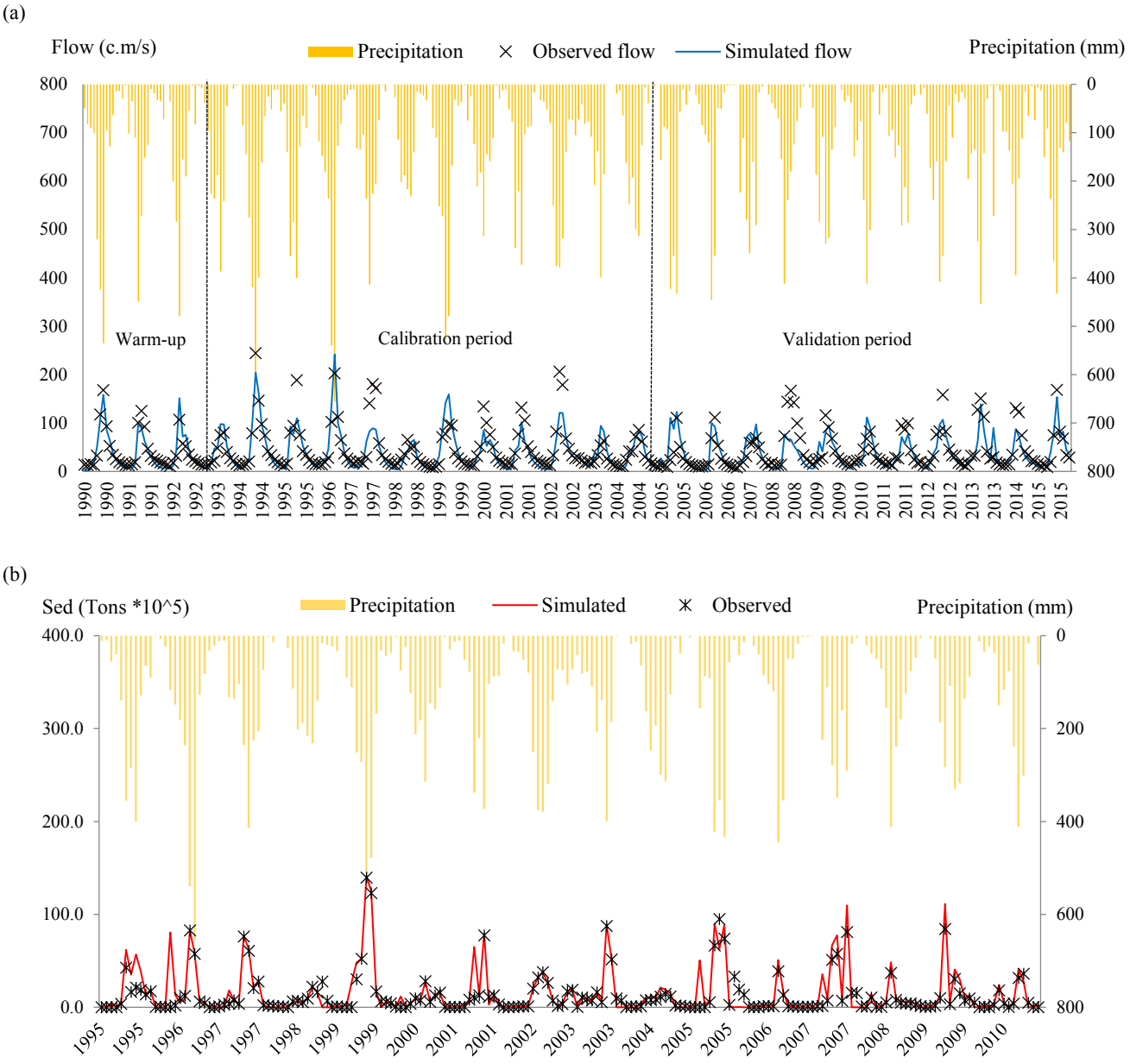

Figure 4. Calibrated and validated flow (a) and sediment (b)

3.2 Impacts of the past LULC and climate change on streamflow, sediment yield, and soil erosion in the basin scale

Under the impact of LULC change, sediment yield and soil loss decreased by 4.3%, 13.7%, and 26.3%, respectively. The above results indicated that the change was influenced by increased forest cover (open and mixed forest) in combination with the decrease of precipitation from 1992-2015. These changes also led for productive use of area by adopting suitable treatment measures, like change in cropping pattern and in soil and water conservation practices. In addition,the results are the same with the findings of Phan et al. (2011) and Khoi and Suetsugi (2014) who found that the conversion of forest land (11.07%) to agricultural land leads to an increase in streamflow by 3.93% because of the fragmentation of soil structure, and scatters of different farming practices which all contribute to an increase in streamflow. Khoi and Suetsugi (2014) also reported that the increase in average annual streamflow (1.2%) was due to rapid deforestation and the expansion of agricultural land. Forest cover stored more water than any other types of land use and the infiltrated rate of forestland is the largest in comparison with other types of land use However, forest in NW has been cut and burned for expansion of agricultural land (corn and cassava, pineapple, and vegetable), therefore causing an increase in average annual streamflow.

Under climate change, sediment yield and soil erosion increased by 12.2% and 52%, respectively. The increase in sediment load and soil erosion could be explained by increasing quantity and intensity of precipitation in the dry season (from December to January) that had a large effect on sediment load. In addition, the traditional farming systems or LULC change in this area are mostly based on the last month of the dry season. Therefore, when precipitation occurs, especially peak precipitation occurs, farmers also start plowing and preparing to sow seed or cultivate plants on their farms. This causes complexity, fragmentation, and scatters of different farming practices which all contribute and encourage soil erosion (Ngo et al., 2015; Li et al., 2011; Phan et al., 2011).

As to the assessment of the combined impacts of LULC and climate change on sediment load and soil loss in the basin scale, Figure 5 presents the compared simulated results of S4 (LULC 2015 and climate change 2004-2015 period) and S1 (LULC 1992 and climate change 1992-2003). Based on the data, compared with S1, S4 showed that the combined impact of LULC and climate change led to a slight decrease in sediment load by -4.9% although soil loss increased by 20%. The increased soil erosion could be caused by increased and altered precipitation patterns such as timing, quantity, and intensity. The rainfall erosivity (R) is mostly related to overland flow which is recognized as a principal factor for soil erosion in the sloping land at Nam Rom Watershed.

For the future assessment of the changing streamflow, sediment yield, and soil loss in the basin-scale under the LULC and climate change scenario, the projected LULC 2030 and climate from 2016 to 2030 were compared to the corresponding current conditions (S4 scenario). Figure 5 (right) indicated that sediment yield and soil loss are projected to decrease by 12 % and 34%, respectively in the future. The decrease is brought about by the increase of forest cover and paddy field (FRST, FSRD, and PDDY) in combination with implementing contour line hedgerow, grass and plastic cover, cropping systems (food production, fruit production, and forest trees) and sustainable agroforestry land technology (SALT) which results in reducing raindrop speed and energy and increasing the rate of infiltration, improving organic matter, reducing soil crusting, and restoring nutrients.

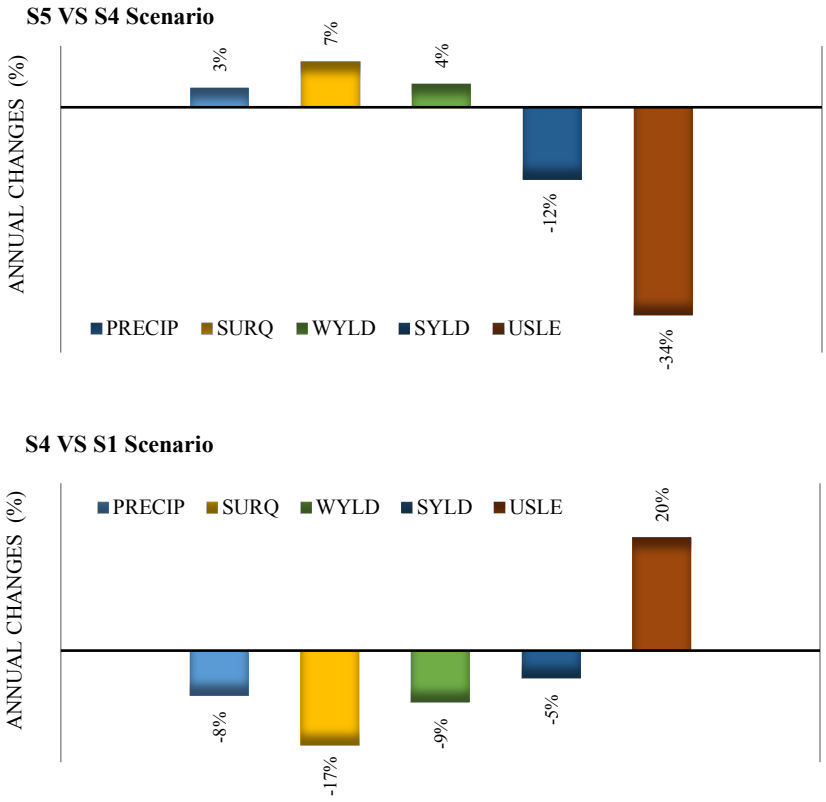

Figure 5. Annual changes of streamflow and sediment yield under different scenarios
(Note: PRECIP: precipitation; SURQ: surface flow; WYLD: water yield; SYLD: sediment yield; USLE: soil erosion)

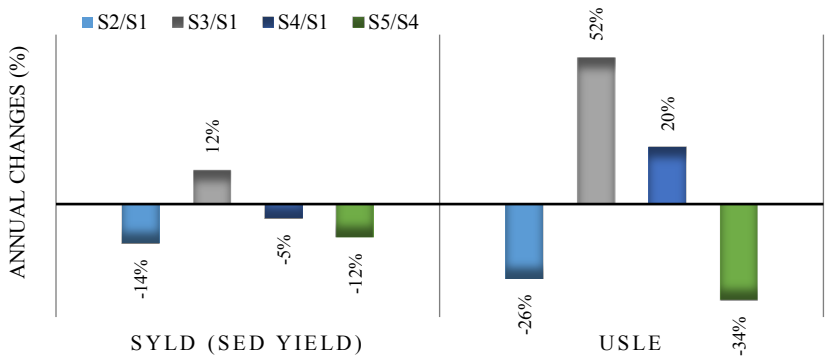

Figure 5. Annual changes of streamflow and sediment yield under different scenarios (cont.)
(Note: PRECIP: precipitation; SURQ: surface flow; WYLD: water yield; SYLD: sediment yield; USLE: soil erosion)

3.3. Contribution of changes for combined LULCs and climate change on runoff and sediment from 1992 to 2015 and 2016 to 2030 in the sub-basin scale

The spatial distribution of changes for the six main LULC classes (open forest, mixed forest, perennial crop, paddy, field crop, and urban area), particularly, the simulated surface runoff and sediment yield between 1992 and 2015 are shown in Figure 6. The decrease in surface runoff and sediment yield in sub-basin 5 and 14 correspond to where the majority of field crop (corn, cassava, sugar cane, potato, etc) was replaced by forest cover and implementation of soil and water conservation (Chen et al., 2019; Duan et al., 2020).

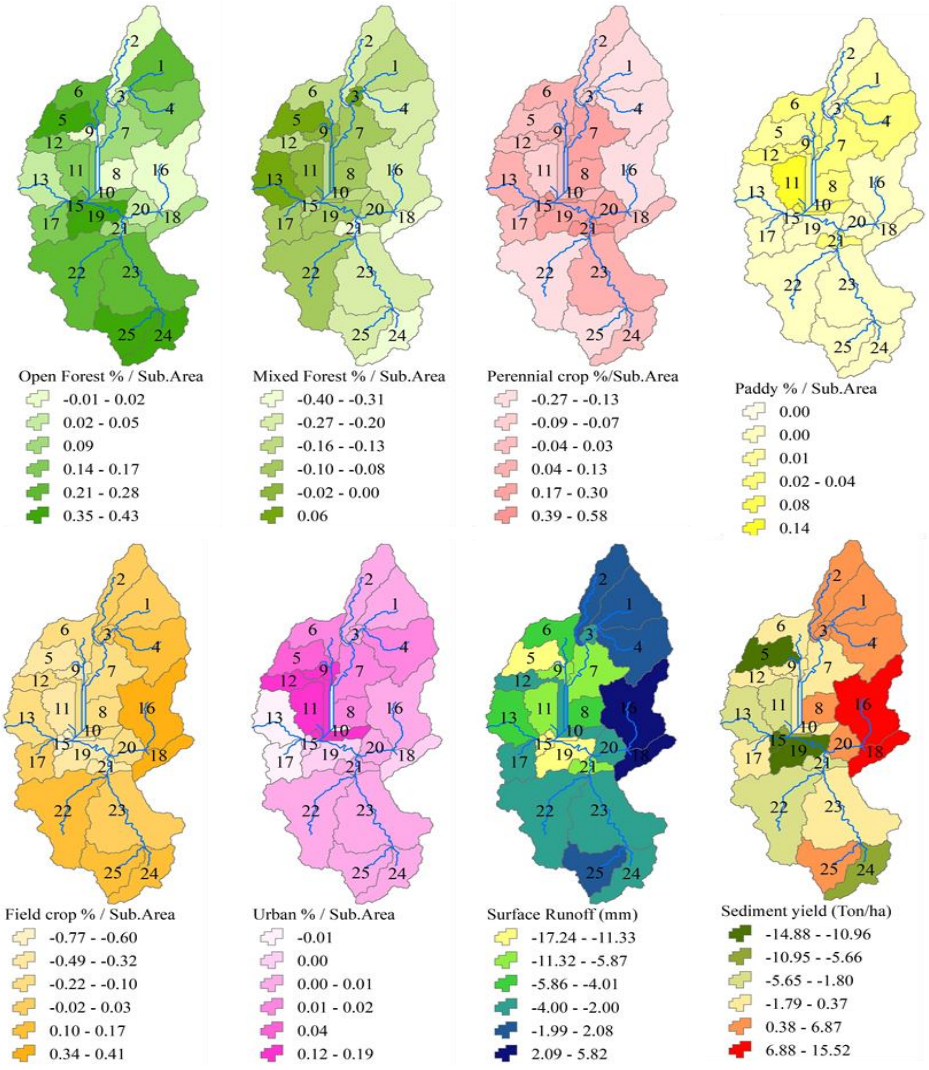

Figure 6. Spatial distribution of LULCs, runoff, and sediment from 1992 to 2015

Similar to the past, the expansion of LULC (open forest, mixed forest, and paddy field) mainly occurred in the northeast of Dien Bien. Due to the increase in forest cover combined with implementing soil conservation practices, the maximum surface runoff and sediment yield decreased compared to land use between 2015 and 2030. This finding largely matches the spatial distribution pattern expansion of FRSE, FRSD, and PDDY and is confirmed by the negative high correlation between its expansion and decrease in surface runoff and sediment yield (Figure 7). The decrease of surface runoff and sediment yield in sub-basin 14 and 20 correspond to where the majority of field crop (corn, cassava, sugar cane, potato, pineapple) was replaced by forest (teak, rubber, bambbo, eucalyptus, and cinnamon).

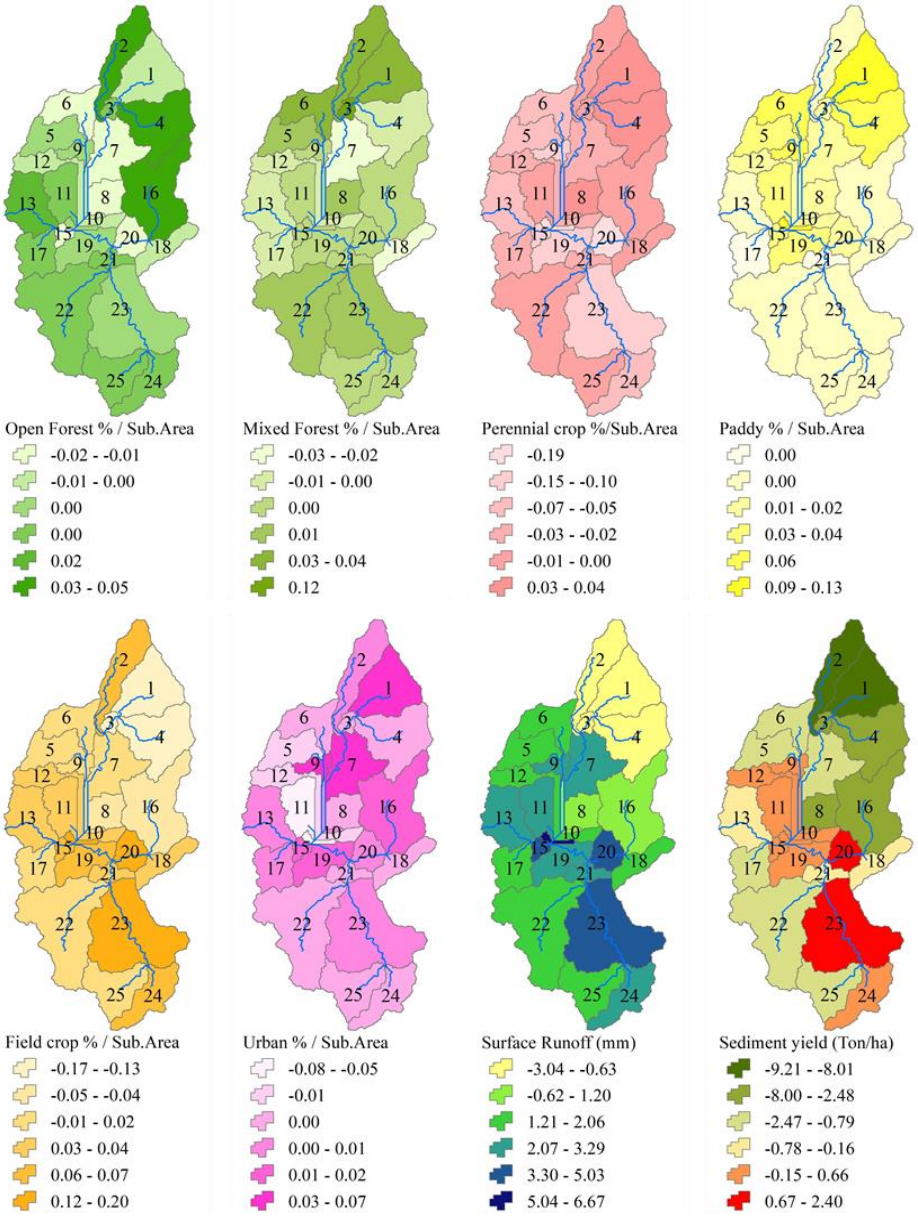

Figure 7. Spatial distribution of LULCs, runoff, and sediment from 2015 to 2030

3.4. Potential soil erosion risk maps under different LULC and climate change scenarios.

The standard soil erosion guidelines recommended by the Ministry of Science and Technology (MOST) in 2009 applied in the present area were categorized into five (5) levels: very low (Soil loss ≤1 ton/ha/year), low (1÷5 ton/ha/year), moderate (5÷10 ton/ha/year), high (10÷50 ton/ha/year), and very high (≥50 ton/ha/year). Areas of soil erosion intensity were significantly changing from nil to weak to high erosion rate. This escalation highlights changes in LULC management practices and climate

change in the period of 1992-2015 as the main reason for the increased erosion. Naturally, the increase or decrease in soil erosion is affected by changes in types of land use as well as the spatial alteration and fragmentation of land use. Aside from this, climate change, in terms of quantity and intensity.

In Figure 8, the soil erosion risk in the Nam Rom watershed mainly shifted from very low and low in 2003 (65.18%) to high and very high in 2015 (58.56%), which suggest that implementation of proper land use planning should be used to avoid conversion of forest land to agriculture land and the built-up area in near future and contributed to reducing soil erosion. From this data, it could be seen that the potential soil erosion in 2030, considering its projected land use and climate scenarios, is a little more serious than soil erosion under current conditions especially when the leaders in the district are planning to increase the evergreen forest as well as expand plantations for the perennial crop like acacia, coffee, and rubber plantation. It must be noted that the potential soil erosion of the Nam Rom watershed may slightly decrease in the future as compared to 2015 since precipitation intensity has been slightly decreasing. However, it must be still be strongly stressed that the complexity, fragmentation, and scattering of different LULC types combined with the increasing precipitation intensity still puts soil erosion in the area at a very high level.

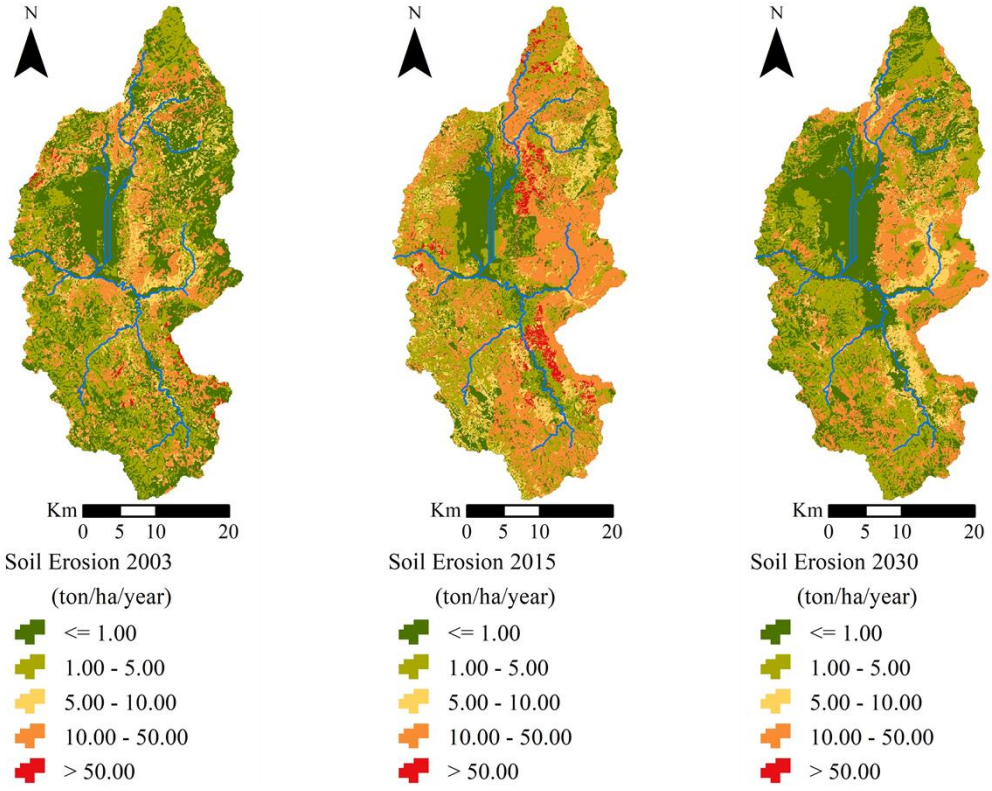

Figure 8. Potential soil erosion in 2003 (left), 2015 (middle), and 2030 (right)

4. CONCLUSION

The present study quantifies the response of streamflow and soil erosion in Nam Rom River Basin of Vietnam. LULC in the Nam Rom River Basin in the past was dominated by converting forests to agricultural land (paddy, maize, cassava) and urban area because of pressure of socio-economic development. In contrast, LULC in the future will shift towards conservation programs by increasing vegetation cover (reclamation, rehabilitation and restoration) and converting ineffective agricultural sloping lands to forest land.

The SWAT model was applied in Nam Rom River Basin of Vietnam in order to simulate the individual and combined effects of land use and climate change on streamflow, sediment yield, and soil erosion. Evaluation results indicated that SWAT performance is from good to very good during calibrated and validated periods. Therefore, SWAT can successfully be used for assessing the impacts of

environmental change including land use change and climate change in Nam Rom River Basin. .

LULC decreased surface flow (4.3%) and sediment yield (13.7%). Climate change increased sediment load by 12% because precipitation from 2004-2015 was significantly higher than 1992-2003. A combination of LULC and climate change impacts leads to a slight decrease in sediment load (4.9%). Overall, climate change strongly affected streamflow and sediment yield than LULC in the study area from 1992 to 2015. Projected LULC and climate change scenarios indicated that sediment yield and soil loss are predicted to decrease by 12% and 34% in the future. It is noted that the combined climate and land use change analysis revealed that sustainable land use planning and management could be adopted to mitigate streamflow and soil loss in the future, in conjunction with the projected direct impact of climate change.

Finally, the results of the present study will contribute useful knowledge, methods, and techniques that could be applied to other regions in Vietnam and the world in terms of land and water conservation.

ACKNOWLEDGEMENTS

Authors would like to take this opportunity to express their deep sense of gratitude to the International Foundation for Science (IFS), Sweden (Grant number: C/5658-1) for funding this research project. Special thanks to Ms. Madonna M. Dimaano for her help in editing grammars on the paper. We also thank two anonymous reviewers for their valuable comments to improve the manuscript.

REFERENCES

Alansi AW, Amin MS, Abdul Halim G, Shafri HZ, Aimrun W. Validation of SWAT model for streamflow simulation and forecasting in Upper Bernam humid tropical river basin, Malaysia. Hydrology and Earth System Sciences Discussions 2009;6(6):7581-609.

Arnold JG, Srinivasan R, Muttiah RS, Williams JR. Large area hydrologic modeling and assessment part I: model development 1. Journal of the American Water Resources Association 1998;34(1):73-89.

Boru GF, Gonfa ZB, Diga GM. Impacts of climate change on streamflow and water availability in Anger sub-basin, Nile Basin of Ethiopia. Sustainable Water Resources Management 2019;5(4):1755-64.

Bouraoui F, Dillaha TA. ANSWERS-2000: Runoff and sediment transport model. Journal of Environmental Engineering 1996;122(6):493-502.

Chen G, Zhang Z, Guo Q, Wang X, Wen Q. Quantitative assessment of soil erosion based on CSLE and the 2010 national soil erosion survey at regional scale in Yunnan Province of China. Sustainability 2019;11(12):Article ID 3252.

Dien Bien People's Committee. Report on Land use Planning of Dien Bien Province. Vietnam: Dien Bien publishing; 2015a. (In Vietnamese)

Dien Bien People's Committee. Report on Soil Map of Dien Bien province. Vietnam: Dien Bien publishing; 2015b. (In Vietnamese)

Do TTD, Son NT. Water use management in the Nam Rom Irrigation System of Muong Thanh Valley, Northwest Vietnam. Vietnam Journal of Agriculture Science 2017;14(10):1518-29.

Duan J, Liu YJ, Yang J, Tang CJ, Shi ZH. Role of groundcover management in controlling soil erosion under extreme rainfall in citrus orchards of southern China. Journal of Hydrology 2020;582:Article ID 124290.

Flanagan DC, Frankenberger JR, Ascough II JC. WEPP: Model use, calibration, and validation. American Society of Agricultural and Biological Engineers 2012;55(4):1463-77.

Huong LH, Phuong TT, Son NT. Assessing correlation between geography and land use changes in Nam Rom River Catchment, Dien Bien Province. Journal of Vietnam Agricultural Science and Technology 2017;(3):71-8. (In Vietnamese)

Jetten V, Govers G, Hessel R. Erosion models: quality of spatial predictions. Hydrological Processes 2003;17(5):887-900.

Khoi DN, Suetsugi T. Impact of climate and land-use changes on hydrological processes and sediment yield: A case study of the Be River catchment, Vietnam. Hydrological Sciences Journal 2014;59(5):1095-108.

Krysanova V, White M. Advances in water resources assessment with SWAT: An overview. Hydrological Sciences Journal 2015;60(5):771-83.

Li Z, Xu Z, Li Z. Performance of WASMOD and SWAT on hydrological simulation in Yingluoxia watershed in northwest of China. Hydrological Processes 2011;25(13):2001-8.

Ministry of Natural Resources and Environment (MONRE). Land Use Planning and DEM Database in Dien Bien Province. Vietnam: Hanoi Publishing House; 2015. p. 1-187.

Ministry of Science and Technology (MOST). TCVN 5299:2009 Soil Quality: Method for the Determination of Soil Erosion. Hanoi, Vietnam: Science and Technology Publishing House; 2009. p. 1-12. (In Vietnamese)

Morgan RP. A simple approach to soil loss prediction: A revised Morgan-Morgan-Finney model. Catena 2001;44(4):305-22.

Moriasi DN, Arnold JG, Van Liew MW, Bingner RL, Harmel RD, Veith TL. Model evaluation guidelines for systematic quantification of accuracy in watershed simulations. American Society of Agricultural and Biological Engineers 2007;50(3):885-900.

Neitsch SL, Arnold JG, Kiniry JR, Williams JR. Soil and water assessment tool theoretical documentation version 2009. Texas, USA: Texas Water Resources Institute; 2011.

Ngo TS, Nguyen DB, Rajendra PS. Effect of land use change on runoff and sediment yield in Da River Basin of Hoa Binh Province, Northwest Vietnam. Journal of Mountain Science 2015;12(4):1051-64.

Nie W, Yuan Y, Kepner W, Nash MS, Jackson M, Erickson C. Assessing impacts of land use and landcover changes on hydrology for the upper San Pedro Watershed. Journal of Hydrology 2011;407(1-4):105-14.

Phan DB, Wu CC, Hsieh SC. Impact of climate change on stream discharge and sediment yield in Northern Vietnam. Water Resources 2011;38(6):827-36.

Shrestha MK, Recknagel F, Frizenschaf J, Meyer W. Assessing SWAT models based on single and multi-site calibration for the simulation of flow and nutrient loads in the semi-arid Onkaparinga catchment in South Australia. Agricultural Water Management 2016;175:61-71.

Son NT, Binh ND. Predicting land use and climate changes scenarios impacts on runoff and soil erosion: A case study in Hoa Binh Province, Lower Da River Basin, Northwest Vietnam. EnvironmentAsia 2020;12(2):67-77.

Thompson JR, Sørenson HR, Gavin H, Refsgaard A. Application of the coupled MIKE SHE/MIKE 11 modelling system to a lowland wet grassland in southeast England. Journal of Hydrology 2004;293(1-4):151-79.

Thuc T, Thang NV, Huong HT, Khiem MV, Hien NX, Phong DH. Climate change and sea level rise scenarios for Vietnam. Hanoi, Vietnam: Ministry of Natural resources and Environment; 2016.

Uniyal B, Jha MK, Verma AK. Assessing climate change impact on water balance components of a river basin using SWAT model. Water Rresources Management 2015;29(13):4767-85.

Van MV. Soil Erosion and Nitrogen Leaching in Northern Vietnam: Expression and Modelling [dissertation]. Wageningen, Netherlands: Wageningen University; 2007.

Van YT, Cochard R. Tree species diversity and utilities in a contracting lowland hillside rainforest fragment in Central Vietnam. Forest Ecosystems 2017;4(1):Article ID 9.

Wischmeier WH, Smith DD. Predicting Rainfall Erosion Losses: A Guide to Conservation Planning. Maryland, USA: Department of Agriculture, Science and Education Administration; 1978.

Wu Y, Liu S, Abdul-Aziz OI. Hydrological effects of the increased CO_2 and climate change in the Upper Mississippi River Basin using a modified SWAT. Climatic Change 2012;110(3-4):977-1003.

Yang Y, Yang Y, Han S, Macadam I, Li LD. Prediction of cotton yield and water demand under climate change and future adaptation measures. Agricultural Water Management 2014;144:42-53.

Young RA, Onstad CA, Bosch DD, Anderson WP. Agricultural Non-point Surface Pollution Models (AGNPS) I and II Model Documentation. Washington D.C., USA: Minnesota Pollution Control Agency; 1985.

Ziegler AD, Giambelluca TW, Plondke D, Leisz S, Tran LT, Fox J, et al. Hydrological consequences of landscape fragmentation in mountainous northern Vietnam: Buffering of Hortonian overland flow. Journal of Hydrology 2007;337(1-2):52-67.

Environment and Natural Resources Journal (EnNRJ)
Volume 18, Number 4, October - December 2020 ISSN: 1686-5456 (Print)
ISSN: 2408-2384 (Online)

LIST OF REVIEWERS IN 2020

Name	Affiliation	Country
Professor Dr. Aye Aye Myint	University of Computer Studies	Myanmar
Professor Dr. Freek van der Meer	University of Twente	Netherlands
Professor Dr. Md Azlin Md Said	Universiti Sains Malaysia	Malaysia
Associate Professor Dr. Daroonwan Kamthonkiat	Thammasart University	Thailand
Associate Professor Dr. Eko Hanudin	Universitas Gadjah Mada	Indonesia
Associate Professor Dr. Kanchana Nakhapakorn	Mahidol University	Thailand
Associate Professor Dr. Le Hung Trinh	Le Quy Don University	Vietnam
Associate Professor Dr. Naiyanan Ariyakanon	Chulalongkorn University	Thailand
Associate Professor Dr. Oliver Ling Hoon Leh	Universiti Teknologi MARA	Malaysia
Associate Professor Dr. Quang Minh Vo	Can Tho University	Vietnam
Associate Professor Dr. Suwit Ongsomwang	Suranaree University of Technology	Thailand
Associate Professor Dr. Takehiko Kenzaka	Osaka Ohtani University	Japan
Associate Professor Dr. Worachart Wisawapipat	Kasetsart University	Thailand
Assistant Professor Dr. Chaiwat Rongsayamanont	Prince of Songkla University	Thailand
Assistant Professor Dr. Chime Mora-Garcia	Caraga State University	Philippines
Assistant Professor Dr. Jenjira Mongon	Mae Jo University	Thailand
Assistant Professor Dr. Nukoon Tawinteung	King Mongkut's Institute of Technology Ladkrabang	Thailand
Assistant Professor Dr. Pantip Klomjek	Naresuan University	Thailand
Assistant Professor Dr. Sureewan Sittijanda	Mahidol University	Thailand
Assistant Professor Dr. Titaya Sararit	Chiang Mai University	Thailand
Assistant Professor Dr. Wiyada Mongkolthanaruk	Khon Kaen University	Thailand
Dr. Abdel Hameed AA.	National Research Centre	Egypt
Dr. Adel Mashaan Rabee	University of Baghdad	Irag
Dr. Allan Sriratana Tabucanon	Mahidol University	Thailand
Dr. Arthur J. Lagbas	Technological University of the Philippines	Philippines
Dr. Chay Asdak	Universitas Padjadjaran	Indonesia
Dr. Chitsanuphong Pratum	Mahidol University	Thailand
Dr. Doungkamon Phihusut	Chulalongkorn University	Thailand
Dr. Erwin Wisnubroto	Tribhuwana tunggadewi University	Indonesia
Dr. Gabriel Salako	Kwara State University	Nigeria
Dr. Hazlina Ahamad Zakeri	Universiti Malaysia Terengganu	Malaysia
Dr. Jakkaphong Thongsawi	Kasetsart University	Thailand
Dr. Kaushala Prasad Mishra	Nehru Gram Bharati University	India
Dr. Kritsadapan Palakit	Faculty of Forestry, Kasetsart University	Thailand
Dr. Kumod Raj Lekhak	Nepal Environmental Resources Organization	Nepal
Dr. Lamthai Asanok	Maejo University	Thailand
Dr. María Menéndez-Miguélez	University of Valladolid	Spain
Dr. Marjorie D	University of the Philippines Los Baños	Philippines
Dr. Merry Krisdawati Sipahutar	Balikpapan University	Indonesia
Dr. Mohamed F. Yassin	Kuwait Institute for Scientific Research	Kuwait
Dr. Mohd. Hafiz Rosli	University Putra Malaysia	Malaysia
Dr. Monthira Yuttitham	Mahidol University	Thailand
Dr. Musingo T. E. Mbuvi	Kenya Forestry Research Institute	Kenya
Dr. Myra Tansengco	Industrial Technology Development Institute	Philippines

Name	Affiliation	Country
Dr. Naphatsarnan Phasukarratchai	Mahidol University	Thailand
Dr. Nazir Ahmad	Sichuan Agriculture University	China
Dr. Nichakorn Khondee	Naresuan University	Thailand
Dr. Noppol Arunrat	Mahidol University	Thailand
Dr. Nguyen Thanh Giao	Can Tho University	Vietnam
Dr. Phonekeo Vivarad	Asian Institute of Technology	Thailand
Dr. Priyom Roy	Indian Space Research Organisation	India
Dr. Raisa Kabeer	Mahatma Gandhi University	India
Dr. Sagar Kafle	Tribhuvan University	Nepal
Dr. Sangay Gyeltshen	APECS	Bhutan
Dr. Selvaraj Vasantha Kumar	Vellore Institute of Technology	India
Dr. Sucheela Polruang	Kasetsart University	Thailand
Dr. Thanh Tien Nguyen	Ha Noi University of Natural Resources and Environment	Vietnam
Dr. Tolera Abera Goshu	Ethiopia Institute of Agricultural Research Institute	Ethiopia
Dr. Trung Thanh Nguyen	An Giang University	Vietnam
Dr. Witchaya Rongsayamanont	Mahidol University	Thailand
Dr. Yutthaphong Kheereemangkla	Kasetsart University	Thailand

GUIDE FOR AUTHORS

Publication and Peer-reviewing processes of Environment and Natural Resources Journal

Environment and Natural Resources Journal is a peer reviewed and open access journal that is published twice a year (January-June and July-December). Manuscripts should be submitted online at https://ph02.tci-thaijo.org/index.php/ennrj/about/submissions by registering and logging into this website. Submitted manuscripts should not have been published previously, nor be under consideration for publication elsewhere (except conference proceedings papers). A guide for authors and relevant information for the submission of manuscripts are provided in this section and also online at: https://ph02.tci-thaijo.org/index.php/ennrj/author. All manuscripts are refereed through a **double-blind peer-review** process.

Submitted manuscripts are reviewed by outside experts or editorial board members of **Environment and Natural Resources Journal**. This journal uses double-blind review, which means that both the reviewer and author identities are concealed from the reviewers, and vice versa, throughout the review process. Steps in the process are as follows:

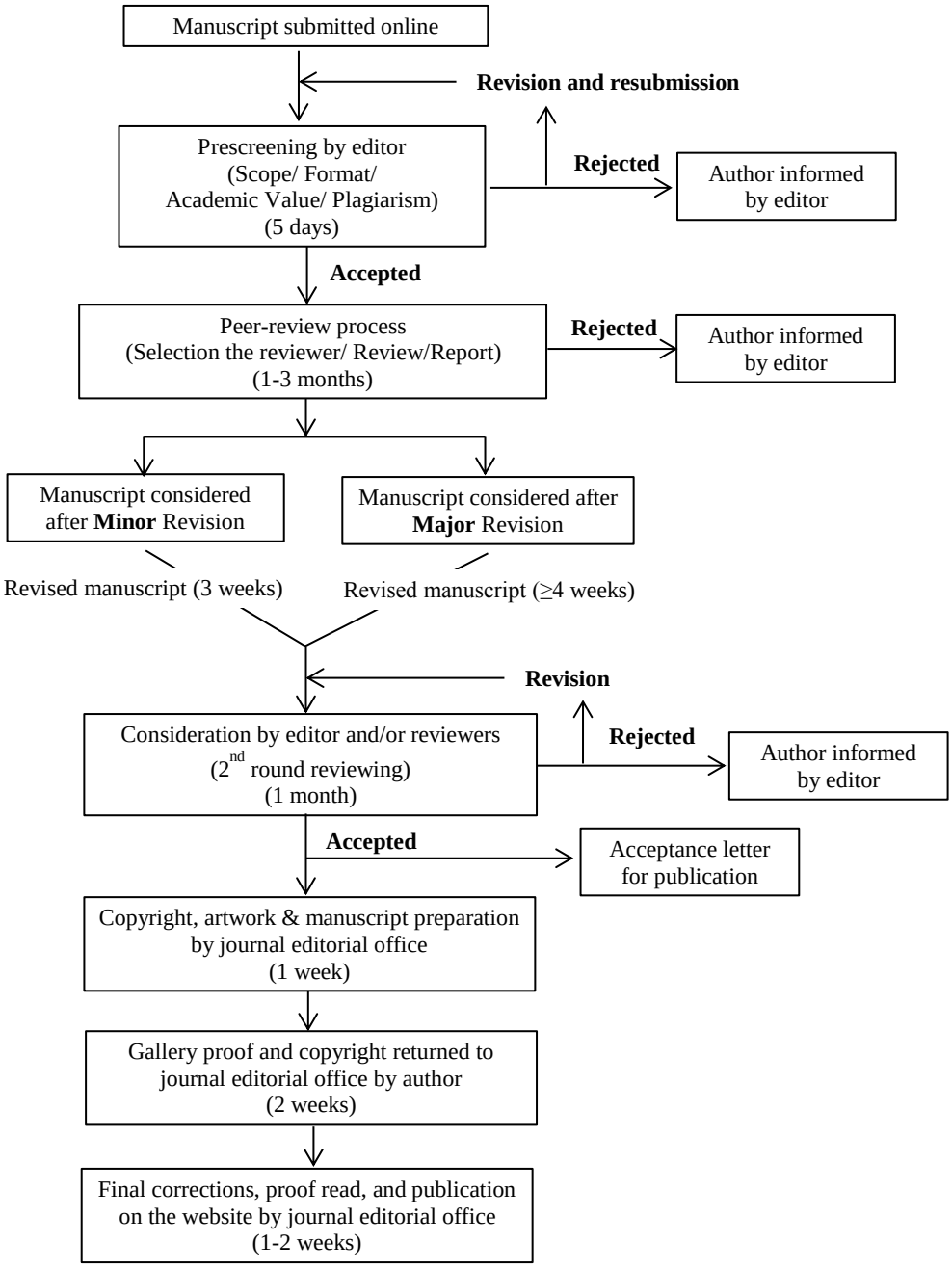

The Environment and Natural Resources Journal (EnNRJ) accepts 2 types of articles for consideration of publication as follows:

- *Original Research Article:* Manuscripts should not exceed 3,500 words (excluding references).
- *Review Article (by invitation):* This type of article focuses on the in-depth critical review of a special aspect in the environment and also provides a synthesis and critical evaluation of the state of the knowledge of the subject. Manuscripts should not exceed 6000 words (excluding references).

Submission of Manuscript

Submitted file(s): The manuscript (A4) must be submitted in Microsoft Word (.doc or .docx).

Reviewers suggestion *(mandatory)*: Please provide the names of 3 potential reviewers with the information about their affiliations and email addresses. *The recommended reviewers should not have any conflict of interest with the authors. Each of the reviewers must come from a different affiliation and must not have the same nationality as the authors.* Please note that the editorial board retains the sole right to decide whether or not the recommended potential reviewers will be selected.

Preparation of Manuscripts

Manuscript should be prepared strictly as per guidelines given below. The manuscript (A4 size page) should be submitted in Microsoft Word (.doc or .docx) with Times New Roman 12 point font and a line spacing of 1.5. *The manuscript that is not in the correct format will be returned and the corresponding author may have to resubmit*. The submitted manuscript must have the following parts:

Title should be concise and no longer than necessary. Capitalize first letters of all important words, in Times New Roman 12 point bold.

Author(s) name and affiliation must be given, especially the first and last names of all authors, in Times New Roman 11 point bold.

Affiliation of all author(s) must be given in Times New Roman 11 point italic.

Abstract should indicate the significant findings with data. A good abstract should have only one paragraph and be limited to 200 words. Do not include a table, figure or reference.

Keywords should adequately index the subject matter and up to six keywords are allowed.

Text body normally includes the following sections: 1. Introduction 2. Methodology 3. Results and Discussion 4. Conclusions 5. Acknowledgements 6. References

Reference style must be given in Vancouver style. Please follow the format of the sample references and citations as shown in this Guide below.

Unit: The use of abbreviation must be in accordance with the SI Unit.

Format and Style

Paper Margins must be 2.54 cm on the left and the right. The bottom and the top margin of each page must be 1.9 cm.

Introduction is critically important. It should include precisely the aims of the study. It should be as concise as possible with no sub headings. The significance of problem and the essential background should be given.

Methodology should be sufficiently detailed to enable the experiments to be reproduced. The techniques and methodology adopted should be supported with standard references.

Headings in Methodology section and Results and Discussion section, no more than three levels of headings should be used. Main headings should be typed (in bold letters) and secondary headings (in bold and italic letters). Third level headings should be typed in normal and no bold, for example;

2. Methodology

2.1 Sub-heading

2.1.1 Sub-sub-heading

Results and Discussion can be either combined or separated. This section is simply to present the key points of your findings in figures and tables, and explain additional findings in the text; no interpretation of findings is required. The results section is purely descriptive.

Tables Tables look best if all the cells are not bordered; place horizontal borders only under the legend, the column headings and the bottom.

Figures should be submitted in color; make sure that they are clear and understandable. Please adjust the font size to 9-10, no bold letters needed, and the border width of the graphs must be 0.75 pt. *(Do not directly cut and paste them from MS Excel.)* Regardless of the application used, when your electronic artwork is finalized, please 'save as' or convert the images to TIFF (or JPG) and separately send them to EnNRJ. The images require a resolution of at least 300 dpi (dots per inch). If

a label needed in a figure, its font must be "Times New Roman" and its size needs to be adjusted to fit the figure without borderlines.
All Figure(s) and Table(s) should be embedded in the text file.

Conclusions should include the summary of the key findings, and key take-home message. This should not be too long or repetitive, but is worth having so that your argument is not left unfinished. Importantly, don't start any new thoughts in your conclusion.

Acknowledgements should include the names of those who contributed substantially to the work described in the manuscript but do not fulfill the requirements for authorship. It should also include any sponsor or funding agency that supported the work.

References should be cited in the text by the surname of the author(s), and the year. This journal uses the author-date method of citation: the last name of the author and date of publication are inserted in the text in the appropriate place. If there are more than two authors, "et al." after the first author' name must be added. Examples: (Frits, 1976; Pandey and Shukla, 2003; Kungsuwas et al., 1996). If the author's name is part of the sentence, only the date is placed in parentheses: "Frits (1976) argued that . . ."

In the list of references at the end of the manuscript, full and complete references must be given in the following style and punctuation, arranged alphabetically by first author's surname. Examples of references as listed in the References section are given below.

Book
Tyree MT, Zimmermann MH. Xylem Structure and the Ascent of Sap. Heidelberg, Germany: Springer; 2002.

Chapter in a book
Kungsuwan A, Ittipong B, Chandrkrachang S. Preservative effect of chitosan on fish products. In: Steven WF, Rao MS, Chandrkachang S, editors. Chitin and Chitosan: Environmental and Friendly and Versatile Biomaterials. Bangkok: Asian Institute of Technology; 1996. p. 193-9.

Journal article
Muenmee S, Chiemchaisri W, Chiemchaisri C. Microbial consortium involving biological methane oxidation in relation to the biodegradation of waste plastics in a solid waste disposal open dump site. International Biodeterioration and Biodegradation 2015;102:172-81.

Published in conference proceedings
Wiwattanakantang P, To-im J. Tourist satisfaction on sustainable tourism development, amphawa floating marketSamut songkhram, Thailand. Proceedings of the 1st Environment and Natural Resources International Conference; 2014 Nov 6-7; The Sukosol hotel, Bangkok: Thailand; 2014.

Ph.D./Master thesis
Shrestha MK. Relative Ungulate Abundance in a Fragmented Landscape: Implications for Tiger Conservation [dissertation]. Saint Paul, University of Minnesota; 2004.

Website
Orzel C. Wind and temperature: why doesn't windy equal hot? [Internet]. 2010 [cited 2016 Jun 20]. Available from: http://scienceblogs.com/principles/2010/08/17/wind-and-temperature-why-doesn/.

Report organization
Intergovernmental Panel on Climate Change (IPCC). IPCC Guidelines for National Greenhouse Gas Inventories: Volume 1-5. Hayama, Japan: Institute for Global Environmental Strategies; 2006.

Remark

** Please be note that manuscripts should usually contain at least 15 references and some of them must be up-to-date research articles.*

** Please strictly check all references cited in text, they should be added in the list of references. Our Journal does not publish papers with incomplete citations.*

Copyright transfer
The copyright to the published article is transferred to Environment and Natural Resources Journal (EnNRJ) which is organized by Faculty of Environment and Resource Studies, Mahidol University. The accepted article cannot be published until the Journal Editorial Officer has received the appropriate signed copyright transfer.

Online First Articles
The article will be published online after receipt of the corrected proofs. This is the official first publication citable with the Digital Object Identifier (DOI). After release of the printed version, the paper can also be cited by issue and page numbers. DOI may be used to cite and link to electronic documents. The DOI consists of a unique alpha-numeric character string which is assigned to a document by the publisher upon the initial electronic publication. The assigned DOI never changes.

Mahidol University

Wisdom of the Land

Research and Academic Service Section, Faculty of Environment and Resource Studies, Mahidol University
999 Phutthamonthon 4 Rd, Salaya, Nakhon Pathom 73170, Phone +662 441-5000 ext. 2108 Fax. +662 441 9509-10
E-mail: ennrjournal@gmail.com Website: https://www.tci-thaijo.org/index.php/ennrj